POINT AND REGIONAL SCALE MODELLING OF VADOSE ZONE WATER AND SALT FLUXES IN AN AREA OF INTENSIVE HORTICULTURE

Thesis submitted by
Graham Paul Green, B.Sc. (Hons)

for the degree of Doctor of Philosophy
in the School of the Environment,
Faculty of Science and Engineering,
Flinders University,
South Australia

August 2010

TABLE OF CONTENTS

LIST OF FIGURES

LIST OF TABLES

ABSTRACT

The introduction of a large volume of reclaimed effluent water for irrigation in the Northern Adelaide Plains (NAP) horticultural area has altered the regional water and salt balance, raising concerns regarding the effects of these on shallow water table elevation and root zone salinity in the highly valued and productive soils.

A methodology is described for constructing and calibrating numerical models of vertical fluxes of soil water and solutes to achieve simulations which match a number of monitored study sites. Extension of these simulations to a period of 20 years, and incorporation of measured soil chemistry variables, enables an examination of the influence of differing irrigation strategies and temporal variations in weather conditions on year-to-year variations in soil water fluxes and root zone salinity. Application of these models to the whole NAP horticultural area was achieved using a system of multiple one-dimensional simulations with variables altered according to their spatial distribution.

The results show large temporal variability in drainage fluxes beneath irrigated plots. Fluxes occur mainly in winter, with annual variations depending primarily on differences in rainfall distribution and evapotranspiration. Annual drainage flux totals were found to correlate poorly with annual rainfall totals.

Spatially, drainage fluxes varied both within and between study sites. Simulations of fluxes at observation points within monitored study sites varied owing to variations in soil hydrological properties. Results of the whole-area simulations suggest that over a larger scale, the majority of variation in drainage fluxes is due to differences in land use and irrigation practices, with a smaller but significant spatial variation due to differing soil types.

Additional simulations, representing the NAP prior to irrigated horticulture, indicates the introduction of irrigation has significantly increased drainage fluxes, but that the major change to the soil water budget in irrigated land areas has been to evaporation from the soil surface, with significant implications for soil salinity development.

DECLARATION OF ORIGINALITY

I certify that this thesis does not incorporate without acknowledgment any material previously submitted for a degree or diploma in any university; and that to the best of my knowledge and belief it does not contain any material previously published or written by another person except where due reference is made in the text.

_____

Graham Paul Green

ACKNOWLEDGMENTS

The author acknowledges and is very grateful to the many people and organisations that have assisted and made contributions to the completion of this research.

Firstly, sincere thanks to my principal supervisor Dr John Hutson, who's patient guidance, unassailable enthusiasm and unfailing willingness to impart his seemingly boundless knowledge have been essential to the completion of this work. John spent many hours over-and-above the call of duty, discussing concepts and checking data files and model code.

Many thanks also to Dr Peter Dillon, who, as co-supervisor of this project, was key to its instigation and provided expert advice, encouragement and support throughout. Professor Craig Simmons provided important guidance and ideas in the early stages of the research, and intellectual support and friendship thereafter. Thanks also to Dr Daryl Stevens for contributions in the early stages of the research.

The Virginia Horticulture Centre provided technical assistance and liaison with horticulturalists. My sincere gratitude is extended to those horticulturalists and property owners of the Northern Adelaide Plains who hosted field study sites and provided assistance in their establishment. Thanks also to Karen Barry, Dallas Baird and David Poulsen for their hard work in assisting with installation and monitoring of field study sites.

Essential operating funds for this research were provided by CSIRO Land and Water, the Northern Adelaide and Barossa Catchment Water Management Board, and the Government of South Australia Environmental Protection Authority. Financial support of the author, in the form of scholarships and stipends, was provided by the Australian Research Council, CSIRO Land and Water (Postgraduate Scholarship) and the Centre for Groundwater Studies (Research Project Support Stipend). The author is sincerely grateful to these organisations.

Lastly, but by no means least, thanks to my endlessly patient wife Niki, who's constant encouragement and moral support have seen me through this task, and to Lewis and Robert, who's welcome arrivals have spurred me to the finish line.

CHAPTER 1: INTRODUCTION

1.1 Wastewater Re-use, Irrigation Drainage, and Irrigation-induced Soil Salinity on the Northern Adelaide Plains

The Northern Adelaide Plain (NAP), approximately 50 km north of Adelaide in South Australia, is an area of extensive broadacre horticulture with approximately 3000 hectares of land under irrigation. Crops grown here are predominantly vegetables, almond trees and grape vines (Figure 1.1). The hot and dry conditions experienced in the area for much of the year demand that vegetable crops are heavily irrigated to maintain a high root zone water content. Irrigation is also used for crop cooling on particularly hot summer days, and for frost protection prior to very cold nights in the winter. The large amount of irrigation that is therefore required for horticultural crops in this area creates a significant risk of high rates of drainage flux to groundwater. Careful management of irrigation is critical to prevent 1) excessive drainage fluxes that may cause a sustained rise in the water table and 2) sustained increases in soil salt concentrations.

In 1999 a scheme for the re-use of treated wastewater began supplying irrigators on the NAP with reclaimed tertiary-treated effluent water from the nearby Bolivar wastewater treatment plant. In 2004 the scheme supplied approximately 14 gigalitres of water per year to irrigators (Collins, J., 7/7/2005, pers. comm.). This has presented water resource and catchment managers with the challenge of ensuring firstly that the available volume of reclaimed water is used conservatively to ensure a sufficient and equitable supply to all subscribers, and secondly that irrigation drainage water does not cause a sustained rise in the shallow water tables in the area. Conversely, the combination of fairly saline irrigation water (average 1200 mg/l TDS), high salinity of the shallow groundwater, and naturally high soil salinity, necessitates the application of sufficient irrigation water to ensure some leaching of salts through the soil profile.

The re-use of urban wastewater for irrigation has great potential to provide a number of benefits. Firstly, it provides a way to dispose of often nutrient-rich treated effluent water, which may otherwise cause environmental degradation in receiving waters. Secondly the new water resource provided by the recycled water reduces the need to

exploit groundwater resources for irrigation, thus reducing draw-down of freshwater aquifers in the area receiving the recycled water. Irrigators can be charged for the supply of the new water, thereby recovering some of the costs of installation and maintenance of the recycling infrastructure. Also, if the recycled water is available in sufficient quantities, then irrigators may be able to increase the area of land under cultivation and increase agricultural production, creating associated economic benefits.

The potential benefits of such a scheme are clearly considerable. However, the potential environmental hazards presented by a water re-use scheme must be carefully considered. If the scheme introduces a large volume of additional water to a given catchment area, as is the case with the Bolivar wastewater re-use scheme and the Northern Adelaide Plains, then the water balance in that area is significantly altered. The additional water and any salts or contaminants it may contain, may have a profound effect on the receiving environment.

In areas of flat topography, such as the Northern Adelaide Plains, there is very little surface drainage. Water tables are fairly shallow, so the introduction of large volumes of recycled water can significantly raise the local water tables if a large proportion of the water leaches to groundwater. Conversely, if most of the relatively high salinity recycled water evaporates from the soil root zone, then there is a considerable risk of raising soil salinity in the valuable agricultural soils receiving the water. It is thus essential to determine appropriate irrigation strategies to ensure the correct balance between salinity control and water table rise.

A requirement for research into the hydrological effects of the reclaimed water irrigation was initiated in response to evidence of a rising shallow water table and consequent surface salinisation observed in areas to the North of Virginia in October 2001 (Good, 2002). Observations of decline in annual and perennial crops in this area prompted the digging of observation trenches, revealing a water table as close as 0.7m to the land surface in some places.

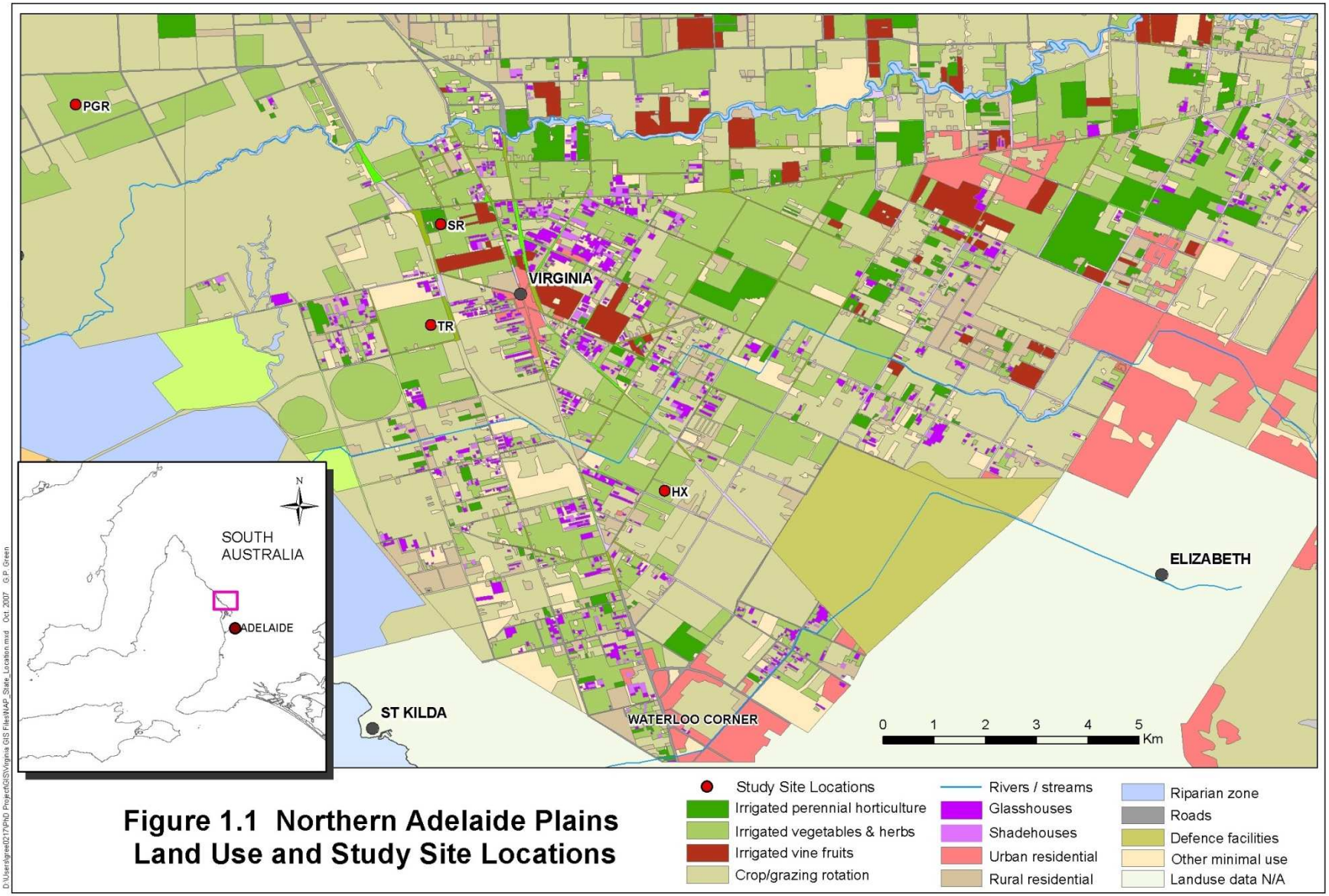

Figure 1.1 Northern Adelaide Plains Land Use and Study Site Locations

Subsequent investigation by Gerges (2002) via a network of fourteen newly-drilled observation wells into the shallow aquifer, suggested a number of potential reasons for the rising water table:

1. The area is a natural low point in the surface topography and would be the first to be affected by a regional rise in the water table
2. The abnormally wet winter of 2001 and above-average rainfall of the past previous two winters, suggesting the water table rise is possibly a cyclic or ephemeral event
3. Poor drainage network management
4. Potential upward leakage from deeper aquifers
5. Surplus irrigation water percolating to the water table aquifer
6. Leakage from new dams and /or wetlands in the area
7. A history of fluctuating water table rise and fall due to abstractions from the deeper aquifers causing periodic changes in the direction of the hydraulic gradient between the water table and the deeper aquifers.

A number of recommendations were made by Gerges for further research to provide a better understanding of the components of the water balance in this area. Subsequently, a first approximation of the NAP shallow aquifer water balances was reported by Gerges and Kelly (2002). This report identified excess irrigation water (mains, bore and reclaimed water) as the greatest potential input to the shallow aquifer, contributing an estimated 75% of accessions to the water table. However, the calculation of drainage to groundwater in this water balance approximation were subject to gross approximations of evapotranspiration and run off. Hence, extensive further research was required into actual drainage fluxes beneath irrigated land in order to provide a reasonably accurate estimation of drainage to the shallow aquifer.

1.2 Research Objectives

In view of the issues present above and the opportunities presented by hydrologic models to provide greater understanding and improved quantification of soil water and salt fluxes in an irrigated setting, the research project presented here was conducted with the following objectives:

1) Through field studies within the NAP, develop a quantitative understanding of fluxes of water and salt draining beneath irrigation areas with different land use types and irrigation management practices.

2) Develop models that predict vertical water and salt fluxes at a number of field study sites in the NAP. Calibrate and verify these models with measurements of soil water, soil salinity and leachate quantity and quality beneath a variety of crops that are typical of those grown in this area.

3) Through integration with geographic information systems, expand the one-dimensional soil water flux models to enable predictions on catchment scale, thereby providing a generic predictive tool to identify areas with large excess drainage fluxes and/or high risk of soil salinity rise.

4) Apply these GIS-integrated models to assess impacts of irrigation management practices on drainage fluxes and soil salinity development on plot and catchment scales.

5) Develop irrigation strategies that minimise the volume of drainage to groundwater while avoiding a sustained rise in soil salinity.

1.3 Rationale for the Modelling Approach

The variety of land uses on the NAP makes the quantification of drainage fluxes over the whole region a complex task. The first steps involve quantifying drainage to groundwater beneath the land use categories that occupy the largest land area and/or use the largest volumes of water. These are various types of irrigated horticulture. Direct measurements of irrigation drainage flux are impractical, firstly because of the difficulty in capturing or monitoring downward flux, and secondly because of the variability of flux from one point to another. There are two problems therefore to overcome: firstly how to determine the vertical water flux between the land surface and the water table and secondly, how to

determine the variation of this flux according to different soil types, crop types, surface topography and irrigation practices.

The NAP is an area of almost uniformly flat topography with a small number of different soil types that are fairly uniformly distributed across the area by alluvial and aeolian deposition. It is posited that, in an area with such topographic and pedologic uniformity, the net downward flux of water and dissolved salts through the unsaturated (vadose) zone to the water table beneath an irrigated plot of land can be quantified using numerical models based on well-established principles of unsaturated soil water flow and soil solution chemistry, which could include ion exchange processes. Ideally such models are constructed and calibrated using measurements of soil water retention characteristics and hydraulic conductivity of the soil profile at a number of points within the study area. Measured rainfall, irrigation, evapotranspiration and crop cover conditions, monitored for a year or more may then provide input data for the soil water flux model relating to each monitored location. Once a soil water flux model is correctly calibrated so that its predictions of soil water contents and drainage fluxes compare well to measured values, the effects of differing irrigation management practices on soil drainage fluxes can be simulated. Thus improved irrigation scheduling regimes can be proposed that minimise excess drainage fluxes and thereby reduce localised water table rises and soil salinisation risks.

Regional estimates of flux to the water table may be obtained by completing similar analyses on several plots that are representative of the major land use categories of the region and combining the one-dimensional flux models with a geographic information system (GIS). The GIS allows the parameterisation of a large area by creating separate thematic maps for each of the variables that affect the soil water balance. By overlaying different thematic maps, all sub-parcels of land sharing common values for each parameter used may be identified. Integration of the one-dimensional soil water transport model with the GIS then allows soil water flux volumes to be calculated for each set of similar land parcels. Thus an assessment of fluxes to groundwater across a large area can be achieved and management policies for irrigators and catchment managers may be developed.

1.4 Why Not Simply Make Direct Measurements of Soil Water and Salt Fluxes?

On a timescale of years, the net drainage flux beneath an irrigated horticultural plot is simply the difference between the sum of irrigation and rain water volume and the sum of evapotranspiration (ET), surface runoff and lateral throughflow. In an area with predominantly flat topography, surface runoff may be negligible such that drainage flux to groundwater over annual timescales is the difference between the total water quantity (irrigation and rainfall) and ET. However, this remains a difficult calculation due to the difficulty of measuring or accurately estimating ET. As drainage is usually a small fraction of the water applied to the soil surface, and ET a large fraction, small errors in ET estimation result in large errors in drainage estimates.

ET calculations in realistic and varying field conditions tend to have a large margin of error because of the number of dynamic parameters involved in their calculation. As a result, the calculation of water fluxes to groundwater by subtracting ET from total precipitation is inherently very inaccurate, because the margin of error in ET estimates is large compared to the net flux to groundwater (Gee and Hillel, 1988; Scanlon et al., 1997).

Direct measurements of drainage fluxes are also very difficult. Lysimeters are commonly used to collect samples of water draining through a soil profile for the analysis of leachate quality, and sometimes to measure volumes of water draining. However, all lysimeters have one or more significant limitations. A conventional drainage lysimeter is simply a box or cylinder that contains a representative volume of soil with a collection chamber at its base into which water leaching through the soil collects and can be withdrawn for measurement or analysis. For the measurement of leachate volumes, all free-drainage lysimeters are compromised by the need to create a discontinuity at some depth in the soil profile in order to incorporate a horizontal surface at which leachate may drain into the collection chamber. This prevents the normal flow of water downwards under the effect of a matric potential gradient and means that water will only drain into the lysimeter under gravity, for which the soil must be at, or close to, saturation. Hence, the unsaturated flow of water through the soil is interrupted and the leachate collected by the lysimeter will only be a proportion of the normal downward flux through the soil profile. Many studies report low and variable leachate collection efficiencies for free drainage lysimeters (Parizek and Lane, 1970; Haines et al., 1982; Radulovich and Sollins, 1987; Jemison and Fox, 1992). For example, Jemison and Fox (1992) tested the collection efficiency of free drainage pan

lysimeters and found an average efficiency of 52% within a range of efficiencies from 13 to 92%.

Tension lysimeters, including porous ceramic suction cup samplers, overcome the matric suction of the sampled soil by applying a suction to the lysimeter's collection surface. However, the applied suction firstly creates an artificial potential gradient between the lysimeter and the soil and, secondly, draws water from an unknown volume of soil such that realistic leachate flux volumes can not be calculated. These problems led van der Ploeg and Beese (1977) to conclude that there is no useful relationship between freely percolating soil water and the amount of soil water extracted by tension and ceramic cup lysimeters. Cochran et al. (1970) recommended the use of tension lysimeters only for monitoring changes in water quality with respect to time.

Weighing lysimeters, which allow measurements of the changes over time in the mass of the contained soil and plants, provide an effective way to measure ET. Over a given time period, the difference between the initial mass of the lysimeter plus the mass of water applied, and the final mass plus the mass of leachate collected is the mass of water evaporated and transpired. These are also subject to the lower boundary condition discussed above, such that the amount of plant-available water may differ to that in normal field conditions. The use of weighing lysimeters in field conditions is limited by the high cost of this type of lysimeter, and by operational difficulties in many agricultural field settings.

1.5 Soil Hydrology Modelling

1.5.1 Opportunities presented by numerical models of soil hydrology

The factors that determine the drainage flux beneath agricultural land include rainfall, irrigation, soil profile type, soil surface condition (e.g. tilled soil), topography, crop types, crop cover fraction, and evaporation conditions: air temperature, wind speed, solar radiation and humidity. These can all be incorporated into models that estimate how drainage fluxes vary according to the combination of these parameters within the prevailing weather conditions, and the crop types, irrigation types and soil types present. Models can be calibrated using in-field measurements of soil water contents such that they estimate the soil water drainage fluxes measured at a number of monitored sites to an acceptable degree of accuracy.

A number of numerical models are available to simulate the movement of water and solutes in unsaturated media and the application of these is demonstrated in numerous research papers. Research is generally aimed at simulating subsurface water fluxes to provide information for the better management of irrigation, either to preserve limited groundwater resources or to minimise accessions to shallow groundwater.

Process-based soil water transport models such as LEACHM (Leaching Estimation And CHemistry Model) (Wagenet and Hutson, 1987) simulates the vertical movement of water through the soil profile in response to water applications and ET conditions. It provides an additional benefit to a simple daily water-ET balance because actual evapotranspiration (ETa) is restricted if soil water becomes limited at the soil surface or in the root zone and can not supply the volume of water that would be assumed in a calculation of ETa based on reference potential ET and crop factors. Thus the ETa calculated within the model does not rely on the assumption that there is a uniform supply of water to be evaporated or transpired.

Importantly, the LEACHM model predicts the soil water contents and soil matric potentials within each layer of the modelled soil profile that result from the combination of processes of infiltration and ET and vertical water movement through the soil profile due to hydraulic potential differences. This feature provides an opportunity to calibrate simulations of a particular soil profile. If the model correctly estimates the ETa and the rate of vertical movement of water between layers then the predicted changes in water content and matric potential in each segment should match the changes observed in the monitored soil profile. Thus the model may be calibrated and verified against measurements of water content or matric potential at a number of depths in the soil. If the predicted changes in potential at two or more depths in the modelled soil profile are in agreement with the observed changes, a degree of confidence is provided in the accuracy of the prediction of water movement between depths. This approach to model verification was demonstrated by Close et al. (1999) and Sarmah et al. (2005), who used soil water content measurements to verify the soil water transport predictions of models of pesticide leaching after the soil hydrologic variables used in the models had been determined experimentally.

A similar calculation of drainage fluxes could be made from historic data of potential differences between two points in depth and an unsaturated hydraulic conductivity function. However, such a calculation provides only a historic estimate of fluxes, whereas

a suitably calibrated model allows the prediction of fluxes under future conditions in which water applications and ET conditions may be different to those during the monitored period.

A study by Ahmad et al. (2002) used the numerical model SWAP (Soil-Water-Atmosphere-Plant) to compute vertical soil water fluxes in the unsaturated zone beneath a cotton/wheat and rice/wheat cropping system in Pakistan. The results of the model showed significant accessions to the water table due to net downward annual flux of soil water induced by over-irrigation, such that the authors were able to make estimates of the required reduction in irrigation required to balance annual water table recharge with groundwater extractions for irrigation.

Wahba et al. (2002) tested the effectiveness of the model DRAINMOD-S (Kandil, 1992) for predicting water table depth fluctuations in response to different irrigation drainage management scenarios and to evaluate the effectiveness of subsurface drainage as a way to manage the water table depth beneath an irrigated field. The DRAINMOD-S model extends the capabilities of DRAINMOD (Skaggs, 1978) to include solute transport modelling. The DRAINMOD model uses a simplified water balance approach, simulating water flow in irrigated soil with a shallow water table in order to predict the depth of the water table and the water content of the soil above the water table in response to hydrologic components of infiltration and evapotranspiration given differing surface and subsurface drainage scenarios. The accuracy of the model output was tested by comparing measured water table depths and tile drain outflow volumes with the model's predictions. In doing this, the study highlighted an important validation test, which is the model's ability to accurately predict fluxes using model parameters that are calibrated using data not from that year.

Several soil water transport models, including LEACHM, MACRO (Jarvis, 1994), NCSWAP (Molina and Richards 1984), SLIM (Addiscott et al. 1986) and SOIL (Jansson, 1991), were evaluated by Jabro et al. (1998) and all found to provide reasonable predictions of water drainage fluxes under irrigated maize crops Statistical analyses of predicted and measured drainage fluxes at 1.2m depth indicated that all five of the models tested made reasonable predictions and were able to accurately predict drainage fluxes without the need to re-calibrate the model for each year (Jabro, 1998).

More recently the vadose zone model HYDRUS (Simunek et al. 1999) has become a standard (at least in Australia) for 1- and 2-dimensional modelling of water and chemical fluxes in variably saturated soil conditions. However, only the most recent version of this software allows sufficient control of temporal variations in crop/vegetation and surface evaporation conditions to undertake the modelling task required in this study. This version of HYDRUS was not available during the period in which this study was conducted.

1.5.2 Underlying principles of soil hydrology modelling

The primary soil properties that affect the flow of water through a soil are its hydraulic conductivity and its water retention characteristic - the ability to store and release water. Hydraulic conductivity is at a maximum when the soil is saturated, and decreases in a non-linear relationship to the soil water content.

Particle size, and size distribution, are key to these properties as they are the primary controller of a soil's porosity and distribution of pore sizes. Pore size distribution largely affects the shape of a soil water retention characteristic curve. Morphological properties, such as bulk density, organic matter content and clay type of a soil also have significant effects on a soil's ability to store and transmit water.

The water retention curve of a soil depicts the relationship between the soil water content and the soil suction or matric potential. The matric potential is the pressure of soil water relative to ambient atmospheric pressure, which is defined as zero. The capillary attraction is greater in smaller pores, and the hydraulic conductivity lower, such that as water is drawn out of a soil (such as under a hydraulic potential gradient), the larger pores release water first, followed by smaller pores under successively higher potential differences between the pore and the lower-potential surrounding environment. Thus the ability of soil to hold or release water is dependent on the size distribution of pores that are in differing states of saturation. For any given soil, the matric potential follows a non-linear relationship to its water content, depicted by its water retention curve. There is a hysteresis effect between the wetting and drying of a soil, due to the entrapment of air between different sized pores when wetting. This effect causes a difference between water retention curves followed when a soil is wetting or drying.

A number of models are available to describe the shape of the water retention curve for a soil. The most commonly used are those developed by van Genuchten (1980), Campbell

(1974) and Brooks and Corey (1964). The van Genuchten model allows the whole water retention curve to be described, whereas the Campbell and Brooks and Corey models do not describe the 'wet' end of the curve at matric potential values greater than the air entry value. Modfications which provide this were described by Clapp and Hornberger (1978) and Hutson and Cass (1987).

A soil's hydraulic conductivity is a measure of its ability to transmit water along a hydraulic potential gradient. In a saturated soil the hydraulic conductivity is affected by the total porosity, pore size distribution and pore continuity, as well as by the density and viscosity of the water transmitted. In unsaturated soil, as the saturation state drops, the hydraulic conductivity falls below the saturated hydraulic conductivity and follows a non-linear function of the soil water content.

The curves followed by the soil retention characteristic and unsaturated hydraulic conductivity of a soil are related by the particle and pore size distributions. The water retention characteristic models of van Genuchten, Campbell and Brookes and Corey have corresponding models for hydraulic conductivity with some common parameter values used in both models for a given soil.

The slope of the water retention curve at any particular water content, $d\theta/dh_m$, is referred to as the differential water capacity, denoted $C(h_m)$. The vertical flow rate of water between two depths in the soil is dependent on the hydraulic conductivity of the soil and the difference in the sum of gravitational potential and matric pressure potential between the two depths. If $K(h_m)$ and $C(h_m)$ are known for a range of values of θ at several depths in the soil profile, then by continuously monitoring the value of h_m or θ at those depths, the flow rate of water through the soil at each monitored depth can be calculated.

Richards's 1931 extension of Darcy's law to form an equation for the flow of water in unsaturated media provides the basis for the modelling of soil water movement.

$$\frac{\partial \theta}{\partial t} = -\frac{\partial}{\partial z}(K \frac{\partial H}{\partial z}) \qquad \text{(Equation 1.1)}$$

(Richards, 1931)

The Richards equation is a non-linear partial differential equation of vertical flow in unsaturated soil. The equation has two dependent variables, θ (volumetric water content) and H (total hydraulic potential, equal to the sum of matric potential and gravitational

potential). By including $C(h_m)$ in the left hand side of the equation, we reduce the number of dependent variables to one.

$$C(h_m)\frac{\partial h_m}{\partial t} = -\frac{\partial}{\partial z}(K\frac{\partial H}{\partial z}) \qquad \text{(Equation 1.2)}$$

In a numerical finite difference model the gravitational component of the total head is known at each spatial interval and the independent variables become θ and h_m (matric potential). If h_m is determined as a function of θ by one of the water retention models cited above, changes in θ over time at each spatial interval can be modelled according to time-varying conditions at the model boundaries.

The main principles of modelling soil water in the unsaturated zone are summarised by Feddes et al. (1988), who describe how to apply a numerical solution to the Richards equation by the finite difference method, enabling computerised modelling of soil water flow if appropriate boundary conditions are applied and appropriate water input and climate data are available.

1.5.3 Laboratory methods for measuring soil hydraulic characteristics

Laboratory based methods allow a wide range of matric potentials to be contrived within a soil sample such that the soil water content at high and low matric potentials can be measured in order to construct soil water retention curves that extend to –1500 kPa. This is considered to be the wilting point or limit for plant water uptake (Briggs, 1912). Gas pressure devices developed by S.J. Richards (1939) and L.A. Richards (1949) allow the soil water content / matric potential relationship to be measured below –100 kPa by applying a pressure to a gas chamber containing the soil sample. The soil sample is placed on, and in hydraulic contact with, a ceramic or cellulose acetate membrane that, when wet, will conduct water but remain saturated. When pressure is applied to the chamber, soil water will flow across the membrane, since the lower surface is at atmospheric pressure. Water will continue to pass from the soil through the membrane until the matric suction in the soil is equivalent (but negative) to the pneumatic pressure applied to the chamber. Incremental water volumes are recorded, and absolute soil water content is measured when the soil is removed from the chamber (Marshall and Holmes 1979).

Measurement of saturated hydraulic conductivity for soil samples is conducted routinely in the laboratory using fixed- or falling-head permeameter apparatus. Measurement of

unsaturated hydraulic conductivity, denoted $K(\theta)$ or $K(h_m)$, is somewhat more difficult. A laboratory-based method for the measurement of unsaturated hydraulic conductivity, $K(\theta)$, is described by Klute (1965). Using pressure cell apparatus, the outflow rate of water from a single soil sample is measured. The outflow rate measurement allows calculation of the soil water diffusivity at the pressure applied to the sample in the cell. Diffusivity, $D(\theta)$ is related to $K(\theta)$ by the relationship $D(\theta) = K(\theta)/C(\theta)$, where $C(\theta)$ is the differential water capacity, equal to the ratio of $d\theta/dh_m$ or the slope of the water retention curve. By increasing the pressure applied to the cell in increments, a range of $D(\theta)$ values can be calculated at a range of pressure potentials. By also monitoring the volume of water expelled from the soil at each pressure increase, a water retention curve is constructed and $C(\theta)$ values are determined, thus $K(\theta)$ can be calculated for each $D(\theta)$ value measured.

1.5.4 Methods of measuring in-field soil hydrologic variables

For soil hydrology models to be representative of field conditions they must be calibrated and/or validated using field measurements of soil water contents. The models can then be applied to the other combinations of soil type, land/crop cover, and irrigation that exist among the various land uses in the NAP. The data required for this exercise requires a number of study sites in which the water applied (irrigation and rainfall), weather conditions, crop type and crop cover percentage, soil water content and soil water potential are closely monitored.

In-situ soil matric potentials can be measured using tensiometers. Developed by Richards and Gardner (1936) after earlier work on retention and movement of water in soil by Buckingham (1907), tensiometers are a simple and low-cost way to measure soil matric potentials in the field at a variety of depths, but have some significant limitations. As matric potential decreases towards -100 kPa, the pressure in the tensiometer drops to that at which the water in the tensiometer will boil at typical ambient temperatures, causing the water column in the tensiometer to break. The useful range of the tensiometer is thereby limited to about –85 kPa matric potential. At this potential in sandy soils not much water is left in the soil, however in clay soils much of the water remains available for plants below the –85 kPa matric potential (Veihmeyer and Hendrickson, 1927). The response of a tensiometer to rapid change in the water content of the soil is determined by the area and

conductivity of the ceramic cup and the sensitivity of the vacuum gauge used with the tensiometer.

Drainage lysimeters provide a way to collect water leaching through a profile, either for measurement of leachate volumes or to collect samples of leachate for analysis. However, as discussed earlier, they suffer poor leachate collection efficiencies. In an effort to overcome these problems, Holder et al. (1991) developed the capillary-wick lysimeter. This is a variation on the pan lysimeter, installed at the base of a soil profile, with a collection of fibreglass wicks that conduct water from the collection plate of the lysimeter and into a collection chamber. The vertical length of the wicks creates a hanging column of water below the collection plate, thus creating a tension to draw water from the base of the soil profile in unsaturated conditions. The tension created is equivalent to the vertical length of the wick beneath the collection surface, so if the wick extends of 0.5m below the collection surface, the tension created at the collection surface will be approximately –5 kPa. Hence water will drain into the collection bottle via the hanging wicks whenever the soil water potential is above –5 kPa. The collection efficiency of this type of lysimeter was tested by Zhu et al. (2002) and compared with the efficiency of zero-tension pan lysimeters. In that study, the capillary wick lysimeters were found to collect on average 2.7 times more leachate than the zero tension lysimeters and, over a 4–year period had a collection efficiency much greater than the zero-tension pan lysimeters.

The construction of the capillary wick lysimeter is described by Holder et al. (1991), while Knutson et al. (1993) describe how to prepare fibreglass wicks for use in these lysimeters to ensure good hydraulic conductivity of the wicks.

1.5.5 Measurement or estimation of evapotranspiration

Evapotranspiration is commonly estimated using a reference or potential evapotranspiration (ETo or ETp) for a given time period and multiplying this by a factor related to the existing plant cover conditions to determine the actual evapotranspiration (ETa). The potential ET may be based on the evaporation of an open pan of water or on a reference vegetated surface against which the potential ET formula has been calibrated. The latter approach, using the Penman-Monteith formula to determine a reference evapotranspiration, ETo, for an ideal well-watered grass reference surface, is commonly used for the purposes of calculating agricultural crop water use. This method is commonly

applied in accordance with the guidelines of the Food and Agriculture Organisation of the United Nations Irrigation and Drainage Paper 56 (FAO 56) (Allen et al., 1998). These guidelines recommend categories of crop development: initial, middle, and end. Recommended crop coefficients for each crop type differ for each of these categories to reflect different stages of crop cover through the life of the crop. Values of these crop coefficients are derived from measurements of the ratio of ETa to Penman-Monteith ETo for sample crops in experimental settings (Allen 1998). This approach makes no allowance for different crop cover development rates that may occur from one site to another due to different weather patterns, seeding patterns, and rates of fertiliser application. There is also no allowance for differing water availability at the soil surface. If a soil surface is kept wet by frequent irrigation applications for the majority of the time, considerably more water may evaporate than if a lower surface moisture level is maintained by more infrequent irrigation, such that the soil surface is sometimes dry and surface evaporation is restricted. With the FAO 56 Penman-Monteith approach, the ETa calculated for one irrigation management strategy is no different to that calculated for another.

The FAO 56 recommendations are necessarily very generalised in order that they can be applied by a variety of users and do not demand specific measures of water availability and crop cover fraction, which would place a greater burden of data collection on the user. Such an approach to determine the ET component of the water balance in a model may result in a poor estimate of the vertical soil water flux. A better estimation of ETa is required, ideally one that is dynamically related to both the crop cover fraction and the availability of water at the soil surface and in the root zone.

A suitably constructed soil water flux model incorporates reference evapotranspiration potential as a time-varying input and can calculate an actual ET flux within each time step according to the leaf area or crop cover and the availability of water to plant roots or at the soil surface. The relationship of actual ET to the reference ET can then be calibrated such that water remaining within the soil correlates with measured values. In this way the actual ET estimated within each time step can be made sensitive to variations in water available and provides a much more accurate estimation of ETa than the simple combination of reference ET and crop coefficients.

1.6 Extending Models to Regional Studies: Dealing with Spatial Variability

A regional estimate of soil water flux to the water table may be estimated by constructing one-dimensional flux models for several plots that are representative of the major land use categories of the area and integrating these models with a geographic information system (GIS). The GIS allows the parameterisation of a large area by creating separate thematic maps for each parameter. By overlaying different thematic maps, all sub-parcels of land sharing common values for each parameter used may be identified. Integration of the one-dimensional soil water transport model with the GIS then allows an areal soil water flux to be calculated for each set of similar land parcels.

A significant problem faced in the estimation of drainage fluxes on the scale of a whole catchment is in determining the spatial variability of the soil hydraulic characteristics. Bosch and West (1998) demonstrated a methodology by which to quantify this variability on the scale of a single paddock and between two paddocks with similar loamy-sand soil profiles. Their statistical analysis of saturated hydraulic conductivity (Ks) values at 28 locations and at 4 depths across each plot indicated a large range of Ks values within a single plot and soil type. However, their analysis also showed that below the surface soil layers of 0 – 20 cm depth, which were often modified by agricultural processes, there was good spatial correlation of Ks, and that differences in conductivity were not random spatially in depth or horizontally. This spatial correlation was found to be sufficient for geostatistical techniques such as kriging to be used to predict or interpolate hydraulic characteristics between spatially separated points at which hydraulic characteristics have been measured.

A study by Li et al. (1999) used a stochastic approach, using probability distribution matrices to characterise the vertical spatial variability of soil textural profiles in a research region. This method was applied to a 15 km^2 area of alluvial soils in northern China to provide variability characterisation to be used in a field water balance evaluation. The results of their field water balance model, based on data derived from the processing of field data through their probability matrix model, illustrated that large differences in the magnitude of field water transport variables occur between different soil profiles within a fairly uniform area of alluvial soils. These findings suggest a need for a large number of soil profiles to be characterised from field data if the field water balance across a region such as this is to be accurately represented.

However, the study by Li et al. only addressed variations in soil hydrologic properties. The actual variation in soil water flux may be dominated by the variation of other factors across a region, such as land use, crop type, irrigation method and ET contributors. Clearly it is important when characterising the vertical soil water fluxes over the scale of a field or region to understand how one-dimensional flux simulations at a single point may vary over a large area which may exhibit considerable spatial variation of several of the factors that affect these fluxes.

The use of geographical information systems (GIS) integrated with hydrological models has been trialed by a number of authors (e.g., dePaz and Ramos, 2001; Romanowicz and Bevan, 1993; Utset and Borroto, 2001; Wang and Cui, 2004), providing a guide to possible methodologies. These attempt to make predictions of hydrological and/or soil chemical fluxes over a large heterogeneous area, over which the effects of hydrologic differences may be minor compared to other factors in controlling soil water drainage fluxes. Typically, these are based on a database of static parameters (such as soil types, topography, land use) and a hydrological model that processes these parameters together with dynamic climate and irrigation variables.

The influence of variables other than the soil hydrologic parameters is demonstrated in a study by dePaz and Ramos (2001). In this, the soil water transport model GLEAMS (Leonard et al., 1987) was linked with a GIS to simulate nitrate leaching under vegetable crops and citrus trees over the scale of a whole catchment with varying agricultural land uses and differing management practices. The soil hydrology sub-model in GLEAMS is a fairly simple 'tipping bucket' type of model, using a water balance between water applied (rain and irrigation) and potential evapotranspiration conditions and assuming piston flow of soil water above a given field capacity. Hence, soil hydrologic parameters and their spatial variability were not fully quantified, however nitrate leaching values predicted by the model were found to show a good agreement with measured values over a one-year monitoring period.

In a further development of the use of integrated GIS/hydrological model arrangements, Utset and Borroto (2001) used the SWAP model to predict water table changes in response to the introduction of a major new source of irrigation water, and then went on to create maps of increased soil salinisation under the combined effects of the newly-introduced irrigation water and regional warming as predicted by a separate climate change model. Their assessment used estimated soil hydraulic properties based on a pedotransfer function

and published soil data. The SWAP model predicted water table rises in the study area using the estimated soil hydraulic properties and daily ET, irrigation and rainfall data. This study by Utset and Boroto is in many ways similar to the requirements of the project for the Northern Adelaide Plains although relying to a greater extent on estimates rather than data collected in the field. The predictions of the SWAP model were not calibrated or cross-checked against field data and the authors acknowledge that their study has a mainly methodological value.

The studies summarised above demonstrate the utility of combining soil hydrologic models with GIS to provide a distributed model of soil water and chemical flux. The research described in this thesis draws from the experience of these and other earlier studies. The application of the LEACHM hydrochemistry model and integration with Arc GIS to create a distributed model structure is demonstrated, allowing a prediction of vertical fluxes of water and salt over the large and spatially heterogeneous area of the NAP. Furthermore the distributed model allows the testing of a number of land and irrigation management scenarios to determine the sustainability of a variety of management policies applied to horticultural irrigation activities in the area.

CHAPTER 2: FIELD AND LABORATORY METHODS

2.1 Study Area

The Northern Adelaide Plains (NAP) covers an area of 750 km^2 and forms part of the Adelaide Plains sub-basin, in turn part of the St Vincent Basin. The majority of literature describing the hydrogeology of the area is by Gerges (1999, 2001). The basin is formed from Tertiary and Quaternary sediments up to 600m thick overlying a Precambrian fractured rock basement. The Quaternary sediments contain up to six aquifers but in most areas contain four. Tertiary sediments contain up to four aquifers, designated T1, T2, T3, T4 in order of increasing depth. Ephemeral watercourses on the NAP include the Gawler and Little Para Rivers and several small creeks rising in the Adelaide Hills (Gerges 2001).

The area is a broad coastal plain with alluvial soils, commonly with a sandy loam top soil of 20 – 50 cm depth overlying a calcareous clay subsoil. The area has a Mediterranean climate, with hot dry summers and cool wet winters. Annual rainfall averages 420 mm/y. Depth to the water table varies across the area from approximately 1.5 m to 12 m with seasonal fluctuations of up to approximately 0.5 m observed in areas where water table depths are monitored (Northern Adelaide and Barossa CWMB, 2004). In many places horticultural crops are grown on land with shallow water tables of 1.5 – 3 m depth.

The NAP has approximately 3000 ha of irrigated horticulture, for which water has traditionally been extracted from the top of the T1 and T2 aquifers via approximately 1200 wells. Prior to 1999, approximately 3500 ML/y was extracted from T1 and 13500-14000 ML/y from T2. Extraction from T2 aquifer is mainly in the Virginia and Angle Vale area while extraction from the T1 aquifer is mainly from three areas in the southern part of the plain. An estimated 500 ML/y is also extracted from the Quaternary aquifers. The highest use of groundwater is in the summer irrigation season from November to January (Gerges 2001). Total licensed bore water allocation in the NAP in 2002 was 26,500 ML/yr. While average annual bore water use is 17-18000 ML/yr, up to 24000 ML/yr is used in dry years. At this rate of extraction, groundwater is being mined, with an annual recharge of the T1 and T2 aquifers estimated to be between 6-10 GL/yr (Gerges, 1999). This over use of groundwater resulted in a significant decline in groundwater head levels and subsequent

decline in water quality to the extent that groundwater in some areas became unsuitable for irrigation of horticultural crops (Stevens, 2002).

In 1999 a water reclamation and reticulation scheme was commissioned to supply more than 200 growers in the NAP area with Class-A reclaimed water, suitable for unrestricted crop irrigation. Tertiary treated effluent water from the Bolivar wastewater treatment plant is delivered by the Virginia Pipeline Scheme (VPS). The reclaimed water was taken up enthusiatically by irrigators and the amount of water supplied by the pipeline has increased rapidly in the six years following the commissioning of the pipeline. Water volumes delivered by VPS from 1999 to 2004 were:

Yr Sept.1999 – Sept. 2000:	4.1 GL
Yr Sept. 2000 – Sept. 2001:	7.9 GL
Yr Sept. 2001 – Sept. 2002:	8.5 GL
Yr Sept. 2002 – Sept. 2003	9.1 GL
Yr Sept. 2003 – Sept. 2004	12.0 GL
Yr Sept. 2003 – Sept. 2004	14.0 GL (estimate, July 2005)

(J.Collins, pers. Comm. July, 2005).

Although groundwater extractions have reduced as more reclaimed water has become available, these reductions amount to less than the additional volume of water supplied via the Virginia Pipeline Scheme. Rather than simply replacing extraction of groundwater from the T1 and T2 aquifers, the availability of the additional water has led to an increase in the amount of land under irrigation. Hence the total amount of water used for irrigation in the area increased over the six year period from 1999-2005.

2.2 Data requirements

The field work program was designed to provide data on the several variables that influence drainage fluxes under irrigated horticultural crops. These were required from study sites that represent the various irrigation, crop and soil most commonly utilised by horticulturalists in the NAP. By selecting study sites with differing crops, soil types, and irrigation methods, approriate models can be developed that combine a number of variables with different values to represent the many combinations of crop, soil, and irrigation type that exist in the NAP area. While a large number of study sites would be ideal, the monitoring requirements at each site are significant, hence the number of

monitored sites had to be kept to an economical minimum. The data required for the hydrological models necessitated a number of study sites in which the water applied (irrigation and rainfall), weather conditions, crop type and crop cover percentage, soil moisture content and soil water potential are closely monitored. These sites were required to be irrigated agricultural plots that are representative of the most common agricultural practices, crop types and soil types in the area.

As the net vertical water and salt flux was simulated using version 4 of the LEACHM model (Hutson, 2003). Continuous records of irrigation, rainfall, reference evapotranspiration (based on temperature, humidity, wind speed and solar radiation data) and crop cover are required to provide input data to the model. Regular measurements of soil moisture content and water potential are used to calibrate the model.

At the study sites identified, the aim of the field monitoring activities was to generate the following data:

1. Records of soil water content and/or soil matric potential at several depths in the soil profile to a depth of up to 1.5m over the monitored time period.
2. Records of rainfall and irrigation water applied to the crops at study sites over the monitored time period.
3. Weather data including all parameters required for ET calculation using the Penman-Monteith method, monitored within the locale of each monitored plot.
4. Records of crop types present and crop cover fraction over the monitored time period.
5. Salinity and, where possible, volumes of leachate draining beneath the root zone in monitored plots.
6. Records of water table depth fluctuation over the monitored time period.
7. One-off measurements of soil water retention curves and unsaturated hydraulic conductivity at a fixed soil matric potential for soil samples at depths where soil matric potential is monitored at each study site.

2.3 Field Data Collection

2.3.1 Selection of study sites

A variety of agriculture types are in use across the Northern Adelaide Plains. Since a monitoring program for all agriculture types was not practical within the scope of this project, it was necessary to select a small subset of agriculture types to represent the broadacre practices within the area. The most recent landuse map of the area (Hogan and Scott, 1999) shows that, of the agricultural landuse in the area, broadacre vegetables make up the highest proportion of irrigated agriculture, with tree crops, vineyards and glasshouse/shadehouse horticulture making up the majority of the remaining irrigated agriculture.

Grazing and cereal crops represent a large part of the agricultural land area, but these are assumed to be un-irrigated. The year-round monitoring of broadacre vegetable plots will involve some monitoring of plots that are left fallow and un-irrigated, or with a cover crop, for part of the year. Data from these periods may be used to provide an indication of drainage fluxes beneath land used for grazing or cereal crops.

Being a flat coastal plain, the weather across the NAP is fairly uniform. However there is a significant difference in rainfall between the north and south of the plain.

To provide the best indication of the general pattern of drainage fluxes, with a minimal number of sites, three primary study sites were chosen for continuous monitoring over a period of eighteen months. Of the three sites selected, two were irrigated broadacre vegetable plots and the third was an irrigated almond orchard. Ultimately only two sites were monitored for the intended time. One of the broadacre vegetable sites was decommissioned after 5 months at the request of the land owner. A replacement site was established and monitored over approximately four months, for the period of one crop of carrots, after which the land owner required the field equipment to be removed to allow harvesting of the crop. No further crops were planted at that location for the duration of the study.

Crops at the selected broadacre vegetable sites were subject to overhead sprinkler irrigation. The almond orchard site was irrigated with micro-jet sprinklers beneath the tree canopy, with one sprinkler between each two trees. All sites were irrigated primarily with Class A reclaimed water (CARW), with an average salinity of approximately 1200 mg/l TDS, from the Virginia Pipeline Scheme.

The four study sites were identified by the designations PGR, TR, SR, and HX, throughout the study period, based on abbreviations of site locations. These identities have been used continuously through the data analysis and modelling phases of this project and are used throughout this report. Figure 1.1 (page 3) identifies which designation applies to which site.

Soil types in the area are fairly homogeneous. Most of the area is covered by a duplex soil type with a loamy-sand A-horizon overlying a loamy-clay B-horizon. The soil classification commonly used by horticulturalists in the area is defined by Matheson and Lobban (1975) and is primarily defined by the thickness of the loamy-sand A-horizon. The exception to this pattern is the dark cracking clay soil adjacent to the Gawler River. Within the Mathesonand Lobban soil classification, three soil types comprise more than 80% of the area used for irrigated agriculture in the NAP. At least one site with each of these three soil types was a priority in selecting study sites.

Soil profile characteristics at each of the four primary monitoring sites can be accurately represented by four soil characterisations identified in the NAP by the PIRSA (2001) soil landscapes database:

- Soil profile at study site PGR is characterised as a ‘sandy loam over dark clay’, as described by PIRSA (2001) at their observation site CL012.
- Study site TR is characterised as a ‘sand over red sandy clay’, as described by PIRSA (2001) at their observation site CL035.
- Study site HX is characterised as a ‘sand over red clay’, as described by PIRSA (2001) at their observation site CL031.
- Study site SR is characterised as a ‘sandy red gradational soil’, as described by PIRSA (2001) at their observation site CL036.

The PIRSA descriptions of these soil profile types are provided below as descriptions of the soil profile structures observed at the four study sites. The depths of transitional boundaries may have differed slightly in the soil profiles at the study sites to those at the PIRSA observation sites and these differences were taken account of when preparing the model soil profile descriptions for the modelling discussed in Chapters 4 to 6.

Also , the upper 40 – 50 cm of the soil at the study sites typically had a higher organic material content than at the PIRSA observation sites as the soil had been developed over a number of years for horticultural purposes.

Study Site PGR

Sandy Loam Over Dark Clay (PIRSA observation site **CL012)**

Soil Description:

Depth (cm)	*Description*
0-10	Dark brown fine sandy loam with weak granular structure.
10-25	Brown massive fine sandy loam.
25-50	Dark brown light medium clay with weak very coarse prismatic structure, breaking to strong subangular blocky.
50-90	Dark greyish brown weakly calcareous medium clay with weak very coarse prismatic structure, breaking to strong subangular blocky.
90-140	Reddish brown and dark brown mottled slightly calcareous medium clay with strong coarse blocky structure (subsoil of an older buried soil profile).
140-180	Orange and light brown weakly structured clayey sand.

Classification: Hypocalcic, Subnatric, Black Sodosol; medium, non-gravelly, loamy/clayey, moderate (PIRSA, 2001)

S**tudy** S**ite HX**

Sand over Red Clay (PIRSA observation site **CL031**)

Soil Description:

Depth (cm)	*Description*
0-12	Red loose sand (drift).
12-23	Dark reddish brown soft loamy sand.
23-44	Reddish brown soft loamy sand.
44-61	Dark reddish brown firm light medium clay with strong coarse subangular blocky structure.
61-100	Yellowish red firm highly calcareous light clay with weak subangular blocky structure and more than 20% calcareous nodules (Class IIIB carbonate).
100-160	Yellowish red and brown soft sandy loam.

Classification: Supracalcic, Mesonatric, Red Sodosol; thick, non-gravelly, sandy / clayey, moderate (PIRSA, 2001)

Study Site TR

Sand Over Red Sandy Clay (PIRSA observation site **CL035**)

Soil Description:

Depth (cm)	*Description*
0-24	Dark reddish brown soft loamy sand.
24-30	Reddish brown firm massive loamy sand.
30-42	Dark red firm sandy light clay with weak coarse prismatic structure and minor nodular carbonate.
42-80	Yellowish red very highly calcareous sandy clay loam with weak subangular blocky structure and minor nodular carbonate.
80-110	Red and brown mottled highly calcareous clay loam with moderate subangular blocky structure.
110-170	Dark brown and orange mottled moderately calcareous fine sandy clay loam with weak subangular blocky structure and 10-20% nodular carbonate.

Classification: Mesonatric, Hypercalcic, Red Sodosol; thick, non-gravelly, sandy / clayey, moderate (PIRSA, 2001)

Study Site SR

Sandy Red Gradational Soil (PIRSA observation site **CL036**)

Soil Description:

Depth (cm)	*Description*
0-15	Soft single grained reddish brown loamy sand.
15-35	Soft massive yellowish red loamy sand.
35-60	Red hard light sandy clay loam with weak coarse prismatic structure.
60-85	Red hard sandy clay loam with weak coarse prismatic structure.
85-150	Red and dark brown mottled moderately calcareous medium clay with strong angular blocky structure and 10-20% soft and nodular calcareous segregations.

Classification: Sodic, Eutrophic, Red Kandosol; medium, non-gravelly, sandy / clay loamy, moderate (PIRSA, 2001)

2.3.2 Monitoring period

Monitoring at two of the initially selected study sites (sites PGR and SR) commenced in August 2003. These included an almond orchard of mature almond trees, and a broadacre vegetable plot with a rotation of crops over the study period including carrots, potatoes and a barley cover crop (Figure 2.1). Monitoring continued at these sites for a sixteen month period in order that the data collected allowed a full one year model calibration. Monitoring at the second broadacre vegetable site (site TR) commenced in September 2003. This site hosted a barley cover crop followed by a crop of onions. This site was monitored for approximately five months, then decommissioned and replaced by another broadacre vegetable site. This site was monitored for nearly five months, the duration of a single crop of carrots.

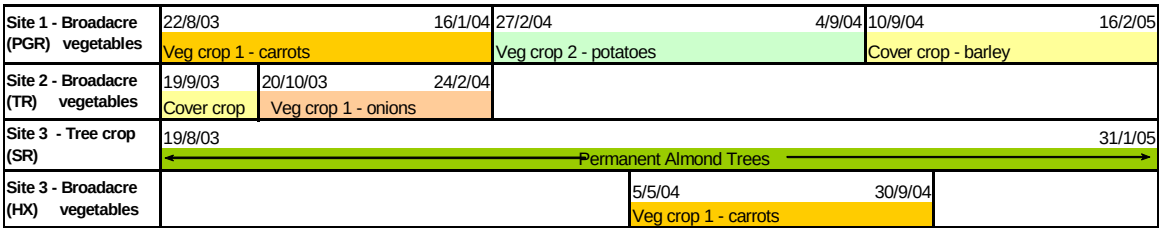

Figure 2.1. Timetable of crops monitored at the four study sites.

As the monitoring program did not provide two successive years of data for each irrigation scenario, inter-annual differences in weather and water applications in successive years on drainage volumes are based on historic weather data and a simulated irrigation schedule. Since weather conditions were continuously monitored, the variation in drainage as a function of weather variations during wet and dry conditions can be considered. As the majority of water falling onto the irrigated plots over the course of a year is irrigation water, the differences between wet and dry years are likely to be masked by irrigation management practices.

2.3.3 Field methods

Irrigation water applied was monitored using a data-logged tipping bucket rain gauge at each monitoring point at each study site. This type of rain gauge is very useful for recording the timing and duration of irrigation and rain events, however, because it only captures water falling at a single point in the plot they give an inaccurate reading of the spatial average amount of water applied in each irrigation event. To overcome this potential inaccuracy, in-line flow meters were installed in the supply pipe to the monitored

sub-plot. In the case of broadacre vegetables the irrigation pipelines were networks of 75 mm diameter aluminium or polypropylene pipes arranged and connected during the preparation of the plot for planting and then dismantled after the crop was harvested. The volume of water through the flow meter was converted to an areal depth of water applied (mm) by dividing the volume measured by the meter by area of the subplot supplied by the lateral spurs of the pipe network in which the in-line flow meter was installed. These measurements were then compared with the depth of water recorded by the raingauges in the plot and used to calibrate the readings of the raingauges.

Evaporation parameters (temperature, humidity, solar radiation and wind speed) were measured with an automatic weather station located at study site PGR, the most northerly study site. This was installed in November 2003 and continuously monitored and logged data for rainfall, temperature, pressure, solar radiation, wind speed, and rainfall at 15 minute intervals for the whole period of the field study program.

Being a flat coastal plain, the weather across the NAP is fairly uniform, however there is a difference in rainfall between the north and south of the plain. As the study sites have more than 6-7 km of north-south separation, the variation in weather conditions between study sites must be considered. To provide additional coverage of rainfall and ET parameters across the region, data from the weather station at the Edinburgh airfield at the Southern side of the NAP is also used.

Weather data was processed into daily minima, maxima and averages prior to calculating daily ETo using the Penman-Monteith formula according to the guidelines of FAO 56 (Allen et al., 1998).

Crop cover fraction was recorded by photographing two 4 m^2 areas of crop at weekly intervals. Photographs were analysed to determine the percentage of ground surface shaded by crop when viewed from above.

Water table depth was monitored by recording measurements of standing water level depth in piezometers adjacent to the study site. This was only monitored at study sites where the water table was at less than three metres depth, where it may effect soil moisture fluxes in the root zone.

Soil matric potential was monitored at three depths at each monitoring station using Soilspec™ tensiometers with a portable vacuum gauge. Readings were taken at approximately weekly intervals and corrected for the pressure drop created in the top of the

tensiometer tube by the length of the column of water within the tube. Tensiometer depths were 30 cm, 75 cm and 110 cm at all study sites. These depths ensured that one tensiometer was in the sandy-loam A-horizon and two were in the clay subsoil at each monitoring station. Vacuum readings were taken at weekly or two-weekly intervals throughout the monitoring period.

Soil moisture contents were monitored using Sentek Enviroscan capacitance soil moisture probes. These monitored soil moisture contents continuously at six depths (10, 30, 50, 70, 110 and 150 cm) at the primary monitoring stations of study sites PGR and SR. These were logged throughout the period of the monitoring program, with values recorded by a data logger at half-hourly intervals.

Soil Hydrologic Characteristics were determined from laboratory analyses of undisturbed soil core samples, collected in brass cylinders from each primary monitoring station. Soil core samples from three depths in the soil profile: 10, 30, and 50 cm, were collected for measurements of water retention unsaturated hydraulic conductivity functions. Undisturbed soil cores were collected in the brass cylinders of a set of Tempe cells. In clay soils, these were taken using a modified drop-hammer, which housed the brass cylinder in a hardened steel outer casing with a sharpened leading edge. Using this device, the cylinder and housing could be forced into the heavy clay subsoils that are typical of the NAP. After removal of the cylinder from the housing, soil protruding from the cylinder was carefully worked off with a hacksaw blade, leaving the brass cylinder neatly packed with a cylinder of soil with the same bulk density and structure as its in-situ state. The laboratory methods for the determination of water retention curves and unsaturated soil hydraulic conductivity are described in Section 2.4, below.

Soil leachate water quality, representing the quality of water that drains to groundwater was monitored by measuring concentrations of nitrate and total dissolved solids in water samples collected in lysimeters installed below the root zone at each monitoring station. Measurements of the volume of water collected in the lysimeters was also useful to provide some verification of the hydrological model's predictions of drainage flux quantities. All lysimeters tend to be problematic for the purpose of measuring net vertical water movement through the soil because the soil water tension at the base of the soil over the leachate collection pan is not the same as the soil water condition at the same depth outside the lysimeter. For this reason, the net vertical water flux will be assessed primarily with the LEACHM model, validated against either soil moisture content or moisture potential

measurements. Measurements of the volumes of leachate collected in the lysimeters is considered to be a secondary purpose of these lysimeters.

Capillary-wick pan-type lysimeters, constructed to a design described by Holder et al. (1991), were installed to collect leachate at a depth of 75 cm. This type of lysimeter was selected to avoid problems that alternative lysimeter types may experience in this application, as discussed in Chapter 1.

Capillary-wick pan-type lysimeters avoid these problems. The effect of the capillary wick is to create a tension at the base of the soil so that both saturated and unsaturated soil water flow is collected. The result is that this type of lysimeter has a much higher collection efficiency than 'zero-tension' types. This lysimeter type is limited to a fairly small surface area (typically a 30cm x 30cm square). Generally, collection efficiency is reduced as surface area of the lysimeter reduces (Jemison and Fox, 1992), however, the additional efficiency provided with the capillary wick make this type, on balance, a better choice. The relative ease of installation and low cost of the smaller lysimeter also enabled the use of two lysimeters in at an observation point to provide a more representative collection area.

2.3.4 Monitoring Site Arrangement

At each of the three primary study sites two duplicate primary monitoring stations were set up (Figure 2.9, page 33), including a tipping bucket rain gauge, a nest of three tensiometers, a Sentek soil moisture capacitance probe (Buss, 1993), and two capillary wick lysimeters. Additionally, two secondary monitoring stations were set up at each study site, each with only a nest of three tensiometers. At primary monitoring stations where it was not possible to install capillary wick lysimeters, suction cup lysimeters were installed instead.

At each study site, an in-line flow meter was used to monitor the total volume of water delivered through the irrigation system between visits. At the PGR study site the meter was installed in the irrigation spur line supplying the monitoed section of the crop. At the other study sites, pre-existing flow meters were used to monitor the volume of water delivered to the whole study site.

The installation of equipment at the three study sites progressed through the whole of August and September 2003. Due to some problems, site TR was only finally complete on the 9th October 2003. At all three study sites the primary monitoring equipment was installed prior to the commencement of irrigation of the Spring 2003 crop. Hence the whole of the summer irrigation season was monitored at all three study sites.

In total twelve capillary wick lysimeters (Figure 2.2) were constructed and eight of these were installed at monitoring locations at sites 1 and 2. The property owner at site 3 belatedly expressed concern about the trenches needed to install the lysimeters, so a decision was made to install suction cup samplers at that site instead of the lysimeters. Hence a total of eight capillary-wick lysimeters were installed: 2 at each of 2 monitoring locations at sites 1 and 2.

The lysimeters were installed in the side of trenches with the lysimeter collection plate installed at a depth of 75cm (Figure 2.3). In each case this was approximately 20cm below the top of the clay B-horizon soil that is expected to limit the downward flux of water in this soil profile due to its low hydraulic conductivity.

Fig 2.2. Capillary wick lysimeter

Figure 2.3 Lysimeter collection plate installation

Collection plates were jacked up against a level surface of undisturbed soil in a cavity carved into the side of the trench (Figure 2.4 (a)). Prior to back-filling the trench, plastic sheeting was placed on the side of the trench to ensure separation of the undisturbed soil above the collection plate from the disturbed soil inside the trench (Figure 2.4 (b)). The leachate collection container is installed at the base of the trench and joined to the collection plate by a rigid PVC pipe.

Figure 2.4 Installation of capillary wick lysimeters

Access tubes from the collection container to the soil surface allow leachate to be pumped out of the collection container after the trench is back-filled. Two lysimeters were installed at each location approximately 1 metre apart. Thus study sites 1 and 2 each have four lysimeters: two in close proximity at each monitoring point, with the two monitoring points being approximately 80 metres apart.

Sentek Enviroscan capacitance type soil moisture probes with sensors at depths of 10, 30, 50, 70, 110 and 150 cm were installed at sites 1 and 2 on the 28th August and at site 3 on the 19th September. For sites 1 and 3, these dates were just after the sowing of the crops at those sites. For site 2, this was about one week before the first irrigation of the almond trees for this growing season. Each site has a soil moisture probe at each of the two monitoring points. Both probes at each site are connected to a single controller and data logger via over-ground cables (Figure 2.5).

Figure 2.5 Soil moisture probes at study site TR.

Three tensiometers were installed at each monitoring point at depths of 30cm, 75cm and 110 cm. These are of a type that uses a separate gauge to measure the vacuum in the tensiometer and hence only allows intermittent measurement of soil water potential, with no data logging. A tipping bucket rain gauge with on-board data logger was installed at each monitoring point to record both irrigation and rainfall reaching the soil/crop.

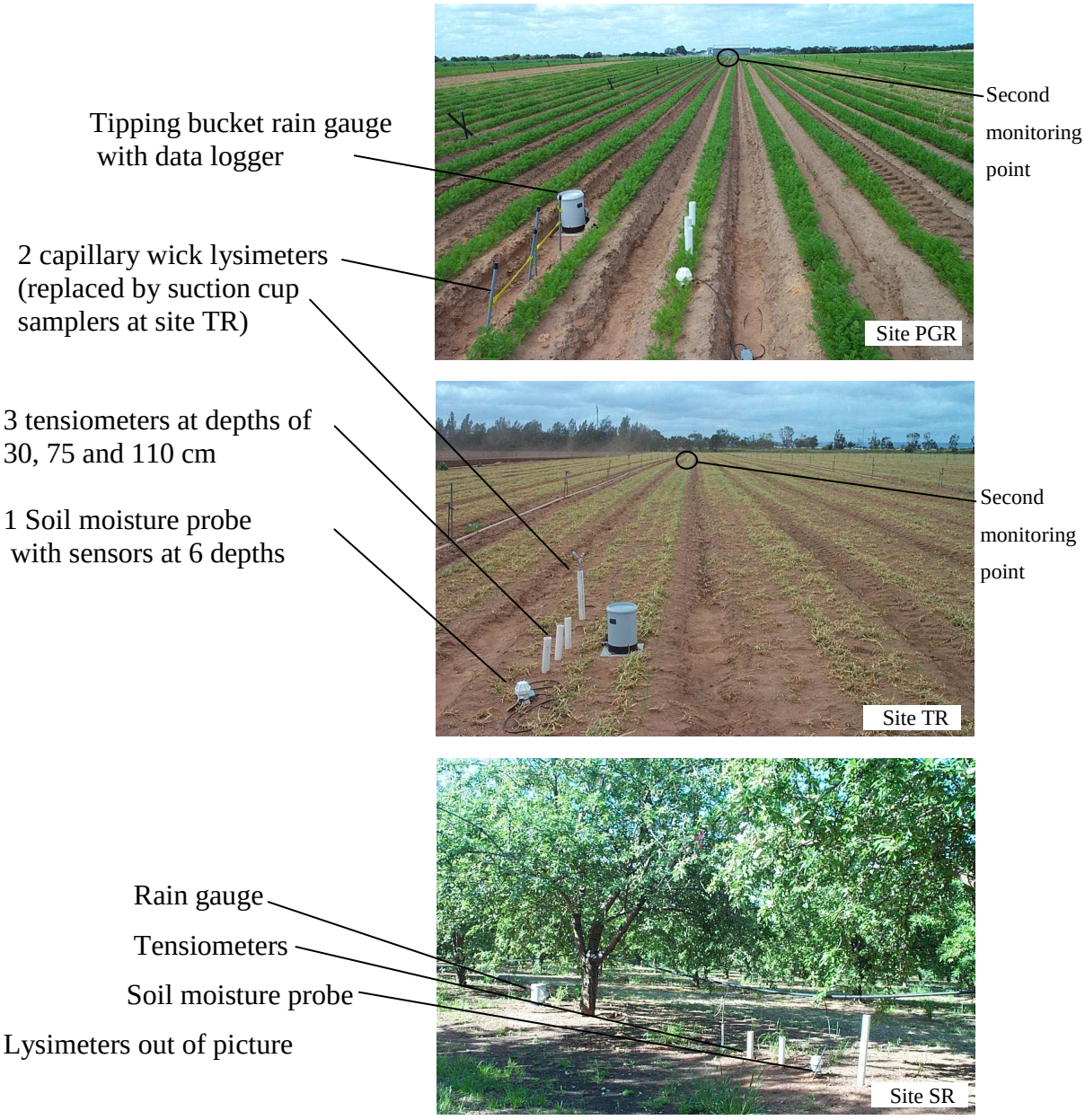

Figure 2.6 Monitoring point configuration at three study sites

The estimation of evapotranspiration requires monitoring of atmospheric parameters that affect evaporation as well as monitoring of crop cover fraction. A data-logging weather station (Figure 2.7) was installed at site PGR for the measurement of climatic parameters. A long delay in the procurement of the weather station meant that it was not installed until late November 2003. For the period of monitoring up to that point, climatic data was available from the BOM Edinburgh airfield weather station. The data from these two sources provided a comprehensive coverage of climate parameters during the period of monitoring.

Figure 2.7 Automatic weather station at study site PGR

Crop cover fraction at the broadacre vegetable sites was monitored by overlaying a grid of four 1-metre squares over the crop and photographing from above (eg. Figure 2.8). This is done periodically throughout the growth of the crop. The photographs are analysed to determine a percentage of crop cover at each photograph date. A uniform rate of growth is assumed between the cover percentages calculated at the date of each photograph. Although the photographs are taken at an oblique angle to the crop, they provide a good indication of the percentage of ground covered by the crop.

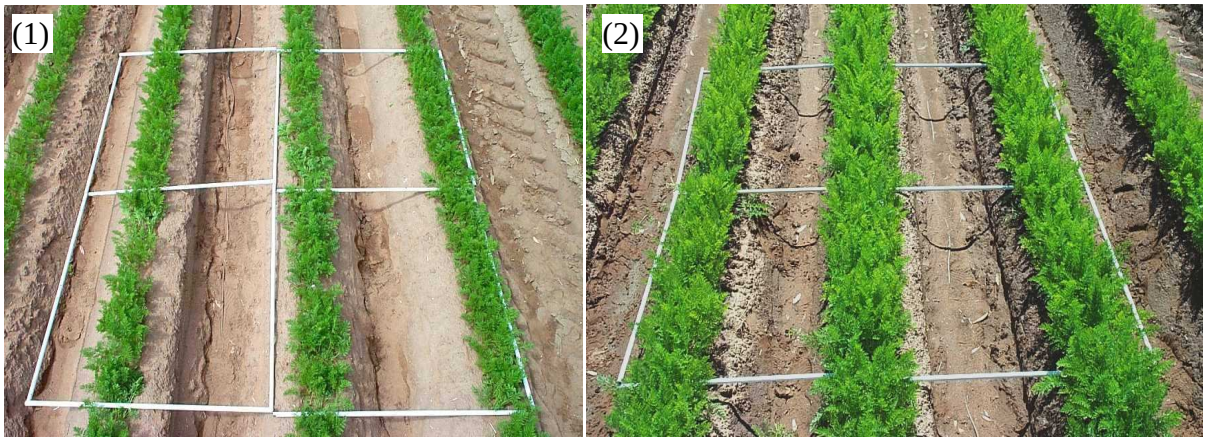

Figure 2.8 Crop cover photographs taken at site PGR; 20/10/03 (1) and 17/11/03 (2).

At the almond orchard site (site SR), it was only possible to make subjective assessments of crop cover fraction. During each site visit, estimates were made of both the coverage of tree canopies as well as grass growth between rows of trees.

Water table depth was monitored using an existing network of piezometers installed by the Department of Water Land and Biodiversity Conservation (DWLBC), as well as individual shallow piezometers installed at each study site. On-site peizometers were installed to between 2.2 – 2.8 metres depth.

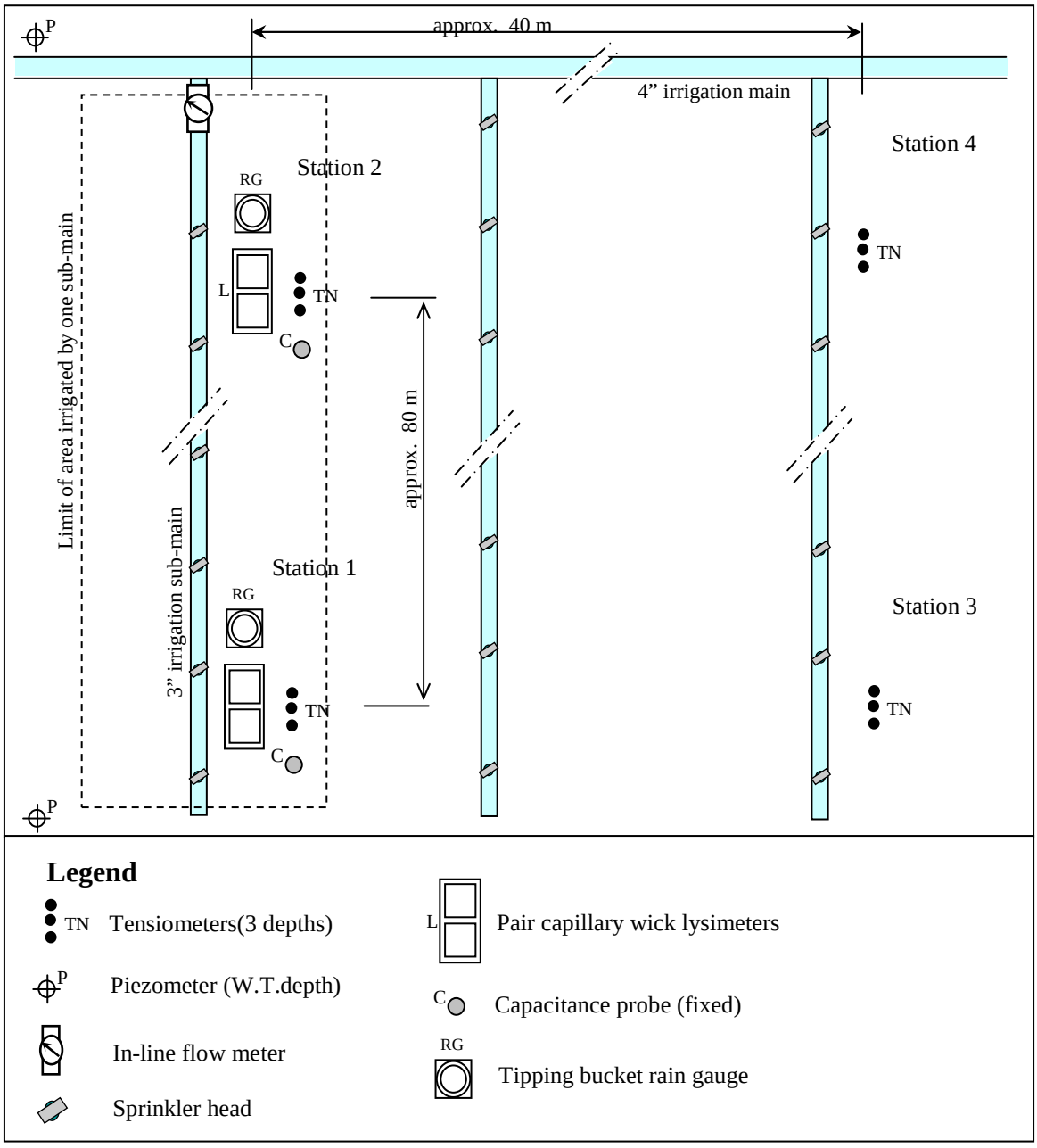

Figure 2.9 Site layout at study site PGR

The diagram in Figure 2.10 is a conceptual arrangement of equipment installed in one primary monitoring station. Actual monitoring station arrangements were altered only as necessary, according to field conditions at each study site.

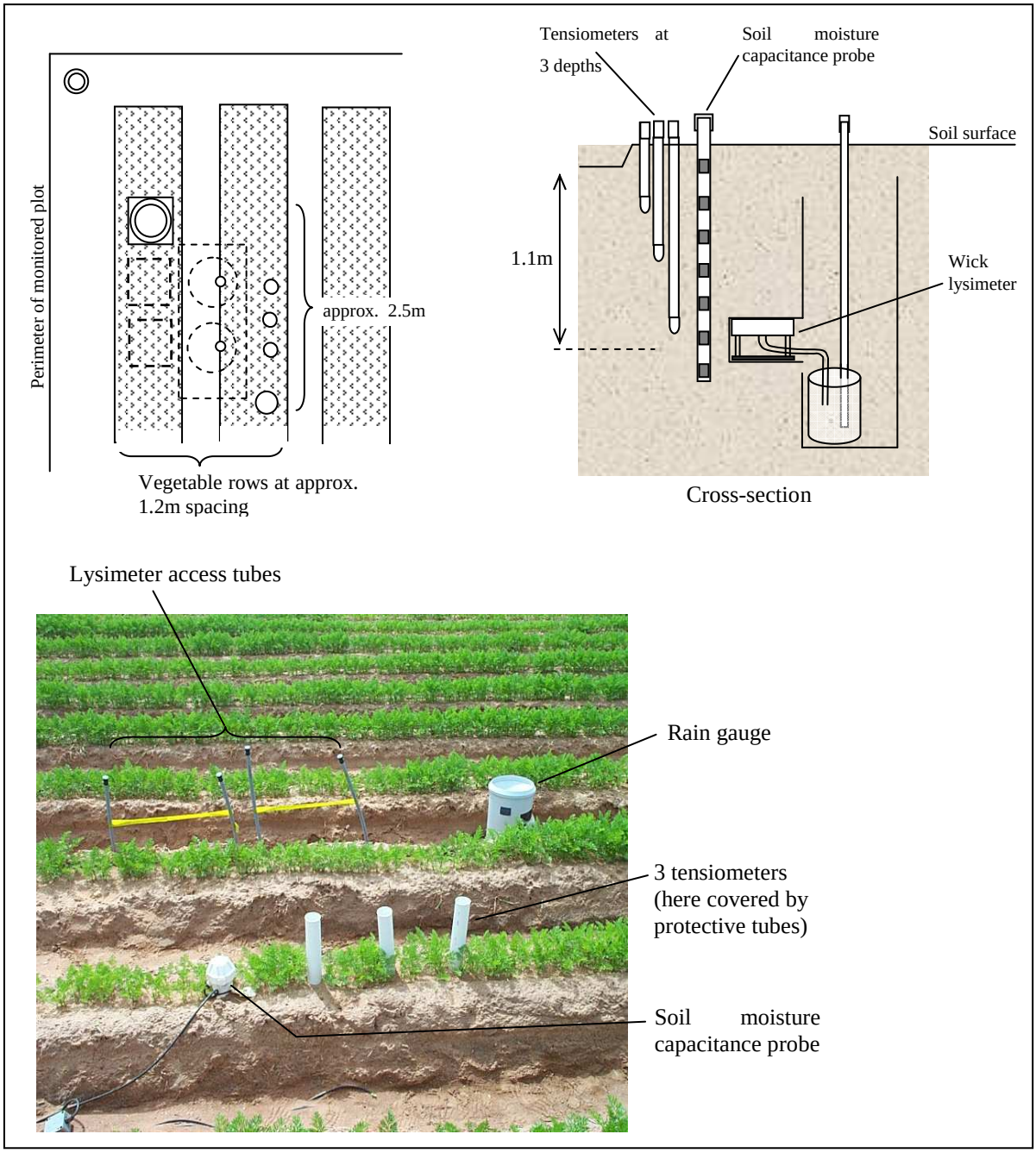

Figure 2.10 Monitoring station arrangement at broadacre vegetable site PGR.

Figure 2.11 shows how the layout of monitoring stations in the one tree crop site (Figure 2.12) differed from that of the broadacre vegetable sites.

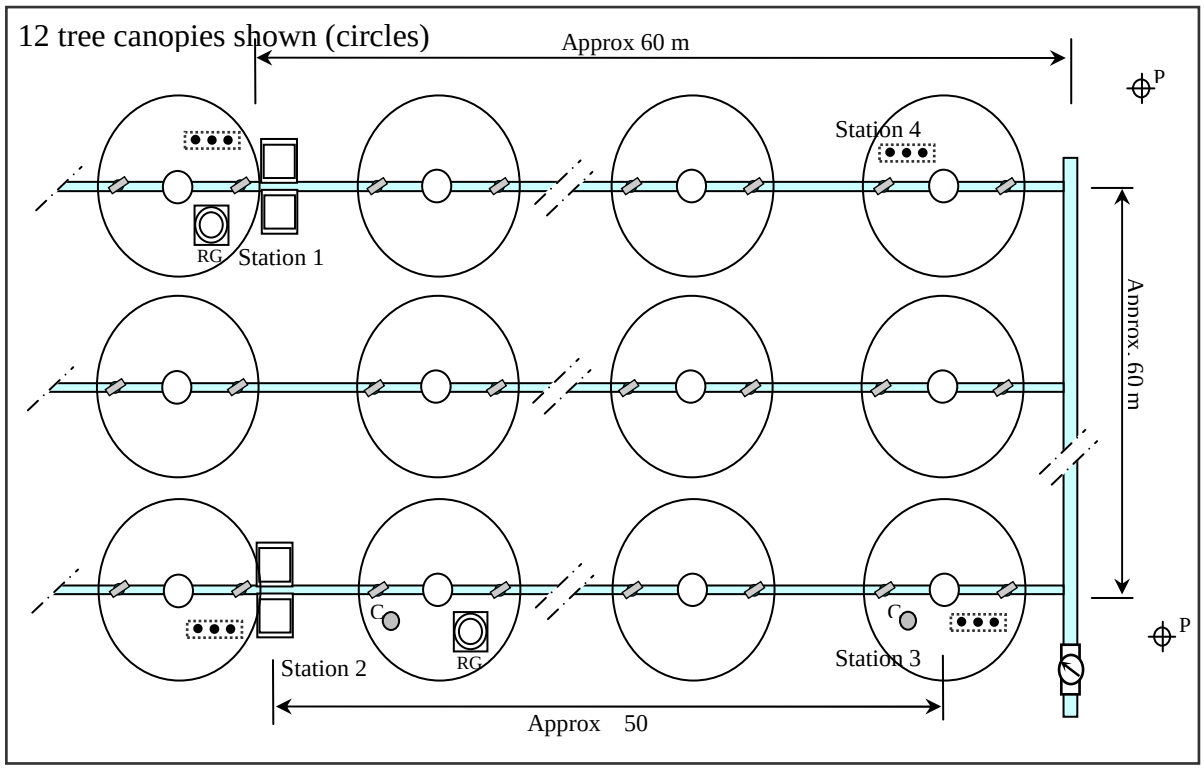

Figure 2.11 Study site layout for almond orchard site (study site SR). Note, circles in this diagram represent tree canopies. Only 12 trees are shown, out of a total of approximately 1200 trees in the orchard.

Figure 2.12 Monitoring station 2 at the SR study site. The area of coverage of the micro sprinklers necessitated spreading monitoring equipment between canopies of two trees.

2.4. Laboratory Methods

2.4.1 Water retention curves and unsaturated hydraulic conductivity

Soil core cylinders for each soil depth sampled were loaded into Tempe pressure cells (Soil Moisture Equipment Corporation stock code 1400B1M3-3) to measure soil hydrologic characteristics including saturated water content (θs), bulk density (ρ), unsaturated hydraulic conductivity at ψ = -10 kPa ($K_{(-10)}$). For each soil sample, several values of water content (θ) and corresponding matric potential (ψ) were measured in order to construct water retention curves. Measurements of water loss were taken at ψ values of 0, -4, -8, -16, -30, -60 and -100 KPa and converted to volumetric water contents. Water retention curves were constructed from measurements from each soil core sample. Campbell's (1974) water retention function (Equation 2.1) was then fitted to the measured water retention curves to determine Campbell's equation parameter values 'a' and 'b' for each soil sample.

$$\psi = a(\theta/\theta_s)^{-b} \qquad \text{(Equation 2.1)}$$

Where 'a' is the air entry water potential, and 'b' is an empirically determined constant.

Unsaturated hydraulic conductivity was measured in the same soil core samples at a matric potential of -10 kPa using the outflow method of Klute (1965). The matric potential of -10 kPa was chosen because it is similar to that in the monitored field study site soil profiles for the majority of the period monitored.

The Klute method is based on measurements of the volume of water outflowing from a soil sample in a pressure cell (here the Tempe cell) as a function of time (Figure 2.13). The measurements are made over the time taken for the soil sample to equilibrate to a small change in pressure. To achieve this, negative matric potentials were applied by means of a 'hanging' column of water, with a 100 cm hanging column applying a matric potential to the sample of approximately -10 KPa. The required pressure change was applied by changing the hanging column length from 90 cm to 110 cm. The method requires that it be assumed that the conductivity K(θ) and the water retention function dθ/d*t* is constant within the range of water content change that occurs through this change in pressure. The change in pressure causes water to flow from the soil sample into the outflow tube and graduated pipette until the matric potential within the soil has equilibrated with the negative pressure in the outflow tube. After the change in pressure is applied, the volumetric outflow rate during re-equilibration is measured, firstly at 1-minute time

intervals, then at longer intervals after the first ten minutes as the rate of outflow slows in response to the reducing difference in pressure between soil and outflow tube. The volumetric outflow rate is measured from the movement of the end of the water column along the graduated pipette.

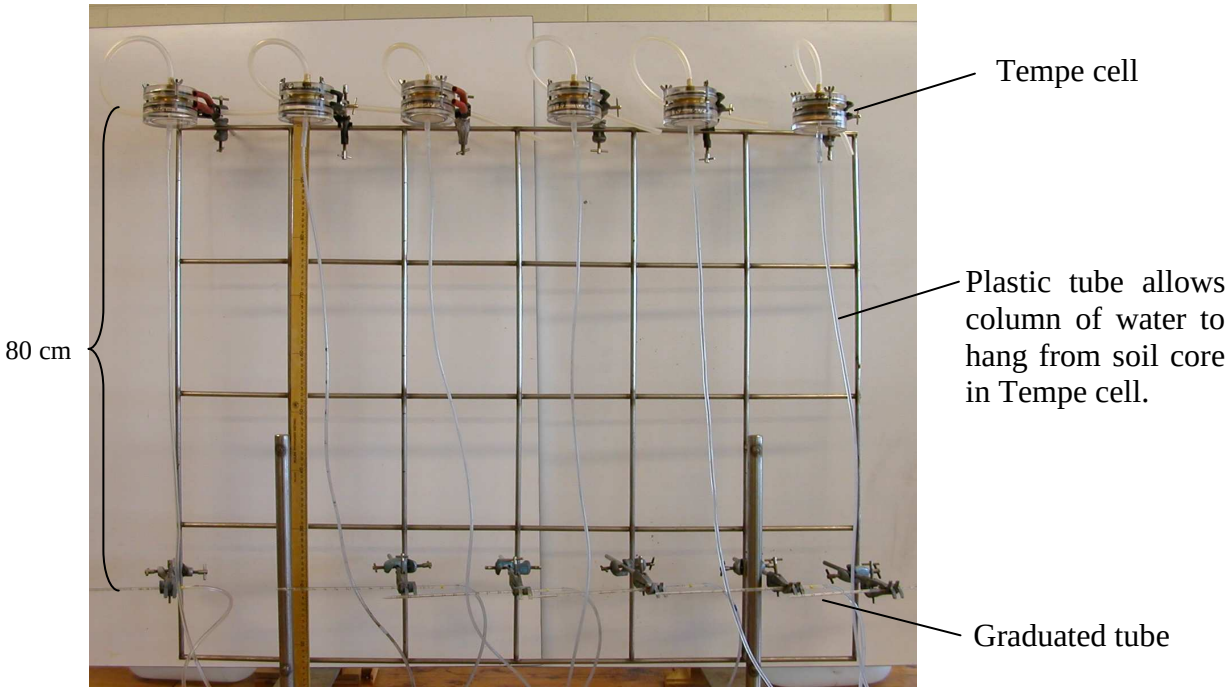

Figure 2.13 Rack of six Tempe cells with hanging tubes allowing water to drain from soil sample cores, here to an equilibrium water potential of -80 cm.

From the volumetric outflow data, the quantity $1 - Q(t)/Q(\infty)$ is calculated, where $Q(\infty)$ is the total volume of outflow required to reach equilibrium. These are then used to construct a plot of $\log [1 - Q(t)/Q(\infty)]$ versus $\log t$. This is overlain on a theoretical plot of the quantities $\log [1-Q(t)/Q(\infty)]$ versus $\log (Dt/4L^2)$. The two plotted curves are brought into coincidence by moving the experimental curve along the $\log (Dt/4L^2)$ axis only. A convenient value of $Dt/4L^2$ is selected and from the theoretical curve and and the corresponding value of t from the theoretical is noted. If the chosen value of $Dt/4L^2$ is represented as w, then the diffusivity, D, is given by

$$\boldsymbol{D = w4L^2/t.} \qquad \text{(Equation 2.2)}$$

Where t is the experimental value of time corresponding to the chosen value of w.

The specific water capacity, C, of the sample is given by

$$\boldsymbol{C = Q(\infty) / V \Delta h.} \qquad \text{(Equation 2.3)}$$

Where V is the volume of the sample.

The mean conductivity within the soil matric pressure increment over which the outflow rate was measured is then given by

$$\mathbf{K = DC} \qquad \text{(Equation 2.4)}$$

(Klute, 1965).

LEACHM uses Campbell's conductivity equation to define hydraulic conductivity at varying states of saturation:

$$K(\theta) = Ks(\theta/\theta s)^{2b+2+p} \qquad \text{(Equation 2.5)}$$

Where 'Ks' is hydraulic conductivity at saturation, 'p' is a pore interaction parameter, often set to 1, and 'b' is the constant determined empirically for the water retention function. Conductivity derived according to this function changes markedly as the soil nears saturation. Hence, if saturated conductivity (Ks) is used to position the K(θ) curve, any inaccuracy in the curve shape can result in significant errors in the derived K(θ) values within the range of θ in which the soil is most commonly found. LEACHM allows the input of a known conductivity value at a stated matric potential value with which to position the K(θ) curve. By using unsaturated conductivity at a matric potential of -10 kPa, the conductivity curve has a known reference point that is close to the state of saturation at which the soil was maintained by irrigation.

2.4.2 Soil water and irrigation water chemistry

Samples of soil solution extract, lysimeter leachate and irrigation water were analysed for major ion concentrations at the Analytical Services Laboratory of CSIRO Land and Water. Major cation analysis was conducted by Inductively Coupled Plasma Emission Spectrometry (ICP-ES). Concentrations of Cl^-, and SO_4^{2-} were analysed by Ion Chromatography (IC). The soil samples were also analysed for exchangeable cation concentrations and their cation exchange capacity (CEC).

Loose soil samples taken at depths of 10, 30 and 50 cm at each of the pimary monitoring points. Solution extracts were prepared from these samples using 5:1 mass ratio of soil to water. Oven-dried soil samples of 20 g mass were shaken end-over-end for 1 hour with 100 ml of de-ionised water, then left to settle for 2 hours, and the supernatant poured off, filtered and sealed in plastic containers.

Lysimeter leachate samples for major ion analysis were taken shortly after the commencement of irrigation. Although these samples were intended to indicate the starting soil chamistry at the start of the study period, no water collected in the lysimeters until irrigation had commenced. Irrigation water samples were taken directly from the irrigation pipes at the study sites during irrigation events.

The data from these analyses provided starting soil solution concentrations used as input data for the chemical equilibrium program Chemeq. The Chemeq program was applied to determine firstly the Gapon selectivity coefficients for the the exchange / solution phase equilibrium, and then soil solution equilibrium concentrations at the starting soil moisture contents at ascribed to the sampled depths in the LEACHM soil chemistry data input file. This was carried out according to the following procedure.

Measured concentrations of exhangeable cations were converted to the equivalent concentration if all exchange cations from 20g of soil is dissolved in 100 ml water.

Exchangeable cation concentrations were added to measured 1:5 solution extract cation concentrations to provide total extractable cations in a 1:5 soil:water mixture.

A composition of anions to balance the charges of the measured cation composition was calculated. Sulphur concentrations measured in solution extracts were assumed to be all in the form of SO_4^{2-}, such that the sulphate anion charge concentration (2 x [S]) provides part of charge balance of cations in solution. The remainder of the ion charge balance was assumed to be from Cl^- after pH was accounted for.

An input data file for the Chemeq program was prepared, containing total extractable cation concentrations and balancing anions for 1:5 soil: water mixtures. Soil bulk density stated in the data file was according to lab measurements of corresponding soil samples. Nominal fractions of gypsum and calcite in the soil are stated according to the presence of these in the soil samples. For example, gypsum ($CaSO_4$) was included if dissolved ions show high concentrations of Ca and SO_4^{2-}. A fraction of calcite was included if calcite fragments were observed in the soil profile at the sample depth. Data files for nearly all soil samples incorporate a fraction of calcium.

Output options in the Chemeq data file were set to output solution and exchange concentrations at 1:5 soil water ratio (same ratio as the input concentrations) and for the soil at saturation water content. Soil saturated water content was as measured on corresponding soil samples in the laboratory.

Nominal starting values were used for Gapon selectivity coefficients. Then, after running the Chemeq program, the exchangeable cation concentrations in the output file were compared with measured exchange cation concentrations in the corresponding soil sample. Selectivity coefficients were adjusted and Chemeq was re-run. This was repeated until the exchange concentrations in the Chemeq output file match the measured exchangeable ion concentrations. When a close match was achieved between modelled and measured exchange cation concentrations, the selectivity coefficients used to achieve the matching results were fixed and recorded.

The data file was adjusted to allow output at 1:5 soil:water ratio and at a water content corresponding to a soil matric potential of -5 kPa. Chemeq is re-run and the exchange cation concentrations and solution phase cation and anion concentrations are recorded for use as initial soil chemistry values in the LEACHM input data files.

CHAPTER 3: RESULTS OF FIELD AND LABORATORY WORK

The results of field and laboratory experiments are discussed and presented in this chapter together with a brief analysis of the data collected from these. The major use of these data will be as input and calibration data for the soil water and salt transport models, the outputs of which represent the major components of this study and are analysed separately in later chapters.

3.1 Results from Field Monitoring Program

The results of the field monitoring program are presented here in graphs of the variation of each monitored variable with time. The results from each study site grouped together, enabling cross-comparison of variables such as lysimeter leachate volume with soil matric potential, such that the variation in time of different variables can be easily compared.

The data are arranged as sets of graphs, with one set for the duration of each crop monitored, as these are the durations over which they have been used in the modelling exercises described in later chapters. The data displayed in this section are the rain and irrigation record, the crop cover percentage, the soil matric potential at three depths, the lysimeter leachate EC and volume and, where used, the EC of suction cup soil solution samples.

The rainfall and irrigation data are as recorded by the tipping-bucket rain gauges and are shown in column charts. The columns represent daily totals of rainfall plus irrigation as the rain gauge provides no distinction between rain and irrigation events.

Results are only provided in this section for the field study sites for which models have been developed in the following chapters, and for the period in time during which model calibration and input data were collected. Further data were collected beyond this period and at study sites that ultimately models were not developed for. These data are not reproduced in this document but are archived at Flinders University.

Although soil moisture capacitance probes were employed at three of the field study sites, the data collected from these was found to be less useful than soil matric potential data for model calibration or verification. Consequently these data are not presented here and are not further discussed in this report.

3.1.1 Port Gawler Road (PGR) study site

A) PGR Crop 1

The first crop monitored at the Port Gawler Road study site, PGR Crop 1, was a carrot crop sown in spring and harvested in mid January. The majority of the water recorded by the rain gauge (Figure 3.1a) is due to irrigation events. It can be seen that the grower at this study site typically applied between 10 mm and 25 mm in an irrigation event. Irrigation commenced on 1/9/2003 and the last irrigation of this crop was on 15/1/2004.

The crop cover percentage of PGR Crop 1 (Figure 3.1b) grew at a fairly linear rate and peaked at approximately 65% in mid January.

The soil matric potential at 30 cm depth was maintained at a high level, greater than -10 kPa, for the duration of this crop. Matric potential at 75 cm depth drops below that at 30 cm and 110 cm as the cover percentage of the carrot crop increases. This is probably due to the roots of carrots taking up water from this depth. Water is also taken up at 30 cm depth, however irrigation water infiltrates more rapidly to that depth and maintains a higher soil moisture content.

Results are shown for lysimeters at monitoring point PGR1. The lysimeters at point PGR2 did not collect any measurable quantities of leachate, probably because of malfunctions due to difficulties with installation. Lysimeters at study site PGR1 did not collect any measurable quantities of water between 20/11/2003 and the end of the first crop growth period.

Prior to 20/11/2003, lysimeter leachate increased in salinity from the start of the crop cycle and seemed to stabilise after about two months into the 4.5 month life of the crop. Leachate volumes collected were generally low. The leachate volume in litres divided by the area of the lysimeter collection plate (0.09 m^2) provides the millimetres of drainage flux at the collection plate. Thus, the 140 mm of leachate collected on 11/9/03 represents approximately 1.6 mm of drainage flux.

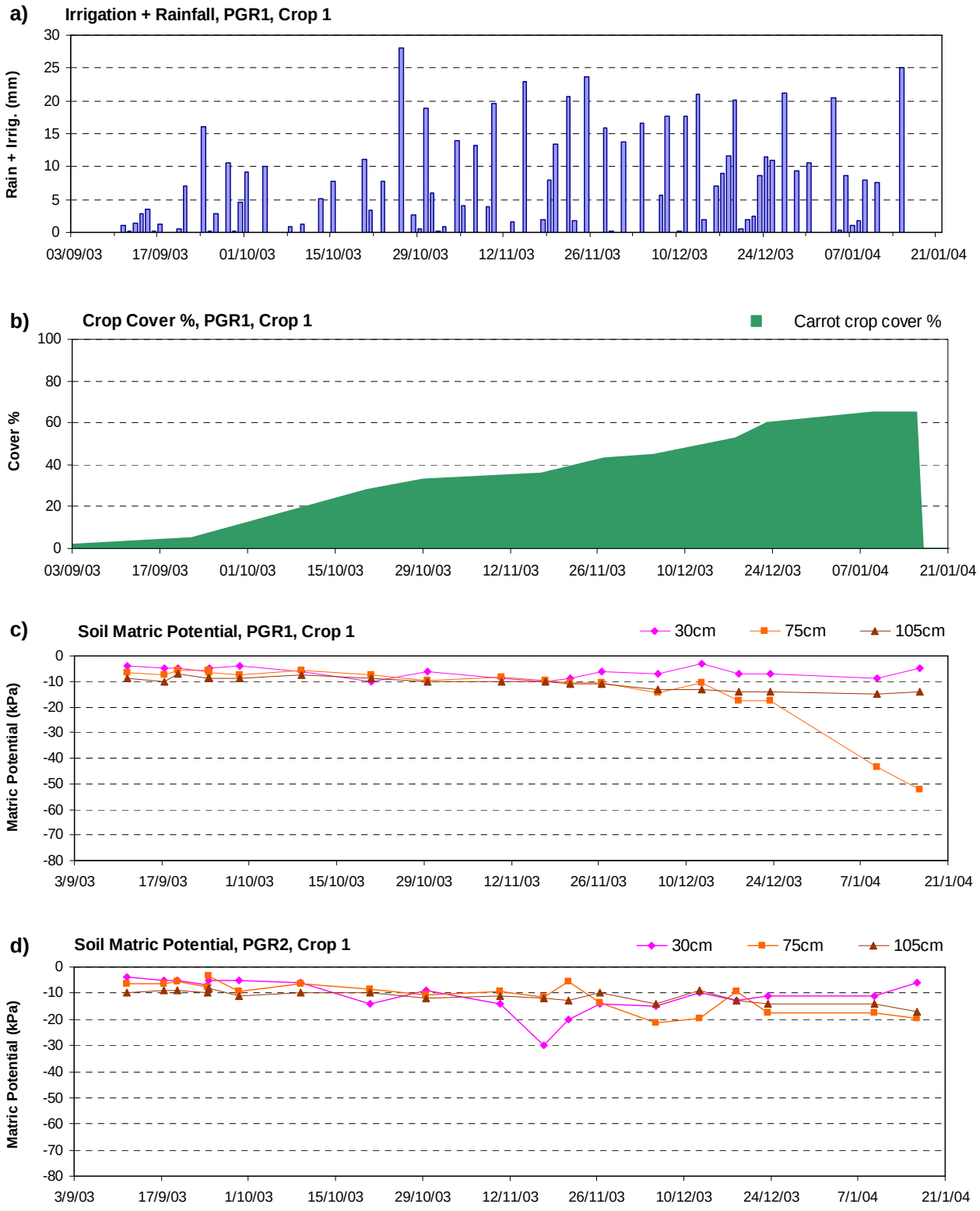

Figure 3.1 Field study data from PGR Crop 1: a) pluviometer record of rain and irrigation, b) crop cover fraction, c) soil matric potentials at point PGR1, and d) soil matric potentials at point PGR2.

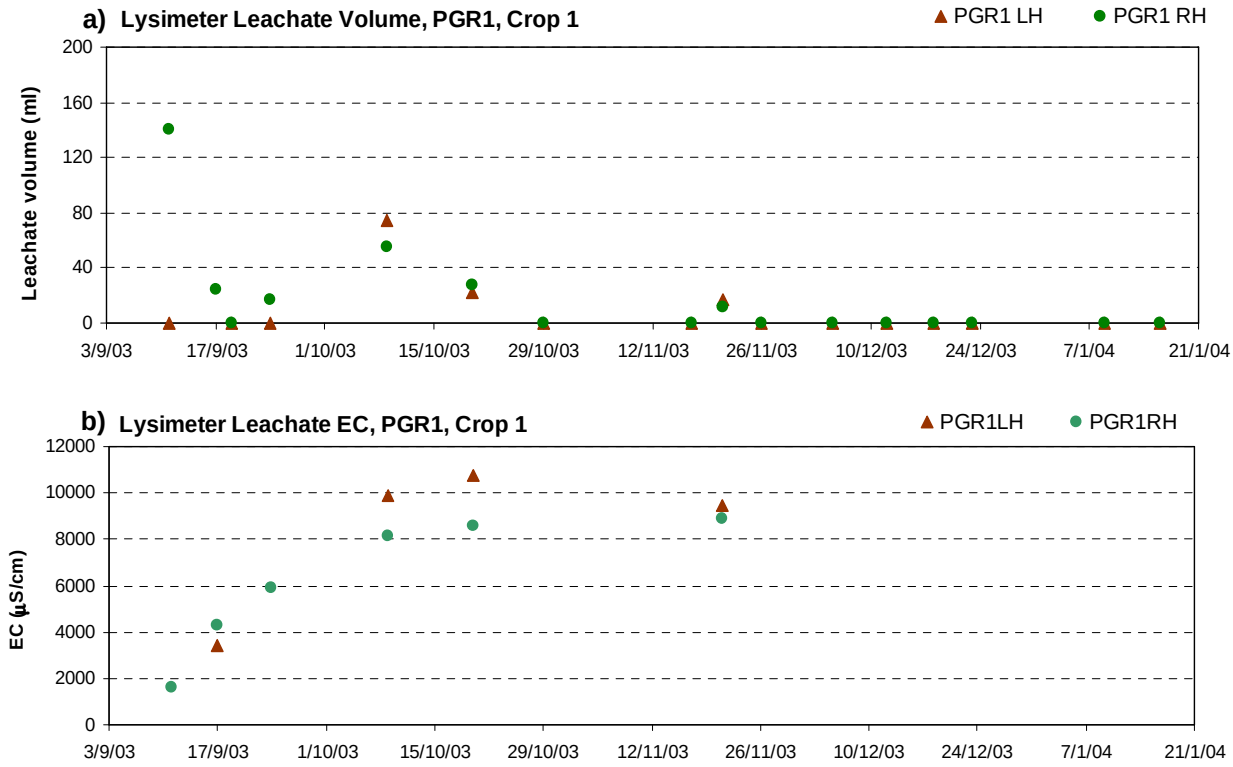

Figure 3.2 Results from lysimeter at point PGR1 during PGR Crop 1: a) leachate volume and b) leachate EC.

B) PGR Crop 2

The second crop monitored at the PGR study site, PGR Crop 2, was a potato crop sown on 27/2/04 grown through the winter, and harvested at the start on 04/09/04.

The first and last irrigation events for PGR Crop 2 (Figure 3.3a) were on 4/3/04 and 25/5/04. Events in the rain and irrigation record after 25/5/04 are rainfall events only. The crop cover (Figure 3.3b) peaked at approximately 70% between late April and mid May in 2004, after which the leaf cover was then allowed to senesce. In mid July the emergence of weeds among the crop resulted in leaf cover that grew to exceed the cover of the senescent potato crop. The crop was harvested on 4/9/2004 and the weed cover removed at the same time.

The soil matric potential throughout the whole depth monitored (110 cm) was maintained at a high potential of less than -10 kPa, for the duration of the crop. A data logger was applied to the tensiometers approximately half way through the crop growth cycle. This was intended to determine whether the reading of tensiometers at weekly intervals was masking shorter-term variations in soil matric potential that would be significant when using the tensiometer data to calibrate numerical models. The results show that there were daily fluctuations in the matric potential but that these were less significant than the longer term changes. It was ascertained from these results that, for calibration purposes, the weekly tensiometer readings provided a sufficiently representative indication of the general trends in matric potential over the timescale of a crop cycle.

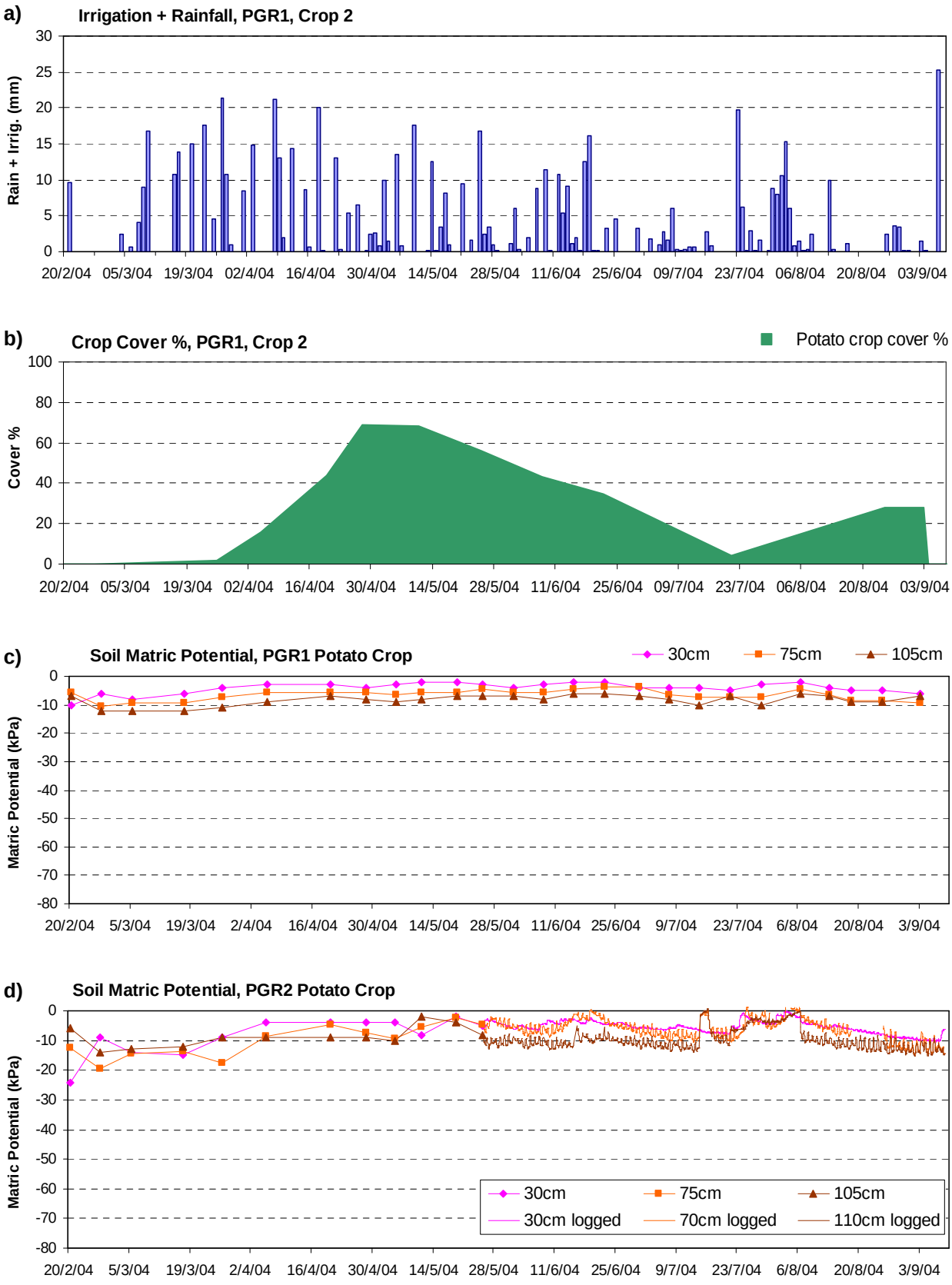

Figure 3.3 Field study data from PGR Crop 2: a) pluviometer record of rain and irrigation, b) crop cover fraction, c) soil matric potentials at point PGR1, and d) soil matric potentials at point PGR2.

Approximately half way through the second crop cycle two additional matric potential monitoring points were installed at points PGR3 and PGR4. These were intended to determine whether the matric potentials measured at the two primary monitoring points were representative of the whole plot. The results (Figure 3.4) show that from the end of May to late August the soil to a depth of 105 cm retained a high matric potential of greater than -10 kPa throughout this depth range, which was similar to that observed at the two primary observation points.

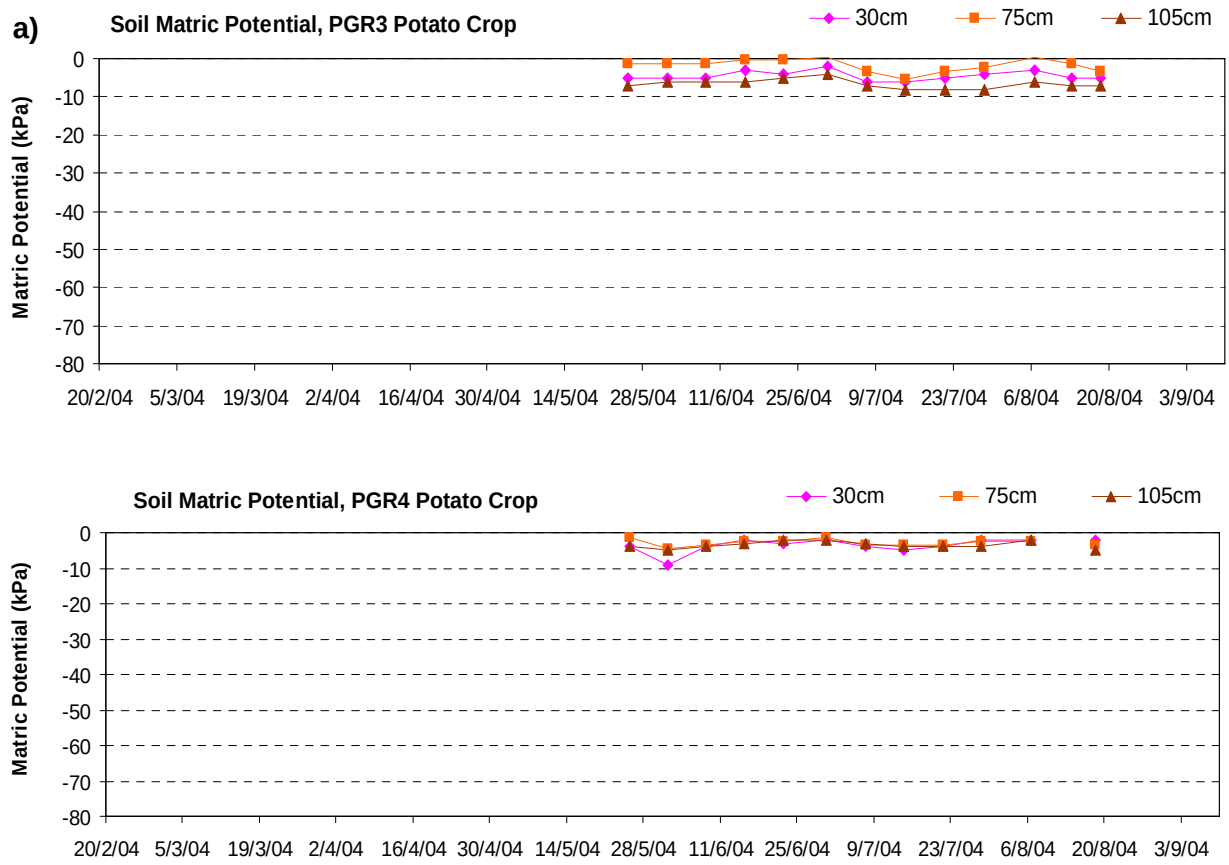

Figure 3.4 Soil matric potentials measured at additional monitoring points for approximately half the duration of PGR Crop 2: a) point PGR3 and b) point PGR4

The PGR1 lysimeters during the term of the second crop (Figure 3.5) collected measurable quantities of leachate between mid April and mid August 2004. Between February and mid April there was no flux of leachate into the lysimeters, even though this was the period of heaviest irrigation of the crop. Soil matric potential measurements through this period (Figure 3.3 c and d, page 46) show that prior to mid April potentials at the depth of the lysimeters (75 cm) were lower than –5 kPa. Water is not expected to leach into the lysimeters at potentials lower than this. After mid August, the matric potential record showed that potentials at 75 cm depth again fell to below –5 kPa and, once again the flux of

leachate into the lysimeters ceased. There was frequently a difference in the volume of leachate captured by the two lysimeters at point PGR1, showing either that there is variability in the drainage flux between these two points, which are only 1.5 m apart, or that one lysimeter is more efficient than the other. Through the period of PGR Crop 2, lysimeter PGR1 LH captured 441 ml of leachate while lysimeter PGR1 RH captured only 291 ml. There were however similar values and similar trends between the EC values of leachate yielded from the two PGR1 lysimeters (Figure 3.5b) through the period of PGR Crop 2

Again, the lysimeters at PGR 2 did not collect any measurable quantities of leachate through the period of this crop despite the high soil moisture content, confirming that the PGR2 lysimeters were not functioning.

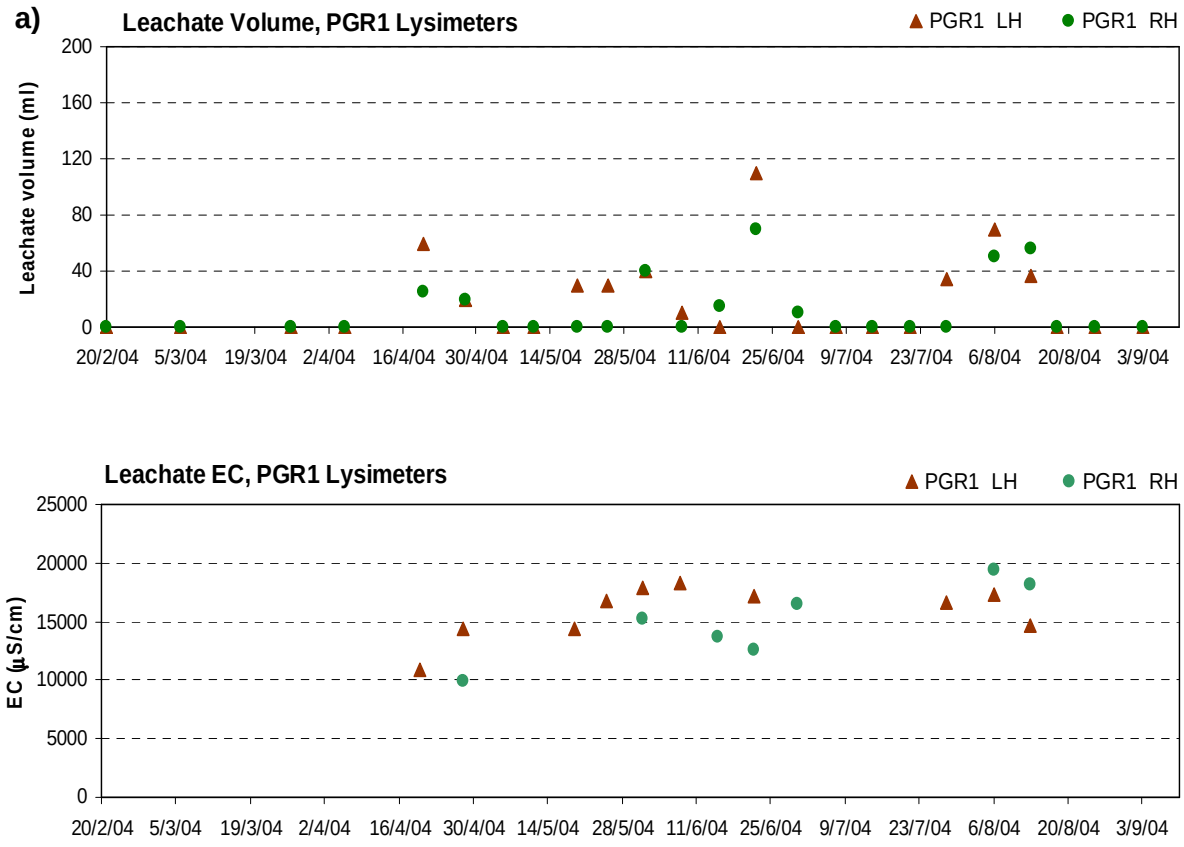

Figure 3.5 Results from lysimeter at point PGR1 during PGR Crop 2: a) leachate volume and b) leachate EC

Suction cup soil solution samplers were installed at points PGR1 and PGR2 in April 2004, when it was determined that the capillary wick lysimeters would not collect sufficient leachate to provide a regular indication of soil solution salinity. These were reliable in providing a sample of soil solution while irrigated crops were in place and through the winter

of 2004. However, after September 2004 when an unirrigated cover crop was in place, the soil moisture content was too low for the suction cups to extract a measurable amount of soil solution. Comparison of the soil solution salinity (Figure 3.6) shows that soil salinity at the two primary monitoring sites did not vary in concert with each other, suggesting that soil water flow at these two sites may have differed significantly, causing differences in the times of solute deposition and removal.

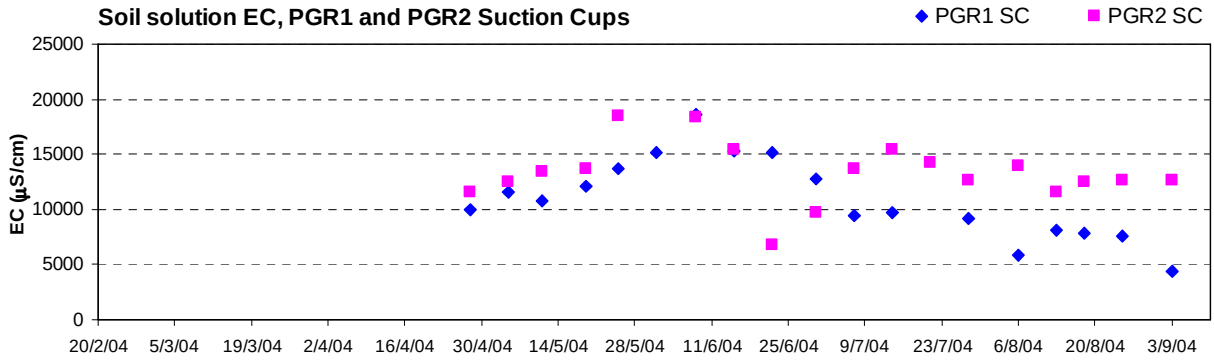

Figure 3.6 EC values of soil solution captured by suction cup soil solution samplers at points PGR1 and PGR2 during the period of PGR Crop 2.

Water table depth at the PGR study site were measured in two piezometers installed at opposite ends of the monitored plot. These were installed later than the other instruments at the site and, hence, water table depth measurements only commenced at the end of June 2004. However, as the results in Figure 3.7 show, the water table depth variations at this site are small. Between the two piezometers, separated by a distance of about 120 m, there was a difference of approximately 0.2 m in water table depth. Over eight months of monitoring, the depth to water at each of the peizometers varied by less than 0.2 m.

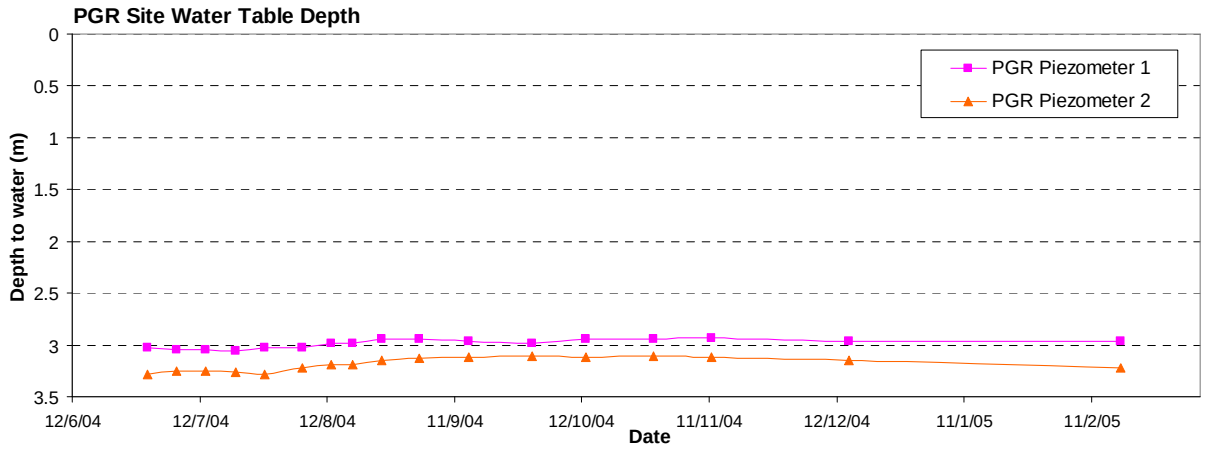

Figure 3.7 Water table depths in two piezometers installed at the PGR study site

3.1.2 Huxtable Road (HX) study site

Only one crop was monitored at the Huxtable Road study site (HX site). This was a winter crop of carrots was sown on 25/4/04 and harvested on 20/9/04.

The majority of the water recorded by the rain gauge at HX1 (Figure 3.8a) is due to rain events. The first and last irrigation events for the HX Crop were on 3/5/04 and 23/8/04, the last being an application of 15 mm. Events in the rain and irrigation record after 23/8/04 are rainfall events only. The irrigator at this study site typically applied between 6 mm and 16 mm in an irrigation event. The crop received a total of 125 mm of irrigation and 305 mm of rain during this period.

The carrot crop at the HX site was planted in closely spaced rows such that the crop cover percentage at the peak of leaf development was approximately 90% (Figure 3.8b).

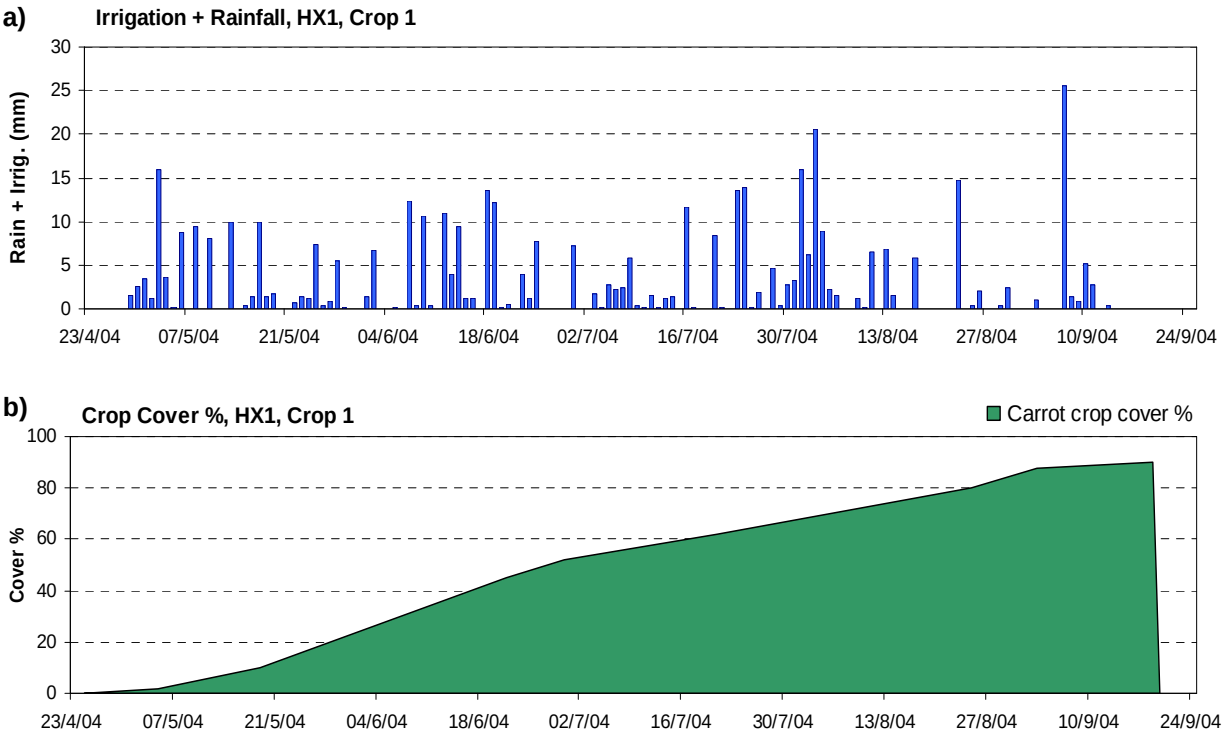

Figure 3.8 Field study data from study site HX carrot crop: a) pluviometer record of rain and irrigation and b) crop cover fraction

The large total irrigation and rainfall received by this crop over the five month period maintained high soil moisture potentials (Figures 3.9a-d), which were frequently at or close to saturation. The periods of soil profile saturation were confirmed by observations of water pooled on the soil surface on two occasions. Even when surface water was not apparent, the

soil could be seen to have a very high water content, close to saturation through the majority of the period of this crop.

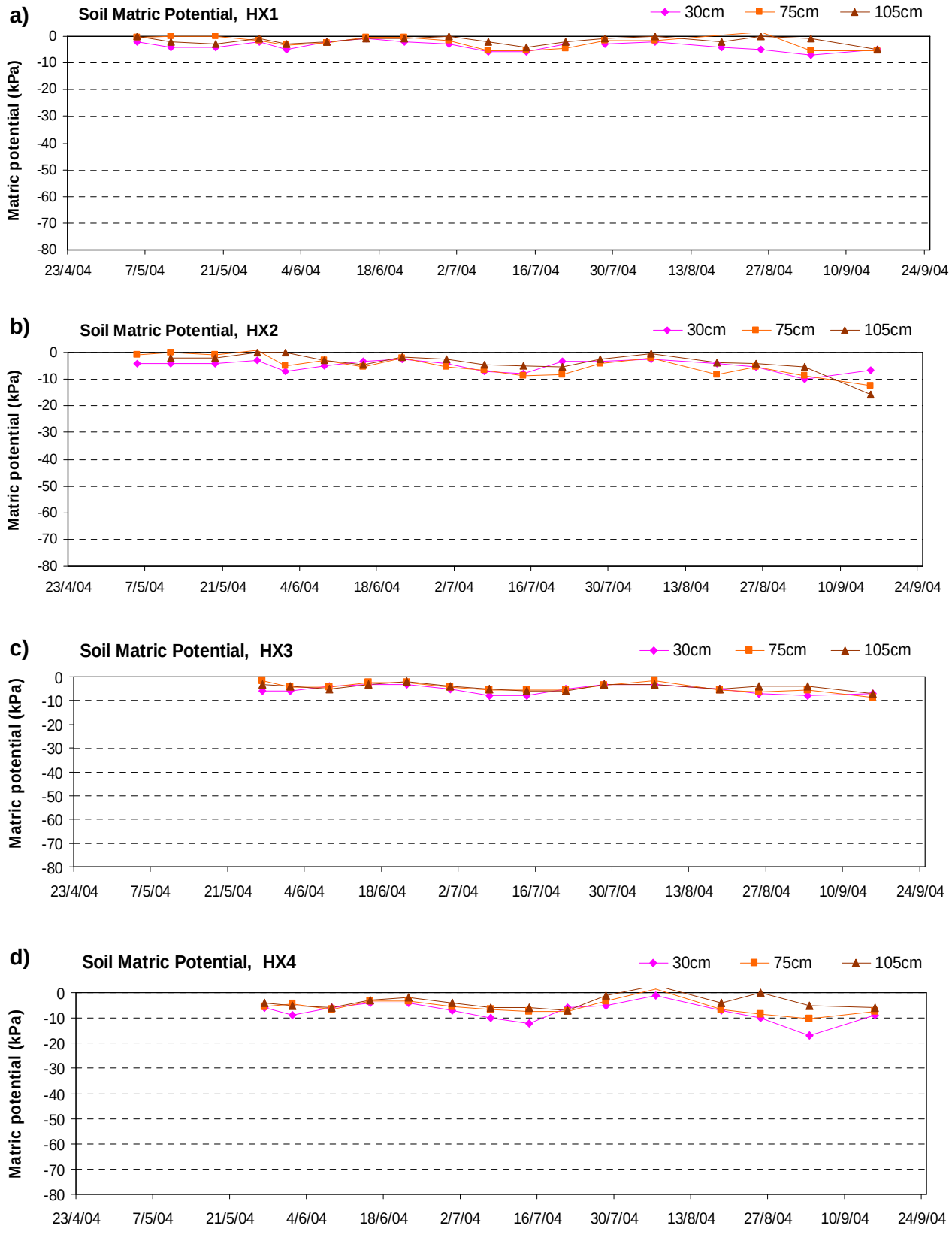

Figure 3.9 Soil matric potentials measured at four monitoring points at study site HX

Soil matric potential monitoring points were also installed at two additional location, HX 3 and HX4, within this crop to ascertain the degree of spatial variability. The results show that potentials were maintained between 0 and –10 kPa at all four points with a few short-term deviations below –10 kPa in the 30 cm at HX4. These results were taken to indicate a sufficient uniformity of soil matric potential to assume soil moisture conditions at each monitored point are representative of the whole plot.

Unfortunately no lysimeters were installed at study site HX as this was a substitute site that was only equipped for monitoring just before the crop was planted, thus not allowing time to install lysimeters. Suction cup soil solution samplers were installed to allow collection of soil solution samples from a depth of 75 cm. The EC of the soil solution captured (Figure 3.10) occupied a fairly high EC range, between 5000 and 12000 µS/cm. While there was a difference between the EC of soil solution between the two sites for the majority of the period monitored, the two monitoring point were seen to follow very similar variations. After the end of July, the EC of the two points became very similar. This was possibly due to the high rate of water flux through the soil at these high water contents having flushed prior concentrations of solutes past the 75 cm depth of the suction cups by that time and that the solute content of water at that depth thereafter was dictated by the salinity of the irrigation water and the concentration of solutes by evapotranspiration, which was effectively the same at both monitoring points.

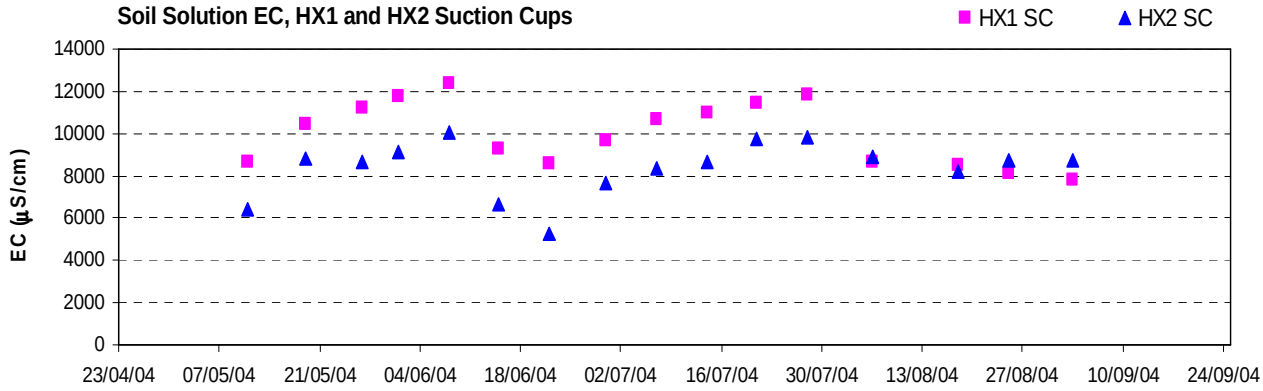

Figure 3.10 EC values of soil solution captured by suction cup soil solution samplers at points HX1 and HX2

3.1.3 Thompson Road (TR) study site

A single crop was monitored at the Thompson Road study site (TR site). This was a summer crop of onions was sown on 20/10/03 and harvested on 24/2/04. However, this was preceded by a cover crop of barley, sown on 10/9/03 and then killed off with herbicide spray in mid October just prior to the sowing of the onion crop. Hence there was an overlapping period of crop cover and there was no tilling of the soil or alteration of irrigation lines between the two crops. These are treated in this study as a single crop cycle. The leaf cover percentage of the barley cover crop (Figure 3.11a) peaked at around 50% just a few days before the onion crop was sown. The leaf cover percentage of the onion crop then peaked at about 75% in early February 2004. The leaf cover was allowed to senesce for about three weeks, reducing to approximately 50%, prior to harvesting on 24/2/04.

This being a summer crop, the majority of the water recorded by the rain gauge at TR1 (Figure 3.11b) is due to irrigation events. The first and last irrigation events for the TR Crop 1 (barley / onion crop combination) were on 19/09/03 and 14/02/04. The final event in the irrigation + rain record on 21/2/04 is a rainfall event of 9.2 mm. The irrigator at this study site typically applied between 6 mm and 18 mm in an irrigation event. The crops received a total of 723 mm of irrigation and 67 mm of rain during this period.

The soil moisture matric potentials recorded at monitoring points TR1 and TR2 (Figure 3.11c,d) show that the intensive irrigation applied here was effective in maintaining the upper 110 cm of soil at a high matric potential. At the 75 cm and 110 cm depths, potential is maintained between approximately –5 kPa and –10 kPa for the whole period of the crop. The potential at 30 cm depth is somewhat more labile, varying between 0 and –17 kPa. The latter occurred in January 2004, when ET conditions were extreme and even the intensive irrigation applied to the crop during that time was insufficient to maintain the moisture content in the root zone at this irrigator's preferred level.

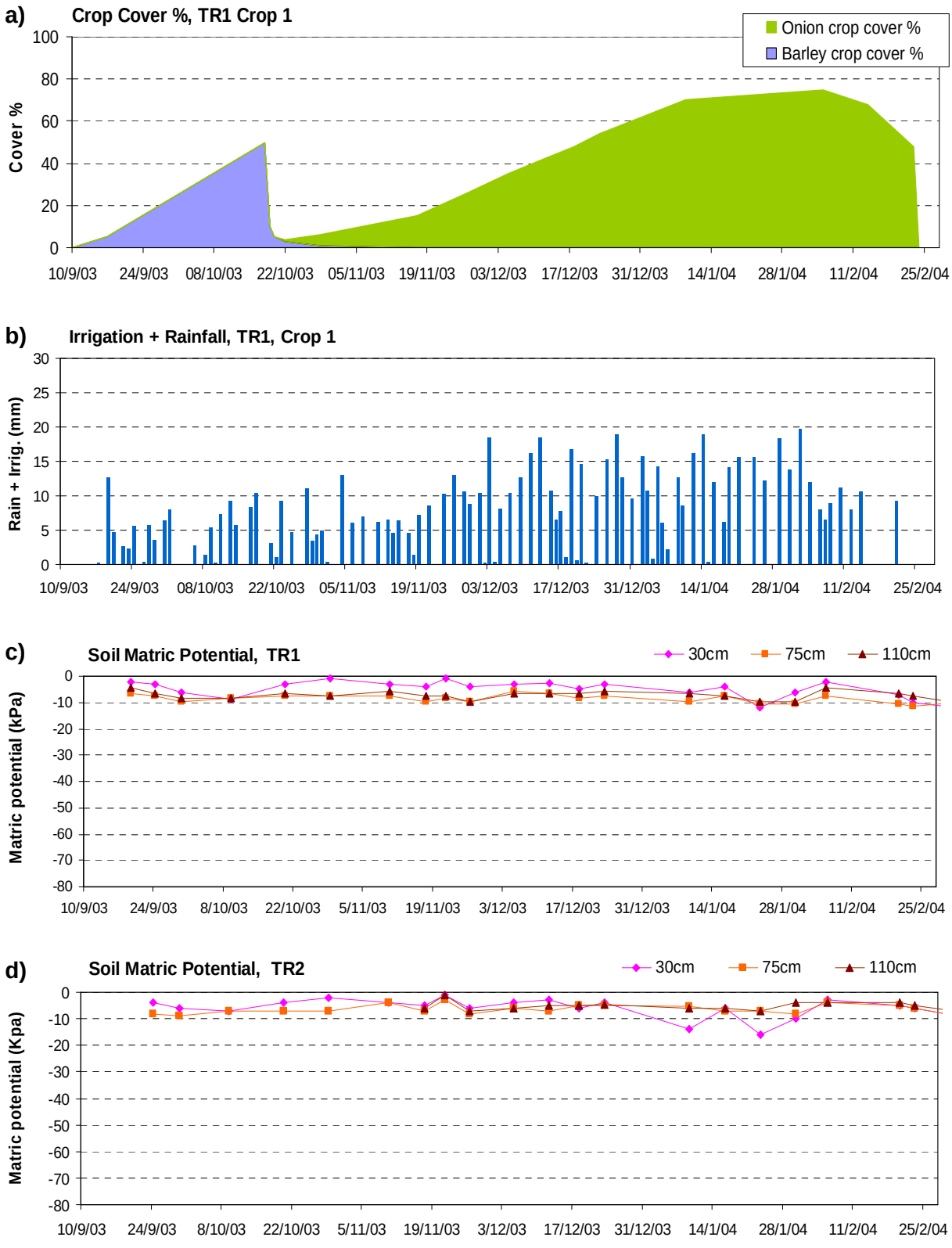

Figure 3.11 Field study data from study site TR: a) crop cover fraction, b) pluviometer record of rain and irrigation, c) soil matric potentials at point TR1, and d) soil matric potentials at point TR2

No lysimeters were installed at the TR study site due to objections from the land owner. Instead, suction cup soil solution samplers were installed to allow collection of soil solution samples from a depth of 75 cm. The EC of the soil solution captured (Figure 3.12) can be seen to occupy a fairly high EC range, between approximately 3,000 and 10,000 µS/cm. While there is a difference between the EC of soil solution between the two sites the two monitoring point are seen to follow quite similar variations. There is a downward trend in EC through much of the period monitored, possibly indicating effective flushing of the solutes through the root zone as a result of the intensive irrigation and high water contents maintained. This would suggest that, despite the extremely high ET potential through this period, there is some drainage occurring leaching soil solutes down through the soil at least to below the 75 cm depth of the suction cup samplers. The difference in EC between the two monitoring points suggests more effective drainage occurs at TR1 than at TR2, indicating spatial variability of drainage characteristics within this plot.

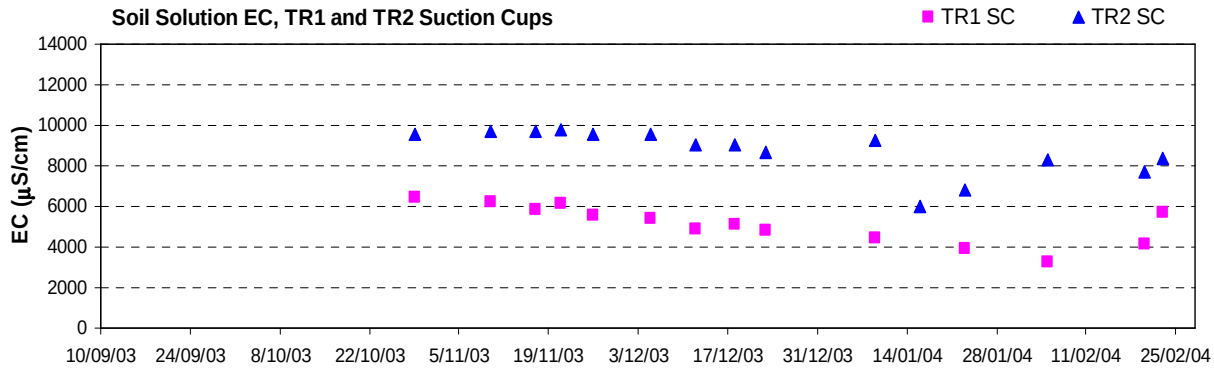

Figure 3.12 EC values of soil solution captured by suction cup soil solution samplers at points TR1 and TR2

3.2 Results from Laboratory Analyses

On the following pages are tables of data resulting from laboratory analysis of soil and water samples from the all four study sites according to methods described in Chapter 2. These data form the basis of 1) the soil hydrologic characteristics used to construct model soil descriptions and 2) initial soil water content conditions 3) dissolved ion composition of initial soil solution and irrigation water and shallow groundwater for the soil water and flux models demonstrated in Chapters 4 – 6.

Table 3.1 provides values resulting from measurements of water outflow from undisturbed soil cores and unsaturated hydraulic conductivity, K_{unsat}, at a soil matric potential of –10 kPa, derived according to the method of Klute (1965), described in Chapter 2. The measured and theoretical outflow curves, from which the values of parameters ***t*** and ***w*** are derived, are reproduced in Appendix 1.

Table 3.2 provides soil physical characteristics of soil samples taken from each of the four study sites. Soil moisture content values (θ and $\theta_{-5\ kPa}$), porosity, bulk and particle densities, unsaturated hydraulic conductivity at –10 kPa (transposed from Table 3.1), and Campbell's water retention equation parameters 'a' and 'b'. Porosity values in the table are calculated from bulk and particle densities where porosity, $\eta = 1 - \rho_p/\rho_b$.

Values of the other soil physical properties were derived experimentally as described in Chapter 2.

Table 3.3 shows values derived from ICP analysis of 1) exchange phase cations and 2) soluble cation and anion concentrations of, respectively, exchangeable cation extracts and soil solution extracts of soil samples from the four study sites. These analyses were conducted by CSIRO Land and Water Analytical Services Laboratory.

Table 3.4 shows derived Gapon selectivity coefficients and concentrations of exchange cations and dissolved ions at soil moisture contents corresponding to soil matric potential of –5 kPa. These values are required as starting compositions for the soil chemistry model in which the initial soil matric potential was set at –5 kPa for the whole modelled soil depth. These are derived using the values in tables 3.2 and 3.3 according to the method described in Chapter 2, section 2.4.2.

Table 3.1 Soil Hydraulic Conductivities (K_{unsat}) Derived From Klute (1965) Outflow Method

Soil K(unsat.) derivations										
Soil Profile / Depth	Values from outflow graphs								K at -10 KPa	
	t (min)	w (= $Dt/4L^2$)	L^2 (cm^2)	D (= $w4L^2/t$)	Δh (cm)	Q() (cm^3)	V (cm^3)	C cm^{-1}	$K_{(-10)}$ (=DC) (cm/min)	$K_{(-10)}$ (mm/day)
PGR1 / 0 - 10 cm	300	0.7	9	0.084	20	1.142	69	0.0008275	6.95E-05	1.001
PGR1 / 30 cm	1320	0.4	9	0.011	10	0.182	69	0.0002638	2.88E-06	0.041
PGR1 / 50 cm	300	0.4	9	0.048	12	0.815	69	0.0009843	4.72E-05	0.680
PGR2 / 0 - 10 cm	180	0.4	9	0.080	20	1.201	69	0.0008703	6.96E-05	1.003
PGR2 / 30 cm	240	0.04	9	0.006	20	0.47	69	0.0003406	2.04E-06	0.029
PGR2 / 50 cm	240	0.1	9	0.015	20	0.347	69	0.0002514	3.77E-06	0.054
SR1 / 0 - 10 cm	180	0.2	9	0.040	20	0.527	69	0.0003819	1.53E-05	0.220
SR1 / 30 cm	240	0.2	9	0.030	14	0.188	69	0.0001946	5.84E-06	0.084
SR1 / 50 cm	240	0.4	9	0.060	14	0.023	69	2.381E-05	1.43E-06	0.021
SR2 / 0 - 10 cm	180	0.07	9	0.014	10	0.73	69	0.001058	1.48E-05	0.213
SR2 / 30 cm	260	0.04	9	0.006	10	0.628	69	0.0009101	5.04E-06	0.073
SR2 / 50 cm	300	0.2	9	0.024	20	0.068	69	4.928E-05	1.18E-06	0.017
HX1 / 0 - 10 cm	140	0.7	9	0.180	20	0.637	69	0.0004616	8.31E-05	1.196
HX1 / 30 cm	330	0.2	9	0.022	20	0.81	69	0.000587	1.28E-05	0.184
HX1 / 50 cm	50	0.1	9	0.072	20	0.041	69	2.971E-05	2.14E-06	0.031
HX2 / 0 - 10 cm	15	0.04	9	0.096	20	1.09	69	0.0007899	7.58E-05	1.092
HX2 / 30 cm	180	0.4	9	0.080	20	0.85	69	0.0006159	4.93E-05	0.710
HX2 / 50 cm	180	0.4	9	0.080	20	0.064	69	4.638E-05	3.71E-06	0.053
TR1 / 0 - 10 cm	300	0.2	9	0.024	20	0.56	69	0.0004058	9.74E-06	0.140
TR1 / 30 cm	180	0.2	9	0.040	20	0.48	69	0.0003478	1.39E-05	0.200
TR1 / 50 cm	300	0.4	9	0.048	20	0.335	69	0.0002428	1.17E-05	0.168
TR2 / 0 - 10 cm	360	0.1	9	0.010	20	0.571	69	0.0004138	4.14E-06	0.060
TR2 / 30 cm	120	0.2	9	0.060	20	0.06	69	4.348E-05	2.61E-06	0.038
TR2 / 50 cm	360	0.4	9	0.040	20	0.172	69	0.0001246	4.99E-06	0.072

Table 3.2 Soil Physical Properties Summary

Soil Physical and Hydraulic Properties								Campbell's Equation Parameters	
Soil sample	Soil texture	θ_{sat}	θ at -5kPa	Porosity	Bulk Density (kg/dm3)	Particle Density (g/cm^3)	K at -10kPa (mm/d)	Campbell's 'a'	Campbell's 'b'
PGR1 0-10cm (1)	Loamy sand	0.48	0.29	0.44	1.58	2.82		-1.67	2.55
PGR1 0-10cm (2)	Loamy sand	0.37	0.23	0.43	1.52	(2.67)	1.000	-1.50	2.52
PGR1 30cm	Sandy loam	0.41	0.29	0.36	1.70	2.67	0.041	-2.37	3.29
PGR1 50cm	Sandy clay	0.31	0.24	0.34	1.74	2.65	0.068	-0.44	7.00
PGR1 70cm	Calcareous sandy clay	0.35	0.26	0.31	1.75	2.53		-0.54	12.00
PGR2 0-10cm (1)	Loamy sand		0.27	0.42	1.59	2.74			
PGR2 0-10cm (2)	Loamy sand	0.36	0.24	0.42	1.56	(2.67)	1.003	-1.50	3.00
PGR2 30cm	Sandy loam	0.27	0.19	0.39	1.64	(2.67)	0.029	-0.50	4.70
PGR2 50cm	Sandy clay	0.33	0.21	0.40	1.65	(2.67)	0.054	-0.30	6.00
SR1 0-10cm	Sandy loam	0.34	0.27	0.39	1.57	(2.67)	0.220	-0.85	7.90
SR1 30cm	Sandy loam	0.30	0.26	0.40	1.61	(2.67)	0.060	-1.80	7.20
SR1 50cm	Calcareous sandy clay	0.33	0.30	0.36	1.70	(2.67)	0.021	-2.00	10.00
SR2 0-10cm (1)	Sandy loam	0.38	0.30	0.43	1.57	2.75	0.087	-0.38	7.21
SR2 0-10cm (2)	Sandy loam	0.31	0.27	0.40	1.59	2.67	0.210	-0.08	10.59
SR2 30cm (1)	Sandy loam	0.33	0.30	0.35	1.73	2.65	0.084	-0.80	12.00
SR2 30cm (2)	Sandy loam	0.33	0.31	0.40	1.61	2.67	0.073	-0.27	11.50
SR2 50cm (1)	Calcareous clay	0.43	0.40	0.43	1.43	2.51		-3.00	12.00
SR2 50cm (2)	Calcareous clay	0.46	0.46	0.46	1.45	(2.67)	0.017	-6.00	25.00
HX1 0-10cm	Sandy loam	0.37	0.31	0.46	1.48	2.76	1.200	-1.00	4.20
HX1 30cm	Loamy sand	0.29	0.29	0.37	1.62	2.59	0.180	-1.50	5.50
HX1 50cm	Sandy clay	0.39	0.39	0.39	1.65	2.70	0.031	-5.00	12.00
HX2 0-10cm	Sandy loam	0.38	0.26	0.43	1.51	(2.67)	1.090	-1.20	3.70
HX2 30cm	Loamy sand	0.31	0.23	0.37	1.68	(2.67)	0.710	-1.80	3.40
HX2 50cm	Sandy clay	0.30	0.30	0.32	1.71	(2.67)	0.053	-5.00	12.00
TR1 0-10cm	Loamy sand	0.32	0.24	0.39	1.64	(2.67)	0.140	-1.00	5.70
TR1 30cm	Sandy loam	0.30	0.27	0.32	1.81	(2.67)	0.200	-1.50	11.30
TR1 50cm	Clay	0.36	0.34	0.37	1.67	(2.67)	0.170	-2.70	12.00
TR2 0-10cm	Loamy sand	0.32	0.30	0.36	1.71	(2.67)	0.060	-3.20	8.00
TR2 30cm	Sandy loam	0.29	0.28	0.33	1.78	(2.67)	0.038	-5.00	12.00
TR2 50cm	Sandy clay	0.33	0.31	0.38	1.67	(2.67)	0.078	-5.00	12.00
TR0 0-10cm	Loamy sand	0.30	0.25	0.30	1.84	2.65		-1.00	12.00
TR0 30cm	Sandy loam	0.46	0.32	0.48	1.51	2.88		-0.60	12.00
TR0 50cm	Clay	0.45	0.36	0.44	1.49	2.65		-0.49	12.00

Note, porosities in the table are calculated from bulk and particle densities ($\eta = 1 - \rho_p/\rho_b$). Particle density values in brackets are in place of measured values and assume similar particle density to quartz. Campbell's equation parameters are from curves fitted to experimental water retention curves (refer Appendix 1).

Table 3.3 Measured Major Soil Chemistry (CSIRO laboratory analysis results)

	Exchange phase cations					Soluble cations and anions in 1:5 solution extracts						
Soil sample	Ca (mmol+/kg)	Mg (mmol+/kg)	Na (mmol+/kg)	K (mmol+/kg)	CEC (mmol+/kg)	Ca (mmol/l)	Mg (mmol/l)	Na (mmol/l)	K (mmol/l)	Cl (mmol/l)	S (mmol/l)	Alk (mmol-/l)
PGR1 0-10cm (1)	22	10	6.2	4.1	44	0.2	0.24	2.62	0.42	3.32	0.2	2.14
PGR1 30cm	18	7	7.9	3.7	42	0.76	0.65	4.35	0.25	5.94	0.74	1.8
PGR1 70cm	29	31	9.2	5.9	71	0.14	0.19	6.52	0.26	6.46	0.83	2.62
PGR2 0-10cm (1)	14	10	8.1	6.2	41	0.27	0.24	2.04	0.27		0.14	
PGR2 30cm	14	7	4.1	3	28	0.15	0.19	2.66	0.23		0.21	
PGR2 75cm	25	45	28	16	121	0.31	0.32	3.2	0.1		0.49	
SR1 0-10cm	54	42	10	14	119	0.38	0.51	2.55	0.32	4.41	0.12	2.25
SR1 30cm	39	27	32	12	100	0.33	1.8	4.15	1.63	9.7	0.17	3.15
SR1 75cm	30	32	40	6.7	97	0.13	0.23	4.78	0.18	4.7	0.49	3.51
SR2 0-10cm (1)	39	34	11	14	104	0.14	0.17	3.36	0.21	2.71	0.74	0
SR2 30cm (1)	59	53	67	30	209	0.08	0.06	4.28	0.14	3.14	0.78	4.05
SR2 75cm	48	53	64	16	182	0.11	0.1	11.3	0.12	10.12	0.86	3.84
HX1 0-10cm	74	9	3.7	9.8	75	8.25	0.81	1.47	0.74	1.57	17.14	0.75
HX1 30cm	78	10	4.3	7.8	72	11.25	1.03	2.08	0.65	1.67	17.51	0.76
HX1 75cm	45	21	13	9.1	89	0.7	0.24	3.53	0.24	2.86	1.43	2.09
HX2 0-10cm	57	9	3.1	9.1	75	3.25	0.49	0.96	0.58		3.44	
HX2 30cm	76	8	3.8	6.6	66	7	0.63	1.54	0.43		8.13	
HX2 75cm	78	28	12	9.3	126	1.24	0.39	2.64	0.18		2.17	
TR1 0-10cm	42	17	11	15	83	0.7	0.37	3.84	0.64	5.8	0.41	2.21
TR1 30cm	55	11	8	9	86	0.82	0.19	4.16	0.25	5.15	0.64	1.79
TR1 75cm	63	19	11	9	130	0.48	0.16	2.47	0.13	3.12	0.38	2.02
TR2 0-10cm	58	15	19	18	124	0.98	0.31	5.22	0.54		0.67	
TR2 30cm	68	13	9.7	14	115	1.47	0.37	4.06	0.42		0.85	
TR2 75cm	61	22	10	12	123	0.8	0.29	2.91	0.28		1.38	

Table 3.4 Soil Chemistry Variables Derived from Chemical Equilibrium Model (Chemeq)

	Derived Gapon Selectivity Coefficients			Chemeq-derived ion concentrations in soil at -5 kPa Water Content										
				Exchange phase cations				Cations and Anions in Solution						
Soil sample	Mg/Ca	Ca/Na	Ca/K	Ca (mmol+/kg)	Mg (mmol+/kg)	Na (mmol+/kg)	K (mmol+/kg)	Ca (mmol/l)	Mg (mmol/l)	Na (mmol/l)	K (mmol/l)	Cl (mmol/l)	SO4 (mmol/l)	Alk (mmol-/l)
PGR1 0-10cm (1)	0.26	6.2	1.5	21.21	9.78	6.97	4.34	2.06	6.32	67.18	10.15	76.82	5.45	6.2
PGR1 30cm	0.26	4.0	0.5	17.97	6.86	8.42	3.75	9.9	20.34	124.5	7.02	144.8	21.69	3.69
PGR1 70cm	0.3	20.0	0.3	29.51	30.92	9.22	5.95	1.19	10.48	129.76	1.27	129.07	8.94	7.15
PGR2 0-10cm (1)	0.9	1.0	0.18	13.64	9.67	8.81	6.28	14.31	8.63	55.86	7.2	89.81	8.24	2.66
PGR2 30cm	0.4	5.0	0.6	13.46	6.67	4.7	3.17	7.88	11.77	109.62	8.91	135.95	9.06	3.76
PGR2 75cm	1.7	1.2	0.03	25.16	44.37	29.48	15.99	15.39	15.84	118.05	1.62	140.64	19.25	2.96
SR1 0-10cm	0.7	4.0	0.3	53.43	41.39	10.96	14.22	13.7	16.59	70.6	6.88	128.22	3.49	2.84
SR1 30cm	0.33	1.8	1.85	37.98	25.48	33.82	12.72	20.51	83.82	164.27	63.67	418.63	7.34	3.33
SR1 75cm	0.9	2.0	0.5	29.79	31.95	40.3	6.66	5.3	7.23	134.86	5.62	133.17	13.88	4.63
SR2 0-10cm (1)	0.65	8.0	0.25	40.69	33.38	10.06	13.87	3.05	4.58	73.71	3.22	55.98	15.29	5.62
SR2 30cm (1)	1.2	2.35	0.18	58.75	52.91	67.26	30.07	4.78	2.55	121.59	4.23	90.54	22.49	4.88
SR2 75cm	1.65	3.2	0.14	47.8	53.14	64.2	16.37	4.78	2.08	200.56	2.26	180.89	15.37	4.8
HX1 0-10cm	0.1	8.0	1.5	73	9.2	4.14	10.18	13.53	19.79	33.01	15.59	37.48	37.23	3.23
HX1 30cm	0.09	12.0	2.0	76.12	10.61	5.07	8.3	12.4	27.07	53.8	15.09	46.64	48.72	3.67
HX1 75cm	0.63	2.43	0.12	44.54	21.02	13.41	9.13	18.92	10.04	66.84	2.19	76.25	24.05	2.55
TR1 0-10cm	0.58	4.1	0.52	41.53	16.77	11.85	14.85	29.16	13.72	138.03	22.1	213.44	16.09	2.21
TR1 30cm	0.42	5.45	0.29	53.8	10.72	8.88	9.2	22.63	4.9	93.74	5.21	121.51	15.1	2.27
TR1 75cm	0.58	3.3	0.2	62.54	18.73	11.3	9.03	12.6	3.25	48.82	2.38	64.57	7.86	2.57

CHAPTER 4: MODELLING OF SOIL WATER AND SALT FLUXES

A number of parameters determine the drainage flux beneath agricultural land: rainfall, irrigation, soil profile type, soil surface condition (e.g. tilled soil), topography, crop types, crop cover fraction, and evaporation conditions: air temperature, wind speed, solar radiation and humidity. These parameters can be incorporated into a model that estimates how vertical flux of soil water varies according to the combination of these parameters within the prevailing weather conditions and the crop types, irrigation types and soil types present. The model can then be calibrated using in-field measurements of soil water contents such that they correctly estimate the soil water drainage fluxes measured at a number of monitored sites. Such models can then be applied to other combinations of the same parameters to provide predictions of the effects of changes in land management practices on vertical water fluxes.

The LEACHC version of the LEACHM solute transport model (Hutson 2003) uses numerical solutions of the Richards equation to simulate the vertical movement of water between discrete layers within a soil profile in response to fluxes of water through the upper boundary of the soil surface. The lower boundary to the soil profile can be defined in several different ways and the model simulates flux through the lower boundary accordingly. The soil profile is defined in the model input file with discrete layers of differing hydraulic conductivity and water retention characteristics. Water and solute movements and resulting changes in water contents and solute concentrations are calculated in response to water and chemical fluxes through the soil surface resulting from precipitation, evapotranspiration and crop cover conditions.

LEACHM is the general acronym (Leaching Estimation And CHemistry Model) for a suite of models that simulate water and solute transport in variably saturated media (Hutson 2003). All variants of LEACHM use a common approach to the simulation of water flow, but they differ in their capability to model organic and inorganic chemical processes within the simulated water flow regime. The LEACHC variant is the inorganic chemistry module that simulates the transient movement of inorganic ions.

The core of LEACHM is a mechanistic model that uses a finite difference approximation of the Richards equation (Equation 4.1) to model 1-dimensional water flow, and the convection-dispersion equation to model solute transport.

$$\frac{\partial \theta}{\partial t} = -\frac{\partial}{\partial z}(K\frac{\partial H}{\partial z}) \qquad \text{(Equation 4.1)}$$

(Richards, 1931)

In the LEACHM application of this equation, z is vertical distance between nodes in the soil profile model. The time increment 't' has a maximum value of 0.1days and is automatically reduced as flux density increases. The total soil moisture head potential, H, is equal to $h_m(\theta)$ + z, where $h_m(\theta)$ is the soil moisture matric potential at soil moisture content θ.

The soil profile is represented as a number of horizontal layers, the thickness and properties of which are specified in the model's input data file. Water retention and unsaturated hydraulic conductivity functions are encoded in the model and parameter values for these functions are user-specified in the input data file. For water retention LEACHM offers a choice of water retention functions, based on either van Genuchten's (1980) equation or a modification of Campbell's (1974) water retention function (Equation 4.2), which at higher potentials replaces the exponential function with a parabolic function to produce a better approximation of the water retention characteristics at the 'wet end' of the water retention curve (Hutson and Cass, 1987).

$$h_m = a(\theta/\theta_s)^{-b} \qquad \text{(Equation 4.2)}$$

(Campbell, 1974)

Three parameter values are required to define the retention function for each soil layer, the air entry value 'a', Campbell's 'b' parameter, and the saturation water content 'θ_s'. LEACHM assumes θ_s is equivalent to porosity and approximates this from the bulk density value 'ρ_b'. Initial values a, b, and ρ_b were determined experimentally for soil at three depths in the monitored soil profile as described in Chapter 2 and are tabulated in Table 3.2. LEACHM uses Campbell's conductivity equation (Equation 4.3) to define hydraulic conductivity at varying states of saturation:

$$K(\theta) = K_s(\theta/\theta_s)^{2b+2+p}. \qquad \text{(Equation 4.3)}$$

(Campbell, 1974)

Here 'K_s' is hydraulic conductivity at saturation, 'p' is a pore interaction parameter, often set to 1, and 'b' is the same constant 'b' used in the water retention function, determined empirically. Conductivity derived according to this function changes markedly as the soil nears saturation. Hence, if saturated conductivity (Ks) is used to position the $K(\theta)$ curve, any inaccuracy in the curve shape can result in significant errors in the derived $K(\theta)$ values within

the range of θ in which the soil is most commonly found. Rather than requiring the saturated conductivity Ks, LEACHM requires a known conductivity at a stated matric potential to position the K(θ) curve. These values were determined from measurements of conductivity in soil cores at a matric potential of -10 kPa, as described in Chapter 2 and are tabulated in Chapter 3. Values of Campbell's pore interaction parameter 'p' were set at values of either 1 or 2 according to the effect on the fit of the resulting simulation to measured data.

The 1.5 m soil profile was defined as 30 layers, each of 5 cm thickness. The number of model soil layers to which each set of parameter values was applied was determined according to observations of horizon thicknesses in the monitored soil profile. LEACHM allows a number of options for lower boundary conditions. The option of a fixed water table depth was used in this study and a depth of 2.6 m was used for the duration of the simulation period. The effect of this lower boundary condition is to create a constant matric potential of -1.1 m (approximately -11 kPa) at the lower boundary of the 1.5 m model soil profile. The upper boundary of the model is the interface between the soil surface, crop and the atmosphere. The input data for individual LEACHM simulations include records of rain and irrigation, potential ET and crop cover development. The common method to estimate ET in agricultural settings is using the Penman-Monteith method according to the guidelines of FAO 56 (Allen et al., 1998). However, the FAO 56 recommendations are necessarily very generalised in order that they can be applied by a variety of users and do not demand specific measures of water availability and crop cover fraction, which would place a greater burden of data collection on the user. The FAO 56 method recommends categories of crop development: initial, middle, and end. Recommended crop coefficients for each crop type then differ for each of these categories to allow for different stages of crop cover through the life of the crop. Values of these crop coefficients are derived from measurements of the ratio of ETa to Penman-Monteith ETo for sample crops in experimental settings (Allen et al., 1998).

Such an approach to determine the ET component of the upper boundary flux in a model may result in a poor estimate of the vertical soil water flux and the resulting chemical flux. A better estimation of ETa at the upper boundary of the model is required, ideally one that is dynamically related to both the crop cover fraction and the availability of water at the soil surface and in the root zone. The LEACHM model allows the ET to be scaled according to the crop cover fraction. The growth and senescence of crop cover between emergence and harvest is simulated by a sigmoidal function that predicts crop cover fraction on each day of

the simulation based on starting and end dates and maximum and final crop cover specified by the user. In addition to this, LEACHM allows an "ET scaling factor" to be applied to the input ETo data. This scaling factor is analogous to the FAO 56 crop coefficient, but is fixed for the duration of the individual crop growth cycle and does not need to incorporate an adjustment for the crop cover development, which is accounted for by the crop growth function within LEACHM. The potential evapotranspiration (PET) for each time step is then equal to the product of the ET scaling factor times the input daily ETo, apportioned into time steps through the day between 7.12 am and 7.12 pm according to a sigmoidal function.

LEACHM then assumes that transpiration occurs over the fraction of the area with crop cover and evaporation from the soil surface occurs over the remaining area. The PET is split into potential evaporation and potential transpiration such that:

Potential Transpiration, T_p = PET x crop cover fraction, and

Potential Evaporation, E_p = PET (1 – crop cover fraction)

The actual evaporation, E_a is limited by the potential flux (q_{max}) through the surface in the time step, which is controlled by the soil matric potential and conductivity corresponding to the water content of the uppermost soil segment, and the potential of the soil surface, which is set at -3000 kPa. Thus,

Actual Evaporation, E_a = minimum of $E_p/\Delta t$ and q_{max}

If E_a in a time step is less than the potential surface flux, then the potential transpiration is increased by the difference between Ep and Ea. However, the potential transpiration is limited by a user-specified maximum ratio of actual to potential transpiration (R_T), such that,

Potential Transpiration, T_p = minimum of T_pR_t and $T_p + E_p - \Delta tE_a$

The resulting amount of water represented by T_p in a time step is then subtracted from the soil segments in proportions determined by the root distribution which is user-specified in the soil physical properties section of the model input file.

Within each of the soil segments that include part of the specified root distribution, water lost to transpiration in a time step is determined by a transpiration sink formula which incorporates terms for an effective water potential in the root at the soil surface (H_{root} > -3000 kPa), a user-specified root flow resistance coefficient, the soil matric potential and osmotic potential, the hydraulic conductivity, the depth to the node at the centre of the soil segment, and an assumed distance (10 mm) from the root to the point at which the soil matric and

osmotic potentials are measured. LEACHM uses an iterative procedure to determine a value for H_{root} that results in the total uptake from all segments in the plant root distribution to be equal to the potential transpiration. In drier soils, the root water uptake is limited by a minimum value for soil matric potential of -1500 kPa, below which LEACHM restricts any loss by transpiration. Thus in drier soils, the actual transpiration may be less than the potential transpiration (Hutson, 2010). While the osmotic potential of the soil is accounted for in LEACHC models and adjusted in each time step according to the concentrations of the major ions in the soil solution, in LEACHP models the osmotic potential of the soil is assumed to be zero. Apart from the effect of the osmotic potential of the soil solution, the LEACHM models do not include a salinity stress response function to adjust plant water uptake if the soil solution becomes highly concentrated.

The ET scaling factor is a measure of the transpiration performance of the subject crop compared to the reference crop that the ETo estimate is based on. This factor is therefore not the same as the time-averaged crop coefficients recommended by FAO 56, which are expected ratios of ETa/ETo within each of three crop growth stages 'ini', 'mid' and 'end'. In a LEACHM model the ETo scaling factor can be calibrated to improve the model's prediction of a measured variable that is influenced by ETa, such as soil moisture change over time. An increase to the ETo scaling factor creates increases ETa in the simulation such that fluxes of water downward through the soil will decrease. If the ETo factor and the soil hydraulic parameters in a model are calibrated correctly, the simulated changes in soil moisture content over the duration of the simulation should be close to observed values at all monitored depths.

The LEACHM Model Description and User Guide (Hutson 2010) contains a full description of the subroutines involved in LEACHM's treatment of evaporation / transpiration partitioning and root water uptake.

4.1 Optimisation of Models

Initial values for Campbell's a and b parameters, and unsaturated conductivity at -10 KPa ($K_{(-10)}$) for the two monitored points at study site PGR were set according to laboratory measurements of soil core samples (refer Table 3.2 and Appendix 2).

Table 4.1 Soil hydrologic parameter values for the two monitored points at study site PGR, from laboratory measurements of $K_{(-10)}$ and Campbell's parameters 'a' and 'b' in soil core samples.

			Lab - derived parameter values		
	Soil layer (depth)	**Soil type**	a	b	$K_{(-10)}$ (mm/d)
Point 1	1 (0 - 5 cm)	sandy loam	-1.5	2.5	1.0
	2 (5 - 30 cm)	sandy loam	-1.5	2.5	1.0
	3 (30 - 50 cm)	transition L1 - L2	-2.4	3.3	0.1
	4 (50 - 150 cm)	sandy calc. clay	0.4	7.0	0.1
Point 2	1 (0 - 5 cm)	sandy loam	-1.5	3.0	1.0
	2 (5 - 30 cm)	sandy loam	-1.5	3.0	1.0
	3 (30 - 50 cm)	transition L1 - L2	-0.5	4.7	0.1
	4 (50 - 150 cm)	sandy calc. clay	-0.3	6.0	0.1

The ETo scaling factors were set to represent the use of crop coefficients according to FAO 56 recommendations, while the crop cover growth function was set to simulate the observed crop cover development at the respective study site.

The irrigation, rainfall and ETo data collected at the study site were arranged into data files and the model was run to simulate the monitored soil profile for the duration of the first crop monitored at the two primary monitoring points at each study site. The fit between measured and model-predicted matric potential values at depths of 30, 70 and 110 cm was assessed to determine the need for further calibration of parameter values (Figure 4.1(a) and (b)).

The poor fit between the observed and model-predicted matric potentials in these graphs suggest that with the initial parameter values, the model was not able to predict the patterns of change in matric potentials at any of the three depths at which they were measured. In view of these results, the output from the initial uncalibrated simulation was deemed to be unsatisfactory and hence parameter optimisation was undertaken.

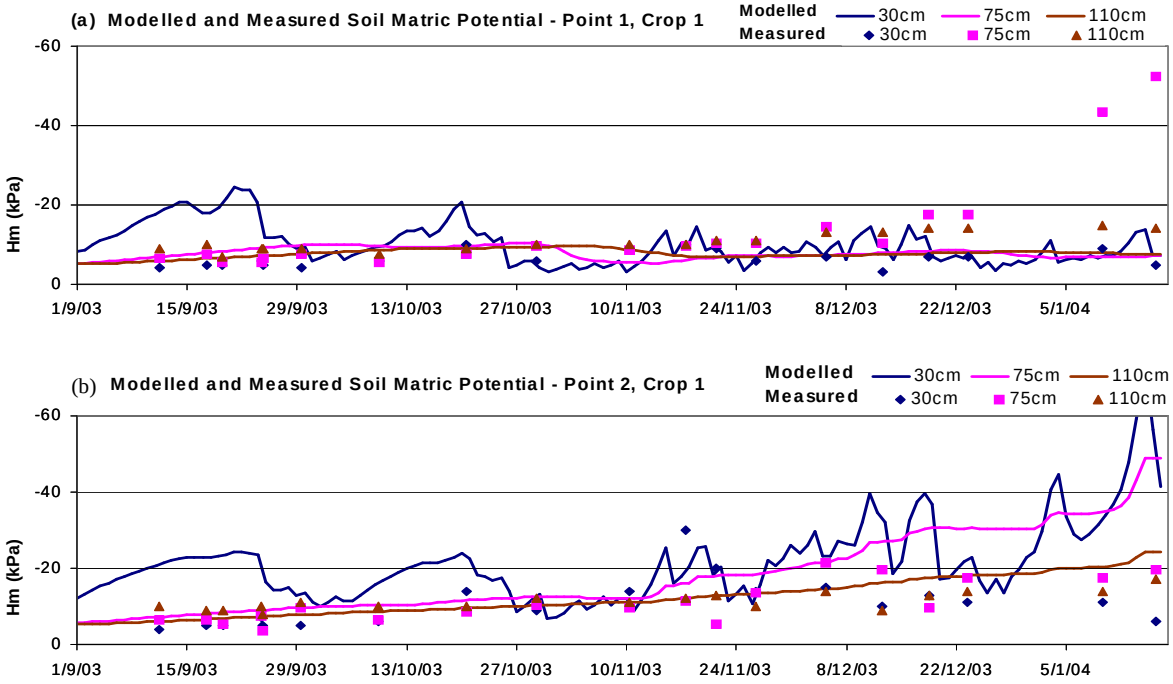

Figure 4.1 Comparisons of simulated matric potential at three depths, 30, 75 and 110 cm at monitoring study site PGR, using measured parameters values with no optimisation, (a) monitored point 1 and (b) monitored point 2

The parameter optimisation program PEST (Doherty, 2004) was used to optimise parameter values to provide a good fit between model-predicted and measured matric potential values. PEST is a model-independent non-linear parameter estimation program that adjusts selected model parameters within a specified range to optimise the residual sum of squares fit between model output and corresponding observed data. The soil hydrologic parameters a, b, and $K_{(-10)}$ were optimised simultaneously, with each parameter allowed to alter within a limited range (Table 4.2).

Table 4.2 Optimisation of soil hydrologic parameter values for soil profiles at study site PGR. Table shows the range of values for optimisation of each parameter and values selected by PEST optimisation.

		Range of parameter freedom for optimisation			Optimised parameter values		
	Soil layer (depth)	a	b	$K_{(-10)}$ (mm/d)	a	b	$K_{(-10)}$ (mm/d)
Point 1	1 (0 - 5 cm)	-3.0 to -0.4	2.5 to 10	0.2 to 20	-0.4	2.5	0.8
	2 (5 - 30 cm)	-3.0 to -0.4	3 to 10	0.2 to 20	-0.4	3	0.2
	3 (30 - 50 cm)	-5.0 to -0.4	5 to 11	0.1 to 10	-3.3	5	0.1
	4 (50 - 150 cm)	-5.0 to -0.4	5 to 12	0.1 to 10	-0.4	12	0.15
Point 2	1 (0 - 5 cm)	-3.0 to -0.4	2.5 to 10	0.2 to 20	-0.5	2.5	5.7
	2 (5 - 30 cm)	-3.0 to -0.4	3 to 10	0.2 to 20	-0.5	3	0.2
	3 (30 - 50 cm)	-5.0 to -0.4	5 to 11	0.1 to 10	-4.3	5	0.47
	4 (50 - 150 cm)	-5.0 to -0.4	5 to 12	0.1 to 10	-5.0	5	0.22

The best fit to the measured data was found when the ETo scaling factor was raised to 1.15 prior to optimising parameters a, b and $K_{(-10)}$. Scaling factor values closer to 1 resulted in the whole modelled soil profile retaining more water than the monitored soil profile, suggesting that the Penman-Monteith ETo calculation method underestimated potential ET at these sites.

The performance of each optimised set of parameters was assessed according to the closeness of fit of the model-simulated matric potential to the measured matric potentials at corresponding depths and times.

This was quantified using three indices. The modeling efficiency (EF) and coefficient of residual mass (CRM) are statistical measures of the total residual errors. The use of these indices for evaluating solute transport models was demonstrated by Loague and Green (1991).

$$EF = (\Sigma^{n}_{i=1} (O_i - O_m)^2 - \Sigma^{n}_{i=1}(S_i - O_i)^2) / (\Sigma_{n}^{i=1} (O_i - O_m)^2)$$

(Equation 4.4)

Where S_i are the simulated values; O_i are the observed values, n is the number of observations; and O_m is the mean of the observed data. The maximum value for EF is 1, indicating simulated values perfectly match measured values. If EF is less than zero, the simulated values are a worse approximation of the observed data than the mean of the observed.

$$CRM = (\Sigma^{n}_{i=1} O_i - \Sigma^{n}_{i=1} S_i) / (\Sigma^{n}_{i=1} O_i) \qquad \text{(Equation 4.5)}$$

A CRM value close to zero indicates a close fit between observed and simulated values. CRM can become increasingly negative or positive, further from zero indicates a worse fit (Loague and Green, 1991).

The correlation coefficient *r* provides a measure of how well the trends in relative high and low values in the observed data match those trends in the simulated data (Rayner, 1967).

$$r = (\Sigma^{n}_{i=1} (O_i - O_m)(S_i - S_m)) / \sqrt{(\Sigma^{n}_{i=1} (O_i - O_m)^2 \ \Sigma^{n}_{i=1}(S_i - S_m)^2)}$$

(Equation 4.6)

Values of *r* are within the range [-1,1]. A value close to 1 indicates a strong positive correlation. A negative value for *r* indicates negative correlation, meaning that trends in relative high values in the observed data correlate with relative low values in the simulated data and vice versa.

The optimisation performance indices for the two optimised simulations are shown in Table 4.3. An index value for EF, CRM and *r* is shown for the fit between observed and simulated matric potentials at each of the three depths at which matric potential was monitored. For both locations (Point 1 and Point 2) it can be seen that the simulated matric potentials at 75 and 110 cm (Matric 2 and Matric 3) have a significantly better fit to observed data than at 30 cm (Matric 1). The reasons for the apparently poor performance at 30 cm is that the values of matric potential at 30 cm were generally closer to zero and occupied a narrower range than those at 75 cm and 110 cm (Table 4.4), causing variations of the simulated values to the observed values to be relatively large proportions of the observed values.

Table 4.3 Model performance for two model soil profiles, optimised for best fit between observed and modelled matric potentials at three depths at study site PGR, monitored points 1 and 2.

	Point 1	Point 2
ETp scaling factor =	1.15	1.15
Matric 1 *r*	0.45	-0.08
Matric 2 *r*	0.86	0.72
Matric 3 *r*	0.8	0.7
Matric 1 EF	-0.44	-0.25
Matric 2 EF	0.7	0.51
Matric 3 EF	0.23	0.42
Matric 1 CRM	-0.57	-0.08
Matric 2 CRM	-0.07	-0.04
Matric 3 CRM	-0.06	0.09

Matric 1,2 and 3 relate to observation/simulation depths 30, 70 and 110 cm respectively.

Table 4.4 Means and ranges of matric potential values measured at PGR site and used in calibration of model-simulated matric potentials at three depths.

	Point 1	Point 2
Mean matric 1	-6.5	-10.7
Mean matric 2	-13.5	-11.0
Mean matric 3	-10.8	-11.4
Min / Max matric 1	-10 / -3	-30 / -4
Min / Max matric 2	-52.5 / -5.5	-21.5 / -3.5
Min / Max matric 3	-15 / -7.5	-17 / -8

The graphical display of the two data sets (Figure 4.2 (a) and (b)) shows the improved fit of the optimised simulation of matric potentials at 30 cm.

Based on the fit of simulated to observed matric potentials as a model performance indicator, the values for a, b and $K_{(-10)}$ resulting from the optimisation (as listed in Table 4.2, page 66) were selected for use in the models for study site PGR.

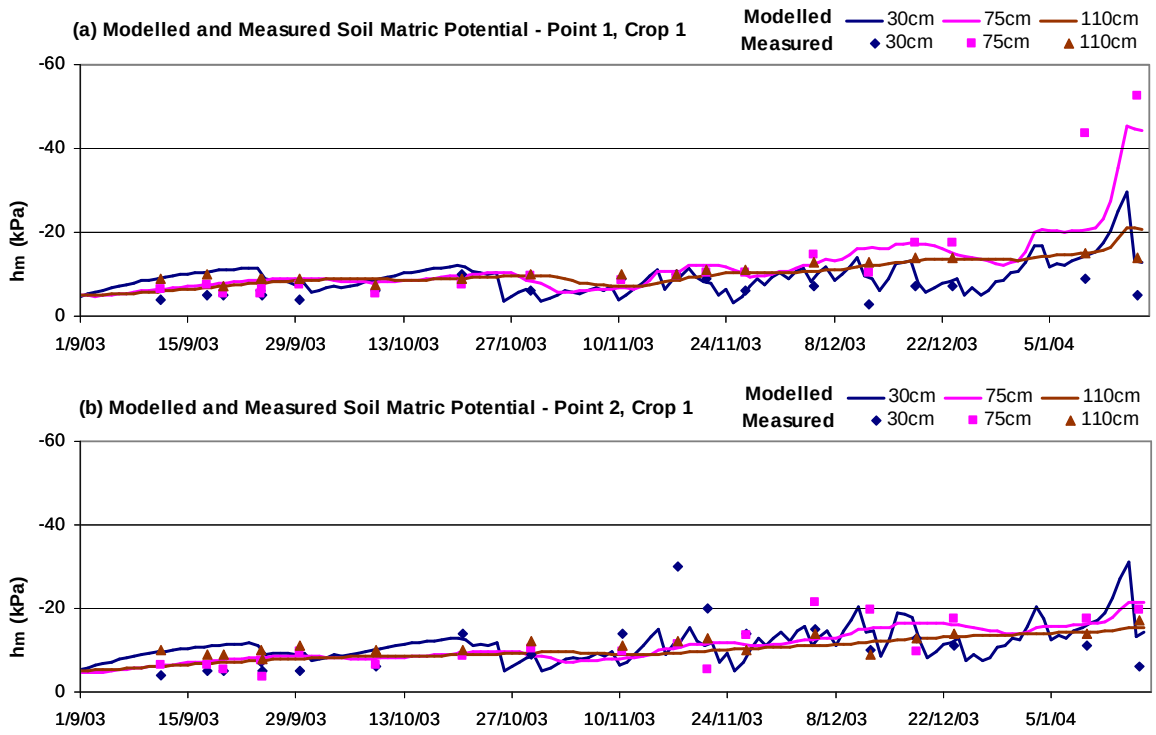

Figure 4.2 Comparisons of simulated matric potential at 30, 75 and 110 cm depths at study site PGR, with PEST optimisation of soil hydrologic parameters at (a) monitored point PGR1, and (b) monitored point PGR2

Following the optimisation of the soil and ETo scaling parameters, the resulting model was verified by running the model with the same model soil profile and ETo scaling factor but with the excitation data (rain, irrigation, ETo and crop cover) for the consecutive 215 days. The study site contained an irrigated potato crop for the first five months of this period, followed by two months of unirrigated weed growth after harvest of the potatoes. The new output from the model was then compared with the calibration data (matric potentials at 30, 75 and 110 cm) for this period to verify the model's ability to simulate soil water transport beyond the period of the data against which the model was calibrated. Graphical comparison of the simulated and observed matric potentials shows that the good fit achieved through the calibration / optimisation period is continued when simulating the consecutive verification period (Figure 4.3).

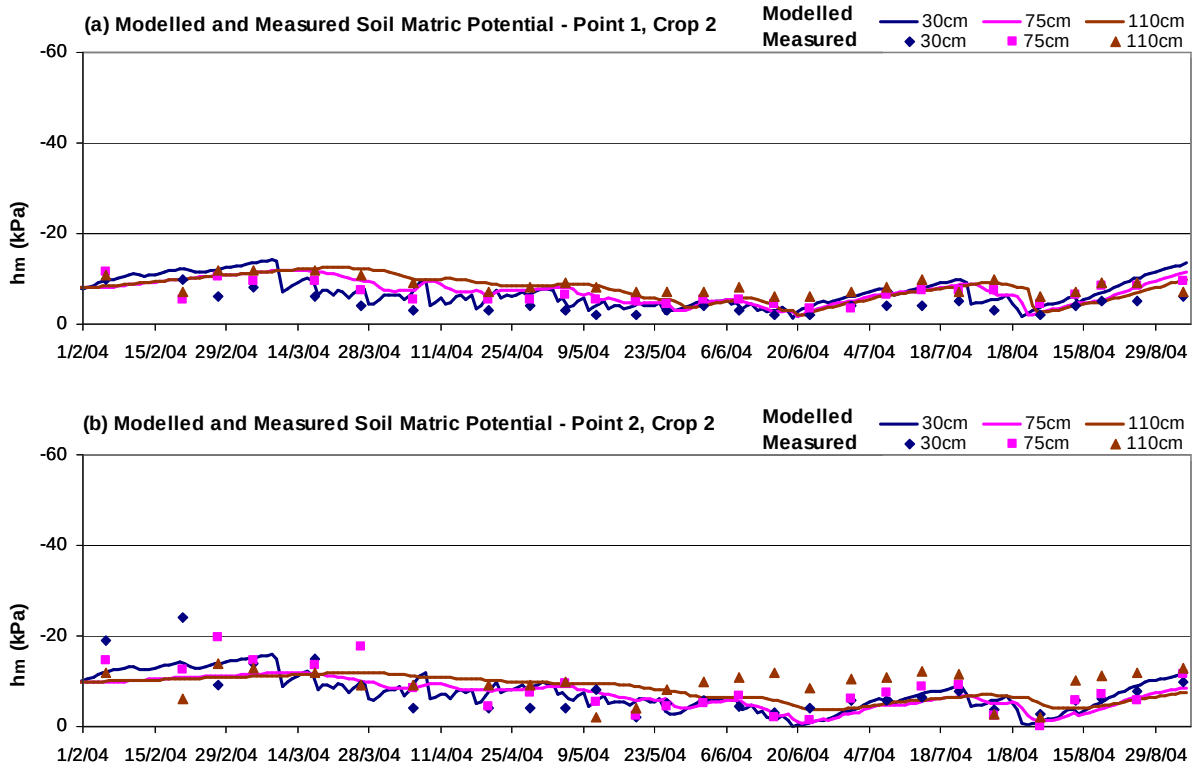

Figure 4.3 Comparisons of simulated matric potential at 30, 75 and 110 cm depths at study site PGR, verifying optimised parameter values with simulated and measured matric potentials from the consecutive 7-month period at study site PGR (a) monitored point PGR1 and (b) monitored point PGR2

4.2 Optimisation of Model Parameters for Other Primary Study Sites.

Having tested and demonstrated the approach to parameter optimisation described above, the same method of parameter optimisation was applied to the soil and crop combinations observed at the other two primary study sites: site HX and site TR. As only one crop cycle was monitored at the two other broadacre vegetable study sites, the soil profile matric potential data collected was only used for calibration, and no verification of the calibrated model was carried out.

Models were created based on the soil hydraulic characteristics at the two primary monitoring stations at each of the three broadacre vegetable crop study sites. The soil profile parameters for each were calibrated against the soil matric potentials measured over the period of at least one crop cycle. Irrigation and rainfall applied in the model were as measured at the individual study site. Whereas the weather data from the on-site weather station at the PGR study site was used to derive the Penman-Monteith (FAO 56) evapotranspiration data used in the calibration of the PGR study site soil profile described above, the ETo data used for the HX study site calibration was derived from BOM SILO Database data from the BOM weather station at the RAAF Edinburgh air field, which is adjacent to the HX study site.

The following graphs show the comparison of model output soil matric potentials with those measured at depths of approximately 30 cm, 75 cm and 110 cm. In each case the matric potential predicted by the LEACHM model is shown by continuous lines, while the measured matric potentials are shown as individual symbols, occurring at each date that matric potential measurements were taken. For each model, the soil hydraulic parameters were calibrated using PEST using the same procedures described above for study site PGR1. The two graphs for each study site show the comparison of outputs from the uncalibrated model (a) and the calibrated model (b) with the measured soil matric potentials. As can be seen in the graphs in Figures 4.4 - 4.7, the uncalibrated models result in a poor agreement between the model-predicted and measured matric potentials, while the agreement is much better in the calibrated models.

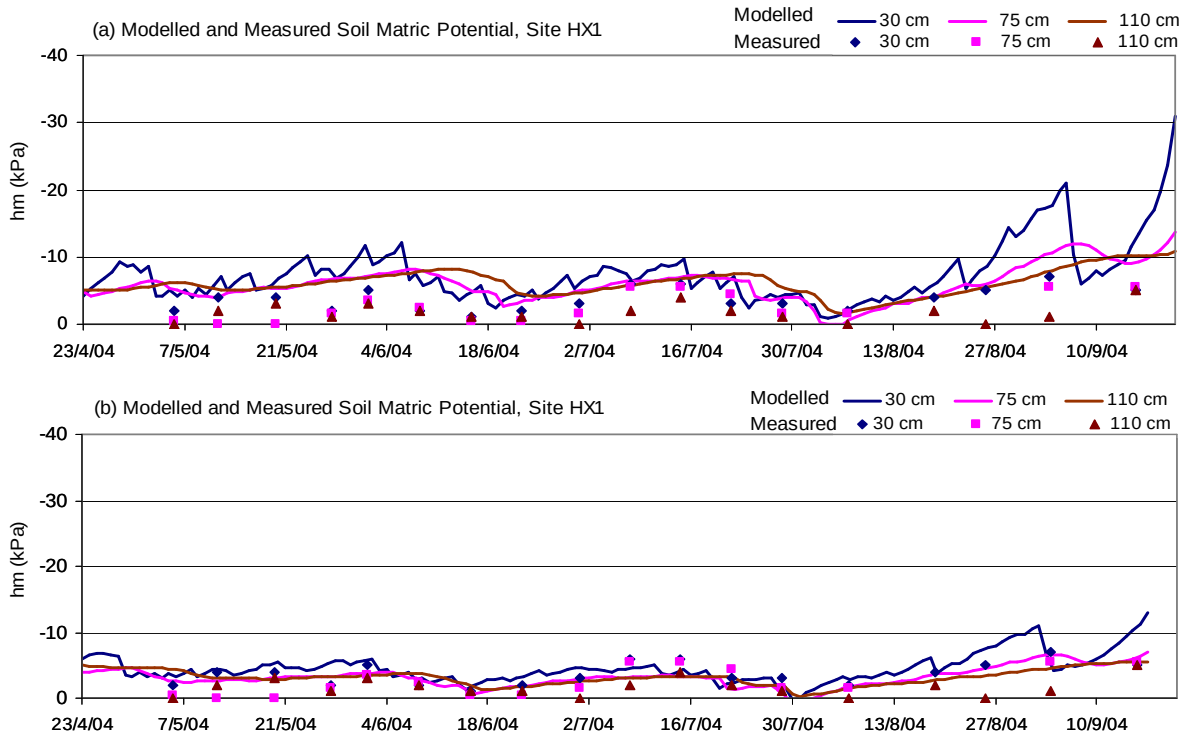

Figure 4.4 Comparisons of measured and simulated matric potential at monitored point HX1 at 30, 75 and 110 cm depths: (a) simulation using measured parameters values, no optimisation, and (b) simulation with PEST optimisation of soil hydrologic parameters and ET scaling factor.

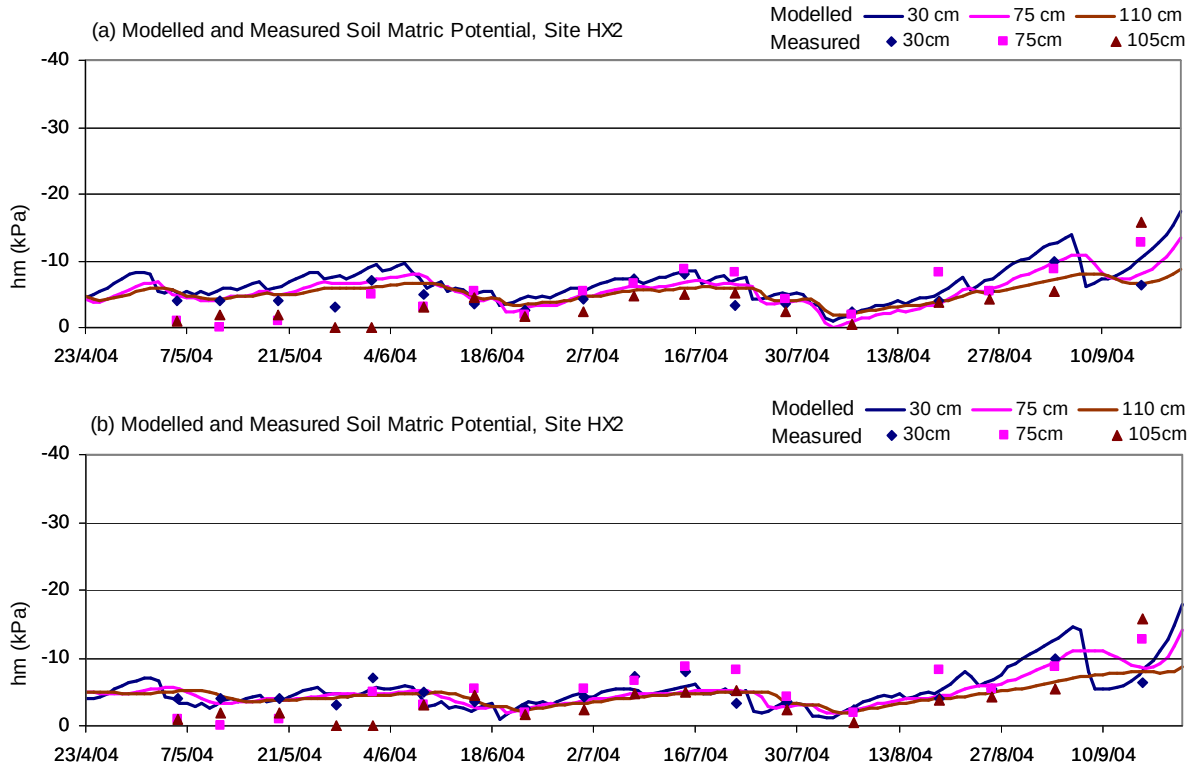

Figure 4.5 Comparisons of measured and simulated matric potential at monitored point HX2 at 30, 75 and 110 cm depths: (a) simulation using measured parameters values, no optimisation, and (b) simulation with PEST optimisation of soil hydrologic parameters and ET scaling factor.

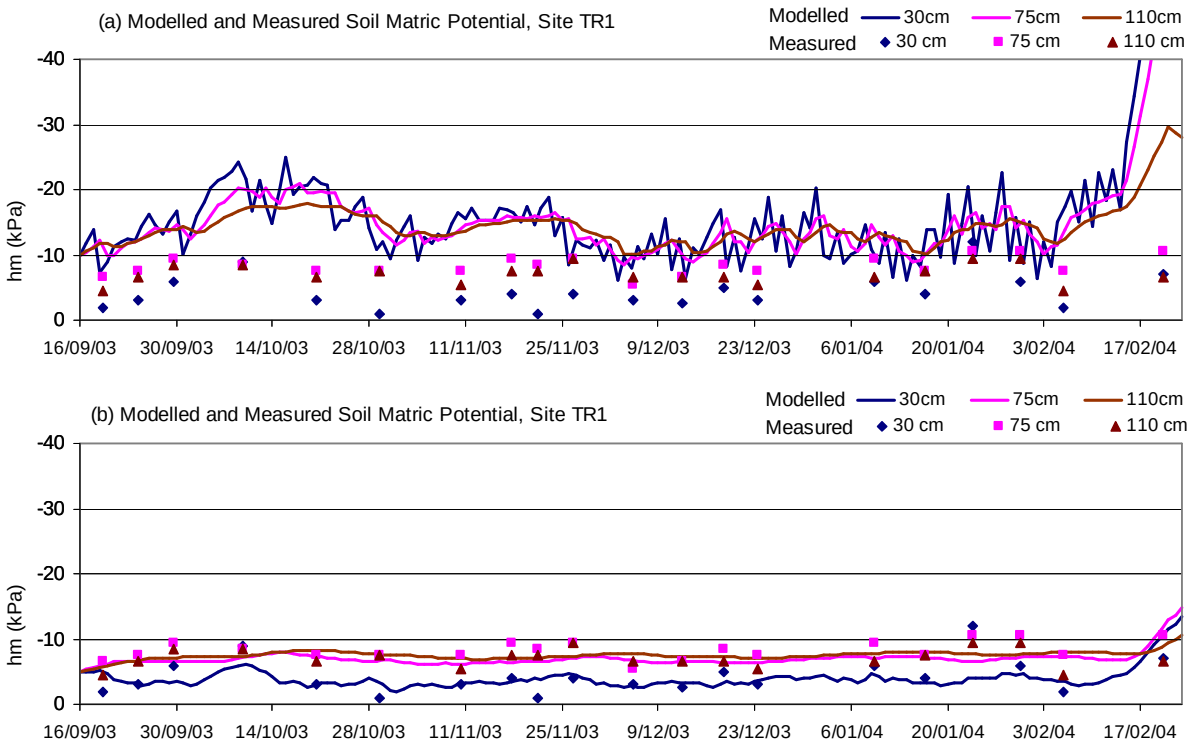

Figure 4.6 Comparisons of measured and simulated matric potential at monitored point TR1, at 30, 75 and 110 cm depths: (a) simulation using measured parameters values, no optimisation, and (b) simulation with PEST optimisation of soil hydrologic parameters and ET scaling factor.

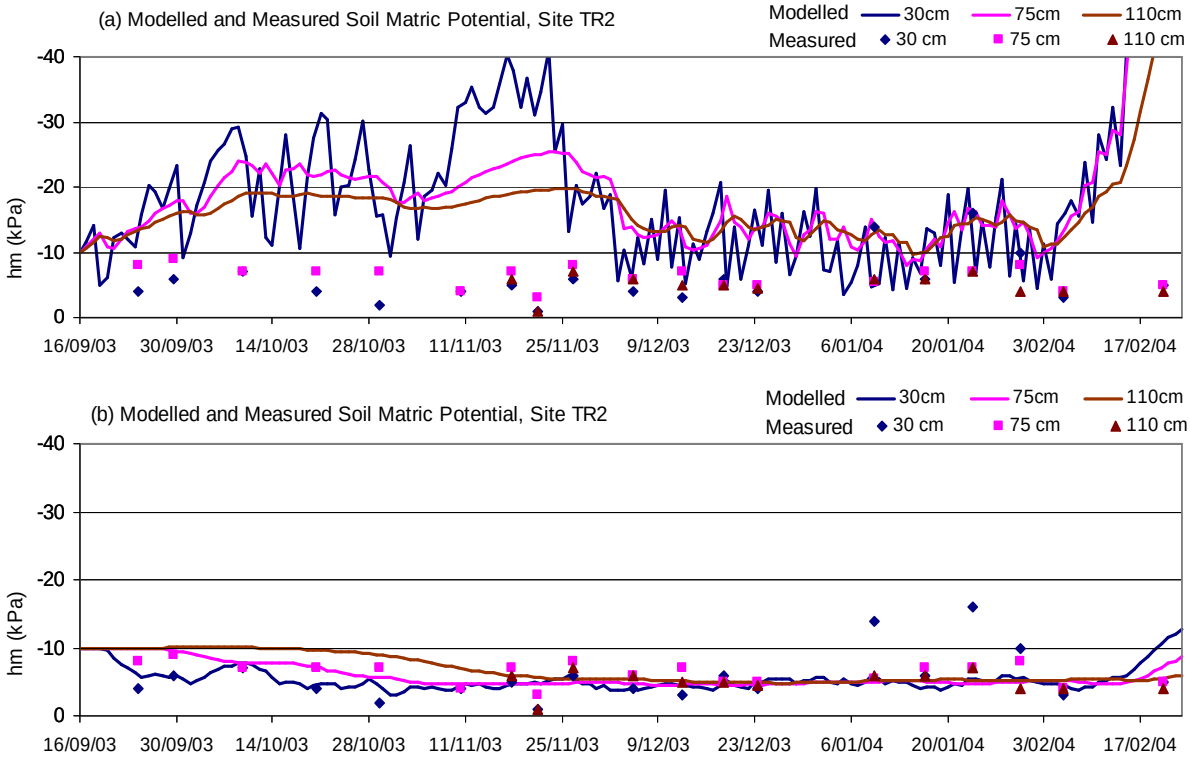

Figure 4.7 Comparisons of measured and simulated matric potential at monitoring point TR2, at 30, 75 and 110 cm depths: (a) simulation using measured parameters values, no optimisation, and (b) simulation with PEST optimisation of soil hydrologic parameters and ET scaling factor.

The soil profile parameters used in the uncalibrated models were as measured in soil samples from the study sites and reported in Table 3.2. The soil hydraulic parameters were altered significantly in most cases during the calibration process. Tables 4.5 to 4.8 show the values of these parameters before and after calibration and the numeric range within which the PEST optimisation process was given freedom to alter the parameter values.

Table 4.5 Soil hydrologic parameter values – before and after optimisation for monitoring point HX1

		Lab - derived parameter values			Range of parameter freedom for calibration			Optimised parameter values		
Soil layer (depth)	**Soil type**	a	b	$K_{(-10)}$ (mm/d)	a	b	$K_{(-10)}$ (mm/d)	a	b	$K_{(-10)}$ (mm/d)
1 (0 - 5 cm)	loamy sand	-1.0	4.2	1.2	-3.0 to -0.5	2.0 to 10.0	0.2 to 20	-1.4	5.7	8.50
2 (5 - 25 cm)	loamy sand	-1.0	4.2	1.2	-3.0 to -0.5	2.5 to 6.0	0.2 to 5.0	-2.3	3.2	1.04
3 (25 - 45 cm)	transition L3 - L4	-1.5	5.5	0.18	-4.0 to -1.0	4.0 to 11.0	0.03 to 2.0	-1.0	11.0	0.21
4 (45 - 150 cm)	calcareous clay	-5.0	12.0	0.031	-6.5 to -0.5	5.0 to 12.0	0.03 to 1.0	-1.6	12	0.06

Table 4.6 Soil hydrologic parameter values – before and after optimisation for monitoring point HX2

		Lab - derived parameter values			Range of parameter freedom for calibration			Optimised parameter values		
Soil layer (depth)	**Soil type**	a	b	$K_{(-10)}$ (mm/d)	a	b	$K_{(-10)}$ (mm/d)	a	b	$K_{(-10)}$ (mm/d)
1 (0 - 5 cm)	loamy sand	-1.2	3.7	1.09	-3.0 to -0.5	2.0 to 10.0	0.2 to 20	-1.3	2.0	0.25
2 (5 - 25 cm)	loamy sand	-1.2	3.7	1.09	-3.0 to -0.5	2.5 to 6.0	0.2 to 5.0	-3.0	4.9	0.20
3 (25 - 45 cm)	transition L3 - L4	-1.8	3.4	0.71	-4.0 to -1.0	3.0 to 11.0	0.03 to 2.0	-2.0	11.0	0.11
4 (45 - 150 cm)	calcareous clay	-5.0	12.0	0.05	-6.5 to -0.5	5.0 to 12.0	0.03 to 1.0	0.95	12	0.133

Table 4.7 Soil hydrologic parameter values – before and after optimisation for monitoring point TR1

		Lab - derived parameter values			Range of parameter freedom for calibration			Optimised parameter values		
Soil layer (depth)	**Soil type**	a	b	$K_{(-10)}$ (mm/d)	a	b	$K_{(-10)}$ (mm/d)	a	b	$K_{(-10)}$ (mm/d)
1 (0 - 5 cm)	Sandy loam	-1.0	5.7	0.14	-2.0 to -0.5	2.5 to 12.0	0.07 to 1.0	-0.9	9.8	0.64
2 (5 - 25 cm)	sandy clay loam	-1.0	5.7	0.14	-2.0 to -0.5	4.0 to 8.0	0.07 to 1.0	-2.0	4.9	0.08
3 (25 - 45 cm)	transition L2 - L3	-1.5	11.3	0.2	-3.0 to -0.75	9.0 to 13.0	0.04 to 0.5	-3.0	9.0	0.05
4 (45 - 150 cm)	calcareous clay	-2.7	12.0	0.2	-5.4 to -1.3	10.0 to 14.0	0.04 to 0.5	-4.0	10.0	0.30

Table 4.8 Soil hydrologic parameter values – before and after optimisation for monitoring point TR2

		Lab - derived parameter values			Range of parameter freedom for calibration			Optimised parameter values		
Soil layer (depth)	**Soil type**	a	b	$K_{(-10)}$ (mm/d)	a	b	$K_{(-10)}$ (mm/d)	a	b	$K_{(-10)}$ (mm/d)
1 (0 - 5 cm)	Sandy loam	-3.2	5.7	0.06	-6.4 to -1.6	4.0 to 12.0	0.07 to 1.0	-1.6	4.0	1.00
2 (5 - 25 cm)	sandy clay loam	-3.2	5.7	0.06	-6.4 to -1.6	4.0 to12.0	0.05 to 1.0	-4.7	4.0	0.10
3 (25 - 45 cm)	transition L2 - L3	-5.0	12.0	0.04	-10 to -2.5	6.0 to 14.0	0.02 to 0.8	-3.8	6.0	0.09
4 (45 - 150 cm)	calcareous clay	-5.0	12.0	0.08	-5.4 to -1.3	6.0 to 14.0	0.04 to 0.8	-1.3	6.0	0.08

4.3 Sensitivity of Model Predictions to Soil Hydraulic Parameters

The example field crop scenarios illustrated and discussed in sections 4.1 and 4.2 provide predictions of drainage volumes from models constructed and calibrated using data from a small number of intensively monitored crops. The resulting outputs from these models provide a prediction of fluxes occurring in those monitored locations and an indication of the main influencing variables. It is important when interpreting the outputs of these models to have an appreciation of the way in which the outputs of interest (in this case the soil water balance components) may change in relation to changes in soil hydrologic variables. Furthermore, if the models demonstrated here are to be used to make more general assessments of the irrigation water flux components in the NAP, it is necessary to determine the sensitivity of the models to changes in soil hydraulic characteristics, which vary significantly over the area of the NAP.

Testing of the sensitivity of individual parameters of the model's soil profile descriptions is a complex task as there are 30 layers in the soil profile description, each with five parameter values (Campbell's 'a', 'b' and 'p', ρ_b and $K_{(-10)}$) that affect the behaviour of soil moisture fluxes. For each model soil profile description these parameters have been optimised with a view to creating a 5 x 30 matrix of parameter values which collectively behave in the same way as the monitored soil profile. Altering individual parameter values within these matrices to test the effect on the drainage characteristics of the whole soil profile description is not useful as the parameters for each soil layer description are not independent of each other: a difference in one parameter value in a real soil will be reflected in differences in the other values. To achieve a practical and realistic analysis of the sensitivity of the model to the key soil hydrologic variables, the effects of the shape of the water retention curve and the unsaturated conductivity value used to position the Campbell's equation unsaturated conductivity curve ($K_{(-10)}$) on the annual drainage were tested as follows.

To create a set of realistic combinations of Campbell's 'a' and 'b' values, the water retention curves for the three primary soil horizons at the PGR1 monitoring point (derived earlier by fitting curves to laboratory data) were used as three base case curves. From these, alternative curves were constructed from random θ values above and below, but within 20% of the base case curve θ values, at several points along the h_m axis. This provided two randomly selected, but realistic, water retention curves positioned either side of the base case curve for each of the three primary soil horizons observed at PGR1 (Figure 4.8).

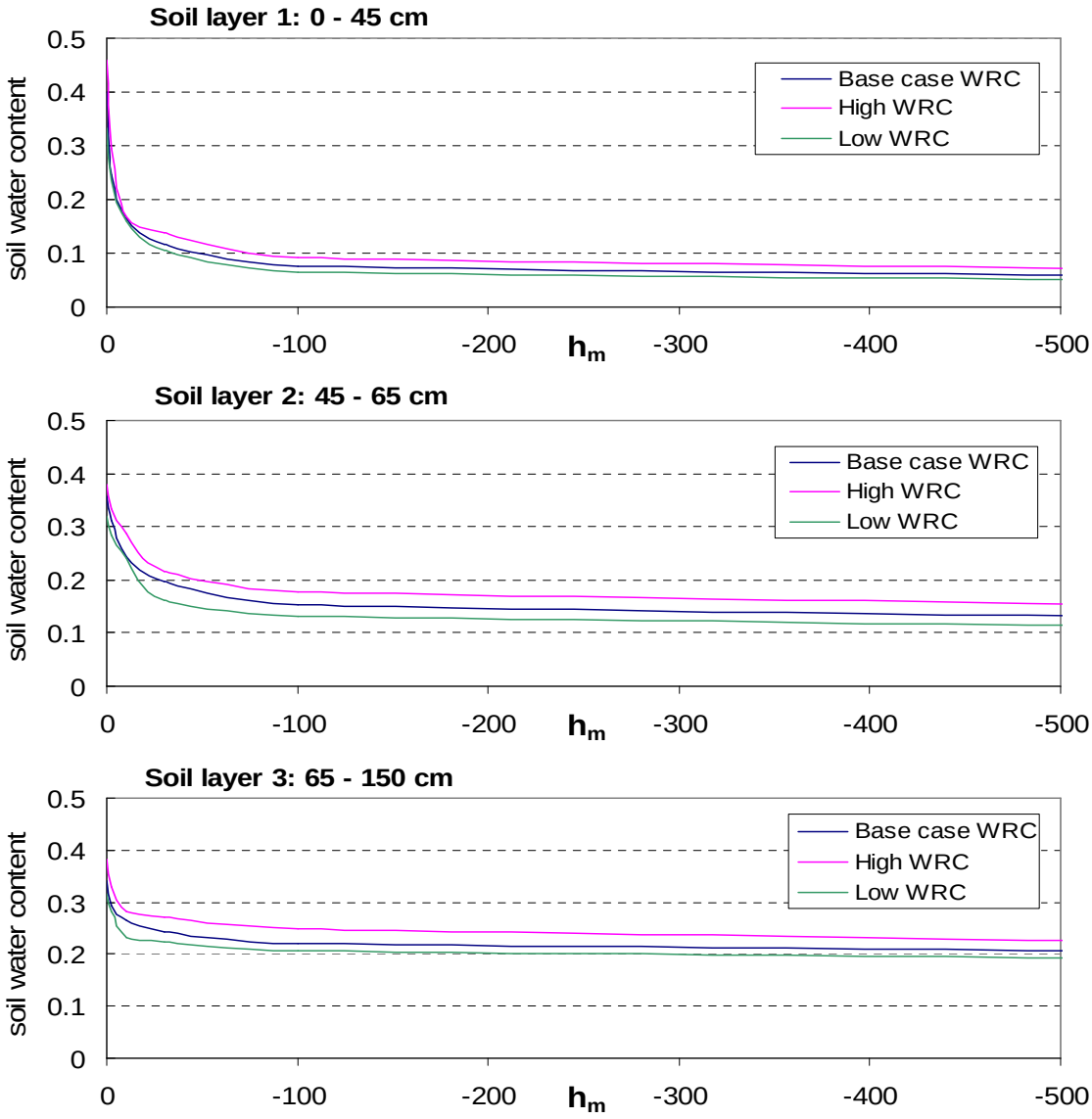

Figure 4.8 Alternative water retention curves for three soil layers at point PGR1, with high and low case curves randomly generated within 20% of the base case curve.

Using inverse modelling, Campbell's equation 'a' and 'b' values were derived for each of these curves. Three soil profile models were then constructed based on each of the base, low and high case water retention curves now available for each of the three main soil horizons.

The resulting three models then had the $K_{(-10)}$ value altered to new values within each depth segment: a low K case in which all $K_{(-10)}$ values from the base case PGR1 soil profile were reduced by a factor of 5; and a high $K_{(-10)}$ case in which all values were increased by a factor of five. The resulting nine soil profile models spanned a realistic range of variations in soil water retention characteristics for a soil of the type at this study site, combined with a range of $K_{(-10)}$ values in which the highest values were 25 times the lowest values.

These model soil profile descriptions were inserted into simulations in which they were subjected to a year of crop, weather and irrigation conditions typical of the PGR study site. Within this scenario, irrigation applications were synthesised in the model such that the soil was maintained close to a matric potential of -10 kPa at 30 cm depth whenever irrigated crops were present, thus maintaining similar soil moisture conditions to those observed.

The models were run for a one-year duration and the resulting total annual drainage was plotted for each water retention curve case against the variations in $K_{(-10)}$ (Figure 4.9).

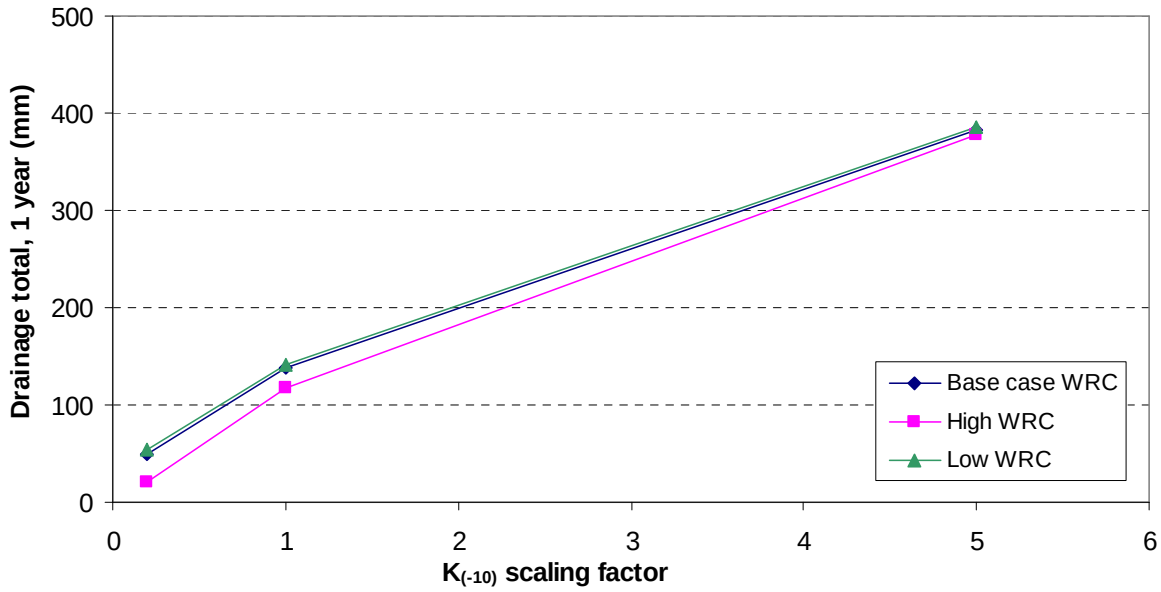

Figure 4.9 Variation of total annual drainage with alternative water retention curve parameters and unsaturated conductivity parameters in the three-layer soil at point PGR1.

It is immediately apparent from these results that the model's predictions of drainage are not particularly sensitive to the water retention curve parameters, but are more sensitive to differences in the $K_{(-10)}$ values. At the lower end of the $K_{(-10)}$ range tested, drainage fluxes approximately halve with a reduction in $K_{(-10)}$ values to 0.2 times the base case values. At the higher end of the range, fluxes are approximately three times as much with $K_{(-10)}$ values increased to 5 times the base case values. The relationship between the drainage and $K_{(-10)}$ values is not quite linear, however, within the range of values tested here, there is no steep part of the curve that would lead to non-unique calibrated parameter value combinations. These results also provide some guidance for interpreting model output results and indicate the likely scale of error in predicted fluxes in comparison to the scale of error in the parameter values used.

Clearly there is the opportunity for errors to be significantly large if erroneous $K_{(-10)}$ values are used in the model. However, the minimal effect of the WRC parameters and relatively

high sensitivity to the $K_{(-10)}$ values indicate that in the automated calibration of models, the optimised $K_{(-10)}$ values would have to be closely matched to the effective values in the real soil profile for the model to achieve an acceptable fit between observed and modelled soil moisture values. Furthermore, dominance in these results of this parameter and the near-linear nature of the relationship between the modelled drainage fluxes and $K_{(-10)}$ values is likely to prevent the creation of non-unique parameter value combinations from the automated calibration process.

4.4 Model Output: Water Flux Estimates for Monitored Study Sites

The outcome of the calibration and optimisation process is a soil water transport model that is intended to be used to estimate the effects of irrigation practices on the components of the soil water balance at the monitored points. The hydrologic conditions at the monitored points are not expected to be representative of the entire irrigated plot because of spatial variability of the soil profile characteristics and other factors affecting the soil water regime, such as crop cover and irrigation distribution. However, a carefully calibrated and optimised model for two points in the plot allows an examination of the effects of differing agricultural management practices on the balance between irrigation, evapotranspiration and drainage amounts in the horticultural setting. These would otherwise be difficult to estimate accurately because of the difficulty in estimating or measuring drainage or actual evapotranspiration.

Figure 4.10 shows the model output for the whole year monitored, from September 2003 to September 2004 for study site PGR, Point 1 and Point 2. Over the two irrigated crops grown through the year, using a total of 917 mm of irrigation water and subject to 352 mm of rain, there was a total of 1148 mm (1145 mm) evaporated and transpired, 169 mm (170 mm) drained below the soil profile, and 48 mm (46 mm) less water in the soil profile at the end compared to the start of the year. Significantly, the majority of drainage in the monitored year appears to occur not as a direct result of excess irrigation applications, but as a result of winter rain falling on soil that already has a high water content due to summer irrigation.

Graphs of the outputs of evaporation, transpiration and drainage predicted by the models for the primary broadacre vegetable study sites provide an indication of the drainage occurring beneath the root zone with the irrigation, rainfall, and evaporation conditions present during the period of the monitored crop. The rainfall and irrigation amounts illustrated in Figure 4.10 are measured amounts rather than model simulation outputs and are shown here to compare with the graphs of model-simulated evaporation, transpiration and drainage.

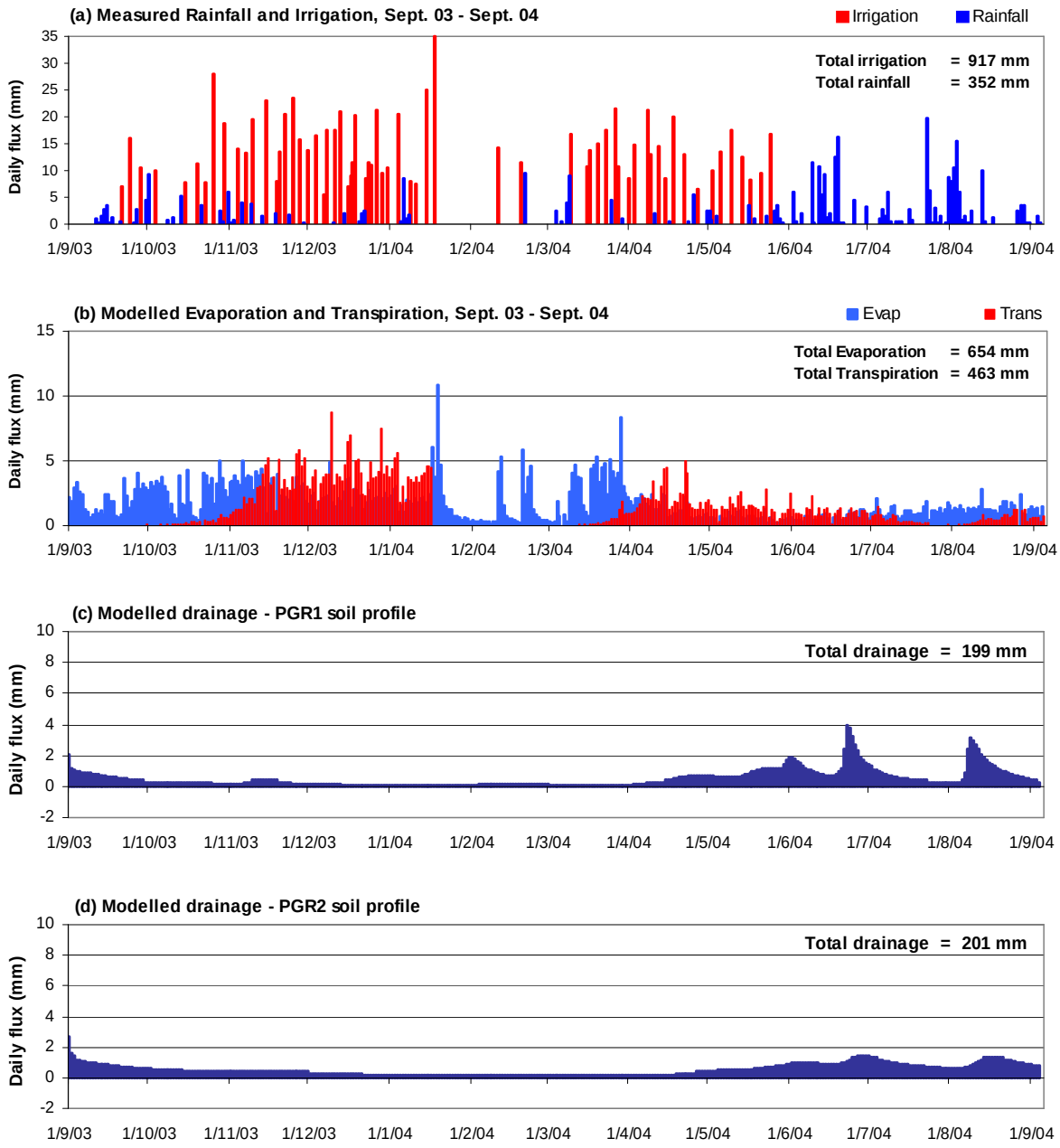

Figure 4.10 (a) Input data of measured rain and irrigation at site PGR result in (b) simulated ETa at study site PGR, (c) simulated drainage in the soil profile at point PGR1, and (d) simulated drainage in the soil profile at point PGR2.

The drainage flux predicted by the models for points 1 and 2 are almost the same, although it can be seen from Figure 4.10 (c) and (d) that drainage flux is less labile at point 2, where daily fluxes vary from 0 mm/d to approximately 1.5 mm/d, than at point 1, where the predicted drainage stops altogether between January and April but reaches peaks of up to 4.8 mm/d in June and August. This is due to differences in the soil hydraulic characteristics in the models for the two points.

Most significant in the outputs from these models is the illustration of the importance of winter rainfall, rather than summer irrigation, in causing drainage to occur. The majority of drainage occurring at the PGR study site occurs between the 26th May and 3rd September 2004, after irrigation had ceased on the 25th May. Conversely, through the summer months from mid October to the end of March, there is almost no drainage even though the majority of irrigation occurs through this period. It is apparent from these model predictions that the irrigation applied during the summer months at the PGR study site was at least balanced by the evapotranspiration demand. In the winter months, when crop cover has reduced, and the potential for both transpiration and evaporation is lower, a significant proportion of the rainfall during this period drains through the soil profile.

Although study site PGR is the only broadacre vegetable study site that was monitored for a full year, the model predictions for sites HX and TR (figures 4.11 and 4.12) provide some important insights into the different rates of evapotranspiration and drainage between summer and winter crops.

The predicted drainage is remarkably similar at points HX1 and HX2 even though there are some distinct differences in the optimised soil hydrological parameters in the two models. Although the modelled period at this study site is only five months, the total drainage is very close to the total for the whole year modelled for study site PGR. However, the crop monitored at study site HX was grown through the part of the year that appears to typically have the highest drainage volumes due to higher rainfall and lower potential ET conditions. Over the a similar five month period at study site PGR, the model-predicted drainage is approximately 144 mm with no winter irrigation occurring during that period at that study site.

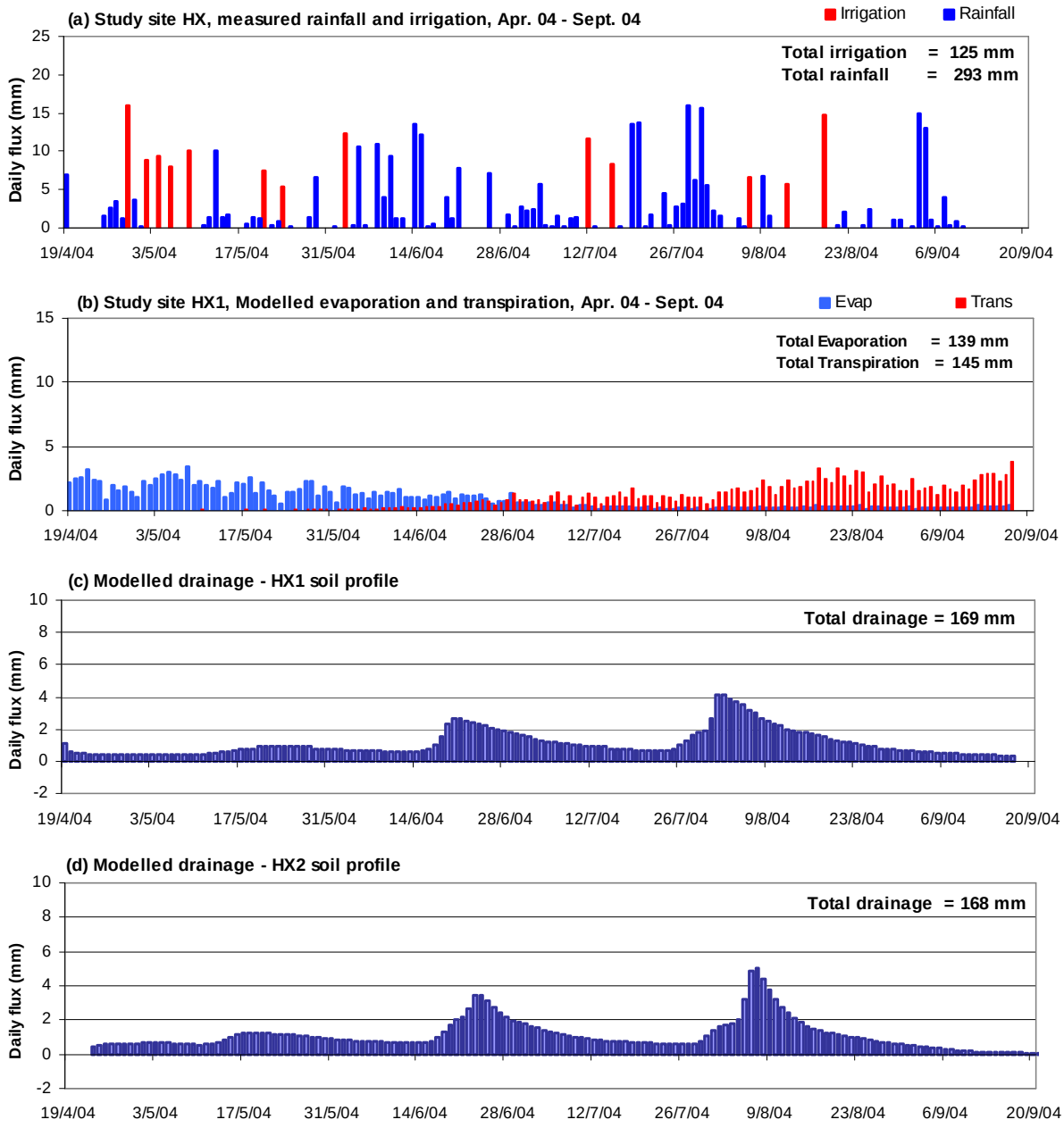

Figure 4.11 Model simulations of ETa and drainage resulting from the measured rain and irrigation (a) and modelled evapotranspiration (b) with the soil profile at monitoring point HX1 (c) and the soil profile at monitoring point HX2 (d).

Drainage beneath the crop monitored at study site TR2 differs significantly between the two models representing the two monitored points, with point TR2 having approximately half of the drainage predicted for TR1. This is a result of differences between the optimised soil hydrological parameters at the two points, and reflects the expected effect of the observed matric potentials at the two points. At point TR1 there was constantly a potential gradient between the 30 cm and 110 cm depths, which would have enhanced downward movement of water. At point TR2 there was a much smaller matric potential gradient, and sometimes a negative gradient, between depths, particularly during the latter three months of the monitored

period. The effect of this would have been to restrict downwards movement of water and subsequently decrease the amount of drainage occurring.

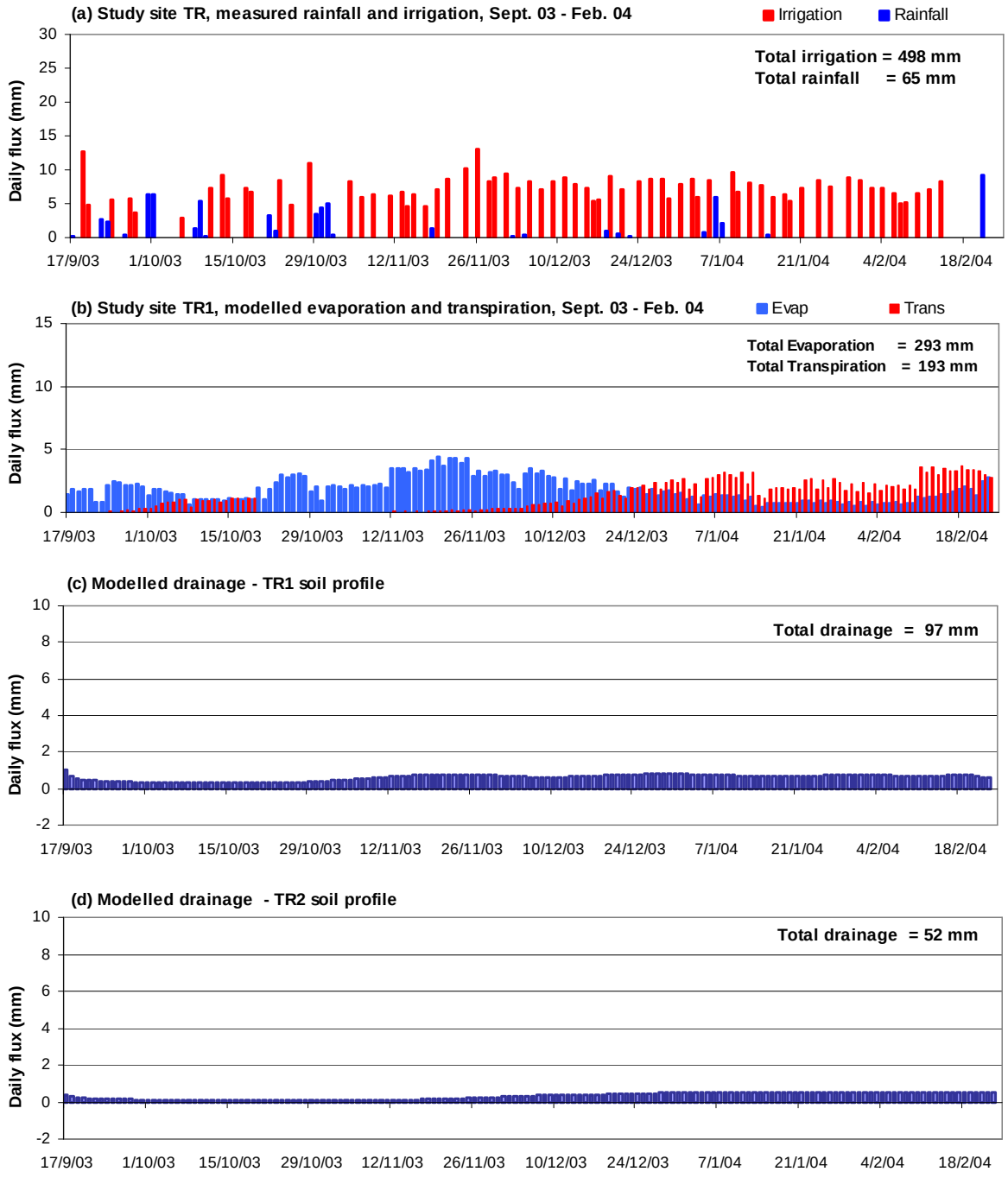

Figure 4.12 Model simulations of ETa and drainage resulting from the measured rain and irrigation (a) and modelled evapotranspiration (b) with the soil profile at monitoring point TR1 (c) and the soil profile at monitoring point TR2 (d).

Although the amount of irrigation applied during the monitored period at the TR site is approximately four times as much as that applied over a similar amount of time to the monitored crop at the HX study site, the predicted drainage flux at the TR study site is significantly less than that predicted at the HX study site. This occurs as a result of the higher

rainfall and lower evaporation experienced by the winter crop at study site HX compared to the summer crop at study site TR. This difference helps to exemplify the importance of to total drainage beneath crops of seasonal differences in rainfall and evaporation conditions. When considering the variables influencing drainage beneath a vegetable crop, these are much more significant variables than irrigation volumes or irrigation scheduling.

4.5 Comparison with Direct Estimates of Fluxes Using Field Tensiometer Readings

The soil matric potential measurements made at the field study sites can be used to determine the soil water potential gradient at each point that readings were taken. The tensiometers readings are corrected for the effect of the length of the water column in the tensiometer and then both the matric potential and the gravitational potential at each depth are summed to give the total head potential at each tensiometer depth. The difference in total potential divided by the distance between measurement depths gives the potential gradient between the two depths. Vertical water movement between these depths, in saturated or unsaturated conditions, should then be in the direction of the potential gradient. Using Campbell's water retention and unsaturated conductivity functions, the hydraulic conductivity of the unsaturated soil can be calculated according to the mean matric potential between the two measurement depths at the time of each measurement. The vertical water flux between the two depths can then be approximated as the product of the potential gradient times the hydraulic conductivity. By applying this approximation of vertical flux for each of the dates on which matric potential measurements were taken, a times series of flux approximations can be created against which the modelled fluxes for each study site. These approximations have been made for one of the monitoring points at each of the three modelled study sites. The soil hydraulic parameters; Campbell's 'a' and 'b' parameters and K(-10), used for these approximations were the same as the optimised values used in the models described in Section 4.4. The value of these approximations is to check that the direction and approximate quantity of water flux indicated by the models is in agreement with that which is indicated by the field measurements of matric potentials. The flux quantities are not expected to match exactly as the matric potential measurements were taken at intervals of 1 – 2 weeks and the fluxes between measurement intervals have been averaged across the interval. In contrast, the LEACHM modelled fluxes result from multiple flux calculations on each day based on the series of head gradients between each soil depth segment, derived from the upper and lower boundary fluxes (rain, irrigation evaporation, transpiration and drainage) and the calculated flux between each

segment in each sub-daily time step. The results of these approximations are shown in the graphs in figures 4.13 to 4.15.

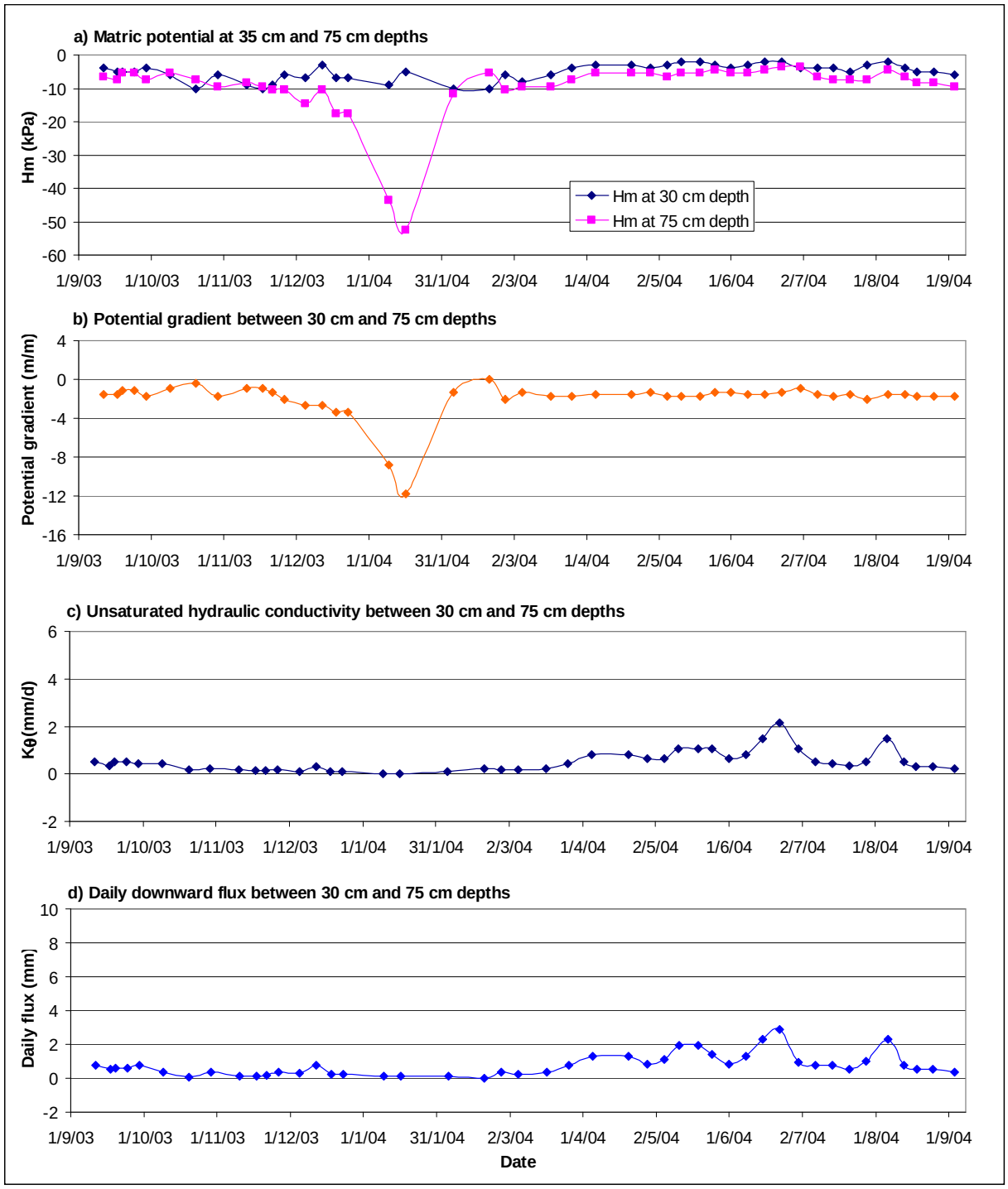

Figure 4.13 Direct approximation of fluxes at monitoring point PGR1, based on a) measured matric potentials at 30 cm and 75 cm, b) soil water potential gradient between these depths, and c) unsaturated hydraulic conductivity at the mean matric potential between 30 cm and 75 cm these depths. Note, positive vertical fluxes shown in (d) are downward.

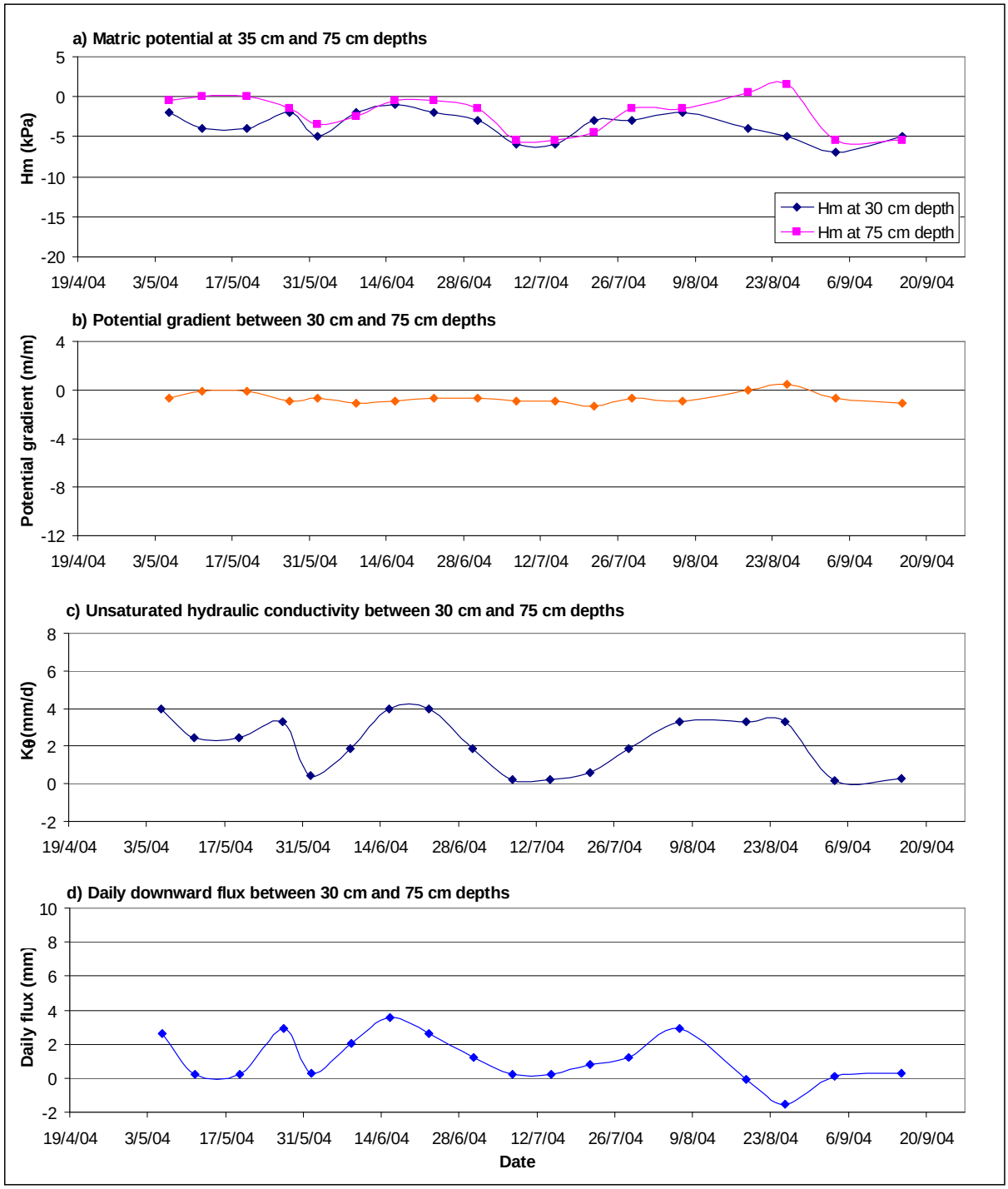

Figure 4.14 Direct approximation of fluxes at monitoring point HX1, based on a) measured matric potentials at 30 cm and 75 cm, b) soil water potential gradient between these depths, and c) unsaturated hydraulic conductivity at the mean matric potential between 30 cm and 75 cm these depths. Note, positive vertical fluxes shown in (d) are downward.

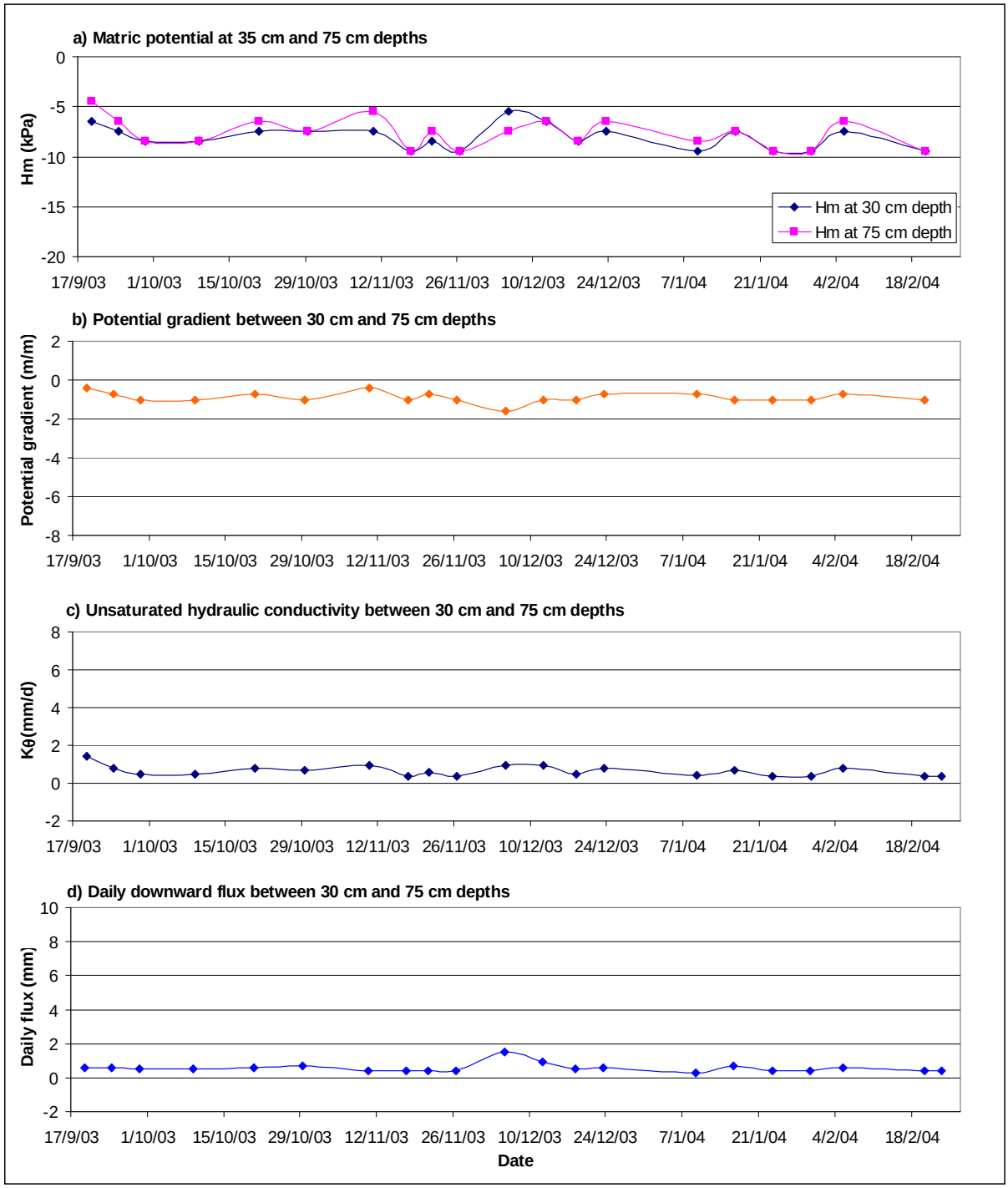

Figure 4.15 Direct approximation of fluxes at monitoring point TR1, based on a) measured matric potentials at 30 cm and 75 cm, b) soil water potential gradient between these depths, and c) unsaturated hydraulic conductivity at the mean matric potential between 30 cm and 75 cm these depths. Note, positive vertical fluxes shown in (d) are downward.

In Figures 4.13 to 4.15, matric potentials were only measured and gradients, K(q) and flux values were only calculated for dates represented by points on the graphs. Lines between points are only an interpolation of these values.

The graphs of the downward flux approximations in Figures 4.13 to 4.15 are comparable to the modelled fluxes shown in Figures 4.10 (c), 4.11 (c) and 4.12 (c). The approximations are

in good agreement with the model predictions of the vertical flux direction and in fairly good agreement with the flux quantities. The total fluxes over the aproximated periods were 242 mm, 141 mm and 87 mm for monitoring points PGR1, HX1 and TR1 respectively. These compare with 199 mm, 169 mm and 97 mm respectively for the LEACHM modelled flux totals. The total fluxes directly approximated for HX1 and TR1 monitoring points are expected to be less than the totals predicted by the models as the first and last matric potential measurements at those sites span a period that was shorter than the modelled period by about 17 days for HX1 and 6 days for TR1. The higher total flux in the approximation for PGR1 is due to the coarse integration of daily fluxes between dates of matric potential measurements, in which the mean of the fluxes calculated on two consecutive measurement dates is taken to occur in every day between those dates.

The key finding here is that the direction and approximate magnitudes of the vertical water fluxes calculated directly from the soil matric potential measurements is in agreement with the fluxes predicted by the models for these monitoring points.

4.6 Sensitivity of Simulated Drainage Fluxes to Modelled Soil Profile Combinations

Further to the previous analysis in section 4.3 of the model's sensitivity to soil hydrologic parameters, it is also useful to test whether the combination of all parameters values derived from the optimisation process has resulted in a set of unrealistic values that only produce sensible model output when the particular combination of crop, weather, and irrigation data used in the optimisation process is applied. Figure 4.16 shows the results of running the model based on 12 months of data from monitoring point PGR1, compared with the output from the same model but with the soil profile description substituted by the soil profile descriptions from the other five primary monitoring points.

With all other model conditions being equal in all six of these models, the differences in the soil profile descriptions can be assessed. The similarity in the patterns of drainage through the 12 months of the model confirm the seasonal nature of the drainage fluxes and the tendency, independently of the soil profile, for fluxes to respond most significantly to periods of more intense rainfall between June and September.

The two modelled soil profiles representing the PGR study site exhibit the greatest drainage flux under these conditions. This is in accordance with the soil profile observed at that site, which had a deep, loamy-sand A-horizon to a depth of greater than 50 cm, and then a deep sandy clay loam B-horizon to a depth of at least 100 cm. This soil structure is expected to be a more freely-draining than that in the soil profiles observed at study sites HX and TR. At site HX, there was a sandy-loam A-horizon to a depth of approximately 40 cm, overlying a sandy clay B-horizon, which is expected to have reasonable drainage characteristics, but not as freely-draining as the soil profile at the PGR site. At the TR site there was a thin loamy-clay-sand A-horizon overlying a sandy clay, which became a calcareous clay below approximately 80 cm. This is expected to have poorer drainage characteristics, as may be reflected by the lower drainage predictions for the TR soil profiles in Figure 4.16(g) and (f).

None of the drainage flux predictions shown in Figure 4.16 are unrealistic and none result in exceptionally high or low drainage fluxes that would suggest a critical error in any of these model soil profiles. The sensitivity of the drainage flux in these models to varying soil profile parameters has particular importance when up-scaling the models to provide predictions for the whole NAP area, as discussed in Chapter 6.

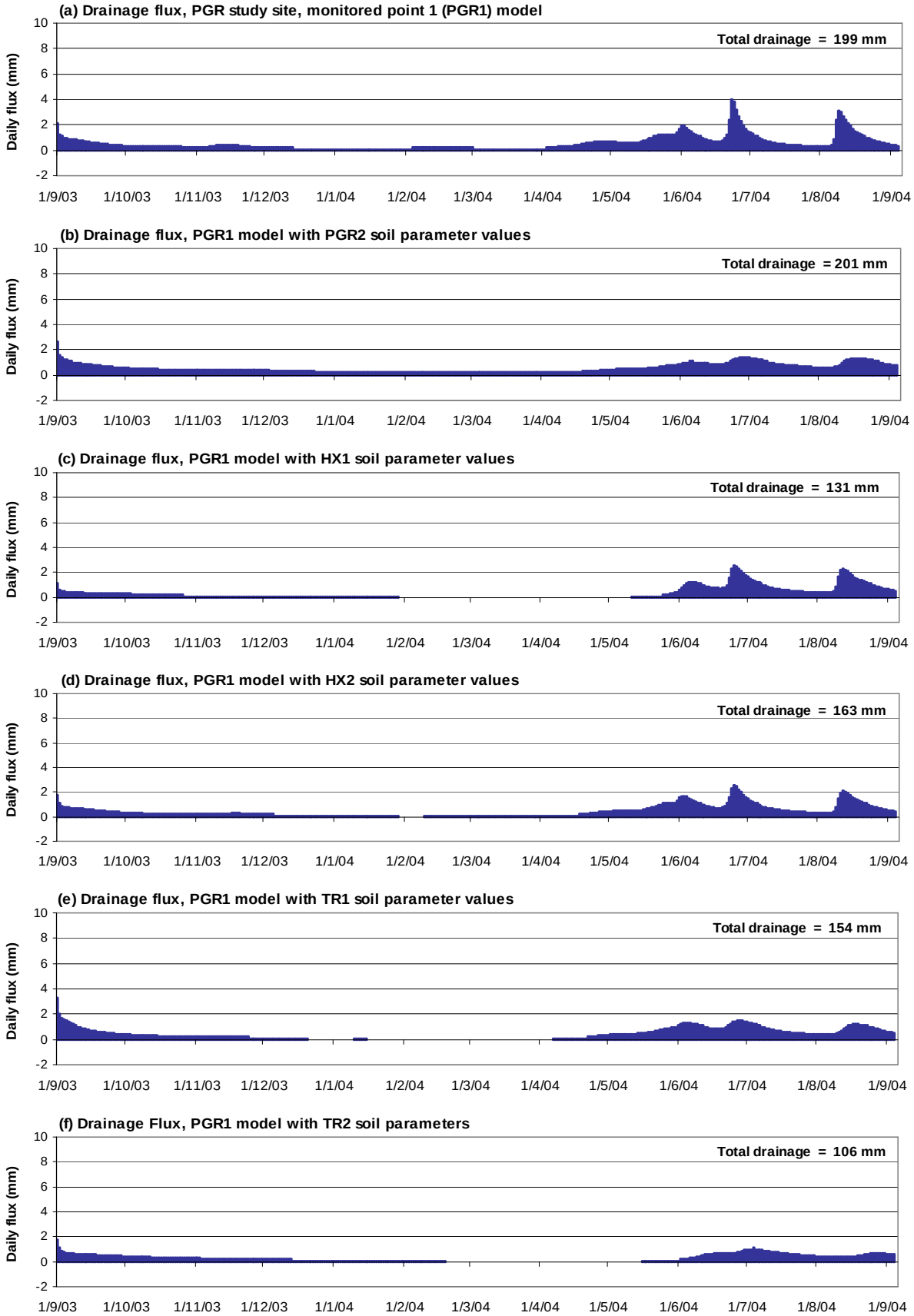

Figure 4.16 Predicted drainage fluxes over a one-year period with soil profile descriptions from models for all monitored sites superimposed on the model of study site PGR1. The model is run with all the same water applications, crop data and weather/ETo data as the original PGR1 model, based on measurements at the PGR study site.

4.7 Sensitivity of Model Predictions to Local and Regional ETo Data

The models discussed in Section 4.4 used potential evapotranspiration data from two sources. The models for the PGR site employed ETo data derived from the weather records collected by the on-site weather station at site PGR. The models for the TR and HX study sites employed ETo data derived from weather records from the BOM weather station at the RAAF Edinburgh air field, which is located closer to these two site than the weather station at the PGR site. While the on-site weather station at study site PGR provides on-site weather conditions at the exact location of the monitored crop, allowing for a very well calibrated model to be developed for that study site, the weather record available from the BOM Edinburgh station covers a longer timescale. If the models are to be run over a longer timescale to provide an understanding of the inter-annual variation of water fluxes, then the later is a more appropriate source of weather data. However, as the outcomes of the model are sensitive to the ETo data employed, and because weather conditions vary across the scale of the NAP area, there is a potential for a degree of inaccuracy to be introduced by the use of ETo data derived from weather data collected at a location other than the study site. By comparing the water flux predictions of models that vary only in their source of ET data, an assessment can be made of the degree of error that may be introduced.

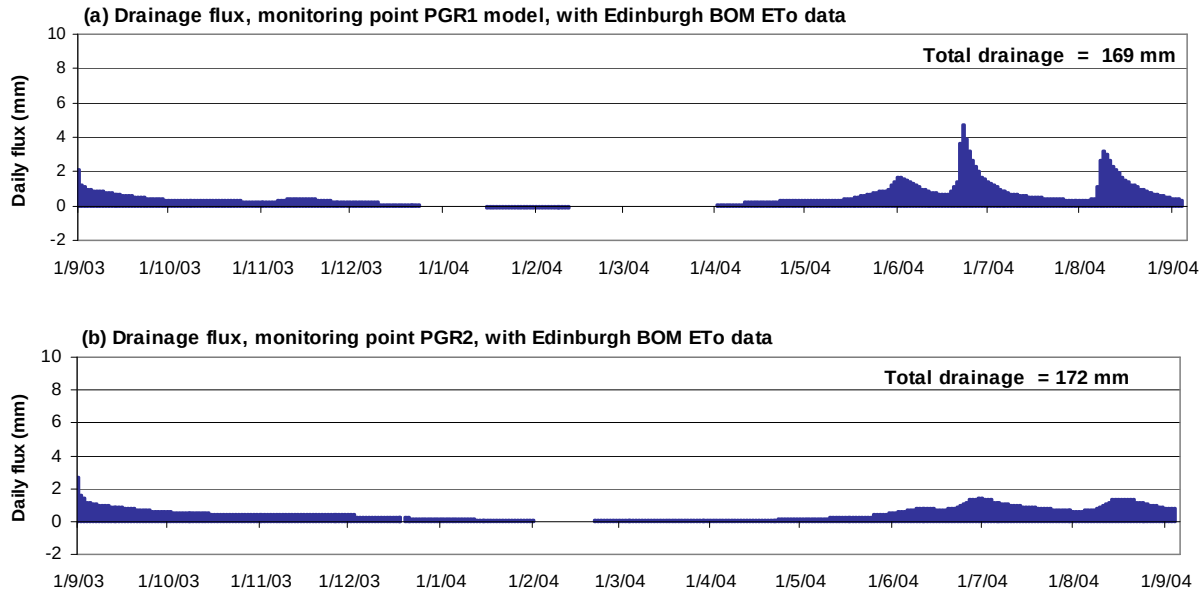

Figure 4.17 Predicted drainage fluxes over a one-year period at the PGR study site when the on-site ETo data are replaced by ETo data derived from weather records from the BOM Edinburgh air field weather station.

Comparison of these outputs with the original outputs shown in Figure 4.17 shows that with the alternative ETo data the seasonal patterns of drainage are preserved, but the overall

drainage over the year has reduced by approximately 15%, from 199 mm to 169 mm at location PGR1 and from 201 mm to 172 mm at location PGR2.

If this comparison is repeated for the modelled study site soil profiles from HX and TR where the original model employed ETo data from the BOM Edinburgh weather station, it is found that there is a consistently lower drainage flux when the BOM Edinburgh ETo data are used than when using ETo data derived from the PGR site (Table 4.9). In simulations of all three study site soil profiles there is approximately 15% – 19% less drainage with the RAAF Edinburgh BOM data than with the PGR study site data. These findings imply firstly that on a yearly time scale, weather conditions at the PGR study site are less conducive to evaporation and transpiration than conditions at the RAAF Edinburgh BOM weather station, approximately 6 km to the south. Secondly, the drainage predicted by the models over a period of a year is sensitive to apparently small differences in evaporation conditions.

The decrease in drainage when using the Edinburgh BOM ETo data differs with soil profile descriptions. There is clearly a greater percentage decrease with the TR study site soil profile than with the PGR study site soil profile. It is thought that this is due to the more clay-rich soils and poorer drainage characteristics of the soils at the TR site, causing more water to be held at the surface and allowing daily ETa to be closer to the daily ETo.

Table 4.9 Comparison of total drainage predicted by 1-year simulation with varying model soil profile descriptions and using 1) reference ET (ETo) data derived from PGR study site weather station data and 2) reference ET data derived from BOM Edinburgh airfield weather station.

Study Site / Monitored Point	1-year drainage using PGR Site ETo data (mm)	1-year drainage using RAAF Edinburgh BOM ETo data (mm)	% Difference
PGR/1	199	169	-15.1
PGR/2	201	172	-14.4
HX/1	131	110	-16.0
HX/2	163	140	-14.1
TR/1	154	127	-17.5
TR/2	106	86	-18.9
	Cummulative Eto, 1/9/03 to 1/9/04		
	PGR Site ETo data (mm)	RAAF Edinburgh BOM ETo data (mm)	% Difference
	1447	1496	3.4

Figure 4.18 illustrates the differences in reference ET at the RAAF Edinburgh airfield BOM weather station compared to the PGR site weather station. While less than 20 high-ET days during the 1-year period resulted in considerably higher ETo at the PGR study site on those days, the majority of days had moderately higher ETo at the RAAF Edinburgh airfield.

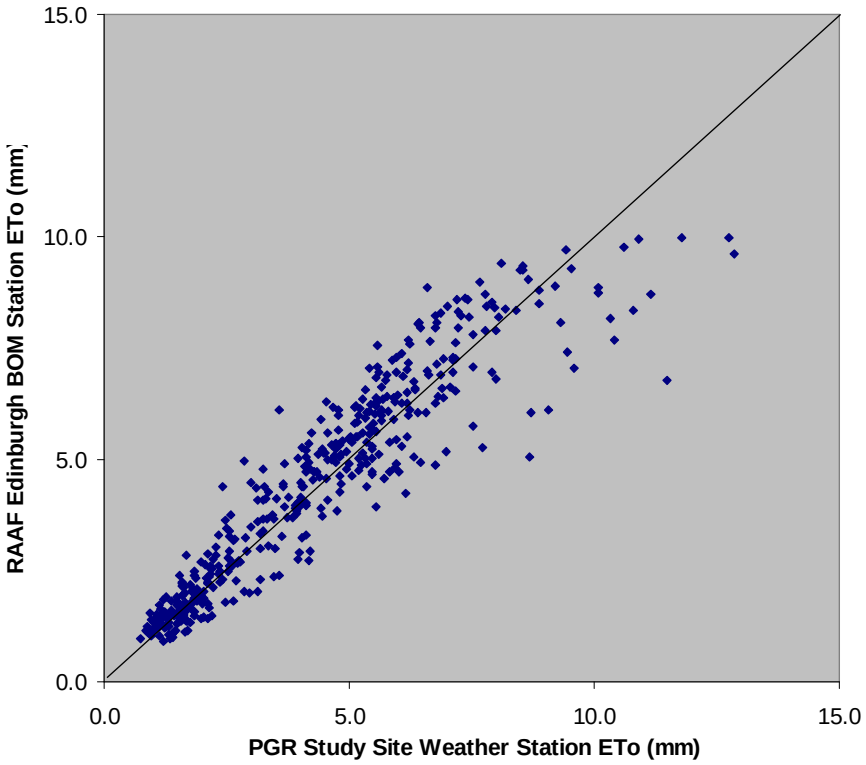

Figure 4.18 Regression of reference daily ETo values derived from PGR study site weather station data and daily ETo values derived from RAAF Edinburgh airfield BOM weather station data over the 1-year period of the model simulations from 1/9/2003 to 1/9/2004.

In summary, the comparisons in this chapter of drainage predicted by LEACHM models with varying soil profiles and evapotranspiration parameters has demonstrated that the model is sensitive to variations in the parameter value combinations that encode these environmental conditions in the model. These model predictions of drainage flux at each study site are also sensitive to different crop growth and crop transpiration parameters. Those demonstrated in this chapter have been calibrated with crop growth and transpiration parameters as recorded at the individual study sites during the period of monitoring. They are intended here to provide an indication of the amount of deep drainage that may be expected in a number of typical and real irrigated crop growth situations in the NAP with typical horticultural practices in the region. Further modelling demonstrated in Chapter 6, in which these models are altered to represent the variety of scenarios across the NAP, will illustrate the impact of differing crop type parameters on deep drainage fluxes.

4.8 Soil Salinity Modelling

The LEACHC model calculates the soil inorganic chemistry for the major dissolved cations: Ca, Mg, K, Na, and anions: Cl, SO_4^{2-}, CO_3^{2-}, HCO_3^-, and takes account of ion adsorption/desorption using Gapon selectivity coefficients for the major cations. Equilibrium concentrations of solution and exchange phase ions are recalculated for each model soil segment after each of a chosen number of times steps (a 20 time step interval was used in the models demonstrated here).

Initial ion concentrations in the exchange and solution phase in the monitored soil profile were approximated for soil at three depths at each of the monitored study sites using a combination of data from analyses of exchange cation concentrations in soil samples and analyses of dissolved ion concentrations in soil solution extracts and lysimeter leachate samples (Tables 3.3 and 3.4). To provide initial soil chemistry data for input to the LEACHC simulation, solution and exchangeable cation extract concentrations were converted to equilibrium concentrations of major ions in solution and exchange phases at a field soil water content considered to be a suitable for each study site. The concentrations of exchangeable cations were converted to concentrations equivalent to all exchange phase cations from 20g of soil dissolved in 100 ml water. Concentrations of exchange phase cations were then added to 1:5 solution extract cation concentrations to provide total extractable cations in a 1:5 soil: water mixture. The sulphur concentrations of the solution extract was assumed to be all in the form of SO_4^{2-} to provide part of the charge balance of cations in solution. A nominal initial carbonate concentration of 5 mg/l was used and the remainder of anions required to balance charges were assumed to be chloride. With these concentrations as input data, the chemical equilibrium program Chemeq (Hutson, 2003), provided with the LEACHM software suite, was used to determine selectivity coefficients and equilibrium concentrations of major cations and anions in the soil at saturation and at the initial soil water content to be used in the LEACHM simulations. The Chemeq program was run several times, with the Gapon selectivity coefficients and initial carbonate concentrations in the input data adjusted between each run, until the equilibrium concentrations of exchange phase cations and ions in solution was in agreement with measured concentrations in the soil samples and soil solution samples (from lysimeters and suction cup samplers).

Irrigation water samples were taken half way through the growing period of the first crop monitored at this site and analysed by ICP for major cation and anion concentrations. These concentrations were used as the dissolved ion concentrations of the irrigation water for the

duration of the simulation. While the salinity of the water delivered by the VPS varies throughout the year, the irrigators at each location simulated here store the water in open agricultural dams prior to use, which has the effect of integrating the quality of water delivered over several days or weeks.

When simulating the vertical water and salt fluxes of the NAP on the broad area scale and over many years, we are concerned with total annual water fluxes and with changes in the total salt content of the soil over a number of years. In this broad scale analysis we are not concerned with changes in the inorganic chemical composition or changes in the concentrations of individual ionic species. In view of this there is an opportunity to simplify the model by treating the total inorganic salt content of the soil as a single chemical and modelling the changes in concentration of that chemical without consideration of ion exchange equilibria. This can be achieved using the LEACHP model to provide an approximation of the changes in total dissolved salt concentration by treating the total of dissolved salts as a single dissolved chemical. Rain and irrigation water salts content are also expressed as a concentration of a single chemical in the model's input data files. The vertical transport of salt through the soil profile is then simulated within the LEACHP model with regard to only to the infiltration and drainage fluxes at the upper and lower boundary and the advective and diffusive transport processes through the soil profile.

The following graphs of simulated EC provide a comparison of the soil salinity modelled in LEACHC, in which all major ion concentrations in solution and exchange phases are considered separately and ion exchange processes are included, and in LEACHP, in which only advective and diffusive transport of the total dissolved salt content in response to the vertical transport of soil water is modelled. In the LEACHC data files, the concentrations of ions in solution in the rain and irrigation water and in the soil water in each segment are listed as individual ion concentrations in mmol/l, and cations in the exchange phase in each soil segment are listed in mmol/kg. Selectivity coefficients are also listed for each soil layer. In the LEACHP data files, concentrations of the sum of the dissolved salts (listed in the LEACHC data files) in each soil layer are listed in mg/kg and those in the rain and irrigation water and in the soil solution are listed in mg/l. No selectivity coefficients are listed as exchange phase equilibria are not calculated in the model.

The EC of the soil solution samples is indicative of the TDS of the soil solution when the soil is at or close to saturation. Water is expected to leach into the lysimeters at soil matric

potentials between 0 kPa (saturation) and -5 kPa. The simulations illustrated here are based on recorded irrigation and rainfall data, and calibrated against soil matric potential data.

The simulated soil moisture EC (Figures 4.16 – 4.18) shows the EC at the model-predicted soil moisture content in the soil at 70 cm depth at the time of each time step.

It is not expected that the simulated soil salinity will match the absolute values and variation of the measured EC in collected lysimeter leachate samples. Firstly, the model provides only an approximation of the flow of water and inorganic solutes through the soil profile and can not exactly match these flows through the real monitored soil profile. Secondly, the simulated EC is expected to differ from lysimeter leachate EC since the simulated EC is based on the soil moisture TDS concentration on each day of the simulation. This concentration increases as the soil moisture content decreases. The lysimeter leachate concentration is an integration of water that has leached from the soil under conditions of near or complete saturation shortly after rain or irrigation events. In these conditions the soil solution is at its least concentrated. For the majority of the simulations illustrated here, the simulated soil water potential was between -5 kPa and -20 kPa, resulting in higher TDS concentration and EC than would be expected in the lysimeter leachate.

However, if the model-simulated EC is able to give an approximation of the absolute values and the trend of soil solution EC under the monitored and modelled conditions, then the model is expected to give a useful indication of the development of soil salinity under differing crop and irrigation conditions in similar soil conditions. Similarly, if the duration of the simulation is extended, the model may provide a useful indication of soil salinity development over a longer timescale than the monitored periods that the models are set up to reproduce here.

The graphs in Figures 4.19 To 4.20 show the simulated soil solution EC at the two monitored points at each of the three study sites over the monitored period simulated within each model. These are a product of the same soil water flux models for the monitored period at each study site discussed and illustrated in section 4.4. Also shown are the measured ECs of lysimeter or suction cup leachate collected at the two monitored points within each study site during the period of monitoring.

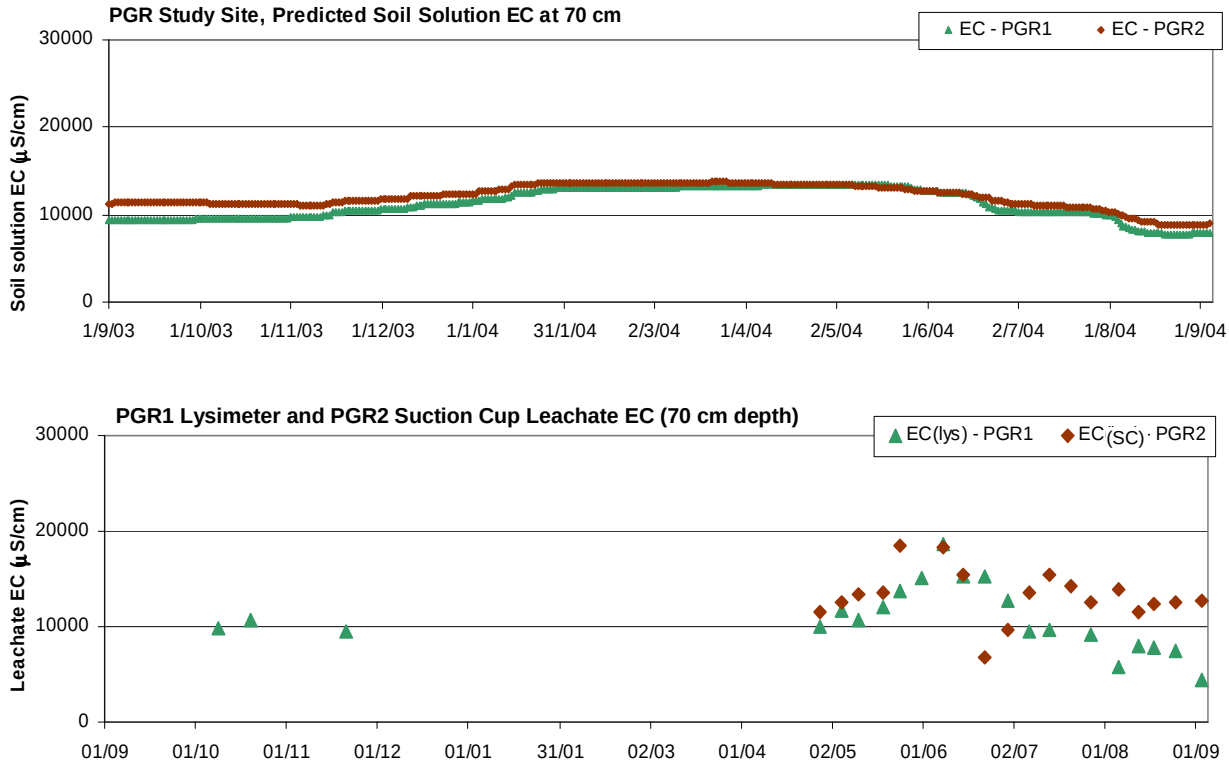

Figure 4.19 Simulated soil solution EC at 70 cm depth in monitored study site locations PGR1 and PGR2, compared with measured EC of leachate collected in lysimeters and suction cup samplers over a period of 1 year from September 2003 to September 2004. The gap of approximately five months in the lysimeter data is due to the absence of leachate in lysimeters and suction cups over the summer months.

The model simulation of soil solution EC and corresponding measurements of lysimeter leachate EC for study site PGR are shown in Figure 4.16. For the limited parts of the year of the simulation during which there are lysimeter leachate measurements to compare with the predictions of the model simulation, the model provides a good simulation of both the range of absolute values of soil solution EC and a fairly good indication of the variation of EC over the final three months of the simulation. There is an absence of lysimeter data for five months in the 1-year simulated period, during which no leachate drained into lysimeters at this study site. The model simulation predicts an elevated EC through that period, which is expected as the soil moisture content was lower at that time, which would have increased the concentration of salts in solution. Significantly, the absence of lysimeter leachate through the five month summer period concurs with the prediction of the soil water flux model discussed in Section 4.4 and illustrated in Figure 4.10, which indicates negligible amounts of soil water flux though the base of the modelled soil profile at this study site through this period.

Furthermore, leachate salinity was higher at PGR2 than at PGR1 over the period when drainage fluxes were predicted to be lower at PGR2 than at PGR 1, consistent with expectations.

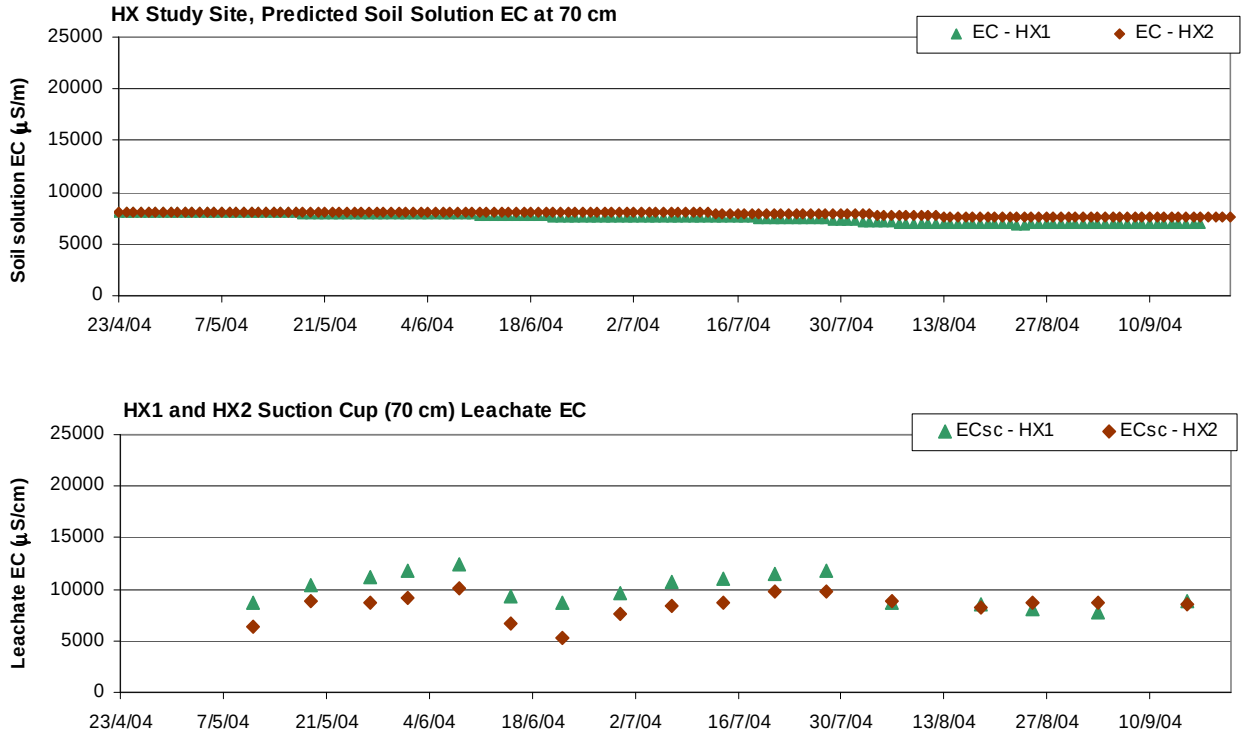

Figure 4.20 Simulated soil solution EC at 70 cm depth at monitored points HX1 and HX2, compared with measured EC of leachate collected in suction cup lysimeters at the same locations over a monitored period of 1 year from April 2004 to September 2004.

The model simulation of EC at the HX study site (Figure 4.20) indicates a narrower range of variation of soil solution EC than indicated by the suction cup lysimeter leachate EC over the monitored period. However, while the model simulation of this study site does not provide a good prediction of the variations in EC, it has predicted the starting and ending soil solution EC quite well and importantly, predicts no significant upwards or downwards trend in EC under the conditions in which this crop was grown, accurately reflecting the overall trend in the leachate EC over this period.

The model simulation of soil solution EC at the TR study site (Figure 4.21) predicts a higher EC than that measured in lysimeters at the study site. The measured ECs at this study site were quite different between the two monitored points, however, the starting soil chemistry in the models representing the two monitored points were both derived from soil chemistry of only one location at the site. Only the soil profiles, crop and irrigation schedules differed in the two models.

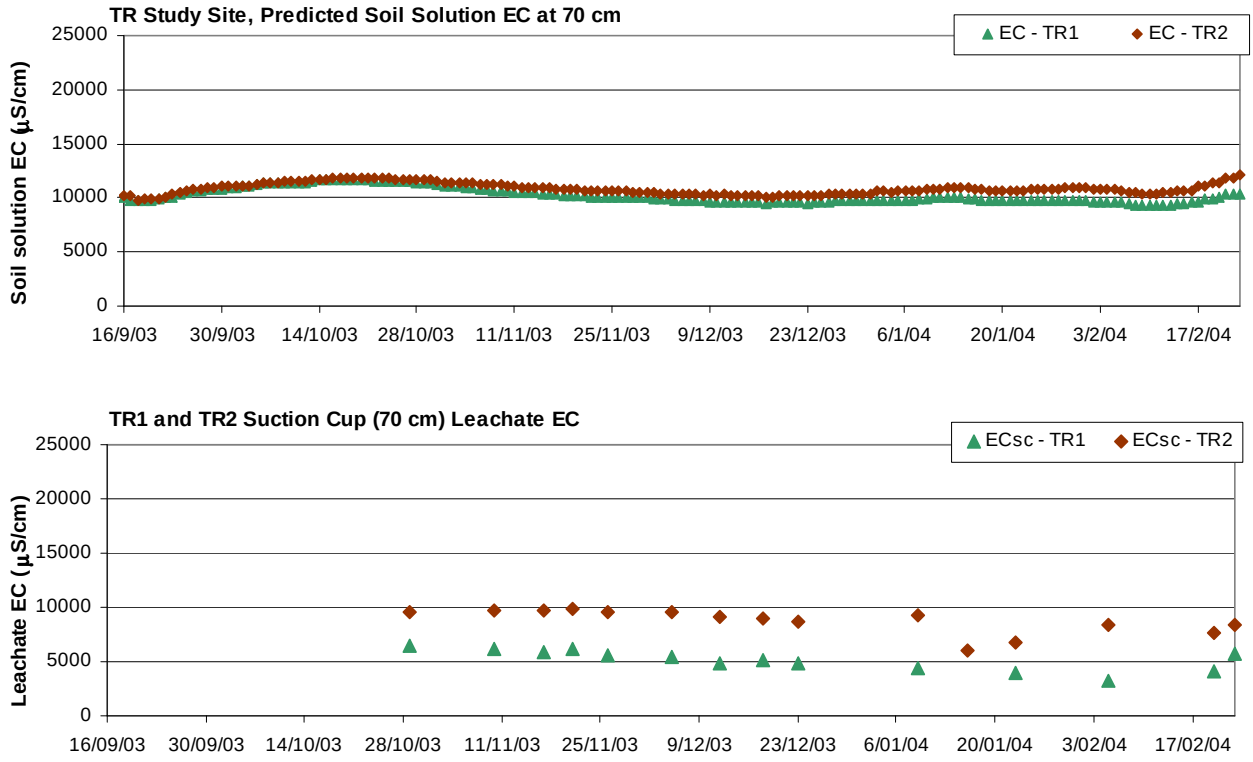

Figure 4.21 Simulated soil solution EC at 70 cm depth at monitored points TR1 and TR2, compared with measured EC of leachate collected in suction cup lysimeters at the same locations over a monitored period of 1 year from September 2003 to September 2004.

The model produces a good prediction of the trend and variation of the real soil solution EC over the period, suggesting that the model is reasonably accurate in its simulation of the soil water and salt flux processes. However, the starting soil chemistry used in the model creates a simulated soil solution EC that is too high to represent location TR1, which has significantly lower EC than location TR2. For location TR2 the pattern of variation of EC over the period for which suction cup leachate measurements are available is fairly well represented by the model simulation, with a slight decrease in soil solution EC between October 2003 and February 2004, with a slight increase at the end of the monitored period.

4.8.1 Modelling soil salts as a single solute

The running of LEACHC with all the combinations necessary for the catchment scale model described in Chapter 6 becomes prohibitively time-consuming as the model for each scenario can take a number of days to run. However, the same scenario can be simulated in a much shorter time by using the LEACHP model, which simulates the soil salinity changes by treating the total of the dissolved inorganic ions in the soil as a single chemical. In this method, the TDS concentrations of the soil solution, irrigation and rain water are listed as the

single chemical for LEACHP to simulate. This allows a time saving approach to the simulation of soil salinity development, but the method must be tested to check its performance compared to the LEACHC model.

The extension of these models over greater lengths of time, as demonstrated in Chapter 5, and over greater area, as demonstrated in Chapter 6, is based on the models developed for study site PGR. This is because that study site has a greater length of monitoring data than the other study sites, which allowed the models to be calibrated more effectively.

The graph in Figure 4.22 shows the soil solution EC at 70 cm depth as simulated by LEACHC and LEACHP models for location PGR1 at the PGR study site. The LEACHC simulation is the same as shown for location PGR1 in Figure 4.10 (page 78). The LEACHP simulation uses the same, soil hydrologic data, crop, irrigation, ETo and rainfall data as the LEACHC simulation but differs in the soil and irrigation chemistry sections of the input data files. Where the LEACHC data file contains concentrations of individual major cations and anions in soil solution and exchange phases and in irrigation and rain water, the LEACHP data file contains only a data of the total salinity, expressed in mg/L TDS in each soil layer segment and the irrigation and rain water.

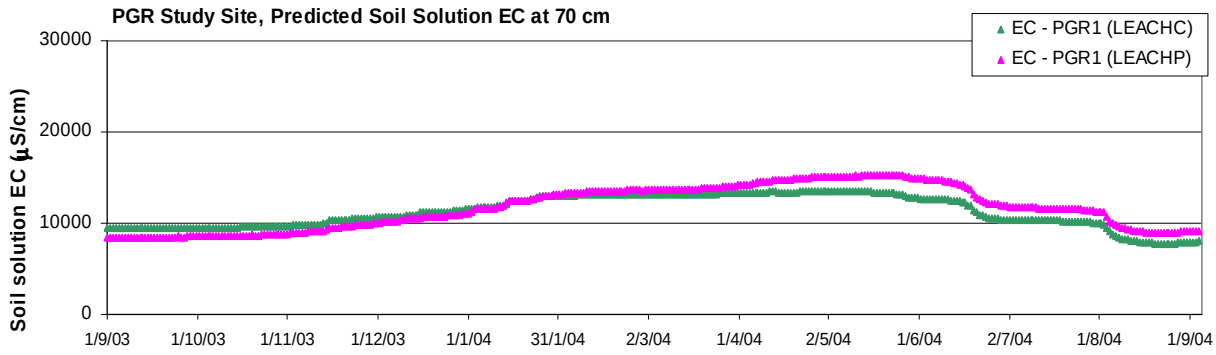

Figure 4.22 Comparison of outputs from LEACHP and LEACHC models simulating soil solution EC at 70 cm depth from Sept. 2003 to Sept 2004 at study site PGR, location PGR1.

The resulting simulated soil ECs shown in Figure 4.22 show a good agreement between the two simulations. Note, the LEACHP model outputs soil salinity at nominated depth intervals in units of mg per kg of soil. The EC shown in Figure 4.22 has been derived from the soil salinity by dividing by the volumetric soil moisture content to provide moisture salinity in mg/l, and then dividing by 0.6 to provide an approximate conversion of TDS concentration (mg/l) to EC (µS/cm).

Both the LEACHC and the LEACHP 1-year simulations provide a good approximation of the observed changes in lysimeter leachate EC over the monitored 1-year period and the

variations in simulated soil solution EC are approximately the same in the each simulation. The LEACHP simulation suggests a slightly greater increase in EC through the summer, which results in a very slight increase in EC over the year, whereas the LEACHC simulation suggests a very slight decrease over the year under the conditions monitored. While these difference are minimal over the one-year period of this simulation, they may become more significant when the simulation is extended over a longer period and this effect must be considered in the longer time scale simulations demonstrated in Chapter 5.

CHAPTER 5: APPLICATION OF MODELS AT A POINT SCALE

The calibration and optimisation process discussed in Chapter 4 provides a soil water transport model that can be confidently used to estimate the effects of irrigation practices on the components of the soil water balance at a specific monitored location. The model is valid only for the particular soil conditions at the point in the landscape which was monitored to provide data with which to construct and calibrate the model. The hydrologic conditions at the monitored point are not expected to be representative of the entire irrigated plot because of spatial variability of the soil profile characteristics and other factors affecting the soil water regime, such as crop cover and irrigation distribution. However, a carefully calibrated and optimised model for one point in the plot allows prediction of the effects of differing agricultural management practices on the balance between irrigation, evapotranspiration and drainage amounts in this horticultural setting. These would otherwise be difficult to estimate accurately from field measurements alone because of the difficulty in estimating or measuring drainage or actual evapotranspiration.

This chapter discusses an application of the one-dimensional models to one of the NAP monitored study sites and demonstrates a methodology for extending the timescale of the model beyond the period of monitoring. This methodology is then used to investigate the inter-annual variability of soil water and salt fluxes and to explore how alternative irrigation strategies may effect the accumulation of irrigation water solutes in the root zone.

5.1 Soil Water Drainage Fluxes at NAP Study Site PGR

The output from the model constructed for the 1-year monitored period at the PGR study site, as illustrated in Figure 4.7 and discussed in Chapter 4 Section 4.3, showed that the majority of drainage in the monitored year appears to occur not as a direct result of excess irrigation applications, but as a result of winter rain falling on soil that already has a high water content due to summer and autumn irrigation. This finding highlights a difficulty in analysing the effects of differing irrigation and crop management strategies on annual ET and drainage volumes. The outcomes of the one-year model suggest that predictions of the effect of irrigation management strategies on the annual ET and drainage balance of a given irrigated crop scenario may be obscured by differing winter rainfall and evaporation

conditions from one year to the next. To reliably assess the effects of differing irrigation scheduling scenarios simulations spanning a number of years of activity are required.

The degree of the inter-annual variations in annual soil drainage fluxes is of particular interest to natural resource managers, as these affect variations in soil root zone salinity and recharge to shallow unconfined aquifers, and subsequently affect shallow water table depths. A simulation of several decades duration also provides an indication of the degree of variability in the annual soil drainage fluxes and root zone salinity due to inter-annual variations in rainfall and evaporation conditions. An understanding of this degree of variability is also of use to other researchers, as a guide to the duration of field study that may be required to provide an indication of typical annual soil water fluxes.

If the soil physical parameters are assumed to be constant for the duration of a simulation, then the model soil profile description calibrated with the field study data can be used for a simulation of any chosen duration. The simulations demonstrated in this chapter use the model soil profile description constructed and calibrated for the two monitored points at the PGR study site. The crop cover at the simulated location can be repeated in each year of the simulation to represent a crop growing practice that is consistent from year to year, or varied within the duration of the model to provide representation of fallow years, or years in which alternative crops were grown in the monitored plot.

To provide a simulation that recreates the inter-annual variability in soil drainage fluxes, a database of real local weather records that covers a period of time of at least the duration of the intended simulation is required. The Bureau of Meteorology (BoM) SILO weather database holds over 100 years of weather records for the weather station at the RAAF Edinburgh airfield. Data from this database was employed in the simulations discussed below. Section 4.5 in Chapter 4 demonstrated that the effect of employing weather records from this weather database with the PGR study site model was acceptable in its effect on the model output. Hence, all the data necessary to run a simulation over a number of years is available apart from a multi-year record of irrigation schedules that can be applied in the specific soil, crop, and weather conditions of the simulated scenario. However, in the absence of several years of irrigation data, irrigation applications can be generated within the LEACHM model.

The model provides an automated irrigation option, which simulates the triggering of irrigation by a soil matric potential sensor placed at a specified depth in the modelled soil

profile. When the simulated soil matric potential at the specified depth drops to a specified matric potential, the model applies an amount of water required to bring the soil moisture content to equal the saturation moisture content in all soil layers down to a specified 'replenishment depth'. This simulates an irrigation event that is triggered by a soil moisture sensor and which instantly saturates the soil to a desired depth. The amount of water required to fill the soil to the specified depth is recorded by the model as an irrigation event. Hence the summary output file from the simulation is able to list the amount of water applied in all the automated irrigation applications that occur during the simulation.

The replacing of the recorded irrigation record for the PGR study site with this simulated automated irrigation and its effect on the outcome of the PGR site 1-year simulation was tested by applying simulated irrigation to the 1-year simulation of monitored point 1 at the PGR study site (PGR1). All other variables were the same as in the 1-year PGR site model discussed in Chapter 4. The model was set up to apply sufficient irrigation to fill the soil to saturation to 30 cm depth whenever a crop was present and the matric potential in the soil at 20 cm depth declined to -10 kPa. This irrigation trigger potential and replenishment depth was found to maintain a degree of soil moisture that was similar to that in the monitored profile during the year of monitoring. Figure 5.1(a) provides a comparison of the matric potentials recorded at site PGR1 and those simulated by the model when the irrigation applications recorded during the monitored period are applied and the ETo record from the BOM Edinburgh airfield weather station is used in place of the on-site weather data. Figure 5.1(b) shows the simulated soil matric potentials when the recorded irrigation events are replaced with simulated auto-irrigation.

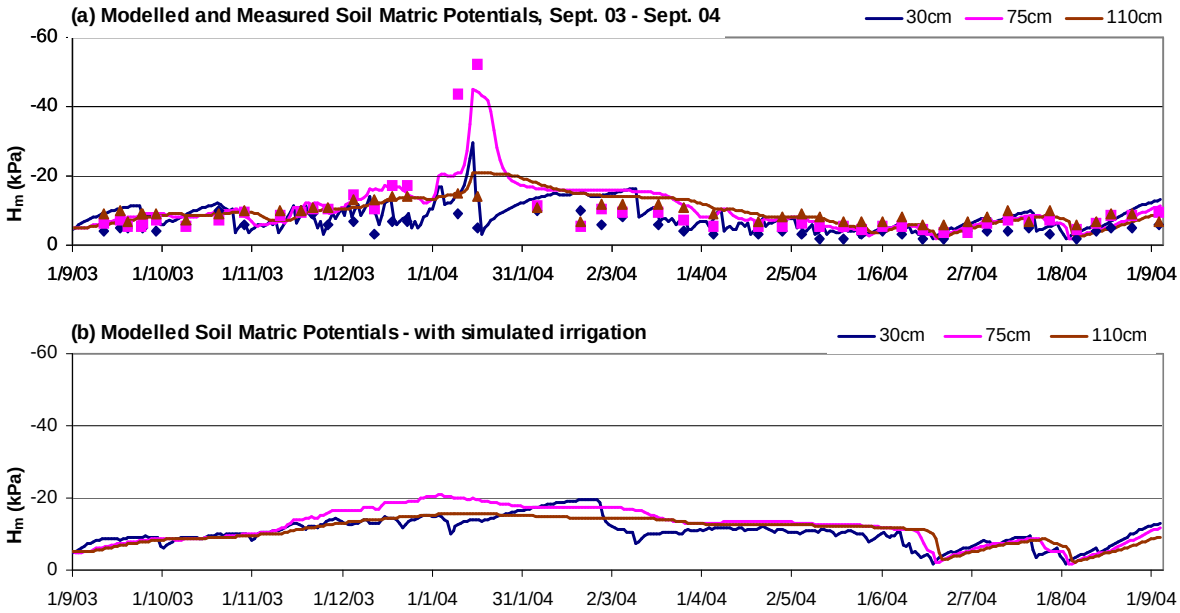

Figure 5.1 Model simulations of matric potentials at 30, 75 and 110 cm resulting from (a) rain, irrigation and potential ET conditions measured on-site, and (b) rain and ET data from local weather station and simulated irrigation.

The matric potentials maintained at the monitored depths with the simulated irrigation are a good approximation to the patterns of matric potential observed during the monitored period, and those simulated by the same model with the recorded irrigation at the study site. A close match between simulated and recorded matric potentials is not expected as, under the simulated irrigation scenario, irrigation was applied more frequently and in smaller amounts .

Figure 5.2(a) shows the simulated irrigation and recorded rainfall events through the period of the simulation as well as the model-predicted ETa, while Figure 5.2(b) shows the model-predicted drainage that results from the balance between these. Significantly, the balance between ET and drainage is altered with the simulated irrigation. When compared to the original simulation that used observed irrigation, the smaller but more frequent applications of the simulated irrigation result in a small overall increase in the amount of irrigation water applied (974 mm compared with 917 mm observed) and a 10% increase in ET, leading to a reduction in drainage from 199 mm to 116 mm for the year. The patterns of drainage through the year however remains similar (refer Chapter 4, Figure 4.8), with the majority of drainage occurring through the winter months, after irrigation has ceased.

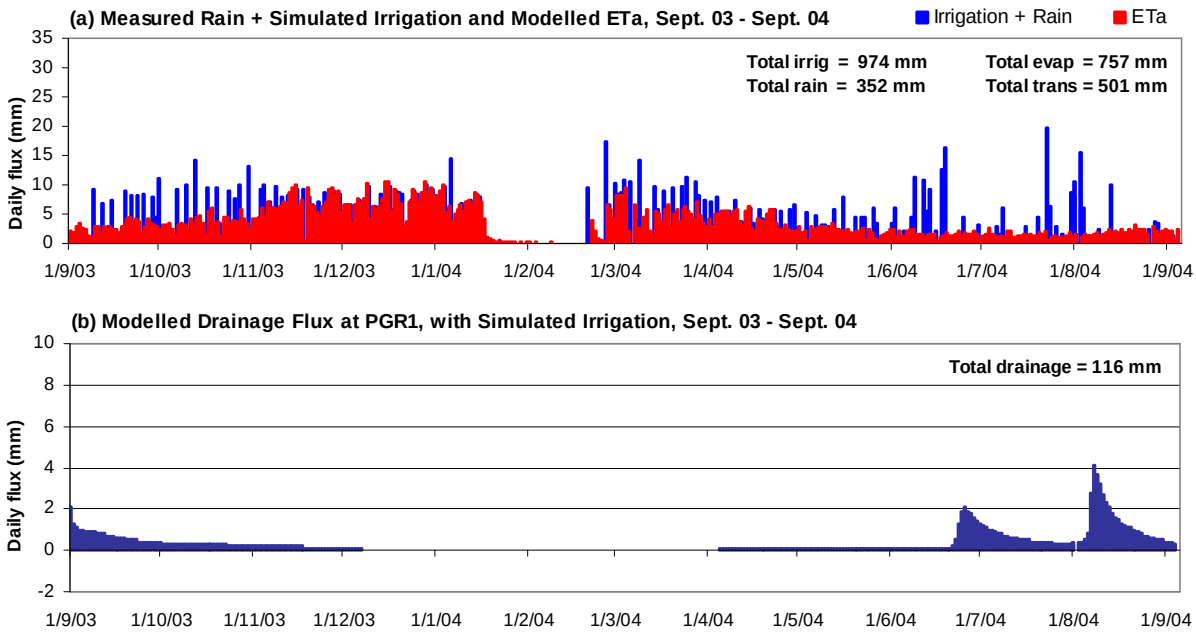

Figure 5.2. Simulated ETa (a) and drainage (b) resulting from applying rain and ET data from local weather station and simulated irrigation, triggered when simulated matric potential at 20 cm depth drops to -10 kPa

The implication of this is that the longer term simulations that are enabled by the generation of irrigation within the model will indicate higher evaporation and lower drainage than could be expected to occur at the PGR study site under the irrigation scheduling currently practiced at that site. However, the intention of the longer term simulations is to a) allow the comparison of differing crop and irrigation scenarios over a number of years and b) reveal the degree of inter-annual variation in the soil water balance components resulting from annual differences in weather conditions. If the simulation of study site PGR1 with simulated irrigation as demonstrated above is used as a baseline scenario, the extension of the model in time allows comparison of variations from year-to-year, and repeated running of the model with differing crop and/or irrigation conditions allows a number of scenarios to be compared to this baseline crop and irrigation scenario. It must be noted however, that the lower drainage fluxes resulting from this scenario compared to that estimated from simulations based on study site data, suggest that any reductions in irrigation and drainage fluxes may be underestimated by crop and irrigation scenario simulations that use the regional weather data.

5.2 Extension of Point Scale Models to a Longer Time Series

5.2.1 Inter-annual variability of water fluxes

In trying to predict the fluxes of ET and drainage from a given soil and crop scenario into the future and under varying conditions of irrigation management, there is a need to account for the effects of inter-annual variability in weather conditions. If winter rains are the cause of a large proportion of leaching and drainage, then variation in the annual rain amount may significantly affect the drainage fluxes occurring in a given year. Hence, predictions of future drainage, ET, and crop water use under varying irrigation management strategies may be difficult to make because the future inter-annual weather variability cannot be known. Whilst the inter-annual variability in weather conditions may be described from historic data, the variability in drainage fluxes from year to year is not easily quantified. The simulations demonstrated here provide a means for quantifying this variability.

Simulations of twenty years of activity at the PGR study site were carried out using the calibrated model soil profiles for the two primary monitored points, PGR1 and PGR2, and a twenty-year record of historic weather data from the BoM Edinburgh airfield weather station for the years 1985 to 2004. While a greater length of weather data is available from the database for the Edinburgh BoM weather station, increasing the length of the simulation causes greater run times and does not add to the utility of the simulation results as long as the period chosen is representative of the variations in weather that may occur in the NAP area. The mean annual rainfall recorded in the Edinburgh database over 104 years is 436.9 mm with a standard deviation of 104.3 mm. The twenty-year period from 1985 to 2004 chosen for this simulation has an average annual rainfall over the twenty years of 422.3 mm, close to the long-term mean, and includes two years that lie within the 10^{th} and 90^{th} percentile of annual rainfall over the whole rainfall record (2002 with 232.5 mm and 1992 with 671 mm) representing the extremes of wet and dry years that may occur in the NAP area. Thus, the chosen simulation period is considered representative of the longer-term weather record.

The same annual crop combination, simulating a carrot crop followed by a potato crop with natural weed growth after harvest, was repeated for every year of the 20-year simulation. This is the same crop cycle observed at the PGR study site during the year of monitoring. The model was set to simulate automated irrigation, again applying sufficient irrigation to replenish soil water to 30 cm depth whenever a crop was present and matric potential at 20

cm depth declined to -10 kPa. This was intended to provide an irrigation policy similar to that followed by the horticulturalist at the PGR study site during the year of monitoring at that site. While the simulation was intended to create results for a period from 1985 to 2004, the simulated period commenced in September 1984 to allow the model soil profile to equilibrate to an approximation of the soil moisture content that would have existed at the start of 1985.

Figure 5.3 shows the annual totals of drainage predicted by the model for the 20 years of the simulation and the corresponding annual rainfall. There is a high degree of variation of drainage from year to year, ranging from as little as -6 mm (representing a net discharge of water from the water table into the soil profile) in 2002, to a maximum of 131 mm in 1992. These results are surprising considering the identical crop covers and highly controlled automated irrigation, which attempted to maintained soil moisture potentials for nine months of each year of the simulation. The reason for the high degree of variation is that, as demonstrated by the one-year simulations in Chapter 4, it is the balance between winter rainfall and evaporation conditions that result in the majority of drainage through the year. In the crop cycle simulated here, there is no crop in place between mid-July and mid-September each year, so there is no irrigation applied during those months in any year of this simulation. Under these conditions, years with low winter rainfall result in very little drainage.

If the coefficient of variance is expressed as a percentage where;

$$\text{variance (\%)} = \frac{\text{standard deviation of annual drainage}}{\text{mean annual drainage}} \times 100$$

the variance in annual drainage over the 20-year simulation was 59% and 41% of the 20-year mean drainage for points PGR1 and PGR2 respectively. The variance in annual rainfall over the same period was much less, only 22%.

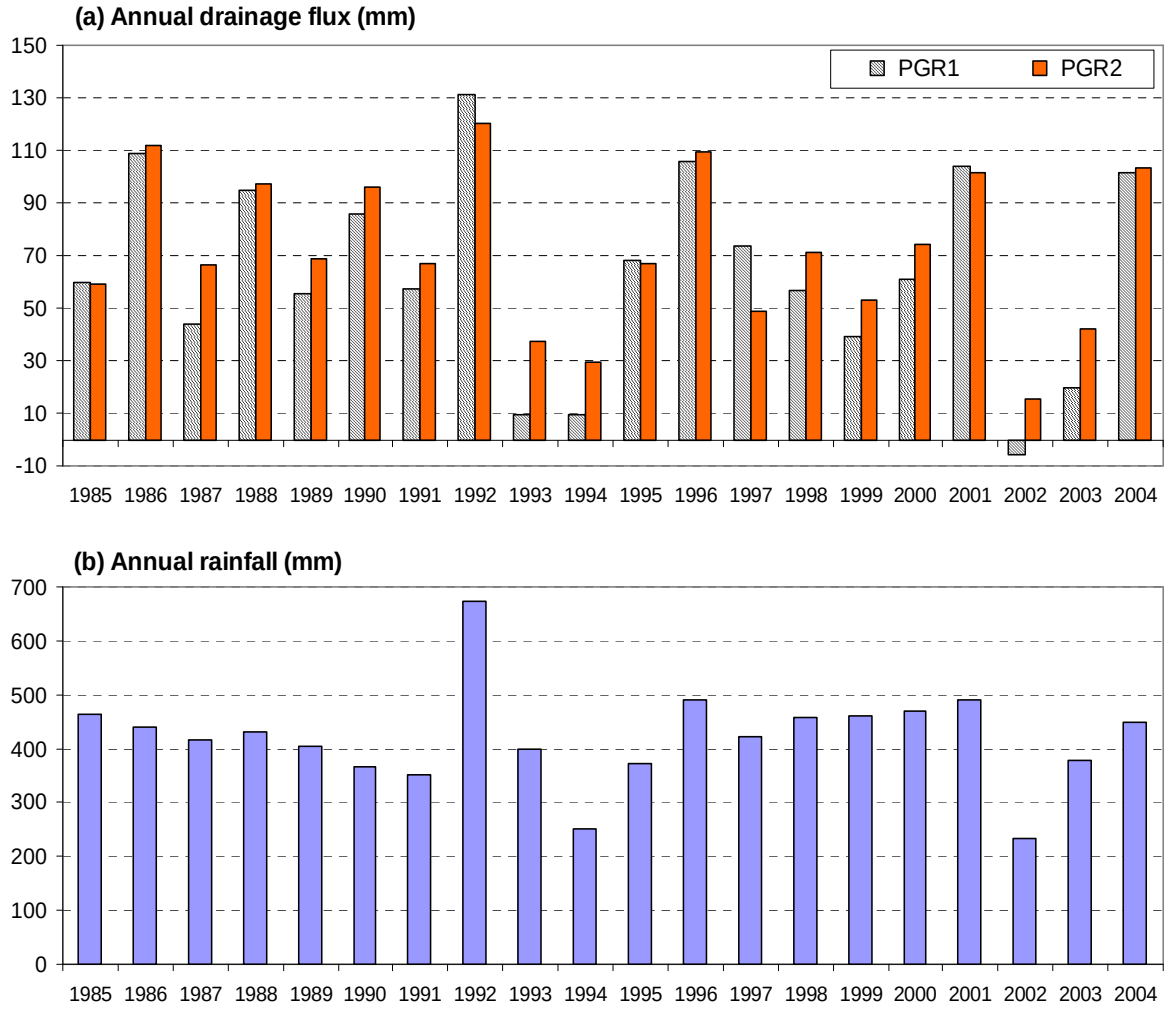

Figure 5.3 (a) Modelled annual drainage totals at monitored points PGR1 and PGR2 for a twenty year simulation from 1985 to 2004, and (b) recorded rainfall for those years.

It can be seen that the rainfall totals for both 2003 and 2004 are higher than that used in the earlier 1-year model of the PGR study site. This is because the weather data applied in this 20-year simulation is from the BOM Edinburgh Airfield weather station, which recorded higher rainfall during that period than the pluviometer at study site PGR. Also, despite the higher rainfall during 2003 – 2004 period in the 20-year model, the earlier 1-year model predicted a higher drainage flux for the Sept. 2003 – Sept 2004 period. This is because the starting moisture content in the 1-year model was significantly higher than the soil moisture content on 1/9/2003 in the 20-year model as the latter was unusually low after the exceptionally dry year of 2002. It is also important to note that the annual totals presented in Figure 5.3 are divided by calendar years and may therefore show some difference from the results of the one-year models previously discussed.

In view of the finding that the majority of drainage in these conditions is caused by winter rainfall rather than irrigation applications, and that rainfall in this region is winter-dominated, it is intuitive to expect that annual drainage totals will be closely correlated with annual rainfall totals. However, the correlation between annual drainage and annual rainfall over the 20 years of the simulation is not strong, with correlation coefficient 'r^2' values of 0.55 and 0.51 for PGR1 and PGR2 respectively. A large part of the correlation that does exist over this period is due to the strong correlation between exceptionally wet or dry years and exceptionally high or low annual drainage totals. Hence, the three exceptional rainfall years in the 20-year simulation period (1992 was exceptionally wet while 1994 and 2002 were exceptionally dry) tend to enhance the correlation. This effect is illustrated by the regression plots of annual drainage over annual rainfall, shown in Figure 5.4. If the three exceptional years are removed, the correlation between rainfall and drainage becomes much weaker, with correlation coefficients 'r^2' of 0.17 and 0.15 for PGR1 and PGR2.

The large variance in drainage has important implications for any efforts to characterise typical drainage volumes under similar combinations of soil, crop, irrigation and climate to those simulated here. For example, a study conducted over two years from 1993 to 1994 or from 2002 to 2003 would have resulted in a significant under-estimate of typical drainage fluxes. A study from 1999 to 2001 or from 2002 to 2004 may have surmised that a dramatic year-on-year increase in drainage fluxes was occurring. A monitoring period of up to 3 years may be largely misleading in its indication of typical drainage volumes.

These findings demonstrate the importance of an appreciation of temporal scale in the analysis of soil water drainage. Long term trends in this variable are difficult to predict from a short term analysis. A one- or two-year analysis of drainage resulting from a particular soil, crop and irrigation combination may provide a misleading indication of average annual drainage fluxes in even the most well-controlled irrigation conditions.

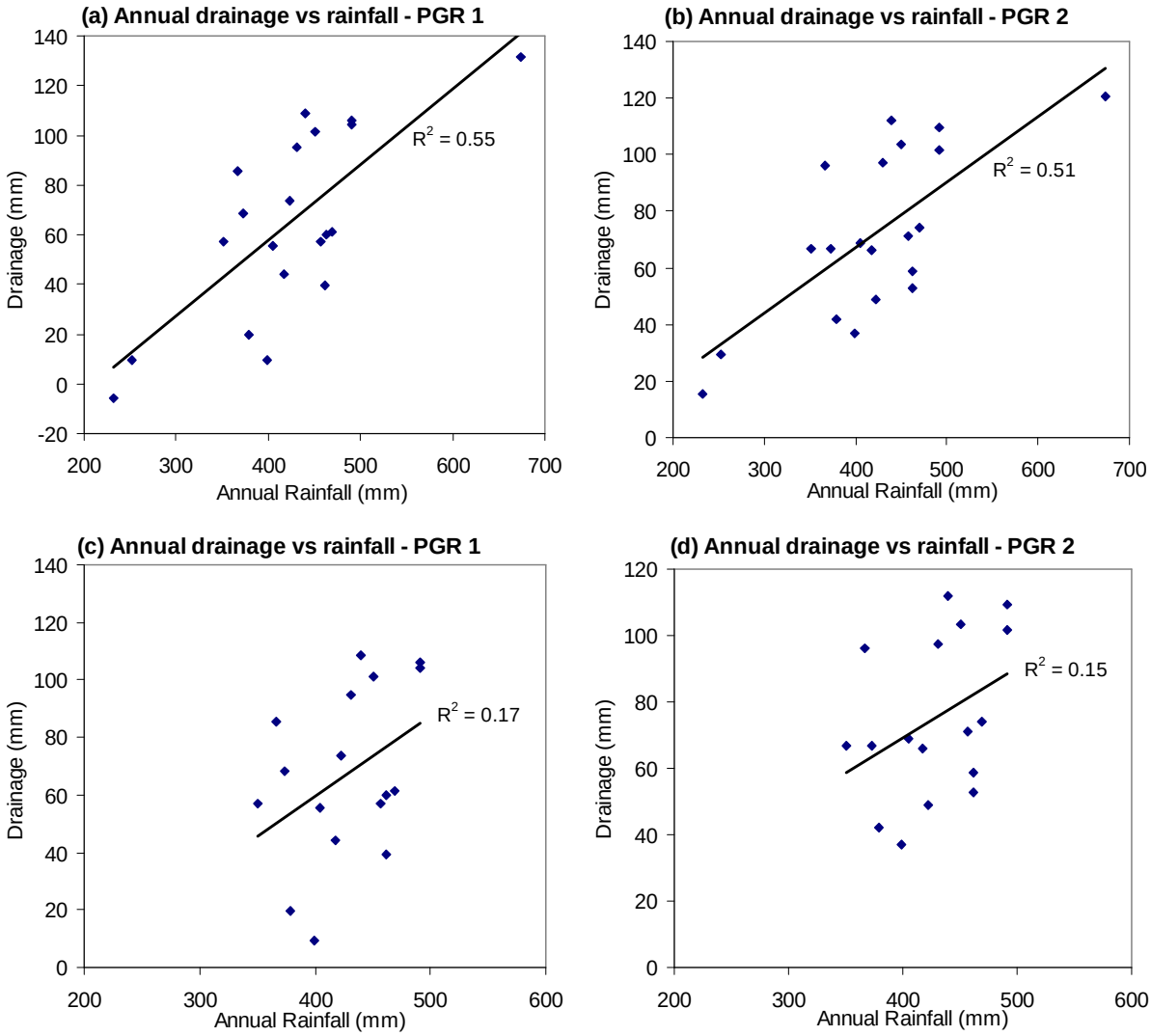

Figure 5.4 Regression plots of annual drainage flux totals versus annual rainfall totals from simulations of twenty years of irrigated crop growth from 1985 to 2004 (a) PGR1 and (b) PGR2. Correlation of rainfall totals with drainage totals decreases significantly when three years of exceptionally high or low rainfall are removed, (c) and (d).

5.2.2 Alternative irrigation scenarios

A simulation model of this type allows predictions of long term trends in drainage under differing scenarios. Plotting the predicted cumulative values of irrigation, evaporation and drainage volumes over time provides a useful way of examining complex transient data in which longer term trends are not always readily apparent. Six further 20-year simulations for PGR1 only were run with simulated irrigation using matric potential triggers of -10, -15, -20, -25, -30 and -35 kPa at 30 cm depth. When plotted cumulatively, the irrigation, evaporation and drainage predicted in the six 20-year simulations increase linearly over time (Figure 5.5, page 107). The inter-annual variation in rainfall and evaporation conditions result in relatively minor fluctuations in an otherwise linear growth of these variables over time. The gradient of the linear trends of these curves is equivalent to the long term average annual flux of the variable over time.

These results reinforce the observation that the effects of timescale are an important consideration in the interpretation of these data. Analyses of drainage occurring under controlled irrigation conditions over a monitored period of one or two years may result in drainage volumes that are significantly different from the long term average drainage resulting from the same controlled conditions. For example, the gradient of the linear trend of the -15 kPa drainage versus time plot is 0.174 mm/day, equivalent to an average annual drainage of approximately 64 mm/year. However, a two-year analysis from 1/1/1993 to 1/1/1995 would have found a total drainage over that period to be 18 mm, whereas a similar analysis of the following two-year period from 1/1/1995 to 1/1/1997 would have found a total drainage of 174 mm. Thus a two-year study of drainage at this site would have the potential to yield a largely inaccurate estimate of the annual drainage amount. This result is unexpected in consideration of the highly controlled irrigation in these simulations, however it is the variability of winter rainfall and evaporation conditions that gives rise to this inter-annual variation in annual drainage volume.

The cumulative fluxes predicted by this simulation over the whole twenty-year period are tabulated in Table 5.1. When plotted cumulatively, the irrigation, evaporation and drainage predicted in the six 20-year simulations are shown to follow linear trends over time (Figure 5.5). The inter-annual variation in rainfall and evaporation conditions result in relatively minor fluctuations in an otherwise linear growth of these variables over time. The gradient of the linear trends of these curves is equivalent to the long term average flux of the variable.

Table 5.1 Average annual fluxes of water at study site PGR1, according to 20-year simulations.

Irrigation trigger soil matric potential	Irrigation mm/year	Rain + Irrigation mm/year	Transp. mm/year	Evap. mm/year	Drainage mm/year	Drainage / Irrigation
-10 kPa	858	1279	485	706	118	0.14
-15 kPa	642	1063	461	539	65	0.10
-20 kPa	545	966	465	463	41	0.08
-25 kPa	494	915	469	423	25	0.05
-30 kPa	458	880	471	399	12	0.03
-35 kPa	433	855	472	379	6	0.01

Average transpiration was found to be similar with all of the six irrigation trigger potentials, ranging from 458 mm/year to 472 mm/year. This similarity is to be expected since the crops present were identical in each year of the simulation and the crops were well watered such that transpiration is not limited. The effects of altering the irrigation trigger point are reflected primarily in changes in the amounts of irrigation water, evaporation and drainage. As the amounts of drainage are approximately one order of magnitude smaller than the irrigation and evaporation amounts, the significant differences in irrigation water used with the range of irrigation trigger potentials are largely a result of reductions in evaporation.

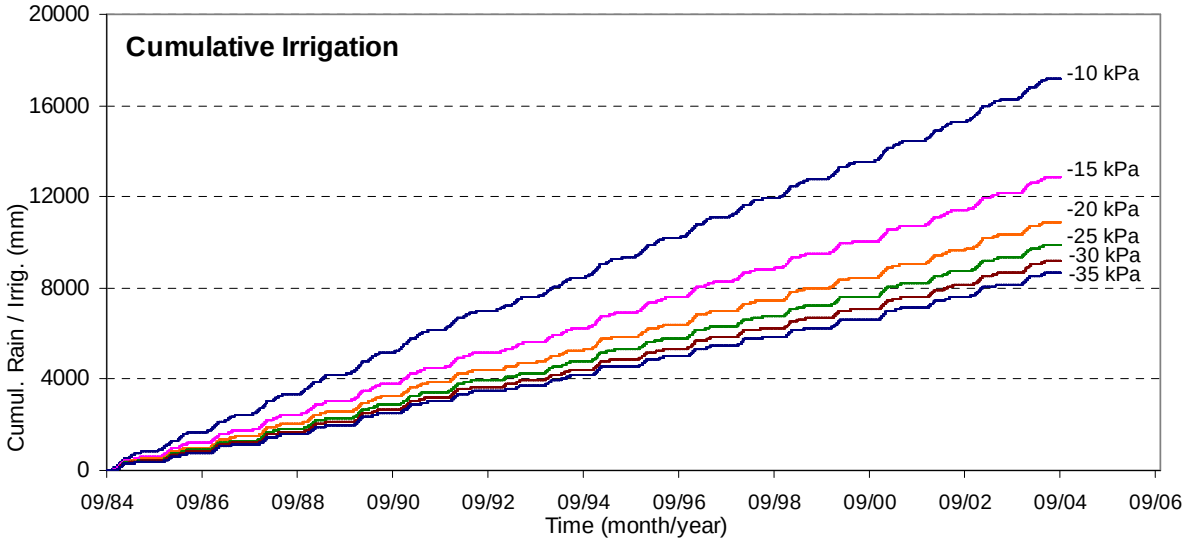

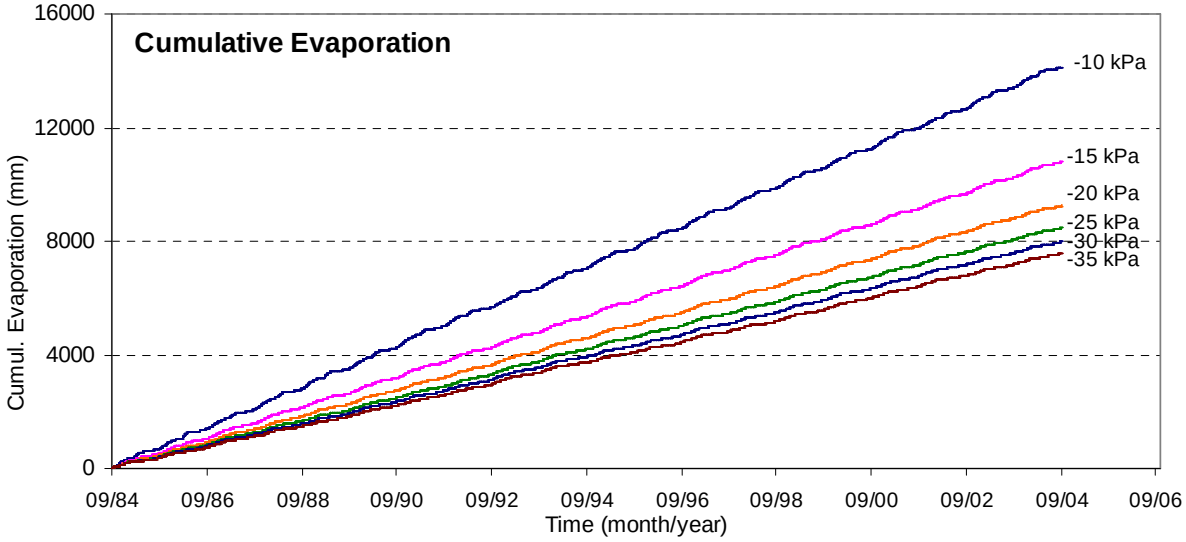

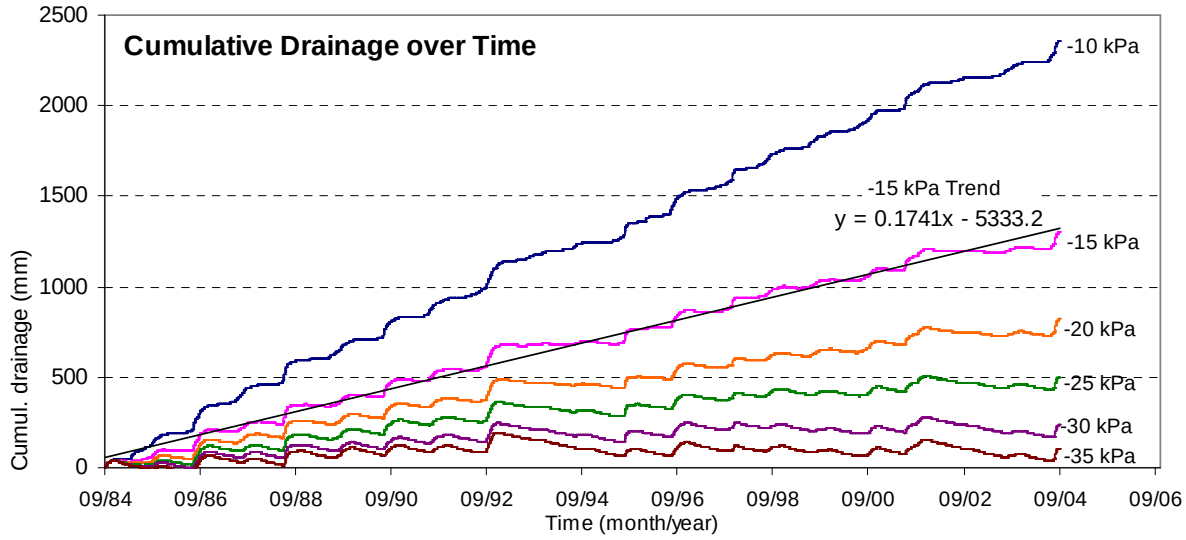

Figure 5.5 Model simulations of cumulative irrigation water, evaporation and drainage over a 20-year simulation with simulated irrigation that is triggered at a specified soil matric potential. Differing trigger potentials result in differing amounts of irrigation, evaporation and drainage.

The benefits of sensor-controlled irrigation policies can be assessed for a given combination of crop, soil and climate, using the methods described. It is clear that in this type of horticulture, in which vegetable crops require maintenance of a high soil moisture content, small changes in irrigation trigger setting, such as from -10 kPa to -15 kPa result in significant savings in irrigation water and that these savings are largely a result of reductions in evaporation from the soil surface. However, as the irrigation trigger potential becomes more negative, further reductions result in smaller changes in irrigation water, evaporation and drainage amounts. Thus, an optimum trigger potential for the soil, crop and irrigation combination evaluated in this study may be -20 or -25 kPa. Potentials lower than this level may not be economically justifiable as the risk of crop yield reductions is not balanced by a significant reduction in water use or environmental impact.

While reductions in drainage are relatively small compared to the savings achieved in irrigation water, they are important when considering the effects of accessions to groundwater and leaching of salts from the root zone. In the setting of the NAP, where irrigation drainage accessions to groundwater may be causing water tables to rise, the reductions in drainage illustrated here are desirable if they do not result in unacceptable increases in root zone salinity either over the long term or periodically while crops are present.

5.3 Soil Salinity Changes Over a 20 Year Simulation

By using the LEACHC model to carry out the simulations described above, changes in salinity in the soil profile can also be simulated. LEACHC calculates the soil inorganic chemistry for the major dissolved cations: Ca, Mg, K, Na, and anions: Cl, SO_4^{2-}, CO_3^{2-}, HCO_3^-, and takes account of ion adsorption/desorption using Gapon selectivity coefficients for the major cations. Equilibrium concentrations of solution and exchange phase ions are recalculated for each model soil segment after each of a chosen number of times steps (a 20 time step interval was used here, with time steps of 0.1 day). Initial ion concentrations in the exchange and solution phase in the monitored soil profile were approximated for soil at three depths using a combination of exchange cation concentrations in soil samples and dissolved ion concentrations in soil solution extracts and lysimeter leachate samples.

To provide initial soil chemistry data for input to the LEACHC simulation, solution and exchangeable cation extract concentrations were converted to equilibrium concentrations of major ions in solution and exchange phases at a field soil water content considered to be

representative of the study site. Measured concentrations of exchangeable cations were converted to concentrations equivalent to all exchange phase cations from 20g of soil dissolved in 100 ml water. Resulting concentrations of exchange phase cations were then added to measured 1:5 solution extract cation concentrations to provide total extractable cation concentrations in a 1:5 soil : water mixture. The sulphur concentrations of the solution extract were assumed to be all in the form of SO_4^{2-} to provide part of the charge balance of cations in solution. A nominal initial alkalinity of 5 mg/l HCO^- was used and the remainder of anions required to balance charges was assumed to be chloride. With these concentrations as input data, a chemical equilibrium program, Chemeq (Hutson, 2003), provided with the LEACHM software suite, was used to determine selectivity coefficients and equilibrium concentrations of major cations and anions in the soil at saturation and at the initial soil water content to be used in the LEACHM simulations. The Chemeq program was run several times, with the Gapon selectivity coefficients and initial carbonate concentrations adjusted between each run, until the equilibrium concentrations of exchange phase cations and ions in solution was in agreement with measured concentrations in the soil samples and lysimeter leachate samples. The resulting equilibrium concentrations are tabulated in Table 3.4 (page 60).

Irrigation water samples were taken half way through the growing period of the first crop monitored at this site and analysed by ICP for major cation and anion concentrations. These concentrations were used as the dissolved ion concentrations of the irrigation water for the duration of the simulation. While the salinity of the reclaimed water delivered by the Virginia Pipeline System varies throughout the year, the irrigator at the location simulated here stores the water in an open agricultural dam prior to use, which has the effect of integrating water delivered over several days or weeks. The TDS of the irrigation water in this simulation was 1260 mg/l, with the composition of major ions determined from ICP analyses of water samples taken from the irrgation lines at the PGR study site. The soil chemistry simulations here do not include additions of fertiliser, which are certainly a part of horticultural practices on this study site. The effect of omitting these from the simulations will be to underestimate the total mass of solutes added to the soil.

When simulating the vertical water and salt fluxes of the NAP on the broad area scale and over many years, we are concerned with total annual water fluxes and with changes in the total salt content of the soil over a number of years. In this analysis the changes in the inorganic chemical composition or changes in the concentrations of individual ionic species

are not reported, however they are provided in the LEACHC output files. Hence, the change in the soil sodium adsorption ratio (SAR) could also be assessed for this study site if required.

The LEACHC output file lists the simulated soil salinity at defined observation depths (30 cm, 70 cm, 110 cm and 150 cm were used here) for each day as the salinity of the soil solution at the simulated water content at that time (EC_θ), in units of mS/m. This salinity of the soil solution is highly dependent on the soil water content; as the soil becomes drier, the same amount of salt is in solution in a smaller volume of water. It is useful, when comparing model output with either measured soil salinity values or simulations with other hydrologic regimes (such as differing irrigation schedules) to convert the EC_θ values to an equivalent salinity that is independent of the soil water content, such as the salinity at saturation water content (EC_{sat}) or the salinity of a 1:5 soil water solution extract ($EC_{1:5}$). These terms are derived from the EC_θ output by LEACHC according to the following formulae:

$$EC_{sat} = EC_\theta \times \theta / \theta_{sat}$$

$$EC_{1:5} = \frac{EC_\theta \times \theta}{5 \times \rho_b}$$

Where θ is the volumetric soil water content and ρ_b is the bulk density of the soil at that depth. The true relationship between EC_{sat}, $EC_{1:5}$ and EC_θ is more complex and is dependent on the composition of the solutes present in the soil (Shaw, 1999). However, these formulae are considered acceptable for the analyses presented here, which only compare solute concentrations derived by differing methods for soil at a specified depth at one location.

Figure 5.6 shows the soil EC at 70 cm depth, predicted according to a one-year simulation of the soil profile at study site PGR1. The model output EC_θ values have been converted to EC_{sat} and $EC_{1:5}$ values in this graph to allow comparison with EC measurements of lysimeter leachate and 1:5 soil:water extracts from samples collected at the study site during the simulated period. The soil chemistry at the start of the simulation was based on equilibrium concentrations of major ions in exchange and solution phases and Gapon selectivity coefficients derived from these as described above. Irrigation, rainfall and ET data applied to the simulation were as measured at that site during the study program. This model's soil hydrologic parameters were the same as for the model calibrated for this site as

described in section 5.1. Figure 5.6 also shows the EC measurements of lysimeter leachate samples and soil 1:5 solution extracts for soil samples collected from 70 – 75 cm depth at the study site during the simulated time period.

The EC of the lysimeter leachate is indicative of the salinity of the soil solution when the soil is at or close to saturation. Water is expected to leach into the lysimeters at soil matric potentials between 0 kPa (saturation) and -5 kPa. When the model is correctly simulating the soil chemistry, the simulated EC_{sat} equivalent shown by the blue line in Figure 5.6 should be comparable to the lysimeter leachate EC values. The simulated $EC_{1:5}$ equivalent shown by the green line should be comparable to the measured soil 1:5 extract EC values. However, the starting soil chemistry was based on results from samples of soil and lysimeter leachate collected on 20/4/04 rather than at the true starting date of the simulation, resulting in the starting soil solute concentrations being higher than they should have been at the starting date of the simulation. This has resulted in the simulated EC_{sat} being higher than the EC of lysimeter leachate samples. Similarly, at the start of the simulation period, the simulated $EC_{1:5}$ equivalent is higher than the $EC_{1:5}$ values of soil samples taken during that time. However, the soil EC predicted by the model shows a rise and fall through the simulation year in line with the trend of the lysimeter leachate samples and is in the right range of EC values for the soil salinity in comparison to both lysimeter leachate and soil solution extracts. In consideration of this, the LEACHC simulation provides a reasonable approximation of the observed changes in soil moisture EC over the monitored 1-year period.

The exclusion of the effects of osmosis on root water uptake is a weakness of the model as applied here. In some of the scenarios modelled, in which soil salinity increased markedly, the vegetation present would in reality have started to take up less water as the osmotic potential difference changed between plant roots and the increasingly saline soil. In the extreme cases, crops may have declined and died. A model response to this should be to either increase irrigation applications, as would be likely if an irrigator was responding to crop condition, or to diminish the occurrence of ETa after the decline of the vegetation. In both cases, an increase in the amount of water in the soil would have resulted, acting as a negative feedback response to the increase in soil salinity.

As the soil chemistry model is not fully calibrated it cannot be used to reliably predict absolute soil salinity values at a point in time. However, the model does have great utility for comparative assessments of soil salinity under differing scenarios and salinity trends in

response to variations in weather, irrigation policies and irrigation water quality. The careful calibration of the underlying soil hydrology model is crucial in the application of the soil chemistry model to ensure that the variations in soil salinity predicted by the chemistry model are a result of realistic fluxes of soil water through the soil profile in response to the applied rainfall, irrigation and evapotranspiration conditions.

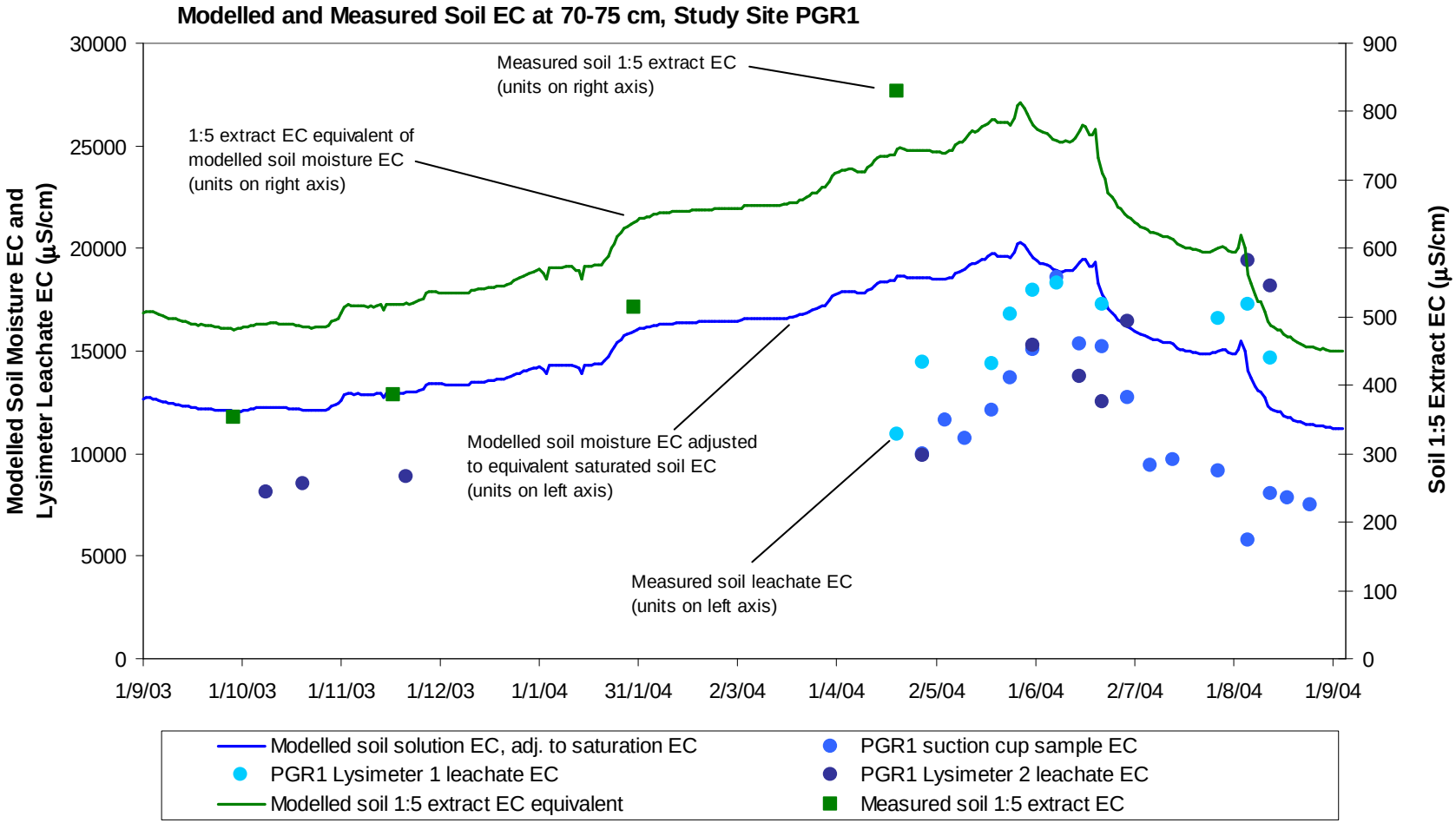

Figure 5.6 Simulated soil solution EC at 70 cm depth from a one-year simulation of point PGR1, shown withEC measurements of soil solution extracts, suction cup samples and lysimeter leachate. Blue and green lines are, respectively, the EC_{sat} and $EC_{1:5}$ equivalents of the EC_{θ} predicted by the LEACHC simulation. Green squares are $EC_{1:5}$ measurements of soil samples taken from 70-75 cm at PGR1 on four dates. Blue dots are EC measurements of samples from suction cups and leachate from capillary wick lysimeters at study site PGR1. No leachate was obtained from lysimeters or suction cup samplers between December and April.

The soil chemistry simulation demonstrated below uses the same soil hydrology model described in section 5.1 and the same rainfall, crop, and ET conditions, applied over a 20-year simulation. Again, the rainfall and ET conditions are as recorded by the BoM weather station at Edinburgh Airfield between 1984 and 2004. The simulated vegetation coverage is of the same rotation of three crops each year as employed in the earlier model, based on the crops monitored at the PGR study site. As with the soil drainage flux models described in Section 5.2, the spring / summer crops are set to be auto-irrigated according to selected soil matric potential trigger settings. The winter cover crop is not irrigated, relying on winter rainfall alone as was the case at the PGR study site during the study period. The same inorganic chemistry data are used for the soil, irrigation and rainfall as were used in the 1-year simulations. The irrigation water solute composition is fixed for the duration of the simulation and is initially set with concentration values of the major ions shown in Table 5.2.

Table 5.2 Composition of irrigation water as used in models

Ca mmol/l	Mg mmol/l	Na mmol/l	K mmol/l	Cl mmol/l	SO4 mmol/l	Alk mmol/l HCO^-
0.72	1.40	15.22	1.13	15.33	2.13	1

This major ion composition results in a total dissolved solids concentration of the irrigation water applied of approximately 1260 mg/l. These concentrations are based on analyses of samples of water taken directly from the irrigation system at the PGR site.

The starting soil solute concentrations used in these simulations are based on the ion concentrations in soil samples taken in early 2004. The concentrations observed will have been due in part to the addition of solutes in fertlisers in the months or years prior to the time of sampling the soil for analysis of these concentrations. As further fertiliser additions are not included in the simulations here, the total salts added to the soil in the simulations is probably less than had historically been applied to the study site. Hence it should be expected that the the simulation predicts a decline in the soil's overall salt content in the first year or two.

The graph in figure 5.7 shows the $EC_{1:5}$ equivalent of the soil at a depth of 70 cm at the PGR1 study site over 20-year simulations from 1984 to 2004, with simulated auto-irrigation scenarios and soil matric potential triggers for irrigation set at -10 kPa, -15 kPa, -25 kPa and -35 kPa. These are the predicted soil salinities at the bottom of a model soil profile depth segment from 30 cm to 70 cm, representing the primary root zone. The 70 cm depth is shown here to be the most representative of the variations of salinity within the modelled soil profile.

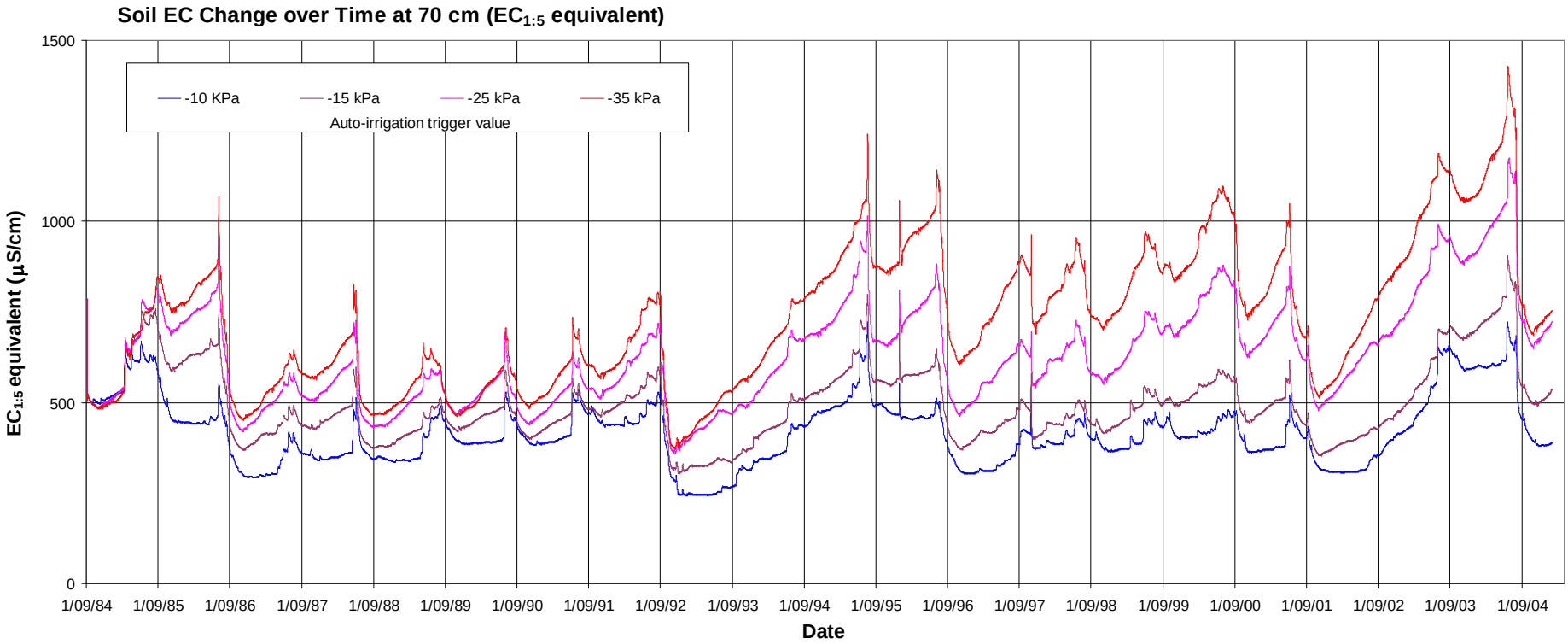

Figure 5.7 Changes in soil salinity ($EC_{1:5}$ equivalent) at 70 cm depth over a 20-year simulation with automated irrigation triggered at soil matric potentials of -10 kPa, -15 kPa, -25 kPa and -35 kPa. Irrigation water used in these simulations has a constant TDS of 1260 mg/l.

The -10 kPa and -15 kPa irrigation trigger scenarios are the most similar to the actual irrigation and soil moisture regime maintained by the grower at this location. Even if the starting soil chemistry composition was somewhat different from the true composition, a well functioning model should start to predict salinity values close to the real values after a few years of the simulation if the soil profile, crop, weather and irrigation conditions of the model are a good representation of the real conditions. That the model predicts a 70 cm $EC_{1:5}$ of close to the observed values in September 2004, at the end of a 20-year simulation is a good indication that the model is representing well the soil salinity fluxes in the real soil profile.

There are a number of significant observations that can be made from the results of these simulations:

1) It is clear that root zone salinity is higher when lower irrigation trigger potentials are used, it is also apparent that the degree of flushing of salts from the profile during winter has a controlling influence on soil salinity trends over the medium to long term.

2) In the majority of years the pattern of salinity variation is comprised of a steady rise through the summer months while irrigation is occurring and evaporation conditions are high, then a sharp decline during the winter and early spring as rain penetrates the soil profile and flushes salts through. This is in agreement with the findings in Section 5.1 that the majority of drainage occurs due to winter rain during low evaporation conditions.

3) In many years there is also a steep rise in salinity immediately before the sharp winter decline. This results from the leaching down to this depth of salts deposited through the summer the soil above, occurring prior to the peak time of leaching of salts from the 30 cm to 70 cm depth segment.

4) The significant effect of the low drainage years identified in Section 5.2 is seen in 1993, 1994 and 2002. Sustained salinity increases are seen to occur as a result of a succession of relatively dry winters, such as from 1993 to 1995. As there is no significant winter flushing of salts in those years to lower the soil salinity, the rise over the next summer occurs on top of the salinity rise of the previous year, resulting in a dramatic year-on-year rise in salinity. This suggests the effects on soil salinity of a series of years of low winter drainage conditions would be severe.

5) Conversely the effects of the years of higher drainage, identified in Section 5.2 as 1986, 1992, 1996, 2001 and 2004, are to cause a larger than normal decline in salinity during the winter. The maintenance of soil salinity levels over the longer term is dependent on any drier than average years being followed shortly afterwards by a wetter than average year.

6) There is an upward trend in the 70 cm $EC_{1:5}$ when the more conservative irrigation triggers are used. Although the starting soil chemistry composition was based on samples taken during April 2004, at the end of the summer irrigation season when annually varying soil salinity is expected to be fairly close to its annual peak, the predicted salinities in the -10 kPa and -15 kPa scenarios for the same time in that year (approx. 600 – 720 μS/cm $_{EC1:5}$ equiv.) are close to the observed values.

7) The degree of winter flushing of salts is the same or greater in the more conservative irrigation scenarios than in the more liberal scenarios. However, the greater increase in EC through the summer months causes the longer term salinity growth trends in the more conservatively irrigated -25 kPa and -35 kPa scenarios.

The range of soil salinity even for the -10 kPa scenrio is high compared to soil salinity that would be recommended for peak production of vegetable crops (Shaw, 1999 after Maas and Hoffman 1977), and is well above ideal growing conditions in the -25 and -35 kPa scenarios. These are reflective of the tendency for soil salinities to be high in the NAP horticultural area and may explain why growers in the region tend to adopt rather liberal irrigation strategies. At these soil salinity levels, plant roots have to take up water against a considerable osmotic potential in the soil solution. By keeping the soil moisture content high, the grower helps to firstly dilute the soil solution and, secondly, reduce the moisture potential against which the plant roots have to take up water. Any increase in soil salinity above the current levels at the PGR location, and similarly high levels at other study locations would be detrimental to crop productivity. Hence, the higher overall salinity and the rising trends of these predicted by the model for the -25 kPa and -35 kPa scenarios need to be avoided. The dilema presented here between providing enough irrigation to flush salts from the soil profile and being sufficiently conservative to prevent water table rise is not uncommon in situations where irrigated crops are grown over shallow water tables.

These simulations suggest that, to maintain soil salinity at a reasonable level, the most appropriate soil moisture regime with this soil and crop rotation cycle is achieved with

irrigation events triggered at soil water contents where matric potential is around -10 kPa to -15 kPa. As shown in figure 5.1, this is close to the soil water content maintained by the grower at study site PGR and probably reflects the grower's experience of the amount of irrigation required to maintain the soil salinity and crop productivity at that site. However, this irrigation regime demands a larger amount of irrigation water than would normally be required for these crops and results in higher drainage fluxes, which in some areas of the NAP may be contributing to rising groundwater levels. Vegetable crops in sandy loam soil such as these would more commonly be grown with root zone soil matric potentials maintained between around -30 kPa to -45 kPa (Shaw, 1999 after Maas and Hoffman 1977).

An ideal irrigation policy for this location would be one in which the amount of irrigation water applied is sufficient to maintain root zone matric potentials around this range while also maintaining root zone salinity levels close to those maintained with a soil matric potential trigger of -10 kPa to -15 kPa. The maintenance of low root zone salinity could be achieved, even when lower irrigation trigger potentials are used, either by using irrigation water of a lower TDS concentration or by introducing irrigation during winter seasons even when the crop in place does not require it. Such irrigation events may be more effective in achieving flushing of solutes from the soil profile than the maintenance of higher soil water contents during the summer, when the high ET conditions prevent significant drainage from occurring.

To test these possibilities, two further 20-year simulations were run. The first uses the same irrigation settings as for the -35 kPa auto-irrigation scenario described above, but with the addition of auto-irrigation of the winter cover crop, with the irrigation trigger set at a high soil matric potential value of -10 kPa. An auto-irrigated winter cover crop does not require much irrigation water as the soil water content is generally high during the winter because of rainfall and lower ET potential. The low irrigation trigger potential of -35 kPa for the spring/summer crops ensures a relatively low irrigation water requirement overall. The addition of winter irrigation takes account of the earlier findings that it is winter flushing by rainfall that is critical in maintaining soil salinity levels. Applying irrigation to maintain the high water content every winter increases the flushing that occurs during average winters and ensures some winter flushing of salts occurs even in the drier years.

The 70 cm $EC_{1:5}$ equivalent resulting from this scenario is shown in Figure 5.8. Over the 20 years of the simulation, the soil salinity trend with this scenario is approximately the same as for the -15 kPa irrigation trigger scenario. However, because the summer irrigation trigger is -35 kPa, the average annual irrigation water demand of 480 mm/y (Table 5.3) is significantly lower than the 662 mm/y for the -15 kPa trigger scenario, and only a little more than the demand of 447 mm/y for the -35 kPa scenario without the winter irrigation.

This decrease in irrigation demand compared to the -15 kPa scenario results from the decrease in evaporation achieved when the -35 kPa irrigation trigger is used for the spring/summer crops. The average annual drainage is reduced under this scenario, lessening the impact on groundwater. Furthermore, the lower volume of irrigation and lower evaporation also reduces the amount of salt added to the soil during summer. However, while the longer-term soil salinity trend in this scenario is acceptable, it rises to a higher peak each summer than the -15 kPa scenario, which may be detrimental to summer crop productivity. The graph in Figure 5.9 shows how significant this is to the overall salt content of the soil profile. Although the simulation indicates that the summer peak $EC_{1:5}$ value at 70 cm is higher with this scenario than with the more liberal irrigation scenarios, the overall mass of salt in the profile between 0 and 110 cm depth is maintained at a lower level with this enhanced winter flushing scenario than for any of the previous four scenarios with summer irrigation only. This is because less irrigation-borne salts are accumulating in the soil profile over time with the enhanced winter flushing scenario.

Table 5.3 Water flux components with scenarios tested to determine soil root zone salinity development

Irrigation policy	Irrigation (mm/y)	Irrigation + rain (mm/y)	Transp. (mm/y)	Evap. (mm/y)	Drainage (mm/y)	70cm $EC_{1:5}$ after 20 yr (µS/cm)	Salt added to soil profile (g/m2/y
-10 kPa trigger	885	1314	472	726	120	389	1115
-15 kPa trigger	662	1092	475	555	66	538	835
-25 kPa trigger	509	939	483	435	25	727	641
-35 kPa trigger	447	877	487	389	5	754	564
-35 kPa with winter flush irrig.	480	910	470	419	26	509	605
-35 kPa with low salinity irrigation	447	877	487	389	5	457	282

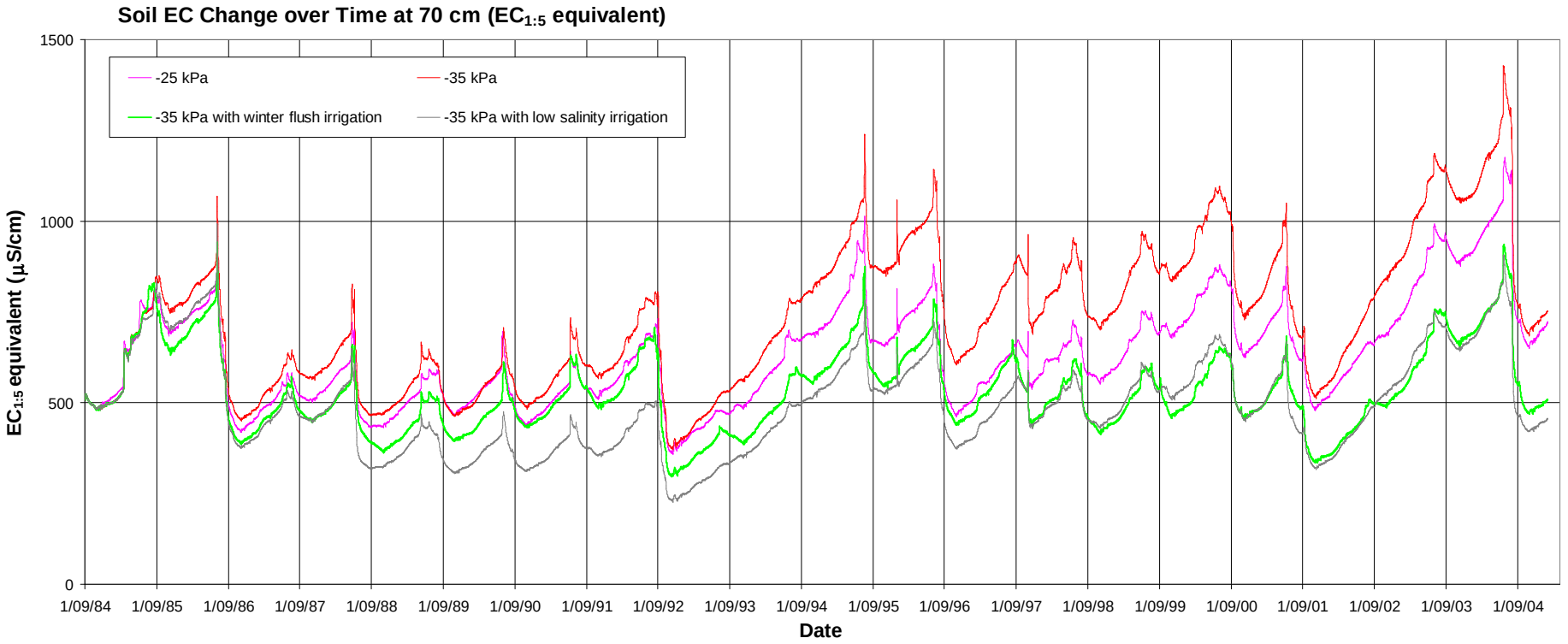

Figure 5.8 Changes in soil salinity at 70 cm depth over a 20-year simulation with varying irrigation trigger potentials and irrigation water TDS. Data shown in green is for 20-year simulation with the same three crops though each year as for the other simulations, but with auto-irrigation of the winter cover crop with an irrigation trigger set at -10 kPa soil matric potential. Data shown in dark grey are for a simulation with a -35 kPa auto-irrigation trigger but with irrigation water of half the TDS of that used in the other simulations.

The final scenario trialed with this model also uses the -35 kPa auto-irrigation trigger, but instead of applying winter irrigation, the salinity (TDS) of the irrigation water is reduced to half that applied in the previous scenarios. This is intended to represent a situation in which the reclaimed water supplied by the Virginia Pipeline Scheme is significantly improved in quality, by means such as partial desalination. This scenario has the dual benefits of low volume as well as low salinity of irrigation water, resulting in much less dissolved salt added to the soil than any of the other scenarios. The resulting development in the simulated 70 cm $EC_{1:5}$ is remarkably similar to the outcome of the previous simulation with the enhanced winter flushing irrigation. Root zone salinity is significantly lower for the first ten years of the simulation, but then for the following ten years is approximately the same as for the -35 kPa scenario with enhanced winter flushing. Again, this leads to a higher summer soil salinity than for the more liberal irrigation scenarios, but follows an acceptable long term trend over the 20-year simulation period. In this scenario, the salt added to the soil profile in the irrigation water is half that of any of the other scenarios (Table 5.3).

The benefit of lower salinity irrigation water is clearly demonstrated in the graph of the total root zone salt content shown in Figure 5.9. Within two years from the start of the simulation the total root zone salt content has dropped to less than with any of the other scenarios, then follows the same trends but at significantly lower values than any of the other scenarios tested, and at the end of 20 years has a significantly lower solute content than any of the other scenarios.

The low salinity irrigation water scenario creates an average annual irrigation demand and drainage that is as low as any of the scenarios tested and results in the lowest amount of salt added to the soil profile overall. However, its application in reality is dependent on considerable financial investment in the irrigation water supply infrastructure. A scheme in which summer irrigation is reduced and winter irrigation of cover crops is applied to enhance winter flushing may provide an acceptable outcome for soil salinity development under broadacre conditions on the NAP, without the need for large investments in water quality improvements.

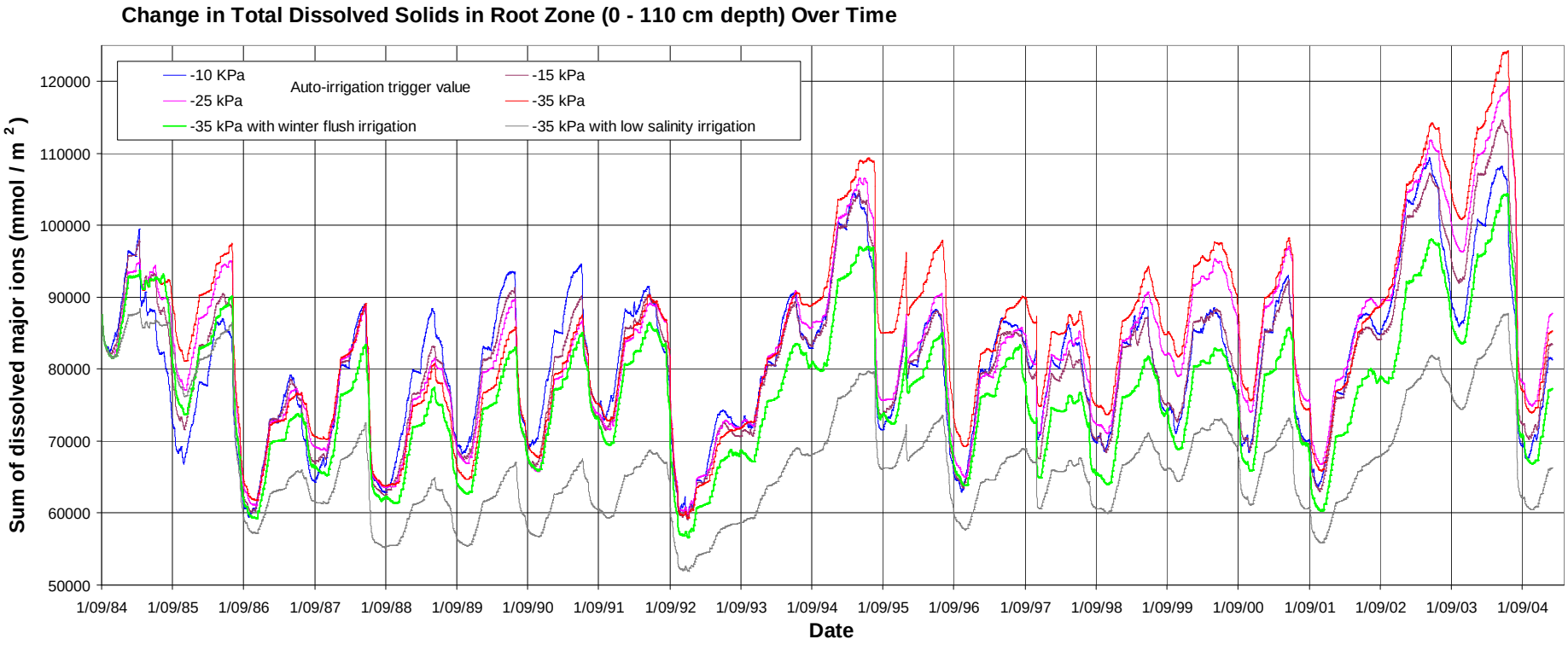

Figure 5.9 Changes in the total solutes in the soil profile from 0 to 110 cm depth over a 20-year simulation with differing automated irrigation scenarios.

5.4 Conclusions from Application of Models at the Point Scale

In the soil, crop, weather and irrigation conditions in a broadacre horticultural setting on the NAP, significant drainage through the soil profile occurs mainly during winter, when the majority of land is not irrigated. This drainage is caused by winter rainfall, occurring when the potential for evapotranspiration is at its lowest. However, the drainage occurring in winter significantly increased if land is irrigated through the summer because the soil has a lower moisture deficit to be replenished before drainage can start to occur in winter.

The amount of drainage occurring each year is highly variable and dependent largely on winter weather conditions. However this amount is poorly correlated with annual rainfall, such that annual rainfall cannot be reliably used as an indicator of the degree of drainage likely to have occurred in a particular year.

These findings demonstrate the importance of an appreciation of temporal scale in the analysis of soil water drainage: long term trends are difficult to predict from a short term analysis. A one- or two-year analysis of drainage resulting from a particular soil, crop and irrigation combination may provide a misleading indication of average annual drainage fluxes in even the most well-controlled irrigation conditions. However, analyses of cumulative drainage, evapotranspiration and irrigation amounts over a simulation period of twenty years show that inter-annual fluctuations in response to rainfall and potential ET conditions, become less significant in the long term trends of these variables. Hence, long-term average annual water use and drainage estimates can be made that are independent of annual fluctuations in weather at this site, assuming similar inter-annual climate variability in future. This may be particularly useful for regional natural resource managers.

The benefits of sensor-controlled irrigation policies can be assessed for a given combination of crop, soil and climate, using the methods described. For the soil, crop and climate combination modelled in this study, it was found that when using automated irrigation triggered by soil matric potentials, small changes in the matric potential trigger point create large changes in the amounts of drainage, evaporation and irrigation water used. However, there is a threshold around -25 kPa beyond which further reductions in irrigation trigger potential create insignificant improvements in average annual water use, evaporation and drainage.

While it is the amount of irrigation water applied during summer that governs the amount of salt added to the soil, it is the degree of winter drainage flux that governs the amount of salt

that drains from the soil root zone. The highly variable drainage flux during winter is the primary influence on the variation of soil salinity. This results in large seasonal fluctuations in root zone salinity, because of the seasonal nature of the effective drainage, and large inter-annual fluctuations due to the highly variable degree of soil flushing and drainage each winter.

In the soil, crop, weather and irrigation conditions in broadacre horticultural setting on the NAP, if high soil water contents are maintained for summer crops, the longer term trend in root zone salinity can be kept stable. However, if soil water contents are maintained at more typical levels for vegetable crops, the removal of solutes from the soil profile is less effective because of the reduction in flushing and drainage. Hence the longer term trend in soil salinity is upward, even though the amount of salt applied to the soil in irrigation water is less.

An irrigation regime that maintains root zone matric potentials around -10 to -15 kPa may maintain root zone soil salinity at an acceptable level, but demands a large volume of irrigation water and results in larger drainage accessions to the underlying water table. If irrigation water with significantly lower salinity is available, its use, even with a more conservative irrigation strategy, results in lower root zone salinity and consistently lower mass of salt in the soil profile than can be achieved with any irrigation strategy with higher salinity water.

Adopting a more conservative summer irrigation policy combined with the enhancing of soil flushing by over-irrigating during winter may be a practical compromise that achieves lower overall root zone soil salt content while using less water than typical current NAP irrigation practices.

CHAPTER 6: APPLICATION OF MODELS AT CATCHMENT SCALE

This chapter describes a methodology to distribute the models across the whole study area of the NAP to provide a tool for a catchment scale analysis and natural resource management based on the water flux models described in Chapters 4 and 5. An application of this methodology to the NAP is described, using soil hydrologic data generated from the laboratory analyses and field program together with landscape data available from existing natural resource databases.

6.1 Considerations When Up-Scaling Models

The one-dimensional models demonstrated in Chapter 5 become more useful for natural resource management if they can be extended to provide predictions for a large heterogeneous area. The one dimensional model can be applied at the scale of an individual plot if the variability of parameters across a plot are quantified. Alternatively an assumption of homogeneity can be made for the controlling parameters over the extent of the plot if the representivity of the model output is treated with sufficient caution.

When scaling up beyond the plot scale, the same assumptions of lateral homogeneity cannot be assumed as there are likely to be changes in land use, soil type, climate, and slope. Similarly, it is unlikely that a full quantification of the lateral variability of many parameters will be possible. For the modelling of hydrologic and hydrochemical processes in the soil zone over a large area, a true three dimensional model is not appropriate as the zone of interest is so much greater in lateral extent than in depth. Over the approximately 12,500 ha of the Northern Adelaide Plains, the 2 – 3 metres of the modelled soil profile has a area-to-depth ratio similar to an A4 sheet of paper. Furthermore, within the unsaturated zone, in which vertical hydraulic gradients are generally much greater than horizontal ones, the horizontal fluxes of water and salt are negligible over this scale. Hence a distributed one-dimensional model, in which the controlling parameters are changed according to a discretised model of their changes across the landscape, is more appropriate than a three-dimensional model.

The decision to upscale the modelling process in this way necessitates either a large amount of data for each of the controlling variables in the model, or a large scale

categorisation of variables derived from knowledge of these in the study area. With the categorisation of parameter values and discretisation of the study area into land area units defined according to their combination of land characteristics (e.g. soil types), there is an inevitable increase in the potential error of the model in its simulation of any point in the landscape. However, the resulting model is of great value for comparing scenarios. While the absolute values of outputs for any particular point in the modelled landscape may have a large margin of error, over the larger area, useful estimates of the direction and magnitude of change between two modelled scenarios are possible.

In order to expand the one-dimensional models examined here to a large and heterogeneous area we must examine the effects of generalising parameters measured at points in the landscape, across relatively large areas.

Bloschl and Sivapalan (1995) identify three components of the analysis of scale: *support*, *spacing* and *extent*. *Support* is the area (or time) over which a measurement averages the underlying conditions, or over which a model assumes homogenous conditions. *Spacing* is the separation between points at which measurements are made, or between computational points in a model. *Extent* refers to the total area (or time) covered by the measurements or model. Measurements of soil moisture characteristics can generally only be considered to have a spatial support of a few centimeters. Soil moisture probes or tensiometers, and laboratory measurements of soil cores provide detailed information on the hydraulic characteristics for a small sample of soil that may only be representative of soil at the point where the measurement or soil core is taken. These measurement techniques can be applied at a large number of points in a given area in order to reduce the spacing between each support area to which the measurement applies. Such techniques are commonly used to determine the variability of soil characteristics across a study area (Biggar and Nielsen, 1976; Braud et al., 2003). With this variability quantified, an average of each hydrological parameter may be found, together with variance limits, to provide data for which the support may be considered to be the whole study area.

An approach such as this, if applied to an area such as the NAP would require an impractical number of centimeter-scale measurement points to assemble a database of average hydrological parameters and their variance limits, for all land parcels in the region.

In estimating the flux to the water table over a large area, the outcome required is essentially the balance between water falling on the soil, water lost to evapotranspiration, and change in soil water storage:

$$\text{Vertical soil water flux} = \text{Rainfall} + \text{Irrigation} - \text{ET} - \Delta\text{storage} - \text{Runoff}$$

In the simplest analysis of such water balance, the difference between rainfall plus average irrigation applied to the area and an average ET estimate for the area provides an approximation for the net flux to groundwater. This simple water balance relies on a highly generalised approximation of ET, prepared without consideration of temporal and spatial variations in soil water availability due to variations in irrigation, crop cover and soil hydrologic characteristics. The most detailed analysis of such a water balance would involve measurements of soil hydraulic characteristics at multiple points in every parcel of land to determine average parameters and variance limits as described above. Similarly, the crop cover, irrigation, and rainfall in every land parcel would have to be monitored and recorded. A model could then be applied that determines the proportion of each water application that is lost to ET while considering both potential ET and the water available at the soil surface and in the root zone.

The latter analysis is impractical to apply in an area with the size and variability of the NAP. A compromise must be found between the simplest and most detailed approaches and its effectiveness tested.

If the outcome of the detailed approach described above is considered, one would derive a water balance for each land parcel and the sum of these would provide the total flux to groundwater for the whole area. The results could then be used to determine the most significant factors contributing to the annual flux in all land parcels. Armed with this information, a simpler model could be developed that would incorporate detailed data for only the most significant parameters and approximations for less significant parameters. In developing a practical approach to a regional estimate of areal recharge, a key challenge is to determine which are the most significant parameters and which can be approximated, without the benefit of such a detailed model.

To enable estimates of areal flux over a large and variable area such as the NAP, we must be able to consider the data used in our estimation to have a spatial support that is at least as large that implied by a land use map of the area. That is, each data item for each parameter involved in the water flux calculation must be applicable to a whole land parcel

or an area that contains a number of land parcels. The characterisation of the spatial variability of soil hydrologic characteristics across a large area requires considerable time and effort. However, such detail may not be required when trying to determine only the annual net downward flux. In field conditions several parameters are more influential on the soil water balance than those related to soil hydraulic characteristics, including the irrigation amounts and timing, crop cover development, and weather-related parameters that determine potential evapotranspiration. In the following analysis, these parameters are considered to have a spatial support equal in size to the individual horticultural plot.

The main influences of the hydraulic characteristics of the soil profile are in their effect on the rate that water infiltrates into the soil or is able to evaporate out of the soil, and the rate that it is able to drain through the soil profile and become unavailable for evaporation or transpiration.

Analysis of the output of soil hydrologic models constructed to represent soils at study sites in the NAP indicates that two components of the soil profile: the water retention characteristics of the upper-most 5cm of the soil, and the hydraulic conductivity of the low-permeability layer below the root zone; have a much greater influence on net flux to groundwater than either the soil water retention characteristics or hydraulic conductivity in other parts of the soil profile.

The soil hydrological characteristics of the upper 5 cm are more dependent on the type of cultivation of each land parcel than on the particular surface soil type prevalent in the area. For example, with vine or tree crop cultivation the surface remains largely undisturbed for long periods, whereas with broadacre vegetable crop cultivation, the soil surface is tilled between 2 and 6 times each year. The latter results in a soil surface that is more loosely consolidated, with greater porosity and lower bulk density, and consequently very different soil hydraulic characteristics. Thus in the case of the NAP, soil surface hydraulic characteristics may be more influenced by land use rather than by regional variations in soil types. The soil surface hydraulic characteristics for each land parcel may therefore also be considered to have a scale support of land parcel size.

The variation of the hydraulic conductivity of the low-permeability B-horizon remains to be examined. The effects of sodicity and clay dispersion in this clay layer must be considered as these factors may cause the conductivity of the layer to vary temporally as well as spatially. A prerequisite to any field study of this variation will be a thorough

analysis of the effect of variations in the conductivity of this layer on annual net vertical water flux predicted by the soil water transport model. An existing soil map of the whole NAP area (Matheson and Lobban, 1975) describes the variation in thickness and texture of the sandy-loam A-horizon across the area and the depth to the interface between the A-horizon and the clay B-horizon. This map provides a template for the generalisation of soil hydrological conditions across the area.

6.2 Methodology for Applying Models to the Whole Study Area

The catchment-scale analysis applies the one-dimensional models described in Chapters 4 and 5 to a large number of discrete land areas which are defined by a combination of the soil type and land use present. For irrigated agricultural land uses, an irrigation schedule or policy was also defined for the crop type. Firstly, thematic maps of the spatial distribution of attributes (hereafter 'spatial variables') such as soil profile types and land use types, that may affect the soil water balance within the study area, are generated using a geographic information system (GIS). In the method used here, vector-based GIS coverages were converted to raster coverages within the GIS, prior to being output as ASCII text-based raster files. The raster files each describe the spatial distribution of a single attribute over a geographical area that is common to all raster files. A modified version of the LEACHP program, termed LEACHPG (Hutson et al., 1997), reads the raster files and performs an operation to effectively overlay the raster images and encode each raster cell with the unique combination of the spatial variables identified in that cell location. This process is conceptually illustrated in Figure 6.1.

The input data for LEACHP are contained in separate data files for soil profile hydrologic characteristics (SOIL.xxx), initial soil chemistry (PPROP.xxx), crop cover (CROPS.xxx), irrigation (IRRIG.xxx), chemical applications (PMANG.xxx) , rainfall (WEATH.xxx), and reference ET data (ETRAN.xxx). Several versions of each data file can then be constructed for as many different soil profile types, crop types, irrigation types and weather regions as are to be included in the analysis. The LEACHPG model requires that input data is prepared in individual data files for each data type so that data can be included for each identified class of each spatial variable existing in the study area. These data files are identical to the corresponding sections describing these variables within the standard LEACHP data file described in chapter 4.1. Separation of the sections into separate data files allows a number of variations of each data type to be described in individual data

files. For example, in the simulation described in section 6.3 (page 131) there are seven soil profile types defined in seven separate dedicated soil profile description data files, and eleven land cover types defined in eleven crop cover description files.

The LEACHPG model constructs and runs the LEACHP model for each unique combination of spatial variables identified by the raster file overlay process described above. The flowchart in Figure 6.2 describes the whole LEACHPG distributed modelling process.

LEACHPG reads the data in the first cell of each of the soil, land use and irrigation rasters and assigns a code to that cell position, representing the combination of the first cell value in each raster. It repeats this for each cell in the rasters and then performs a LEACHP simulation for each unique combination code identified, taking the data required for the simulation from the spatial variable data files designated by the raster cell's combination code. LEACHPG creates output files (.OUT, .SUM and .BTC) for each simulation, with the same format as the corresponding output files from a LEACHP simulation. The output files are named by combining the land use, and irrigation category number (two digits each, allowing up to 100 categories) with the soil, rainfall, ET, chemical application and soil chemical properties category numbers (single digits, allowing up to 10 categories). For example, files resulting from a simulation of a combination of soil class 2, soil chemistry class 1, land use class 12, irrigation class 12, and with uniform ET and weather classes of 0 for the whole study area, would create output files 21121200.OUT, 21121200.SUM, and 21121200.BTC. After all combination simulations are complete, individual output variables, such as root zone drainage, may be written to raster image files and read back into the GIS to create maps to illustrate the variation of that variable over the simulated study area. Finally, LEACHPG creates a text file (SPREAD. OUT) which lists totals over the whole simulation period for water and chemical balance components for each combination simulated.

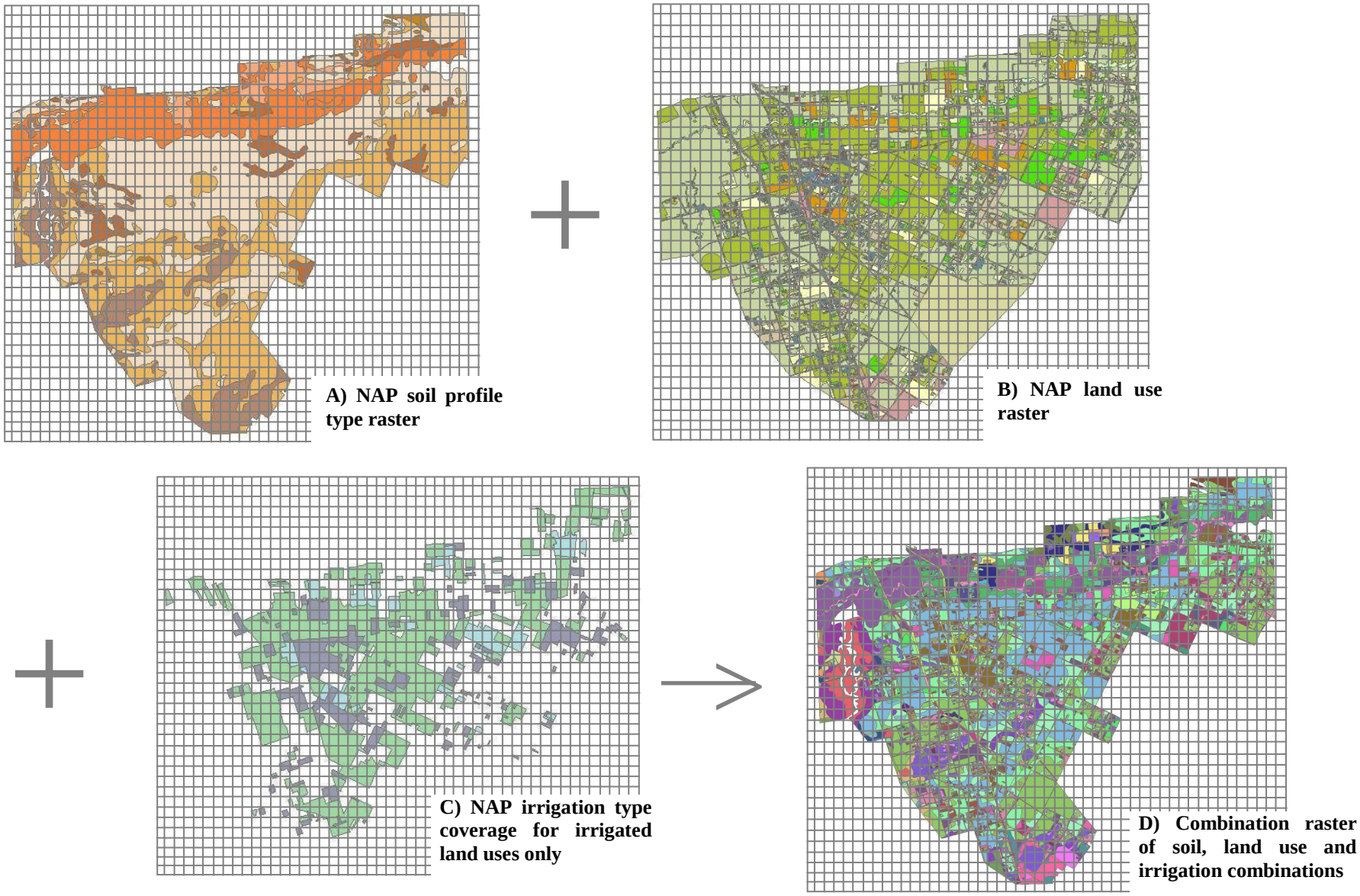

Figure 6.1 A GIS coverage of soil profile types (A) is overlain by a coverage of land use (B) and an irrigation coverage (C) for the horticultural district of the NAP . The intersection of the three coverages results in a coverage (D) containing over 4000 individual land parcels defined by their combination of soil, land use, and irrigation types. More than one parcel can have the same soil/land use combination but parcels with this commonality are spatially separate.

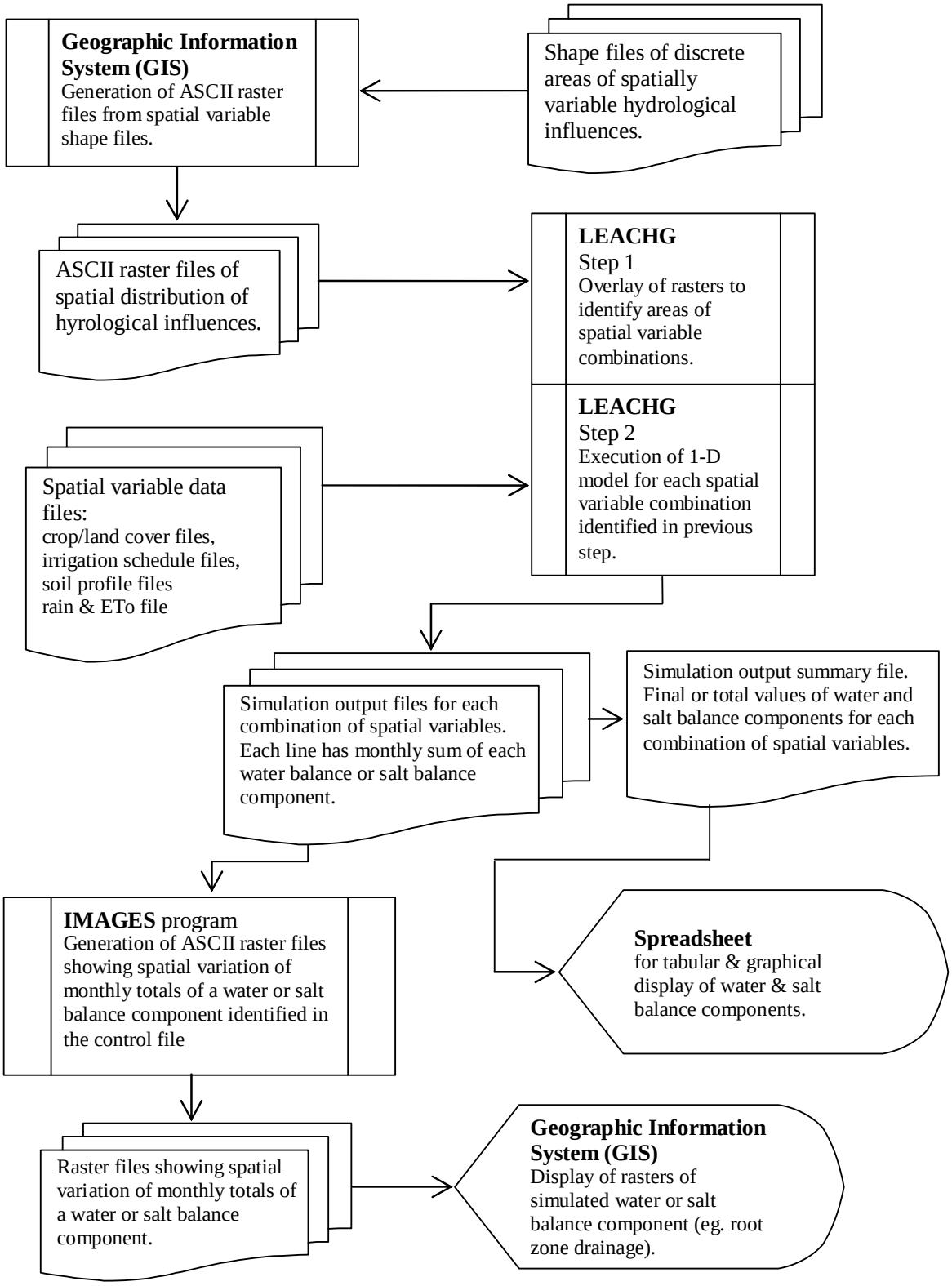

Figure 6.2 Flowchart of the distributed modelling process using the LEACHPG program.

6.3 Catchment-Scale Annual Water Balance Derived from a 20-Year Simulation Distributed Across the NAP Agricultural Area

A catchment-scale assessment of the whole NAP horticultural area was achieved using seven soil profile type descriptions and 11 land use categories. Soil descriptions are derived from a combination of the soil profile descriptions in the Northern Adelaide Plains Suitability of Land for Irrigation map of Matheson & Lobban (1975), and soil profile hydrologic characteristics are taken from the soil profile description of the most reliable LEACHM models of the PGR study site. The thicknesses of each soil horizon in each of the seven soil profile types is determined from the descriptions of the seven soil profile types listed in the Matheson & Lobban (1975) map. Areas of the respective soil type zones are derived from a GIS coverage in the Primary Industries and Resources, South Australia (PIRSA) 2002 state soils database. The zones on the PIRSA soil map are coincident with those on the Matheson & Lobban map, and are assumed to have been derived from the latter.

Vegetation coverage for the various land uses was assessed according to observations at the various study sites, together with a synthesised vegetation coverage for natural grass and weed growth. The vegetation coverage for all broadacre vegetable growing land is intended to simulate the crops grown at the PGR site during the monitored period. Other synthesised vegetation coverages are used for grazing/crop rotation, urban residential, and rural residential land use categories, as well the category of “other minimal use”, which is a generalised category for farm tracks, yards and other small areas of minimal vegetation coverage.

Rainfall is the same for the whole region and uses 20 years of data from the Edinburgh SILO weather station. ETo is calculated according to the Penman-Monteith (FAO 56) method using weather data from the Edinburgh SILO weather station with a daily time increment.

For irrigated land uses, a simulated irrigation scheme is applied wherein the crop is irrigated after the soil water potential falls to a set trigger potential. Once irrigation commences, due to a trigger potential having been reached, it will continue until sufficient water has been applied to fill the soil to saturation to a chosen depth. The trigger potential is set according to the crop type. For vegetable crops the trigger is -10 kPa, which results in a soil water potential while crops are in place that is similar to that observed at the

vegetable study sites. Lower trigger potentials were used to simulate the more conservative irrigation applied to in areas of irrigated perennials (almonds and olives) and grape vines.

Two simulations of 20 year duration have been completed: one intended to represent the current coverages of crops and current irrigation practices across the NAP region, and one intended to represent the same area without irrigated land uses. The latter simulation is intended only to provide an indication of the proportion of drainage that can be ascribed to horticultural practices in the study area.

In reporting the results of this analysis, we have to make a distinction between drainage flux and volume. The flux is considered to be the 1-dimensional transfer of water over time and here is measured in mm/year. The volume is the flux multiplied by the area over which that flux applies and is reported for a given time period in megalitres (ML). This distinction is illustrated in Figure 6.4, which shows separate graphs of drainage flux per year and drainage volume per year for the 11 different land uses and 7 different soil profile types employed in the model.

The total land area covered by the model is 12,561 ha, which is divided into eleven land use categories as shown in Table 6.1 (page 134). Among the land use categories described in the model, only three have irrigation applied in this simulation, these being broadacre vegetables, irrigated perennial horticulture, which in the NAP area mostly represents almond tree cultivation, and irrigated grape vines. The category of irrigated broadacre vegetables includes a variety of vegetable types such as carrots, potatoes, brassicas, and onions. The study area cannot be divided into sub-areas of these individual vegetable types for a long-term simulation because vegetable crop types are rotated on each area of vegetable growing land. Commonly more than one type of vegetable will be grown on a plot of land in a singe year. For the purposes of this simulation, all the broadacre vegetable areas have been treated with the same annual rotation of a carrot crop, potato crop and barley cover crop as used in the single-point simulations described in sections 5.1 to 5.3. The total area of the three irrigated landuses in this simulation is 3603 hectares, representing 29% of the 12561 hectares covered by this simulation. The land area covered by the simulation is also divided according to the seven soil profile types identified identified by the PIRSA 2002 database. The areas of the various combinations of land use category and soil profile type are illustrated in Figure 6.3.

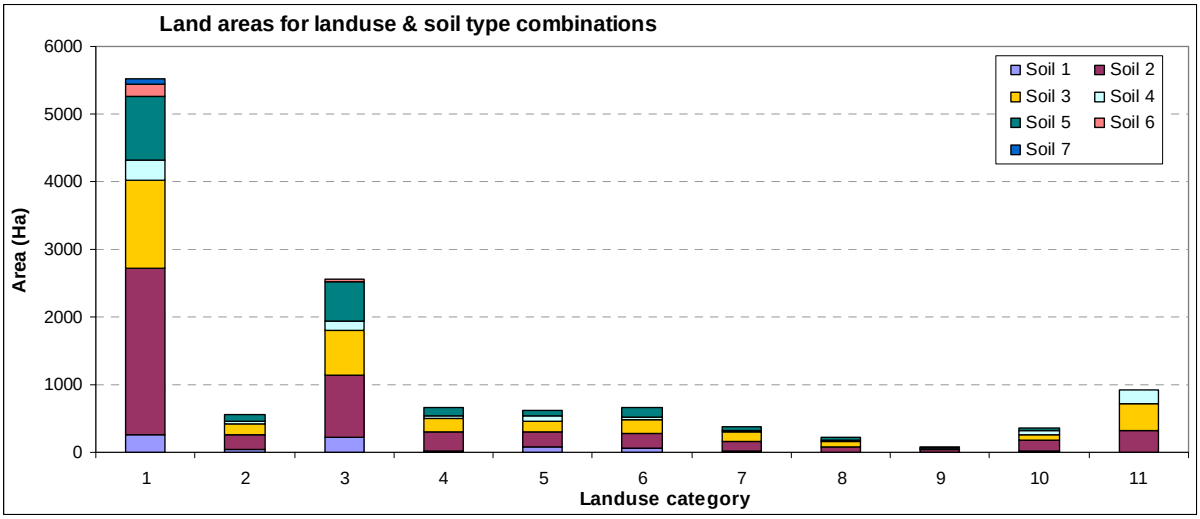

Figure 6.3 Areas of the 11 land use categories and soil profile types incorporated in the 20-year simulation. Land use categories are numbered: 1. Grazing/crop rotation, 2. Roads, 3. Irrigated broadacre vegetables, 4. Other minimal use, 5. Rural residential, 6. Irrigated perennials (almonds), 7. Irrigated vine fruits (grape vines), 8. Glass houses, 9. Shade houses, 10. Urban residential, 11. Defence facilities.

The majority of land in the study area is in the grazing/crop rotation land use category, which represents land that is either used perennially for grazing or is rotated between grazing and fodder crops or nitrogen-fixing land cover. Second in land area to this category is the irrigated broadacre vegetables category. The other irrigated land use categories, of irrigated perennials (primarily almond trees) and vines, are relatively minor in area and similar in overall area to roads, rural residential land and a grouping of other miscellaneous areas of minimal use. The distribution of soil types is fairly similar between these categories closely related to the distribution of the total area of these soil types in the study area. Soil types 1,2 and 3 are sandy loams overlying a clay subsoil, type 1 having the deepest sandy loam and type 3 the shallowest of these three. Soil type 2 is the most favoured for irrigated horticulture in the NAP. Soil type 1 is also favoured but is limited in extent, and hence does not represent a large proportion of the area of any of the land use categories. Soil type 5 is a dark cracking clay soil on the Gawler River floodplain. Types 5 and 3 are adequate for horticulture and are extensive across the study area, which is why they both represent fairly large areas of the irrigated horticultural and grazing land use categories. Types 4, 6 and 7 are less suitable for irrigated horticulture and represent only small areas of these land use categories.

In the rural residential and miscellaneous categories, the majority of the land is commonly left to for development of grass and weeds. In the whole-area model, these are given a

common vegetation cover description intended to simulate grass/weeds growing through the autumn and winter and then senescing in late spring and summer.

6.3.1 Whole area model output.

Table 6.1 shows the annual mean quantities of the inputs and outputs of water to the whole study area, distributed across the eleven land use categories. The values shown are annual averages of the total water volumes determined from the 20-year simulation. The high degree of annual variability that is typical for these water flux volumes was demonstrated in Section 6.2. It must be considered that in any one year, flux volumes may differ markedly from the mean values shown in Table 6.1. Simulated runoff was less than 0.5% of rainfall and is not included in the table.

Table 6.1 Summary of output from 20-year whole area simulation

Land Use ID	Land Use Description	Total Area (Ha)	Annual Rain (ML)	Mean Annual Irrigation (ML)	Mean Annual Drainage (ML)	Mean Annual Evap (ML)	Mean Annual Transp (ML)
1	Crop/grazing rotation	5522	23186	0	2155	1680	19355
2	Roads	568	2383	0	633	1751	0
3	Irrigated vegetables	2562	10708	21856	3003	17828	11740
4	Other minimal use	667	2801	0	444	1580	778
5	Rural residential	627	2633	0	246	187	2201
6	Irrigated perennial hortic.	662	2770	4816	456	3011	4120
7	Irrigated vines	378	1587	1989	205	1303	2068
8	Glasshouses	214	896	0	536	360	0
9	Shadehouses	72	303	0	102	201	0
10	Urban residential	363	1527	0	69	576	882
11	Defence facilities	925	3896	0	340	276	3281
Whole study area totals:		**12561**	**52692**	**28661**	**8188**	**28752**	**44425**
Irrigated areas totals:		**3603**	**15065**	**28661**	**3663**	**22142**	**17928**

There are a number of notable observations that can be made with regard to the values in Table 6.1. The simulated mean annual drainage volume for the whole study area over 20 years is 8,188 ML/year. The annual drainage volume from irrigated areas alone is 3663 ML. Irrigated areas represent 29% of the total area and generate 45% of the drainage volume.

The greatest proportion of drainage from irrigated land uses results from the irrigated vegetable category. This is because these occupy a greater area than the other two irrigated land use categories and because irrigated vegetable horticulture generates greater drainage fluxes than perennial horticulture land uses. These quantities are illustrated in Figure 6.4.

Evaporation from the soil surface is significantly greater in areas of irrigated land use than in other areas. Over the whole study area, transpiration is greater than evaporation. But

within the irrigated areas, evaporation is significantly greater than transpiration. This is because of the large amount of water applied in the summer months in irrigated areas and because of the cycles of crop growth and removal in the irrigated vegetable horticulture areas, leaving the soil exposed for part of each year. In areas of grass or natural vegetation cover, the soil surface is covered with vegetation for the whole year, allowing year-round transpiration to occur across the whole land surface. Figure 6.4 further illustrates how drainage fluxes and annual drainage volumes are distributed across different land uses and soil profile types.

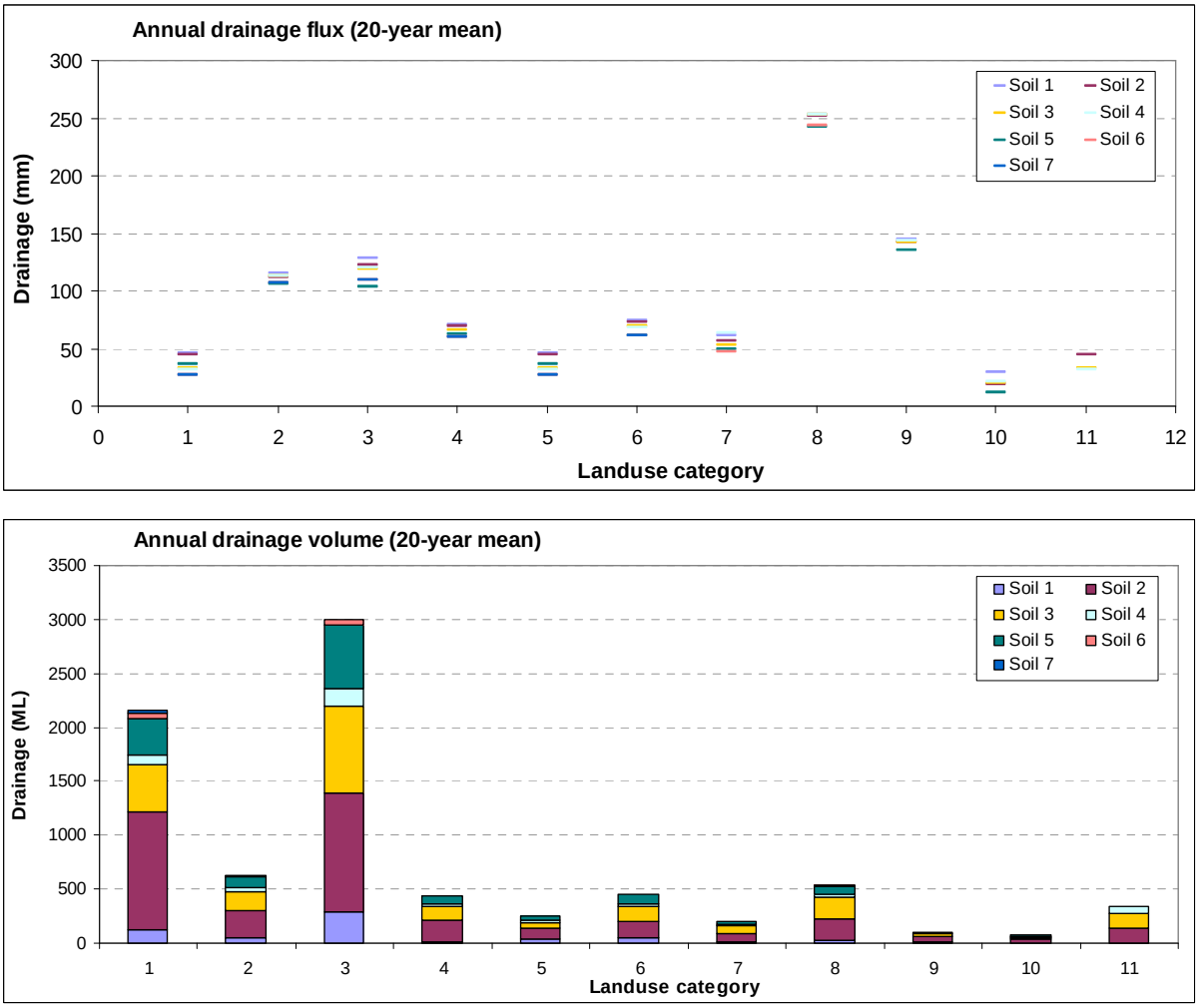

Figure 6.4 Annual average drainage fluxes and drainage volumes for the each land use / soil type combination (refer to Figure 6.3 for land use categories)

The results illustrated in Figure 6.4 suggest that differences in land use create significantly more variation than differences in soil type. Within the irrigated vegetables land use category there are large variations in annual drainage volumes between different soil types because of the differences in area of the seven soil profile types with this land use. For

example, there is a particularly large volume of drainage resulting from irrigated vegetables on soil type 2 because of the combination of relatively high drainage flux and large land areas with this soil and land use combination. Of the irrigated horticultural land uses, the three that create the highest drainage fluxes were irrigated vegetables, ranging from 103 mm/yr to 128 mm/yr depending on soil type, followed by irrigated perennials (mainly almonds), ranging from 61 mm/yr to 74 mm/yr, then irrigated grape vines with 48 mm/yr to 61 mm/yr.

Areas with no vegetation have the highest drainage fluxes, particularly roads and glass houses, which are treated in the model as mostly impervious surfaces from which runoff is channeled, reducing evaporation and enhancing infiltration. Areas of grazing/crop rotation have low drainage fluxes but have the highest drainage volumes because of their large areas.

The 3663 ML mean annual volume of drainage from the irrigated land is approximately 45 % of the annual mean drainage volume of 8188 ML for the whole area covered by the simulation. As discussed in Section 5.2, drainage fluxes can vary by more than one order of magnitude from year to year. Hence when interpreting the annual mean fluxes stated here it must be considered that the annual flux in any one year may differ significantly from the 20-year mean. The single point simulations discussed in section 5.2 showed standard deviation values of up to 59% of the mean annual drainage for irrigated vegetable crops with sensor-controlled irrigation. The cause of this variation is the annual variability in rainfall and ET conditions, and this variability can be expected to occur across the study area. Hence, similar inter-annual variations are expected in the annual drainage for the whole-area. A SD of 50% of mean annual drainage values for all the areas of irrigated vegetables in this simulation would result in a range of annual drainage values from 54.5 mm/yr to 192 mm/yr.

6.3.2 Whole area water balance

Using mean annual water volumes from the 20-year simulation the annual water balance is as follows:

For the whole study area:

	Rain	+	Irrigation	=	Drainage	+	Evaporation	+	Transpiration	+	Runoff	+	ΔSoil storage
ML:	52692	+	28661	=	8188	+	28752	+	44425	+	221	-	223
%:	64.8%		35.2%		10.0%		35.4%		54.6%		0.3%		-0.3%

For only the irrigated crop areas:

	Rain	+	Irrigation	=	Drainage	+	Evaporation	+	Transpiration	+	Runoff	+	ΔSoil storage
ML:	15065	+	28661	=	3663	+	22142	+	17928	+	113	-	120
%:	34.5%		65.5%		8.4%		50.6%		41.0%		0.3%		-0.3%

The average percentage of water going to drainage from the irrigated areas is quite low at only 8.4% of the total (irrigation and rain) water volume. However, this drainage volume is 8.4% of a much larger volume of water that would have been received by these areas prior to irrigation, hence drainage fluxes are large compared with non-irrigated areas.

This simulation provides an estimate of the relative proportions of the components of the whole-area water budget according to the current land use status of the NAP area. It is useful in considering the present-day water budget to have an indication of how it may differ from that which would exist in the absence of irrigated agriculture. In a repeat of this simulation, all the land use areas that currently have irrigated crops have been replaced with areas of natural vegetation growth. This is achieved by replacing the crop descriptions for the irrigated horticultural land uses (irrigated vegetables, perennials and grape vines) with a vegetation cover description representing natural grass and weed growth and deleting the simulated irrigation for these land uses. Table 6.2 summarises the output of this alternative simulation. The resulting water balance is as follows:

Annual water balance for the whole area without irrigation:

	Rain	+	Irrigation	=	Drainage	+	Evaporation	+	Transpiration	+	Runoff	+	ΔSoil storage
ML:	52692	+	0	=	5397	+	7207	+	40158	+	157	-	227
%:	100%		0%		10.2%		13.7%		76.2%		0.3%		-0.4%

Annual water balance for the now-irrigated areas when under natural vegetation:

Rain	+	Irrigation	=	Drainage	+	Evaporation	+	Transpiration	+	Runoff	+	ΔSoil storage
ML:												
15065	+	0	=	1399	+	1073	+	12656	+	51	-	114
%:												
100%		0%		9.3%		7.1%		84.0%		0.3%		- 0.7%

Comparison of these volumes to the simulation with present-day irrigation practices shows that total drainage volumes may have increased considerably: by 162% for the areas of irrigated horticulture and by 52% for the whole area compared to volumes draining without horticulture in the area.

It is also apparent that when land is converted from natural vegetation to irrigated horticulture, the proportion of water that is transpired decreases significantly and the proportion evaporating and draining increases. Note that the volume of transpiration from the irrigated areas is significantly greater (42% more) than from the same areas with natural vegetation, however this volume transpired results from a much greater volume of water applied, leading to transpiration being a considerably lower proportion of the overall water budget for the irrigated land.

Table 6.2 Summary of output from 20-year whole area simulation with irrigated crop areas replaced by areas of natural vegetation

Land Use ID	Land Use Description	Total Area (Ha)	Total Rain (ML)	Annual Mean Irrigation (ML)	Annual Mean Drainage (ML)	Annual Mean Evap (ML)	Annual Mean Transp (ML)
1	Crop/grazing rotation	5522	23186	0	2155	1680	19355
2	Roads	568	2383	0	633	1751	0
3	Formerly irrigated land use	2562	10756	0	997	763	8998
4	Other minimal use	667	2801	0	444	1580	778
5	Rural residential	627	2633	0	246	187	2201
6	Formerly irrigated land use	662	2780	0	257	197	2327
7	Formerly irrigated land use	378	1590	0	146	113	1332
8	Glasshouses	214	898	0	82	64	753
9	Shadehouses	72	304	0	29	22	253
10	Urban residential	363	1527	0	69	576	882
11	Defence facilities	925	3896	0	340	276	3281
Whole study area totals:		**12561**	**52755**	**0**	**5397**	**7207**	**40158**
Irrigated areas totals:		**3603**	**15126**	**0**	**1399**	**1073**	**12656**

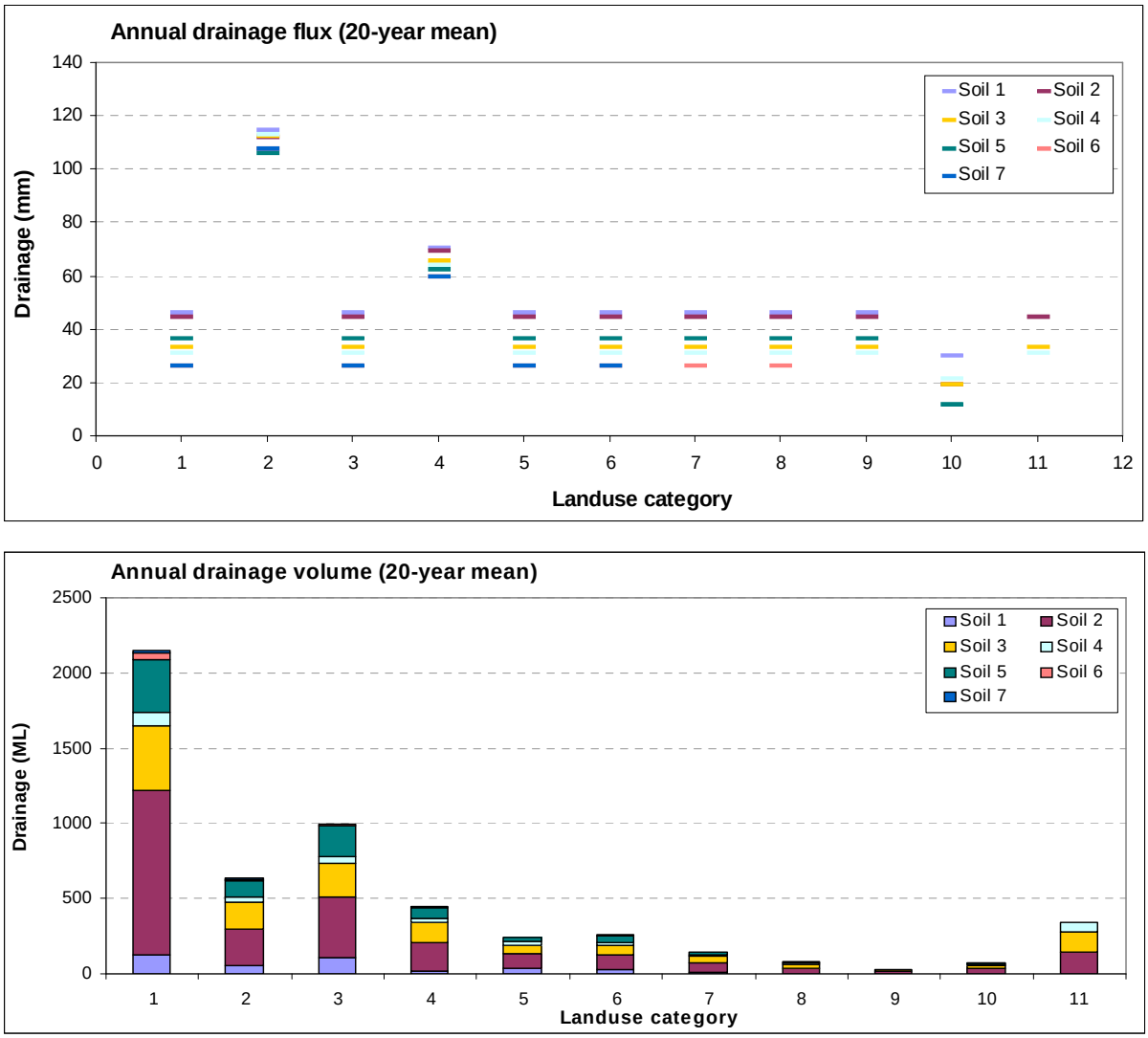

Figure 6.5 Drainage fluxes (1) and volumes (2) for the each land use / soil type combination irrigated crop areas replaced by areas of natural vegetation.

The simulated mean annual drainage volume for the whole study area with no irrigated horticulture is 5397 ML/y. This compares to an annual mean of 8,188 ML/y in the simulation of present-day irrigation, an area-wide increase of 52 % in drainage volume compared to the no-irrigation scenario.

Areas that now have irrigated crops (replaced in this simulation with natural grass /weed vegetation) have average annual drainage flux of 39 mm/y and annual drainage volume of 1399 ML/y. This compares with a mean annual drainage flux of 102 mm/y and mean annual drainage volume of 3663 ML/y over the same areas with their present-day irrigated land uses, an increase of 162%. Areas without irrigation have the same fluxes as they do in the no-irrigation simulation. However, their proportion of overall drainage volumes is

now less significant because of the considerably larger volumes of drainage from irrigated crop land.

The increase in evaporation over transpiration is converse to what would be desirable in irrigated horticulture. Ideally, most of the water would be transpired from the irrigated crop and a small amount, around 10%, would be a leaching allowance intended to go to drainage. Any water that is evaporated deposits its dissolved salts in the soil while not being used by the crop. Under the scenario simulated here, it would be unwise to attempt to alter irrigation to reduce drainage since the proportion of drainage from the irrigated areas is already fairly low, at an average of about 8%. Further reductions would be likely to lead to an increase in soil salinity over the long term. An important objective of any new irrigation strategy would be to reduce evaporation, increasing the proportion of water supplied that is used by the crop, and decreasing the total irrigation water volume. Several methods for reducing evaporation are available and are already used by horticulturalists in the NAP area, including drip irrigation, irrigating at night, mulching, and sub-surface irrigation.

In the setting of the NAP, where there is an available volume of reclaimed water for irrigation, there is no requirement to reduce the overall irrigation water use in order to reserve more water for other purposes. The savings in irrigation water resulting from measures to reduce evaporation could then be redirected to supply to an expanded area of irrigated land.

6.3.3 Effects of water table depth change

The simulations described here assume a fixed water table depth of 2.6 m across the whole study area. While this is a typical depth for the water table aquifer under the NAP, in reality seasonal and spatial variations may cause the water table depth in the uppermost unconfined aquifer to vary from this value by about 1 metre, as shown by the depth-to-water records of a number of state government observation wells in this aquifer in the vicinity of the TR and HX study sites during the period of the field study (Figure 6.6). The measurements from the PGR study site piezometers, illustrated in Figure 3.7 in Chapter 3, showed the water table depth in that location to have seasonal variation of about 0.2 m and spatial variation across the study site, also of about 0.2 m.

The water table depth fluctuations in the upper unconfined aquifer remain fairly small (~ +/- 1 m) because this aquifer is a thin aquifer of Quaternary silts and sand, which is not developed for water supply. The all groundwater used in this area is pumped from the deeper, confined Tertiary limestone aquifers. The large seasonal fluctuation in those aquifers is not significantly reflected in the water levels of the upper unconfined aquifer.

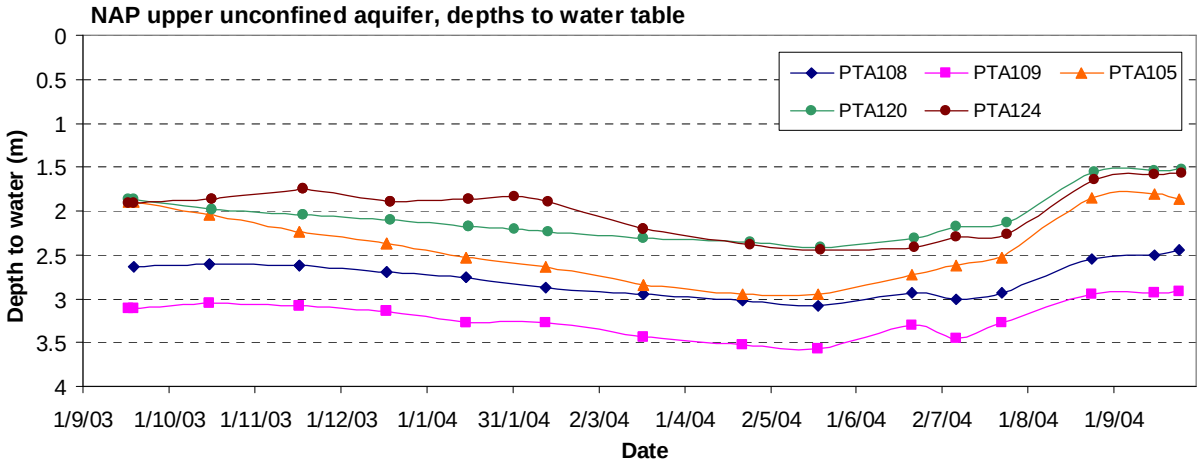

Figure 6.6 Water table depths in SA state government observation wells in the vicinity of study sites HX and TR

It is somewhat unpredictable whether a change in water table depth will increase or decrease drainage fluxes. A shallow water table may in some cases increase drainage fluxes as the whole soil profile is maintained at a higher water content, with a consequently higher unsaturated hydraulic conductivity of the soil. In other cases a shallower water table may cause a decrease in drainage fluxes as 1) the higher soil moisture content causes greater evaporation so net drainage fluxes are lower and 2) the hydraulic potential differences between the soil surface and deeper soil layers are reduced.

The 20-year whole-area simulation described above was run two more times to test the effect on drainage fluxes of altering water table depth to 0.5 m deeper and 0.5 m shallower than the 2.6 m depth of the original model. With the deeper water table, the mean annual drainage volume for the whole study area increased to 8527 ML, an increase of about 4% compared to the original model's 2.6 m water table depth. With the shallower water table, the mean annual drainage decreased to 7423 ML, a decrease of approximately 10%. These changes in flux indicate that in the soil profiles simulated here, the increased hydraulic potential differences and reduction in surface evaporation resulting from a greater water table depth has more effect on vertical water flux rates than the increased soil hydraulic conductivity that may result from a rise in soil water content due to a shallower water table

depth. The implications of this sensitivity to water table depth is that if there were a widespread rise in water tables over the modelled area, the net drainage fluxes of water to the water table would be likely to reduce compared to the model results described in this chapter. This reduced drainage flux would also result in decreased flushing of salts from the soil root zone and hence a rise in root zone salt content.

6.4 Recommendations for Irrigation Management

There is scope for a significant reduction in the volume of irrigation water used per hectare for broadacre horticulture, and for the drainage flux to the underlying unconfined aquifer to be reduced. However, irrigation policies to achieve this must take account of the potential increases in root zone salinity that may result.

It is clear from the results presented in this chapter that a major impact of the introduction of irrigation of broadacre crops to the NAP has been a great increase in the proportion of the soil water budget that is lost to evaporation. This is counter-productive to any irrigation scheme as it results in much of the irrigation water applied being ineffective and increases the accumulation of water-borne salt in the root zone. There is therefore a need for irrigators and natural resource managers to tackle the proportion of irrigation water applied that is lost to evaporation. Reductions in evaporation have the potential to reduce irrigation water requirements, and reduce the accumulation of salts in the root zone without increasing the fluxes of water draining to the underlying groundwater. This could be achieved using well established methods such as sub-surface drip irrigation or mulching. However these methods are often not practical for broadacre vegetable horticulture which requires frequent replanting and dismantling of irrigation structures.

The proposal for winter flushing irrigation, combined with a more conservative summer irrigation policy, is a possible approach to reducing evaporation in broadacre vegetable irrigation. Such an approach should result in less evaporation of irrigation water applied in summer because the soil is maintained in a drier state, and also a low proportion of evaporation of irrigation applied in winter (for flushing) because potential ET is lower at that time.

The introduction of soil moisture sensor-controlled automated irrigation has the potential to reduce irrigation water volumes and without significantly reducing soil root zone water contents below levels currently maintained by growers. Once such systems are

established, the irrigation trigger levels should be experimented with, starting cautiously by initially maintaining high root zone water contents. It is expected that small changes in irrigation trigger points will create large changes in the amounts of drainage, evaporation and irrigation water used. However, there is a threshold beyond which further reductions in irrigation trigger potential create insignificant improvements in average annual water use, evaporation and drainage. Low trigger potentials may not be economically justifiable as the risk of crop yield reductions is not balanced by a significant reduction in water use or environmental impact. If lower root zone water contents are trialed, it is important that root zone salinity is monitored and that any sustained increase in salinity is responded to by appropriately adjusting irrigation applications. However, it may take several growing seasons to determine a trend in soil salinity development.

It is recommended that the NAP NRM authority should establish a trial site in which enhanced winter flush irrigations are trialed along with a fairly conservative summer irrigation strategy. The root zone salinity in this trial site should be closely monitored and compared with an accompanying trial site that uses the same conservative summer irrigation but no enhanced winter flush irrigations. Developing soil salinity may become a significant issue and a limit to productivity in NAP horticultural plots in the near future. The establishment of a monitoring program for soil salinity in irrigated broadacre horticulture plots is recommended.

CHAPTER 7: CONCLUSIONS

The outcomes of this research can be divided in to two principal parts; 1) the development and application of one-dimension soil water and solute flux models for a number of monitored study sites, and 2) extension of these models to quantify soil water fluxes across the whole NAP horticultural area.

7.1 One-Dimensional Soil Water and Solute Flux Models

The first part of the study described a methodology for constructing and calibrating models of soil water and solute flow to achieve a realistic simulation of vertical fluxes in a number of study sites that were monitored for up to 18 months. Extending these simulations to a period of 20 years allowed examination of the degree of temporal variability in soil water drainage, including both seasonal variation within each year and inter-annual variation over a number of years. Further to this, incorporation of measured soil chemistry variables into the calibrated soil water flux models, enabled the examination of soil salinity development in irrigated crop scenarios with varying irrigation management strategies.

Key findings from this first part of the study, relating primarily to the 20-year simulation achieved using data from study site PGR, are:

1. Most drainage occurs in winter, when irrigation is not occurring. Summer season irrigation does significantly increase annual drainage compared to no irrigation at all, as it raises soil water content prior to the start of winter. However It is probably only late summer/autumn irrigation contributes to this effect and promotes winter drainage and soil salt flushing.

2. Irrigation leaching allowances in spring and summer under these soil and climate conditions may be ineffective as high ET prevents any significant drainage from occurring. The majority of the annual drainage flux occurs during winter, some time after irrigation has ceased for the year. Hence the amount of rainfall and the evapotranspiration potential through winter are highly influential on the annual drainage flux.

3. Drainage fluxes are highly variable from year to year, even when crops and irrigation management criteria are identical. Although drainage is caused mainly by winter

rainfall, the annual totals of drainage and rainfall are not well correlated. In some years a slightly lower than average annual rainfall causes a major reduction in total drainage, whereas in other years, low rainfall can result in average annual drainage. This finding is significant for other studies of drainage from irrigated soils, indicating that a) the duration of field study or model simulation must be sufficient to encompass the variation, and b) variations in annual rainfall are not a good guide to variations in annual drainage. The findings are also important when considering the possible effects of climate variability on drainage and unconfined aquifer recharge in this location, which could suffer a relatively major decline if there were a small but persistent reduction in rainfall and increase in evapotranspiration potential.

4. In general, soil root zone salinity increased in years of low drainage. However, the resulting elevated salinity levels are effectively reduced by flushing during winters when average or above average drainage fluxes occur.

5. Irrigation strategies that maintain higher soil water contents tend to promote higher annual drainage fluxes and maintain soil salinity levels within acceptable limits. More conservative irrigation strategies, that have benefits in reducing groundwater accessions and irrigation water requirements, result in greater increases in salinity, particularly during years with lower winter rainfall. Hence, strategies that increase irrigation efficiency in these field conditions need to be accompanied either by a reduction in irrigation water salinity, or by strategies to reduce the proportion of water that evaporates rather than transpires or drains.

The models developed for three field study sites suggest that typical drainage fluxes beneath irrigated broadacre horticulture on the NAP has a range extending between 52 mm/y to 201 mm/y with current irrigation practices. The upper end of this range is considerably less than the drainage fluxes estimated by Gerges and Kelly (2002), who used a water balance approach in their estimations and may have significantly under-estimated the evapotranspiration component. Furthermore, the models have demonstrated that automated irrigation controlled by soil moisture sensors could significantly reduce the drainage fluxes that result from current irrigation practices.

7.2 Extension of Models to the Whole NAP Area

The second part of the study demonstrated a methodology for extending the one-dimensional soil water flux models using a spatially distributed model structure, enabling assessment of soil water balance components over a large and heterogeneous area.

The approach taken was to use multiple one-dimensional model simulations which encompassed the coarse spatial variations of the landscape, such as differing land uses, vegetation types, soil profile types and irrigation practices. These contribute to a spatial assessment of irrigation, evaporation, transpiration and drainage to the water table across the whole study area.

This approach was applied to the whole study area of the NAP using spatial soil and land use data derived from the field study program and state databases. After simulating the soil water balance components (fluxes and volumes) across the whole area, the simulations were repeated, but with areas of irrigated horticulture replaced by areas of unirrigated grass, intended to represent land use in the area prior to horticulture. The key findings from this can be summarised as follows:

1. With the 2002 coverage of irrigated horticultural and other land uses, the simulated mean annual drainage volume for the whole study area over 20 years is 8,188 ML/year. The annual drainage volume from irrigated areas alone is 3663 ML. Irrigated areas represent approximately 29% of the total area but generate approximately 45% of the area's mean annual soil water drainage volume.

2. With automated, sensor-controlled irrigation, the range of drainage fluxes under the various combinations of soil and land use type would be lower than those determined for the three study sites under the observed irrigation practices. Drainage from the modelled combinations range between 48 mm/y to 128 mm/y under irrigated broadacre horticulture, including vegetables, vines and tree crops. This range is lower than anticipated for drainage fluxes in these areas, but is an increase of approximately 162% compared to the estimated drainage fluxes prior to irrigation.

3. Of the irrigated horticultural land uses included in the simulation, irrigated vegetables had the highest drainage fluxes, ranging from 103 mm/yr to 128 mm/yr depending on soil type, followed by irrigated perennials (mainly almonds), ranging from 61 mm/yr to 74 mm/yr, then irrigated grape vines, with 48 mm/yr to 61 mm/yr.

4. Other land use categories in the simulation, particularly roads and glasshouses produce more drainage flux than irrigated horticultural categories. This is because the model treats these as mainly impervious areas from which rainwater runs off and accumulates in a small proportion of the area, causing a high proportion of the water to infiltrate. However, because the land area occupied by these categories is relatively small, their total contribution to drainage fluxes is also small.

5. Comparing the whole-area soil water budget with and without irrigated horticulture, the major change in the soil water budget in the irrigated areas is in evaporation rather than drainage. Drainage volumes increased by 162% in areas of irrigated horticulture and by 52% for the whole area.

6. The aggregation of drainage fluxes predicted by the multiple simulations across the whole area suggests that, even under irrigation more controlled than current NAP horticultural practices, as applied in the model, the shallow aquifers beneath the NAP may receive approximately an additional 2.26 GL per year of additional recharge compared to prior to irrigated horticulture. This flux is considerably less than is likely to be occurring under current irrigation practices in broadacre horticulture on the NAP.

It could be argued that drainage fluxes predicted for irrigated areas by the distributed model are too low. Leaching allowances for irrigated crops are typically expected to be about 10% of the irrigation applied. The whole-area model results indicate that average drainage fluxes under irrigated areas with automated sensor-controlled irrigation were only approximately 8% of the total of rain plus irrigation. This could be interpreted as suggesting either that the soil hydrologic parameters used result in unrealistically low hydraulic conductivity of the soils, or that the scaling factors applied to the reference evapotranspiration are too high. However, in the application of the distributed whole-area model to the scenario without irrigation, which uses the same distribution of soil hydraulic parameters across the plain and similar ETo scaling factors, the average annual drainage flux for the whole area is 38 mm/year. This is approximately 9% of the average annual rainfall in the 20-year period modelled, and is a reasonable, or possibly erroneously high estimate of the average recharge flux to the water table aquifer under non-irrigated conditions in such a low-rainfall area. This provides some confirmation that the average conductivity of the variety of the soil characteristic across the area in the distributed model is not too low and that the average of the ETo scaling factors is not too high.

It is counter-intuitive that introducing such a large volume of irrigation water to an area, and applying most of this intensively through only a part of the year, does not cause a greater increase in drainage of water to the underlying water table than the average 162% increase suggested by the model results. However, the simulation results show that the application of the majority of this water through the summer months causes a large percentage of it to be lost to evapotranspiration.

With the modelling method applied and the assumptions adopted regarding spatial variability, the smaller-scale variations that occur within discrete land parcels were not quantified. The true variability of water fluxes within land parcels is not provided by the model results. The results of the distributed whole-area model suggest that the seven different soil profile descriptions used to represent the spatial variability of soil hydraulic parameters across the study area are a relatively minor contributor to spatial variations in drainage. This is likely to be partly due to the way in which the soil types were categorised. Further field and laboratory investigation into the true spatial variability of soil hydraulic characteristics across the study area could provide a more robust analysis of the effects this variability on soil water budget fluxes.

A natural progression for the application of the distributed model and its utility to estimate fluxes draining to the shallow unconfined aquifer would be to couple this model's output of drainage flux estimates to a model that predicts water table rise across the NAP. This further development was beyond the scope of this study. However, if such a model of the unconfined aquifer systems of the NAP were developed in future, the time-varying predictions of drainage fluxes under various irrigation and regional management scenarios would provide recharge input data for the groundwater model that would be superior to those that are typically applied in groundwater models, which are frequently just a fixed percentage of annual rainfall. That there is poor correlation between annual rainfall totals and annual recharge fluxes in the conditions of the NAP (Chapter 5), strongly supports the need to couple two such models to produce accurate predictions of shallow groundwater response.

The limited drainage characteristics of many of the soils used for horticulture on the NAP make it possible to keep root zone water content high while keeping drainage fluxes relatively low. However, this is achieved at the expense of high levels of evaporation from the soil surface and an accumulation of irrigation-borne salts in the soil root zone. There is considerable scope to reduce both irrigation volumes and drainage fluxes generated by

current irrigation practices, while keeping root zone water contents within a range that is normally recommended for these types of crops, by using soil moisture sensing. However, achieving this while maintaining root zone salinity at an acceptable level is more difficult.

At the time of the field study component of this research, soil salinity under irrigated NAP horticultural plots were already high. If the major source of irrigation water continues to be the Bolivar wastewater reclamation scheme and the water supplied continues to have an average TDS concentration of around 1200 mg/l, then soil root zone salinity in irrigated horticultural plots is likely to increase, particularly if irrigation strategies that are more conservative than current practices are adopted without regard to the need to somehow enhance the leaching of salts from the root zone.

The most effective way to prevent further rise, and to even cause a decline in root zone salinity would be to use irrigation water of a lower salinity. This may however require large investments in infrastructure to allow partial desalination of the reclaimed water, either in the supply chain or by the individual horticultural enterprises.

A further option that may result in lower irrigation water demand and lower drainage fluxes while also maintaining root zone salinity levels, is to enhance winter flushing of salts by irrigating during winter to maintain high soil water content while ET potential is low. This must be accompanied by more conservative irrigation of spring and summer crops such that the overall amount of irrigation water used is less. The modelling described in Chapter 5 showed that in the conditions of the PGR study site, this should result in lower drainage fluxes than scenarios with more heavily irrigated summer crops (similar to current practices), and also significantly lower root zone salinity. This is effectively an approach to reducing evaporation, since it results in less evaporation of irrigation water applied in summer because the soil is maintained in a drier state, and also a lower proportion of evaporation of irrigation applied in winter (for flushing) because potential ET is lower at that time.

If the spatially-averaged values within each category of land use and soil type are reasonably accurate, then this modelling approach will provide a sufficiently accurate assessment of the larger area on which to base resource management decisions and policies. This is most useful if the model is used in a comparative way, such as for comparing the outcomes of two different land use or irrigation management scenarios. If a regional natural resource manager maintains such a model over time, the accuracy of

spatial parameter values can be improved over time as more data becomes available. Furthermore, the number of variables that are categorised in the distributed model can be increased to include, for example, water table depths, potential ET, and rainfall, which in this study were all assumed to be uniform across the modelled area. Hence, the system of modelling demonstrated has considerable scope for a more comprehensive application, either to the NAP or to other study locations.

The volume of reclaimed wastewater delivered from the Bolivar wastewater reclamation scheme to horticultural enterprises on the NAP is in excess of 14 GL per year. While this has reduced the volume of irrigation water drawn from the underlying confined Tertiary limestone aquifer, the overall volume of water now used for irrigation in the NAP is much greater than it was prior to the establishment of the water reclamation scheme in 1999. This has inevitably led to a substantial change in the water balance of the region. With very little loss via surface runoff, the large increase in water input to the area has to be balanced primarily by increases in evapotranspiration and drainage to the underlying unconfined aquifers. For natural resource management in the NAP area, perhaps the most significant outcome of this study is the finding that, of the changes to the region's water balance, the largest change to the water outputs is the increase in evaporation from the soil surface in areas under irrigation. The increase in soil water drainage is secondary to this and the typical leaching fluxes achieved by NAP irrigators are possibly no more than are required to flush irrigation-borne salts from the root zone.

In view of these findings the focus of natural resource management authorities should shift from an aim of reducing irrigation drainage fluxes, to a concerted effort to reduce evaporation rates in irrigated plots. A successful campaign to promote techniques that reduce evaporation would have the multiple benefits of slowing soil salinity increases, minimising drainage fluxes, reducing pumping costs for irrigators and reducing irrigation water demand from existing irrigators, possibly making water available for an expanded irrigation area.

APPENDIX 1

Unsaturated hydraulic conductivity measurements: soil moisture outflow curves

Curves were constructed from soil moisture outflow measurements resulting from laboratory tests on undisturbed soil cores, as described in Chapter 2, Section 2.4.1, according to the method of Klute (1965).

From the volumetric outflow data, the quantity $1 - Q(t)/Q(\infty)$ is calculated, where $Q(\infty)$ is the total volume of outflow required to reach equilibrium. These are then used to construct a plot of log $[1 - Q(t)/Q(\infty)]$ versus log t (shown in blue in the graphs below). This is overlain on a theoretical plot of the quantities log $[1-Q(t)/Q(\infty)]$ versus log $(Dt/4L^2)$ (shown in black in the graphs below). The two plotted curves are brought into coincidence by moving the experimental curve along the log $(Dt/4L^2)$ axis only. A convenient value of $Dt/4L^2$ is selected (indicated with a red ring in the graphs below) and from the theoretical curve and and the corresponding value of t from the theoretical is noted. If the chosen value of $Dt/4L^2$ is represented as w, then the diffusivity, D, is given by

$$\boldsymbol{D = w4L^2/t}. \qquad \text{(Equation 2)}$$

Where t is the experimental value of time corresponding to the chosen value of w.

The specific water capacity, C, of the sample is given by

$$\boldsymbol{C = Q(\infty) / V \Delta h}. \qquad \text{(Equation 3)}$$

Where V is the volume of the sample.

The mean conductivity within the soil matric pressure increment over which the outflow rate was measured is then given by

$$\mathbf{K = DC} \qquad \text{(Equation 4)}$$

(Klute, 1965).

A1.1 Outflow curves for soil cores from study site PGR

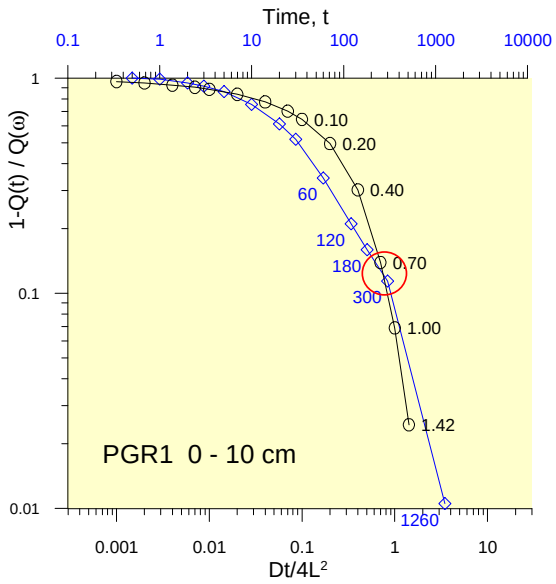

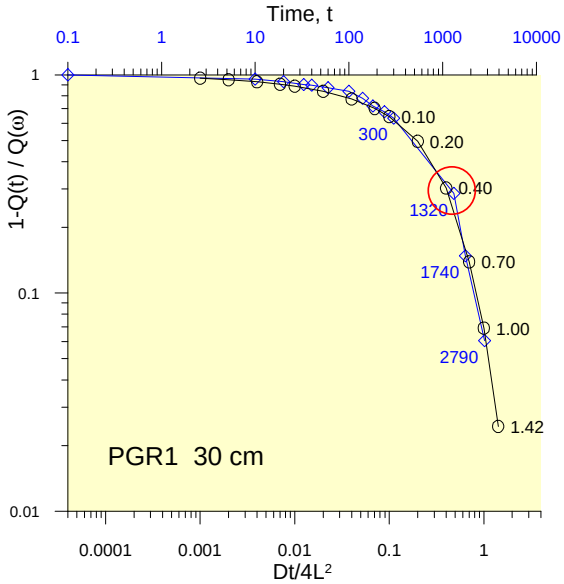

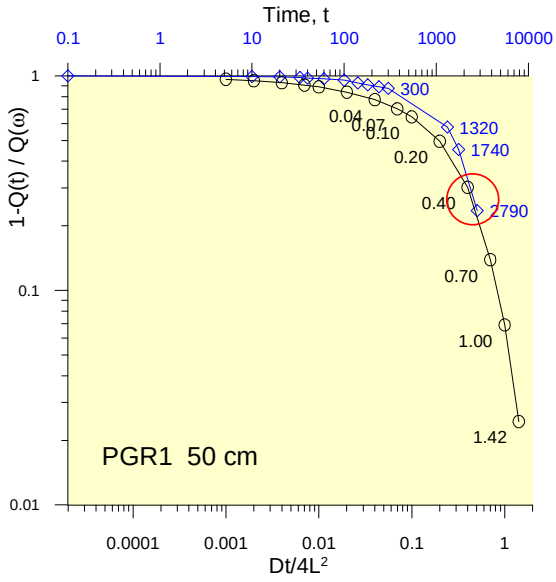

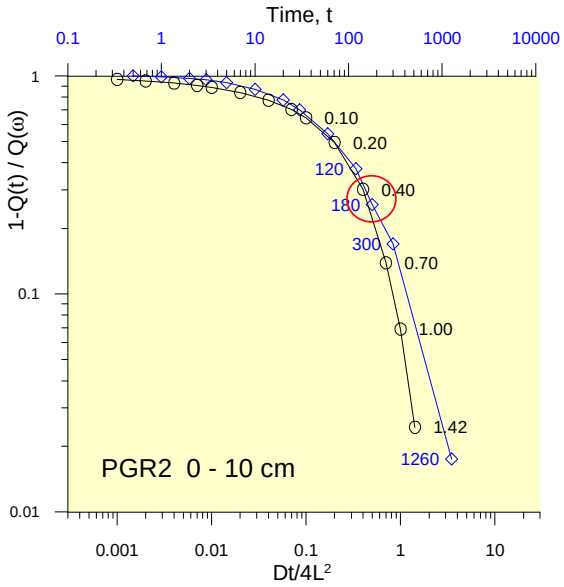

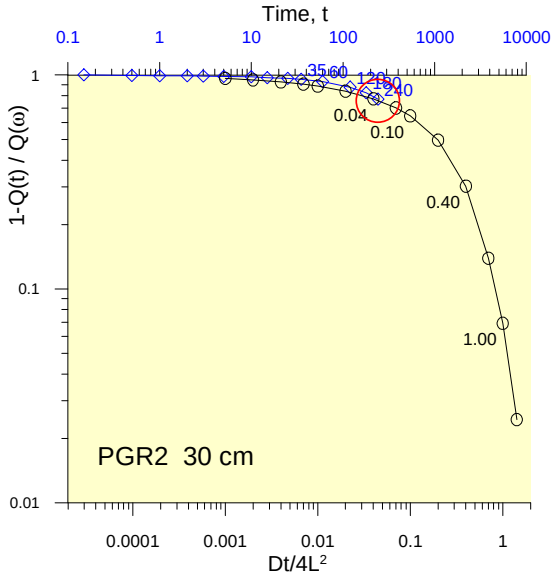

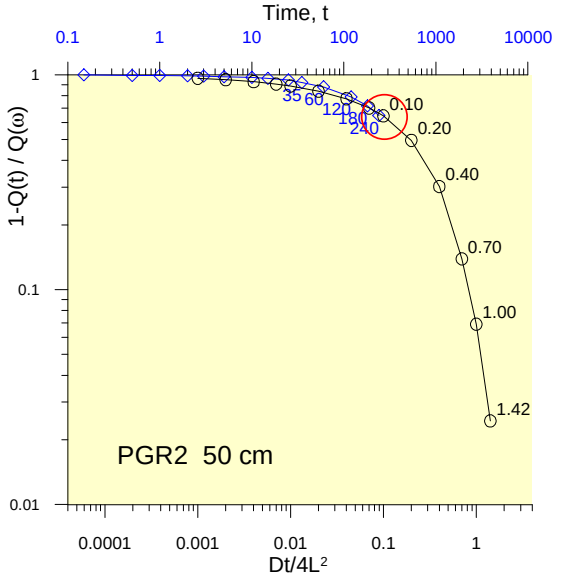

A1.2 Outflow curves for soil cores from study site HX

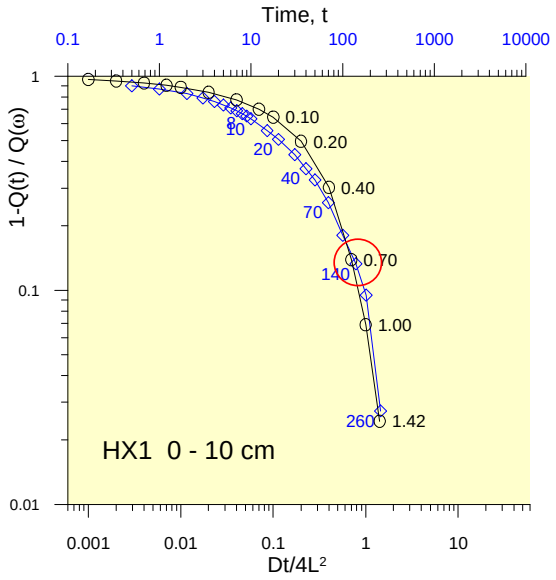

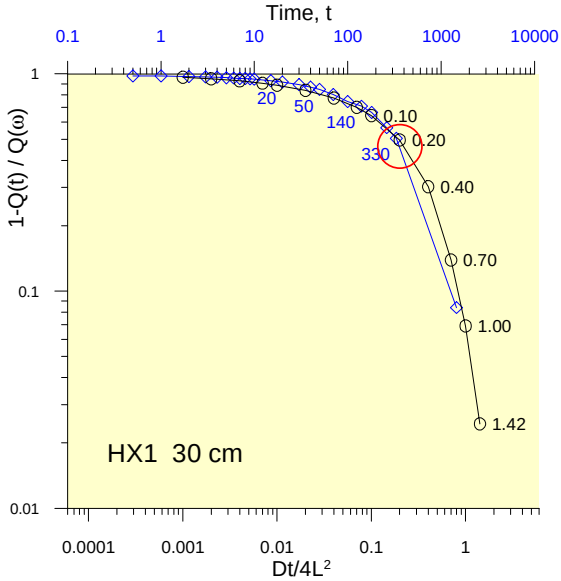

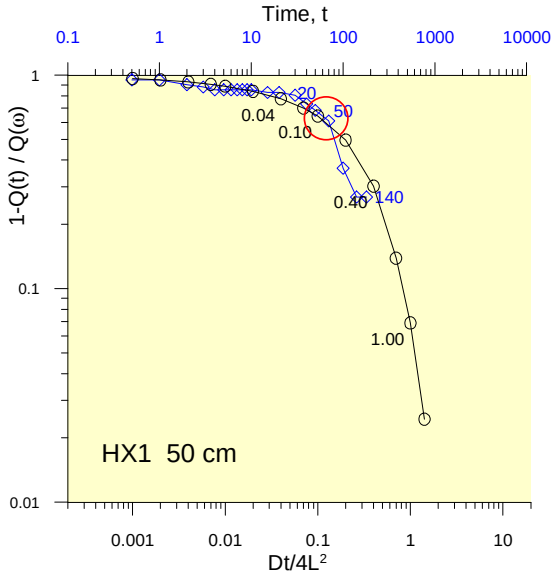

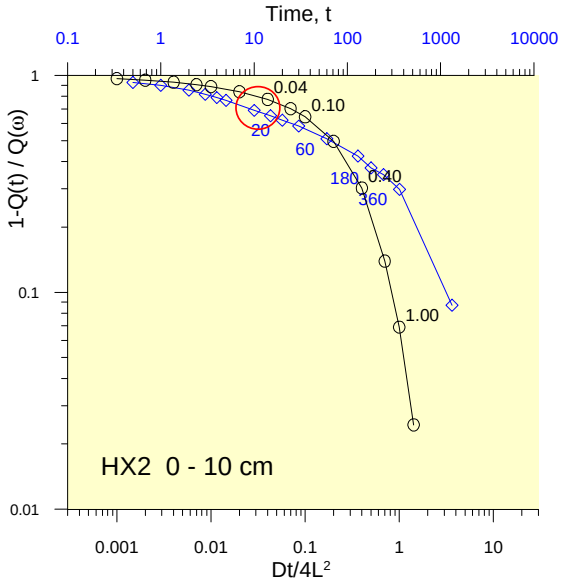

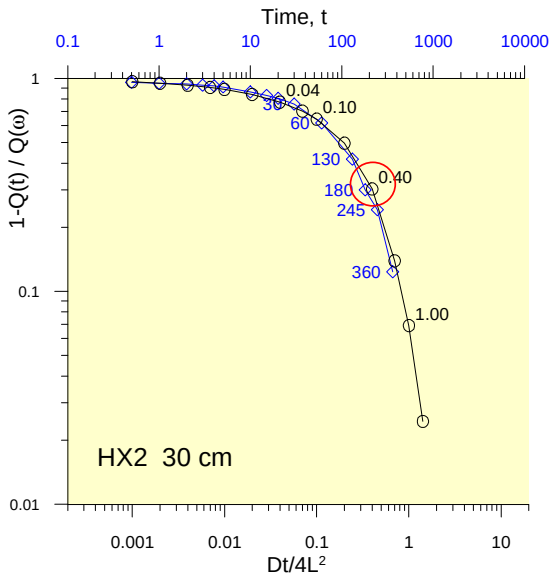

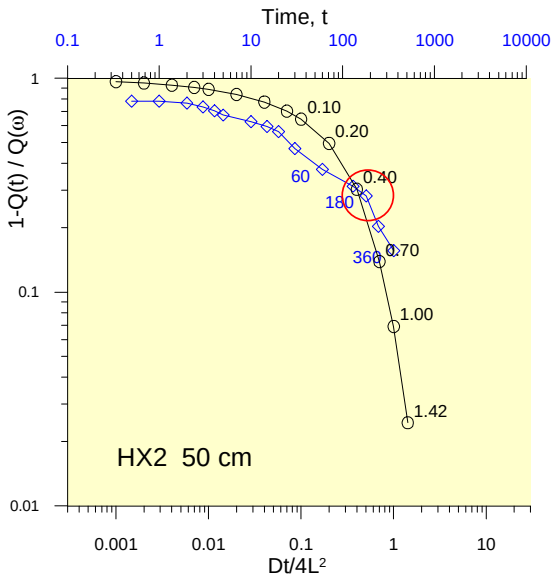

A1.3 Outflow curves for soil cores from study site TR

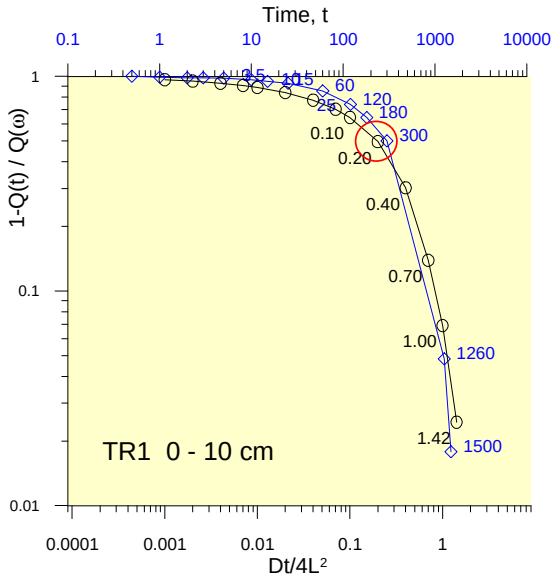

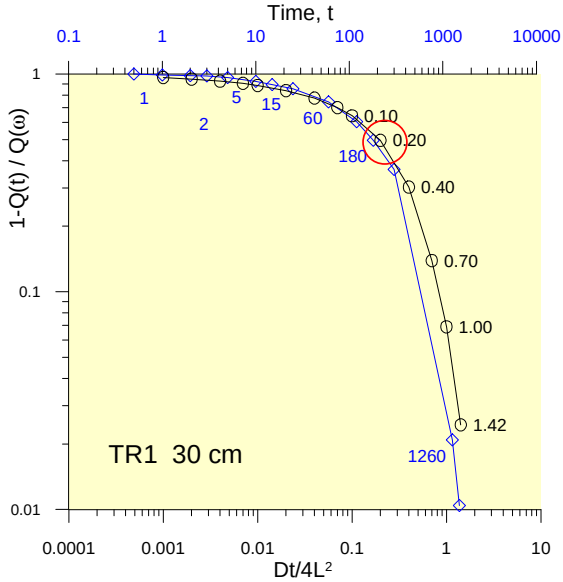

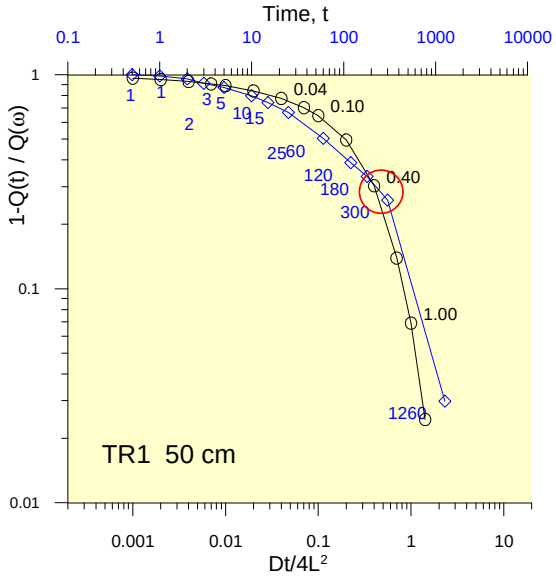

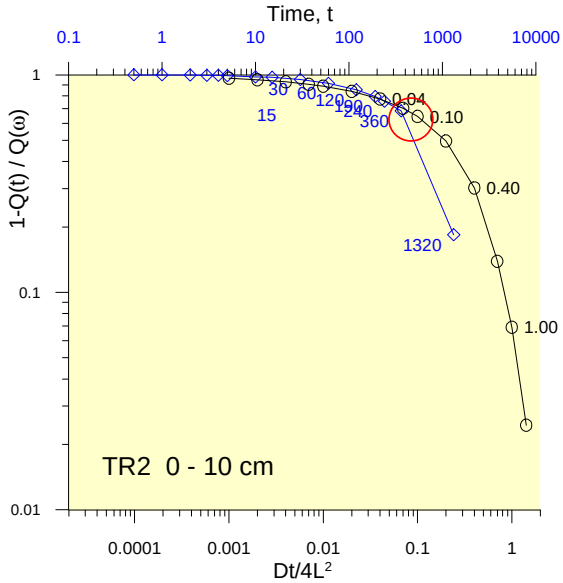

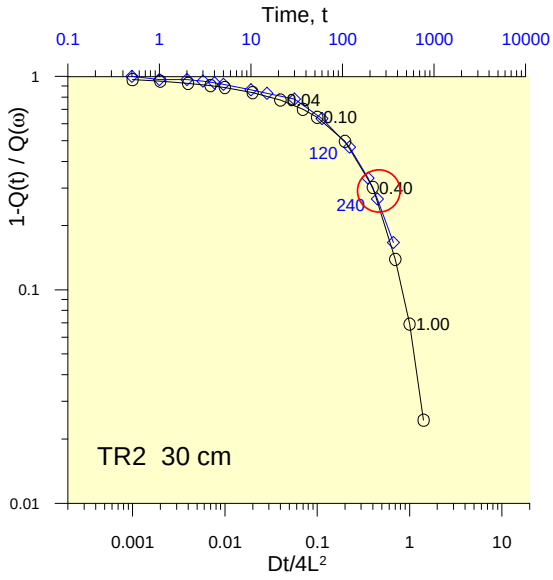

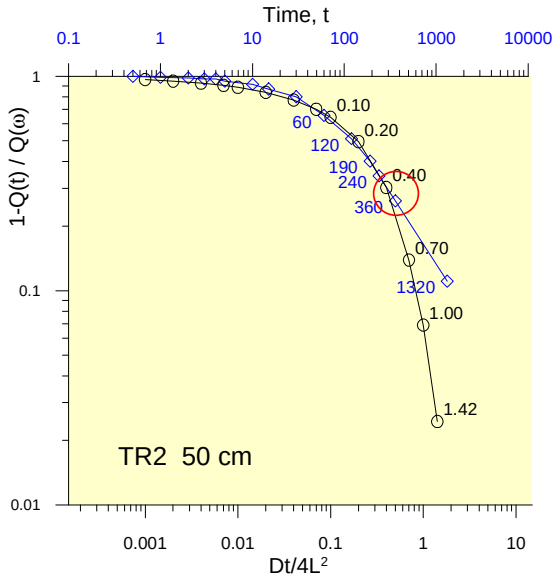

A1.4 Outflow curves for soil cores from study site SR

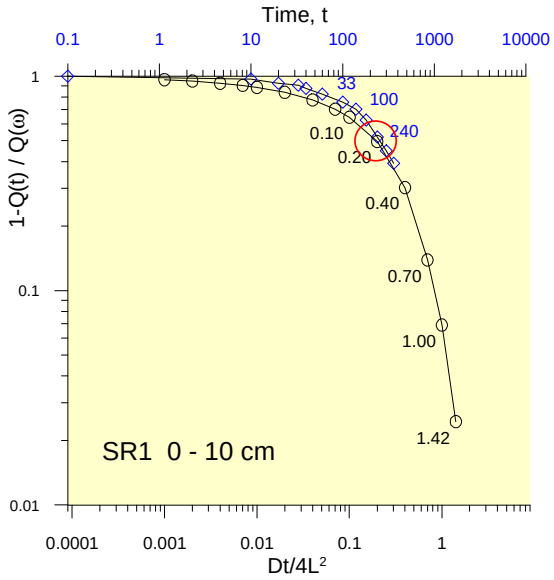

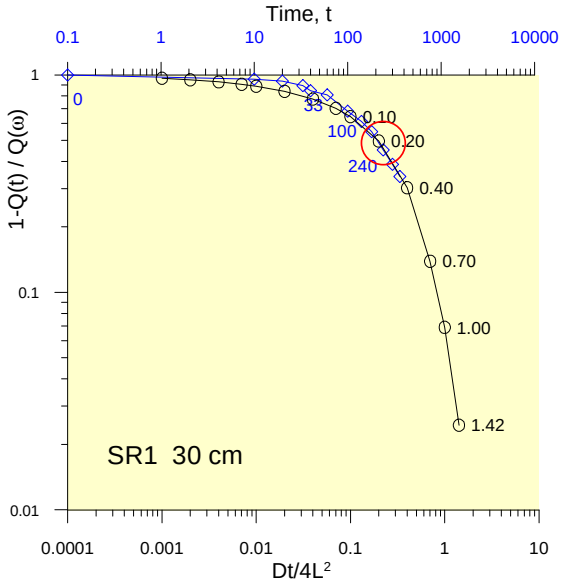

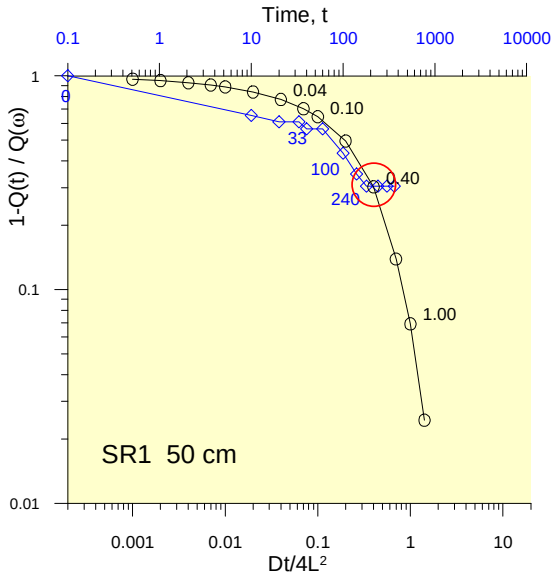

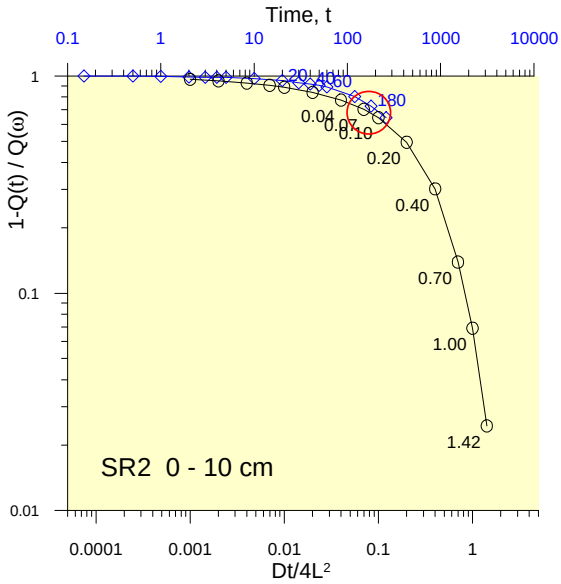

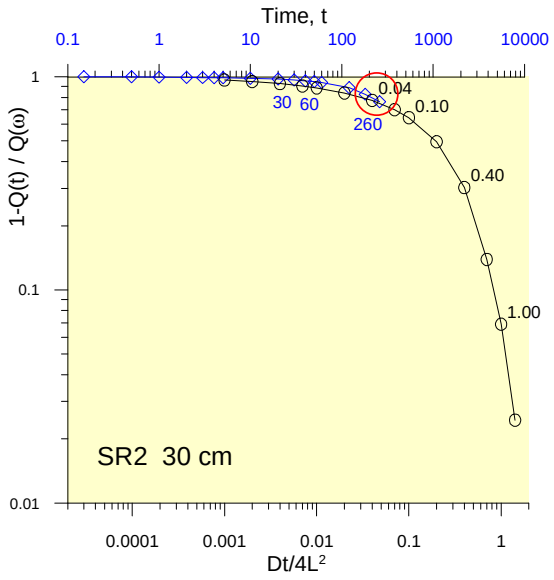

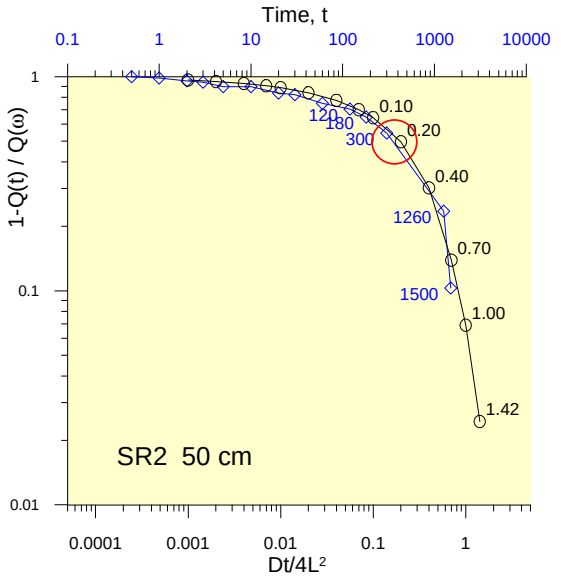

APPENDIX 2

Measurements of Soil Water Retention variables and derivation of Campbell's equation parameters from soil water retention curves

TABLES A2.1 to A2.15

FIGURES A2.1 to A2.5

1. Study Site PGR

Table A2.1 Calculations of soil sample porosity, bulk density and in-field water contents (monitoring point PGR1)

Sample	Mass, cell at 15 kPa (g)	Band + Cloth mass (g)	Mass, soil + cylinder at -15 kPa (g)	Oven dry mass with cylinder (g)	Brass cylinder mass (g)	Mass of water at -15 kPa (g)	Mass of dry soil (g)	Grav. water content (θ_g) at -15 kPa	Soil Volume	Dry bulk density	Vol. Water Content (θ_v) at -15 kPa	Particle density (g/cm^3)	Porosity (from bulk and particle densities)
PGR1 0cm	485.06	1.95	483.11	443.85	163.28	39.26	280.57	0.14	177.11	1.58	0.22	2.82	0.44
PGR1 30cm	515.6	1.65	513.95	481.80	162.85	32.15	318.95	0.10	187.29	1.70	0.17	2.67	0.36
PGR1 50cm	560.98	1.54	559.44	519.78	162.63	39.66	357.15	0.11	205.61	1.74	0.19	2.65	0.34
PGR1 70cm	563.77	1.72	562.05	522.80	162.00	39.25	360.80	0.11	206.41	1.75	0.19	2.53	0.31

Table A2.2 Soil water retention measurements for soil core samples (monitoring point PGR1)

Soil core matric potential	h_m (KPa)	PGR1 0cm core mass	PGR1 0cm vol. water content	PGR1 0cm θ/θs	PGR1 30cm core mass	PGR1 30cm vol. water content	PGR1 30cm θ/θs	PGR1 50cm core mass	PGR1 50cm vol. water content	PGR1 50cm θ/θs	PGR1 70cm core mass	PGR 70cm vol. water content	PGR1 70cm θ/θs
At Field Water Content		461.70	0.090		513.10	0.158		589.40	0.331		571.80	0.229	
Saturated	0.0	531.50	0.484	1.000	560.68	0.412	1.000	585.10	0.310	1.000	596.16	0.347	1.000
-5 cm	-0.5	526.19	0.454	0.938	555.42	0.384	0.932	582.46	0.297	0.959			
-10 cm	-1.0	518.79	0.412	0.852	550.76	0.359	0.872	580.11	0.286	0.922	589.00	0.312	0.900
-20 cm	-2.0	516.52	0.399	0.825	548.82	0.349	0.846	578.70	0.279	0.900			
-40 cm	-4.0	494.67	0.276	0.570	532.53	0.262	0.636	574.95	0.261	0.841	584.48	0.290	0.837
-80 cm	-8.0	494.11	0.273	0.564	531.85	0.258	0.627	575.17	0.262	0.844	580.63	0.272	0.783
-150 cm	-15	485.06	0.222	0.458	515.60	0.172	0.416	560.98	0.193	0.622	579.43	0.266	0.766
-50 Kpa	-50	467.00	0.120	0.247	512.75	0.156	0.379	553.11	0.155	0.498	574.75	0.243	0.701
-100 Kpa	-100	464.28	0.104	0.216	507.12	0.126	0.306	550.54	0.142	0.458	573.48	0.237	0.683
-200 Kpa	-200	462.72	0.096	0.197	504.62	0.113	0.274	549.40	0.137	0.440	572.44	0.232	0.669
-400 Kpa	-400	458.77	0.073	0.151	498.76	0.082	0.198	546.30	0.121	0.392	563.77	0.190	0.548

Note, core mass = mass of soil core, brass ring, cloth cover and rubber band.

Table A2.3 Data for curves fitted to measured water retention curves using Campbell's equation (monitoring point PGR1)

	Campbell's equation 'a' & 'b' parameters		θ/θs :																		
	-b	a	1	0.95	0.9	0.85	0.8	0.75	0.7	0.65	0.6	0.55	0.5	0.45	0.4	0.35	0.3	0.25	0.2	0.15	0.1
PGR1 0 cm	-2.55	-1.67	-1.67	-1.90	-2.18	-2.53	-2.95	-3.48	-4.15	-5.01	-6.14	-7.67	-9.78	-12.79	-17.28	-24.29	-35.98	-57.28	-101.18	-210.71	-592.54
PGR1 30 cm	-3.29	-2.37	-2.37	-2.81	-3.35	-4.05	-4.94	-6.11	-7.66	-9.78	-12.72	-16.94	-23.18	-32.79	-48.30	-74.95	-124.46	-226.74	-472.45		
PGR1 50 cm	-7	-0.442	-0.442	-0.63	-0.92	-1.38	-2.11	-3.31	-5.37	-9.02	-15.79	-29.03	-56.58	-118.29	-269.78	-686.98					
PGR1 70 cm	-12	-0.54	-0.54	-1.00	-1.91	-3.80	-7.86	-17.05	-39.01	-94.94	-248.07	-704.76									

These 'a' and 'b' values adjusted from values provided by Retfit curve fitting program to provide best fit to curves of measured data.

Figure A2.1 Fitted and measured water retention curves for PGR1 soil samples, according to data in Tables A2.2 and A2.3

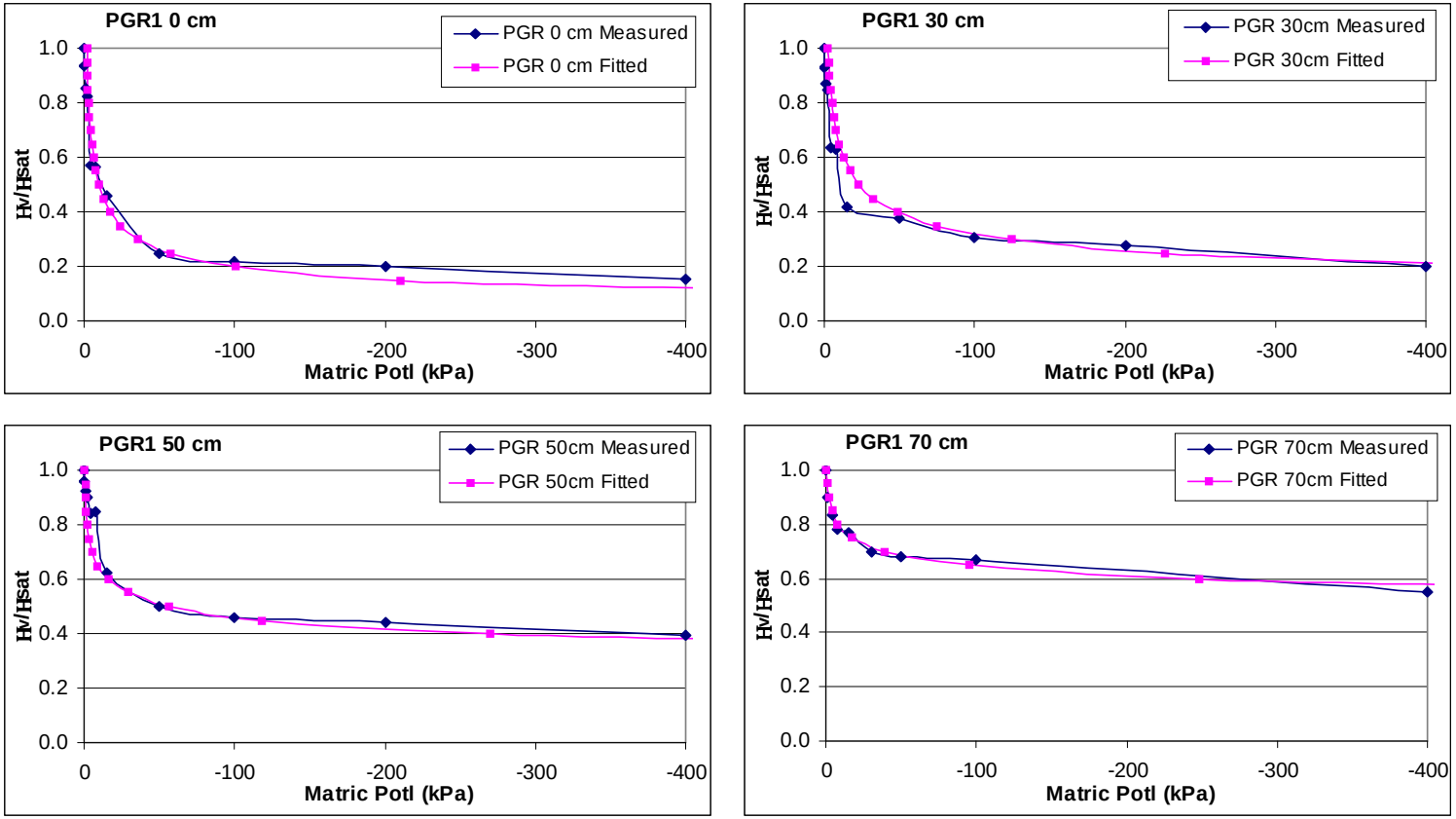

Table A2.4 Calculations of saturation and –100 kPa water contents, bulk density and soil sample porosity (monitoring point PGR2)

Sample	Mass of cell at saturation	Mass of cell at -100 KPa	Water Lost (mL)	Mass of soil + cyl at -100 kPa	Mass of brass cyl	Mass of soil at -100 kPa	Mass of soil +cyl at air dry	Mass of soil at air dry	Volume of soil core (cm^3)	θv at -100 kPa	θv at satur-ation	Dry bulk density	Particle density	Porosity (from bulk & particle densities)
PGR2 0 cm	571.02	552.37	18.65	184.91	71.03	113.88	178.68	107.65	69	0.09	0.36	1.56	2.67	0.42
PGR2 30 cm	568.74	556.35	12.39	191.78	70.81	120.97	183.81	113	69	0.12	0.30	1.64	2.70	0.39
PGR2 50 cm	570.1	559.41	10.69	192.31	70.81	121.5	184.59	113.78	69	0.11	0.27	1.65	2.76	0.40

Table A2.5 Soil water retention measurements for PGR site soil core samples (monitoring point PGR2)

	PGR2 0cm			PGR2 30cm			PGR2 50cm		
Soil core matric potential (-KPa)	Total outflow (ml)	θv	θv/θsat	Total outflow (ml)	θv	θv/θsat	Total outflow (ml)	θv	θv/θsat
0	0	0.36	1	0	0.30	1	0	0.27	1
-4	6.21	0.270	0.75	3.6	0.248	0.83	2.55	0.233	0.86
-9	10.15	0.213	0.59	9.15	0.167	0.56	6.05	0.182	0.68
-30	16.02	0.128	0.36	11.42	0.134	0.45	9.4	0.134	0.50
-50	17.67	0.104	0.29	11.87	0.128	0.43	10.12	0.123	0.46
-100	18.65	0.090	0.25	12.39	0.120	0.40	10.69	0.115	0.43

Table A2.6 Data for curves fitted to measured water retention curves using Campbell's equation (monitoring point PGR2)

	Campbell's equation 'a' & 'b' parameters		θ/θs:																
	-b	**a**	1	0.95	0.9	0.85	0.8	0.75	0.7	0.65	0.6	0.55	0.5	0.45	0.4	0.35	0.3	0.25	0.2
PGR2 0 cm	**-3**	**-1.5**	-1.5	-1.75	-2.06	-2.44	-2.93	-3.56	-4.37	-5.46	-6.94	-9.02	-12.00	-16.46	-23.44	-34.99	-55.56	-96.00	-187.5
PGR2 30 cm	**-4.7**	**-0.5**	-0.5	-0.64	-0.82	-1.07	-1.43	-1.93	-2.67	-3.79	-5.52	-8.30	-13.00	-21.32	-37.09	-69.48	-143.4	-337.8	-964.1
PGR2 50 cm	**-6**	**-0.3**	-0.3	-0.41	-0.56	-0.80	-1.14	-1.69	-2.55	-3.98	-6.43	-10.84	-19.20	-36.13	-73.24	-163.2	-411.5	-1228.8	

Figure A2.2 Fitted and measured water retention curves for PGR2 site soil samples, according to data in Tables A2.5 and A2.6

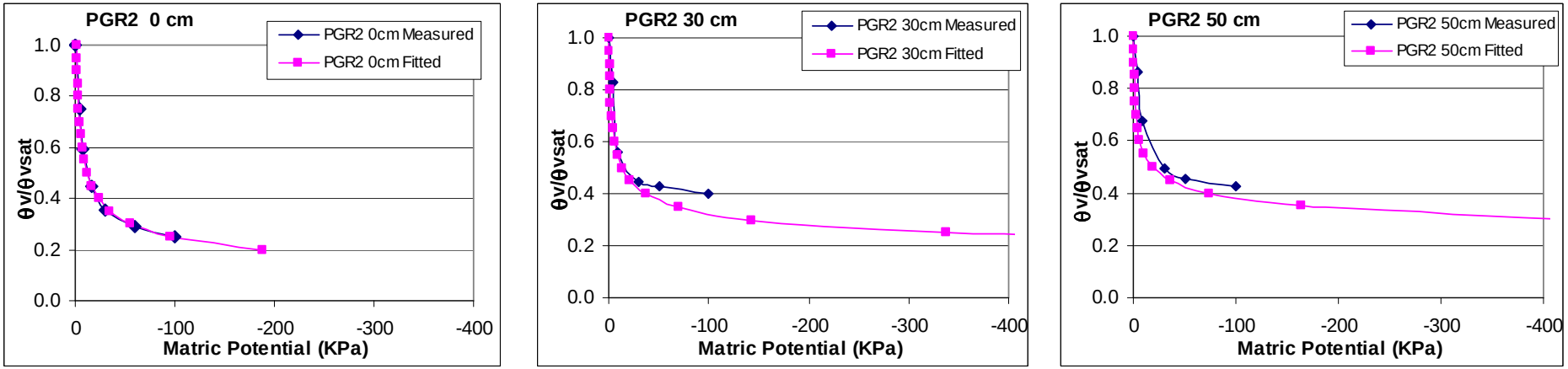

2. Study Site HX

Table A2.7 Calculations of –100 KPa and saturation water contents, dry bulk density and soil sample porosity (Study Site HX)

Sample	Mass of cell at Saturation	Mass of cell at -100 KPa	Water Lost (mL)	Mass of soil + cyl at -100 KPa	Mass of brass cyl	Mass of soil at -100 kPa	Mass of soil +cyl at air dry	Mass of soil at air dry (g)	Volume of soil core (cm^3)	θv at -100 kPa	θv at satur-ation	Dry bulk density	Particle density	Porosity (from bulk & particle densities)
HX1 0cm	541.56	525.11	16.45	182.08	70.81	111.27	173.23	102.42	69	0.13	0.37	1.48	2.76	0.46
HX1 30cm	546.05	535.49	10.56	192.43	70.81	121.62	182.66	111.85	69	0.14	0.29	1.62	2.59	0.37
HX1 50cm	550.8	547.58	3.22	208.31	70.81	137.5	184.71	113.9	69	0.34	0.39	1.65	2.70	0.39
HX2 10 cm	568.5	550.11	18.39	183.11	70.74	112.37	175.24	104.5	69	0.11	0.38	1.51	2.67	0.43
HX2 30 cm	572	561.73	10.27	197.77	70.58	127.19	186.7	116.12	69	0.16	0.31	1.68	2.67	0.37
HX2 50 cm	580.48	577.6	2.88	213.5	70.99	142.51	195.41	124.42	69	0.26	0.30	1.80	2.67	0.32

Table A2.8 Soil water retention measurements for HX site soil core samples

	HX1 0cm			HX1 30cm			HX1 50cm		
Soil core matric potential (-KPa)	Total outflow (ml)	θv	θv/θsat	Total outflow (ml)	θv	θv/θsat	Total outflow (ml)	θv	θv/θsat
0	0	0.370	1.00	0	0.290	1.00	0	0.390	1.00
-4	6.75	0.272	0.74	2.55	0.253	0.87			
-8	11	0.211	0.57	4.76	0.221	0.76			
-15	13.19	0.179	0.48	7.1	0.187	0.65	1.52	0.368	0.94
-30	14.74	0.156	0.42	8.73	0.163	0.56	2.03	0.361	0.92
-60	15.49	0.146	0.39	9.8	0.148	0.51	3.1	0.345	0.88
-100	16.45	0.132	0.36	10.56	0.137	0.47	3.22	0.343	0.88
	HX2 10cm			**HX2 30cm**			**HX2 50cm**		
Soil core matric potential (-KPa)	Total outflow (ml)	θv	θv/θsat	Total outflow (ml)	θv	θv/θsat	Total outflow (ml)	θv	θv/θsat
0	0	0.380	1.00	0	0.310	1.00	0	0.300	1.00
-4	4.6	0.313	0.82	2.5	0.274	0.88	0.5	0.293	0.98
-8	9.8	0.238	0.63	6.9	0.210	0.68	0.75	0.289	0.96
-30	15.59	0.154	0.41	12.22	0.133	0.43	1.9	0.272	0.91
-60	16.77	0.137	0.36	14.01	0.107	0.35	1.9	0.272	0.91
-100	18.34	0.114	0.30	15	0.093	0.30	1.94	0.272	0.91

Table A2.9 Data for curves fitted to measured water retention curves using Campbell's equation (Study Site HX)

	Campbell's equation 'a' & 'b' parameters																		
	-b	**a**	1	0.95	0.9	0.85	0.8	0.75	0.7	0.65	0.6	0.55	0.5	0.45	0.4	0.35	0.3	0.25	0.2
HX1 0cm	**-4.2**	**-0.8**	-0.8	-0.99	-1.25	-1.58	-2.04	-2.68	-3.58	-4.88	-6.84	-9.85	-14.70	-22.89	-37.54	-65.77	-125.66	-270.24	-689.86
HX1 30cm	**-5.5**	**-1.5**	-1.5	-1.99	-2.68	-3.67	-5.12	-7.30	-10.67	-16.03	-24.90	-40.19	-67.88	-121.18	-231.61	-482.74			
HX1 50cm	**-12**	**-5**	-5	-9.25	-17.70	-35.15	-72.76	-157.85	-361.24	-879.04									
HX2 10cm	**-3.7**	**-1.2**	-1.2	-1.45	-1.77	-2.19	-2.74	-3.48	-4.49	-5.91	-7.94	-10.96	-15.60	-23.03	-35.61	-58.36	-103.24	-202.68	-462.78
HX2 30cm	**-3.4**	**-1.8**	-1.8	-2.14	-2.58	-3.13	-3.84	-4.79	-6.05	-7.79	-10.22	-13.74	-19.00	-27.19	-40.58	-63.89	-107.91	-200.57	-428.32
HX2 50cm	**-12**	**-5**	-5	-9.25	-17.70	-35.15	-72.76	-157.85	-361.24	-879.04									

NB. These a and b numbers adjusted from retfit numbers to provide better fit to curves of measured data

Figure A2.3 Fitted and measured water retention curves for HX site soil samples, according to data in Tables A2.8 and A2.9

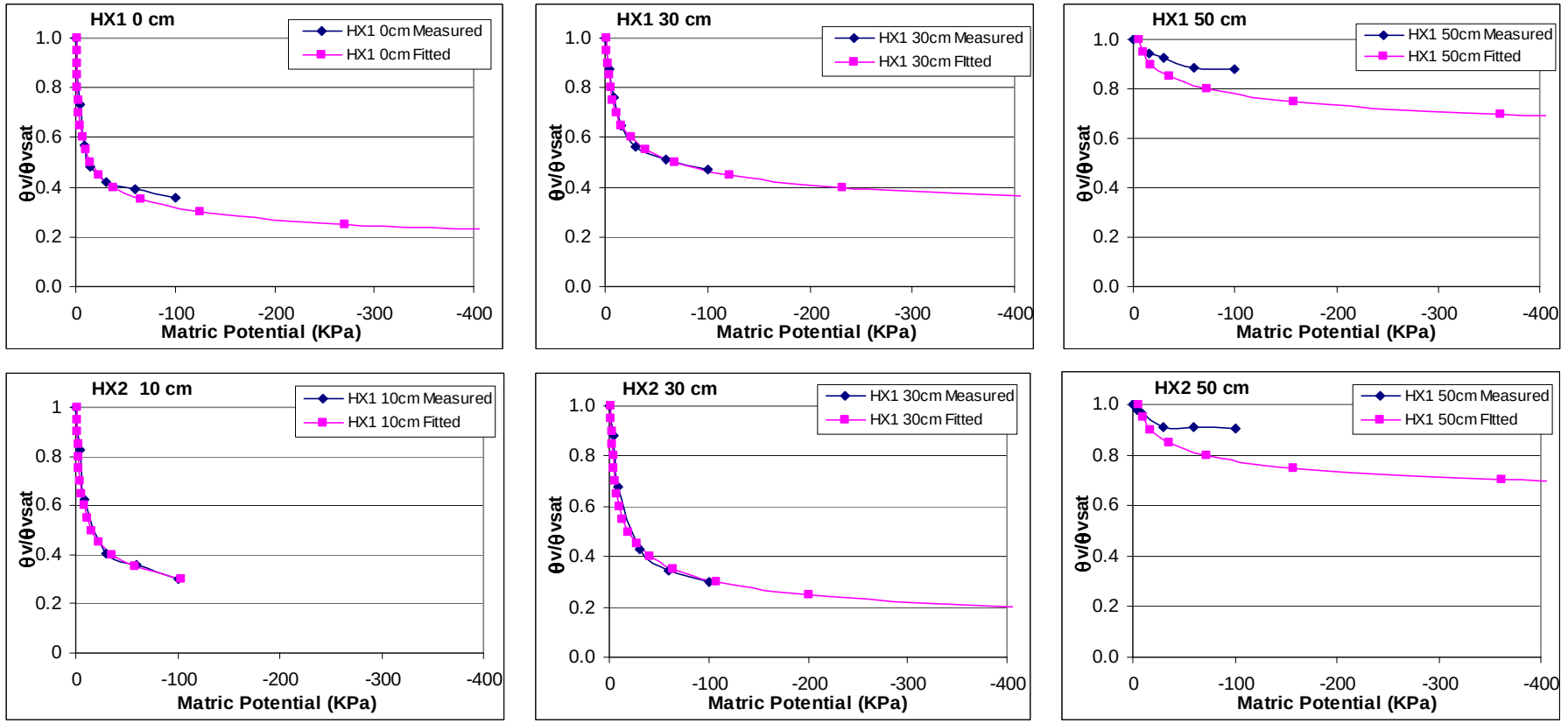

3. Study Site SR

Table A2.10 Calculations of –100 KPa and saturation water contents, dry bulk density and soil sample porosity (Study Site SR)

Sample	Mass of cell at Saturation	Mass of cell at -100 KPa	Water Lost (mL)	Mass of soil + cyl at -100 kPa	Mass of brass cyl	Mass of soil at -100 kPa	Mass of soil +cyl at air dry	Mass of soil at air dry (g)	Volume of soil core (cm^3)	θv at -100 kPa	θv at satur-ation	Dry bulk density	Particle density	Porosity (from bulk & particle densities)
SR1 0 cm	566.59	556.03	10.56	192.24	70.81	121.43	179.29	108.48	69	0.19	0.34	1.57	2.59	0.39
SR1 30 cm	558.92	550	8.92	194.12	70.81	123.31	182.05	111.24	69	0.17	0.30	1.61	2.67	0.40
SR1 50 cm	575.02	567.56	7.46	203.57	70.81	132.76	188.39	117.58	69	0.22	0.33	1.70	2.67	0.36
SR2 0cm	557.61	548.83	8.78	193.1	70.81	122.29	180.71	109.9	69	0.18	0.31	1.59	2.67	0.40
SR2 30cm	559.22	551.64	7.58	197.24	70.81	126.43	181.89	111.08	69	0.22	0.33	1.61	2.67	0.40
SR2 50 cm	566.85	563.43	3.42	199.11	70.6	128.51	170.79	100.19	69	0.41	0.46	1.45	2.67	0.46

Table A2.11 Soil water retention measurements for SR site soil core samples

	SR1 0cm			SR1 30cm			SR1 50cm		
Soil core matric potential (-kPa)	Total outflow (ml)	θv	θv/θsat	Total outflow (ml)	θv	θv/θsat	Total outflow (ml)	θv	θv/θsat
0	0	0.340	1	0	0.300	1.00	0	0.330	1.00
-4	2.7	0.301	0.8849	1.85	0.273	0.91	0.9	0.317	0.96
-9	5.85	0.255	0.7506	3.65	0.247	0.82	2.65	0.292	0.88
-30	8.56	0.216	0.6351	6.48	0.206	0.69	5.31	0.253	0.77
-50	9.61	0.201	0.5904	7.77	0.187	0.62	6.43	0.237	0.72
-100	10.56	0.187	0.5499	8.92	0.171	0.57	7.46	0.222	0.67

	SR2 0cm			SR2 30cm			SR2 50cm		
Soil core matric potential (-kPa)	Total outflow (ml)	θv	θv/θsat	Total outflow (ml)	θv	θv/θsat	Total outflow (ml)	θv	θv/θsat
0	0	0.310	1	0	0.330	1.00	0	0.460	1.00
-4	4.75	0.241	0.7779				0.2	0.457	0.99
-8							0.56	0.452	0.98
-11	6.23	0.220	0.7087	3.74	0.276	0.84			
-16							1.39	0.440	0.96
-30	8.24	0.191	0.6148	5.39	0.252	0.76	1.88	0.433	0.94
-60	8.6	0.185	0.5979	6.76	0.232	0.70	2.52	0.423	0.92
-100	8.78	0.183	0.5895	7.58	0.220	0.67	3.42	0.410	0.89

Table A2.12 Data for curves fitted to measured water retention curves using Campbell's equation (Study Site SR)

	Campbell's equation 'a' & 'b' parameters													
	-b	**a**	1	0.95	0.9	0.85	0.8	0.75	0.7	0.65	0.6	0.55	0.5	0.45
SR1 0cm	**-7.9**	**-0.85**	-0.85	-1.27	-1.95	-3.07	-4.95	-8.25	-14.23	-25.55	-48.09	-95.62	-203.03	-466.70
SR1 30cm	**-7.2**	**-1.8**	-1.8	-2.60	-3.84	-5.80	-8.97	-14.28	-23.47	-40.02	-71.22	-133.25	-264.66	-565.12
SR1 50cm	**-10**	**-2**	-2	-3.34	-5.74	-10.16	-18.63	-35.52	-70.80	-148.56	-330.76	-789.59		
SR2 0cm	**-10.6**	**-0.3**	-0.3	-0.52	-0.92	-1.68	-3.19	-6.33	-13.15	-28.86	-67.41	-169.54	-465.63	
SR2 30cm	**-11.5**	**-1.3**	-1.3	-2.34	-4.37	-8.43	-16.92	-35.54	-78.58	-184.26	-462.60			
SR2 50 m	**-12**	**-5**	-5	-9.25	-17.70	-35.15	-72.76	-157.85	-361.24	-879.04				

NB. These a and b numbers adjusted from retfit numbers to provide better fit to curves of measured data

Figure A2.4 Fitted and measured water retention curves for SR site soil samples, according to data in Tables A2.11 and A2.12

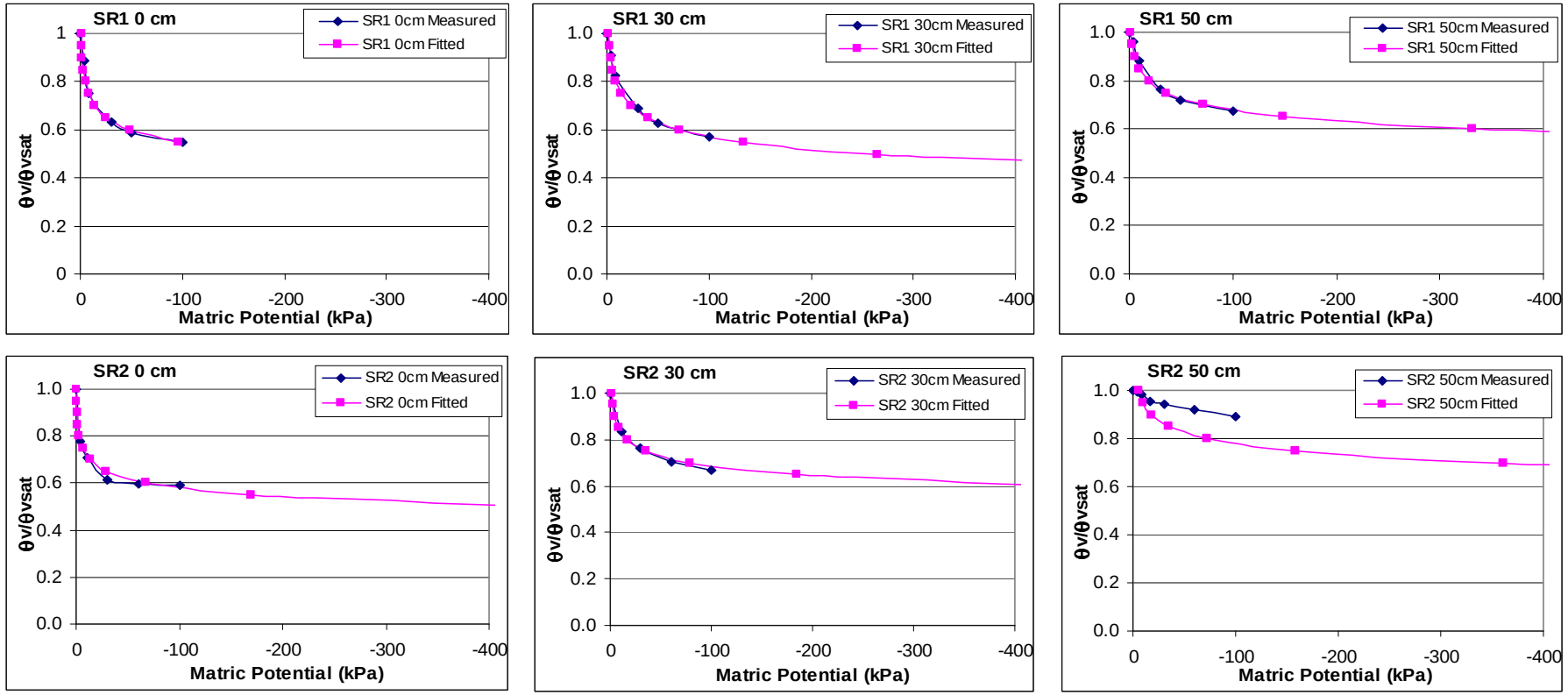

4. Site TR

Table A2.13 Calculations of –100 KPa and saturation water contents, dry bulk density and soil sample porosity (Study Site TR)

Sample	Mass of cell at Saturation	Mass of cell at -100 KPa	Water Lost (mL)	Mass of soil + cyl at -100 kPa	Mass of soil at -100 kPa	Mass of soil +cyl at air dry	Mass of soil at air dry (g)	Mass of brass cylinder	Volume of soil core (cm^3)	θv at -100 kPa	θv at saturation	Dry bulk density	Particle density	Porosity (from bulk & particle densities)
TR1 0 cm	563.70	551.50	12.2	193.76	122.78	184.00	113.02	70.98	69	0.14	0.32	1.64	2.67	0.39
TR1 30 cm	580.08	573.67	6.41	209.68	138.88	195.57	124.77	70.80	69	0.20	0.30	1.81	2.67	0.32
TR1 50 cm	572.00	565.59	6.41	204.51	133.65	186.02	115.16	70.86	69	0.27	0.36	1.67	2.67	0.37
TR2 10 cm	572.56	564.32	8.24	202.7	131.86	188.90	118.06	70.84	69	0.20	0.32	1.71	2.67	0.36
TR2 30 cm	578.36	575.04	3.32	210.37	139.37	193.76	122.76	71.00	69	0.24	0.29	1.78	2.67	0.33
TR2 50 cm	566.55	562.34	4.21	204.11	133.32	185.75	114.96	70.79	69	0.27	0.33	1.67	2.67	0.38

Table A2.14 Soil water retention measurements for TR site soil core samples

	TR1 0 cm			TR1 30 cm			TR1 50 cm		
Soil core matric potential (-Kpa)	Total outflow (ml)	θv	θv/θsat	Total outflow (ml)	θv	θv/θsat	Total outflow (ml)	θv	θv/θsat
0	0	0.320	1.00	0	0.300	1.00	0	0.360	1.00
-4	3.95	0.263	0.82	1.56	0.277	0.92	1.78	0.334	0.93
-8	7.88	0.206	0.64	3.06	0.256	0.85	2.69	0.321	0.89
-16	9.25	0.186	0.58	4.14	0.240	0.80	3.65	0.307	0.85
-30	10.15	0.173	0.54	4.95	0.228	0.76	4.64	0.293	0.81
-60	11.24	0.157	0.49	5.72	0.217	0.72	5.63	0.278	0.77
-100	12.20	0.143	0.45	6.41	0.207	0.69	6.41	0.267	0.74

	TR2 0 cm			TR2 30 cm			TR2 50 cm		
Soil core matric potential (-Kpa)	Total outflow (ml)	θv	θv/θsat	Total outflow (ml)	θv	θv/θsat	Total outflow (ml)	θv	θv/θsat
0	0	0.320	1.00	0	0.290	1.00	0	0.330	1.00
-4	0.40	0.314	0.98	0.3	0.286	0.99	0.45	0.323	0.98
-9	2.70	0.281	0.88	0.75	0.279	0.96	1.00	0.316	0.96
-30	5.98	0.233	0.73	3.08	0.245	0.85	3.57	0.278	0.84
-60	6.37	0.228	0.71	3.13	0.245	0.84	4.19	0.269	0.82
-100	7.36	0.213	0.67	3.59	0.238	0.82	4.81	0.260	0.79

Table A2.15 Data for curves fitted to measured water retention curves using Campbell's equation (Study Site TR)

	Campbell's equation 'a' and 'b' parameters															
	-b	**a**	1	0.95	0.9	0.85	0.8	0.75	0.7	0.65	0.6	0.55	0.5	0.45	0.4	0.35
TR1 0 cm	**-7.5**	**-0.25**	-0.25	-0.37	-0.55	-0.85	-1.33	-2.16	-3.63	-6.33	-11.53	-22.14	-45.25	-99.73	-241.26	-656.79
TR1 30 cm	**-9.5**	**-0.25**	-0.25	-0.41	-0.68	-1.17	-2.08	-3.84	-7.40	-14.97	-32.03	-73.20	-181.02	-492.52		
TR1 50 cm	**-9.5**	**-0.25**	-0.25	-0.41	-0.68	-1.17	-2.08	-3.84	-7.40	-14.97	-32.03	-73.20	-181.02	-492.52		
TR2 10 cm	**-8**	**-3.2**	-3.20	-4.82	-7.43	-11.74	-19.07	-31.96	-55.51	-100.43	-190.52	-382.16	-819.20			
TR2 30 cm	**-12**	**-5**	-5.00	-9.25	-17.70	-35.15	-72.76	-157.85	-361.24	-879.04						
TR2 50 cm	**-12**	**-5**	-5.00	-9.25	-17.70	-35.15	-72.76	-157.85	-361.24	-879.04						

NB. These a and b numbers adjusted from retfit numbers to provide better fit to curves of measured data

Figure A2.5 Fitted and measured water retention curves for TR site soil samples, according to data in Tables A2.14 and A2.15

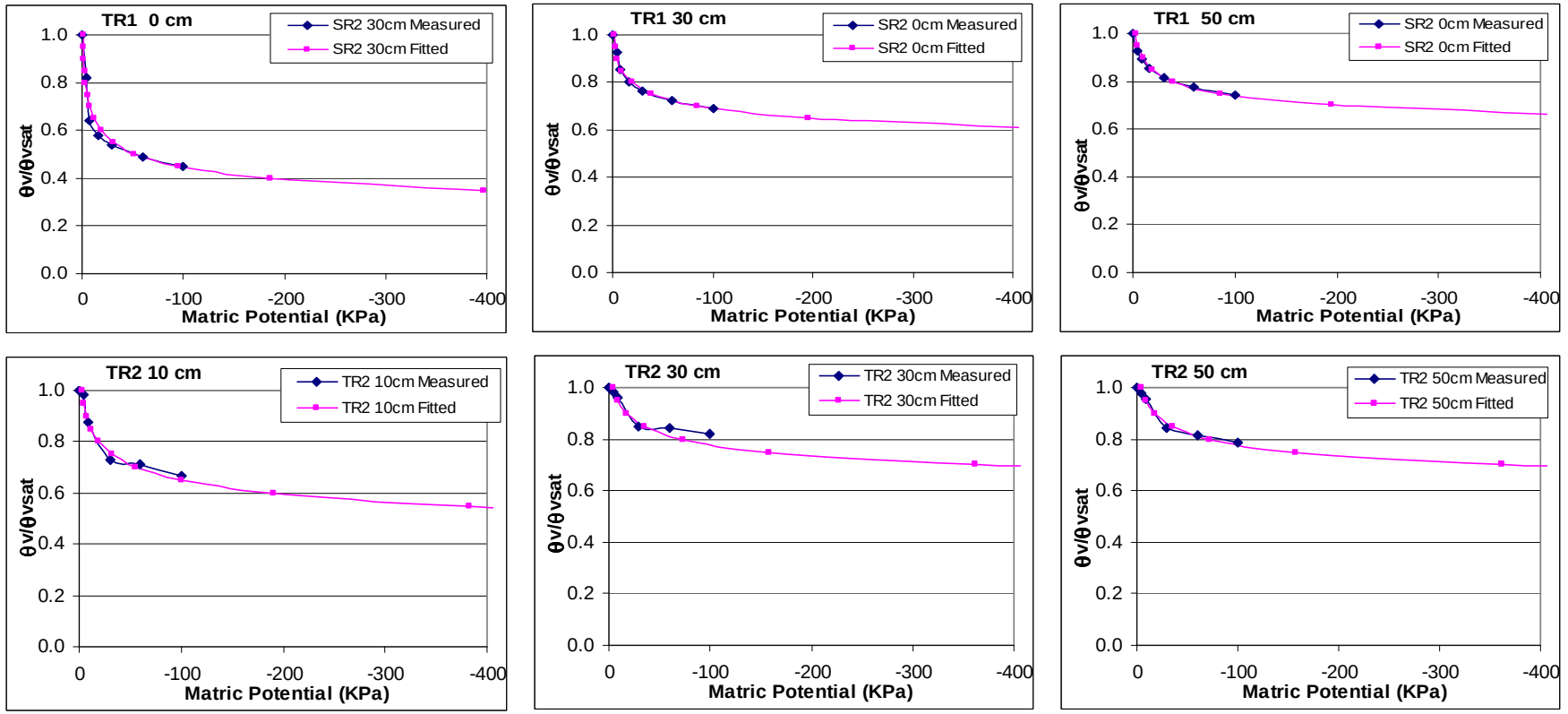

REFERENCES

Addiscott, T.M., Heye, P.J. and Whitmore, A.P. (1986). *Application of simple leaching models in heterogeneous soils.* Geoderma, 38: 185-194.

Ahmad, M., Bastiaanssen, W.G.M. and Feddes, R.A. (2002). *Sustainable use of groundwater for irrigation: a numerical analysis of the subsoil water fluxes.* Irrigation and Drainage, 51: 227-241.

Allen, R. G., Pereira, L.A., Raes, D., Smith, M. (1998). Crop evapotranspiration: guidelines for computing crop water requirements. FAO Irrigation and Drainage Paper 56, Food and Agriculture Organisation of the United Nations, Rome, Italy.

Baver, L.D. (1940). Soil Physics. John Wiley and Sons, New York & London.

Biggar, J.W. and Nielsen, D.R. (1976). *Spatial Variability of the Leaching Characteristics of a Field Soil.* Water Resources Research, 1 (12): 78-84.

Bosch, D.D. and West, L.T. (1998). *Hydraulic Conductivity Variability for Two Sandy Soils*. Soil Sci Soc. Amer. Jnl., 62: 90-98.

Bloschl, G and Sivapalan, M. 1995. Scale Issues In Hydrological Modelling: A Review. John Wiley & Sons, New York.

Braud, I., Haverkamp, R., Arrue, J.L. and Lopez, M.V. (2003). *Spatial variability of soil surface properties and consequences for the annual and monthly water balance of a semiarid environment.* Journal of Hydrometeorology, 4: 121-136.

Briggs, L.J. (1912). *The wilting Coefficient for different plants and its indirect determination*. US Dept of Agr. Bureau of Soils (Bulletin 230).

Brooks, R.H. and Corey, A.T. (1964). *Hydraulic Properties of Porous Media*. Hydrology Paper 3, Colorado State University, Fort Collins, Colorado.

Buss, P. (1993). *The use of capacitance based measurements of real time soil water profile dynamics for irrigation scheduling.* Proc. Natl. Conf. Irrig. Assoc. Austr., Launceston, Tasmania, May 1993.

Buckingham, E. (1907). Studies on the movement of soil moisture. U.S. Dept. Agric. Bur. Soils (Bulletin 38), Washington, D.C.

Campbell, G. S. (1974). *A simple method for determining unsaturated conductivity from moisture retention data.* Soil Science 117(6): 311-314.

Childs, E.C. (1969). An Introduction to the Physical Basis of Soil Water Phenomena. John Wiley and Sons, New York & London.

Clapp, R.B. and Hornberger, G.M., (1978). *Empirical equations for some soil hydraulic properties*. Water Resources Research, 14(4): 601-604.

Close, M.E., Watt, J.P.C. and Vincent, K.W. (1999). Simulation of picloram, atrazine and simazine transport through two New Zealand soils using LEACHM. Australian Journal of Soil Research, 37: 53-74.

Cochran, P.H., Giles, M.M. and Leaf, A.L. (1970). Variations in Tension Lysimeter Leachate Volumes. Soil Science Society of America Journal, Vol. 34: 309-311.

Darcy, H. (1856). Les fontaines publiques de la Ville de Dijon. Dalmont, Paris.

Day, P.R. (1942). *The moisture potential of soils*. Soil Science 54(6): 391-400.

dePaz, J.M. and Ramos, C. (2001). *Linkage of a geographical information system with the GLEAMS model to assess nitrate leaching in agricultural areas*. Environmental Pollution, 118: 249-258.

Doherty, J. (2004). PEST Model-Independent Parameter Estimation, Watermark Numerical Computing.

Feddes, R.A., Kabat, P., van Bakel, P.J.T., Bronswijk, J.J.B. and Halbertsma, J., (1988). *Modelling soil water dynamics in the unsaturated zone. State of the art*. Journal of Hydrology, 100: 69-111.

Gardner, W.R. (1956). *Calculation of capillary conductivity from pressure plate and flow data*. Proc. Soil Sci. Soc. Amer., 20: 317-320.

Gee, G.W. (1988) *Groundwater Recharge in Arid Regions: Review and Critique of Estimation Methods*. Hydrological Processes Vol. 2: 255-266.

Gerges, N.Z. (1999). The Geology & hydrogeology of the Adelaide metropolitan area [PhD thesis manuscript]. Flinders University, South Australia.

Gerges, N. Z. (2001). Northern Adelaide Plains Groundwater Review. Adelaide, SOuth Australian Government Department for Water Resources

Gerges, N. (2002). 'Hydrogeological Investigations of the Shallow (Perched) Water Table Aquifer North of Virginia.' Consultancy report to the NABCWMB, March 2002.

Gerges, N. and Kelly, J. (2002). 'A First Approximation of the Shallow Aquifer Water Balances on the Northern Adelaide Plains.' Consultancy report to the NABCWMB, March 2002.

Good, K. (12/09/02) Letter to South Australia Water Resources Minister John Ringham re. 'Rising Groundwater Threatening Northern Adelaide Plains Horticulture.'

Haines, B.L., Waide, J.B. and Todd, R.L. (1982). *Soil Solution Nutrient Concentrations Sampled with Tension and Zero-Tension Lysimeters: Report of Discrepancies.* Soil Science Society of America Journal, Vol. 46(3): 658 - 661.

Hogan, G. and Scott, V. (1999). "Land Use – Northern Adelaide Plains" 1:10,000 capture scale GIS mapping. Primary Industries and Resources South Australia (PIRSA).

Holder, M., Brown, K.W., Thomas, J.C., Zabcik, D. and Murray, H.E. (1991). *Capillary-Wick Unsaturated Zone Soil Pore Water Sampler*. Soil Sci. Soc. Am. Jnl. (55): 1195-1202.

Hutson, J. L., Cass, A. (1987). *A retentivity function for use in soil water simulation models*. Journal of Soil Science 38: 105-113.

Hutson, J.L., Waganet, R.J. and Niederhofer, M.E. (1997). LEACHM, Leaching Estimation and Chemistry Model. A process-based model of water and solute movement, transformations, plant uptake and chemical reactions in the unsaturated zone. Versions LEACHF and LEACHG. Research Series No. R97-1, January 1997. Department of Soil, Crop and Atmospheric Sciences, Cornell University, Ithaca, New York.

Hutson, J. L. (2003). Leaching Estimation and Chemistry Model, Version 4. Research Series R03-1, March 2003, Department of Crop and Soil Science, Cornell University, Ithaca, New York.

Jabro, J. D., Toth, J.D. and Fox, R.H. (1998). *Evaluation and comparison of five simulation models for estimating water drainage fluxes under corn*. Journal of Environmental Quality, 27(6): 1376-1382.

Jansson, P.E. (1991). *SOIL water and heat model. Technical Description.* Dept. of Soil Sciences, Swedish University of Agricultural Sciences, Uppsala, Sweden.

Jarvis, N. (1994). *The MACRO model (Version 3.1), Technical description and sample simulation.* Department of Soil Sciences, Swedish University of Agricultural Sciences, Rep and Diss. 9, Uppsala, Sweden.

Jemison, J.M. and Fox, R.H. (1992). *Estimation of zero-tension pan lysimeter collection efficiency*. Soil Science, 154(2): 85-94.

Jhorar, R.K., van Dam, J.C., Bastiaanssen, W.G.M. and Feddes, R.A. (2004). *Calibration of effective soil hydraulic parameters of heterogeneous soil profiles.* Journal of Hydrology 285: 233-247.

Kandil, H.M. (1992). *DRAINMOD-S: a water management model for irrigated lands.* PhD thesis, North Carolina State University, Raleigh, USA.

Kelly, J. and Stevens, D. (2000). "From Problem to Profit - Wastewater reclamation and reuse on the Northern Adelaide Plains." Water, Journal of the Australian Water Association (Sept./Oct. 2000): 37-41.

Kendy, E., Gerard-Marchant, P., Walter, M.T., Zhang, Y., Liu, C. and Steenhuis, S. (2003). *A soil-water balance approach to quantify groundwater recharge from irrigated cropland in the North China Plain*. Hydrological Processes, 17: 2011-2031.

Klute, A. (1965). 'Water Diffusivity' in Methods of Soil Analysis, Part 1. American Society of Agronomy Inc., Madison, Wisconsin.

Knutson, J.H., Lee, S.B., Zhang, W.Q. and Selker, J.S. (1993). *Fibreglass wick preparation for use in passive capillary wick soil pore-water samplers*. Soil Sci. Soc. Am. Jnl. (57): 1474-1476.

Leonard, R.A., Knisel, W.G. and Still, D.A. (1987). GLEAMS: Groundwater Loading Effects of Agricultural Management Systems. Transactions of the American Society of Agricultural Engineers 30: 1403-1418.

Li, W., Li, B. and Shi, Y. (1999). *Markov-chain simulation of soil textural profiles*. Geoderma (92): 37-53.

Li, W., Li, B. and Shi, Y. (2001). *Effect of spatial variation of textural layers on regional field water balance*. Water Resources Research, 37 (5): 1209-1219.

Loague, K. and Green, R.E. (1999). *Statistical and Graphical Methods for Evaluating Solute Transport Models: Overview and Application*. Journal of Contaminant Hydrology, 7: 51-73.

Maas, E.V. and Hoffman, G.J. (1977). *Crop salt tolerance – current assessment.* Journal of the Irrigation and Drainage Division, Proceedings of the American Society of Civil Engineers 103: 115-130.

Marshall, T.J. and Holmes, J.W. (1979). Soil Physics. Cambridge University Press.

Marshall, T.J., Holmes, J. W. and Rose, C.W. (1996) Soil Physics, Third Edition, Cambridge University Press.

Matheson, W.E. and Lobban, B.L. (1975). "Northern Adelaide Plains Suitability of Land For Irrigation." (map), Design Branch, Engineering and Water Supply Department, Government of South Australia.

Molina, J.A.E. and Richards, K. (1984). *Simulation models of the nitrogen and carbon cycle in the soil-water-plant system, NCSWAP; Guide for the Preparation of input*

data files and execution of NCSWAP. Soil Series 116, Dept. of Soil Science, University of Minnesota, St. Paul.

Northern Adelaide and Barossa Catchment Water Management Board (2004) Groundwater Trends in the Northern Adelaide Plains. Northern Adelaide and Barossa Catchment Water Management Board, Salisbury, South Australia.

Olyphant, G.A. (2003). Temporal and spatial (down profile) variability of unsaturated soil hydraulic properties determined from a combination of repeated field experiments and inverse modeling. Journal of Hydrology, 281: 23-35.

Parizek, R.R. and Lane, B.E. (1970). Soil-Water Sampling Using Pan and Deep Pressure-Vacuum Lysimeters. Journal of Hydrology, Issue 1: 1-21.

PIRSA (2001). Soil Data Sheets: A Compilation of Data from Soil Characterisation Sites Located Across Souuthern South Australia. PIRSA Land Information, Primary Industries and Resources South Australia, Government of South Australia.

Radulovich, R. and Sollins, P. (1987). *Improved Performance of Zero-Tension Lysimeters.* Soil Science Society of America Journal, Vol. 51: 1386-1388.

Rayner, A. A. (1967). A First Course in Biometry For Agriculture Students, University of Natal Press, Pietermaritzburg.

Richards, L.A. (1931). *Capillary conduction of liquids through porous medium*. Physics, Vol. 1: 318-333.

Richards, L.A. and Gardner, W. (1936). *Tensiometers for Measuring the Capillary Tension of Soil Water*. Journal of of the American Society of Agronomy, Vol. 28: 352-358.

Richards, L.A. (1949). *Methods of measuring soil moisture tension*. Soil Sci. (68): 95-112.

Richards, S.J. (1939). *Soil Moisture Content Calculations from Capillary Tension Records*. Soil Science Society of America Journal 3: 57-64.

Romanovicz, R. and Beven, K. (1993). *GIS and distributed hydrological models*. Chapter in Mather, P.M. (Ed.), Geographical Information Handling – Research and Applications. John Wiley and Sons, London.

Sarmah, A. K, Close, M.E., Pang, L., Lee, R. and Green, S.R. (2005). *Field study of pesticide leaching in a Himatangi sand (Manawatu) and a Kiripaka bouldery clay loam (Northland). Simulation using LEACHM, HYDRUS-1D, Gleams, and SPASMO models*. Australian Journal of Soil Research, 43: 471-489.

Scanlon, B.R., Keese, K. E., Flint, A.L., Flint, L.E., Gaye, C.B., Edmunds, M.W., Simmers, I. (1997) Global Synthesis of Groundwater Recharge in Semiarid and Arid Regions. Hydrological Processes, 20: 3335-3370.

Shaw, R.J. (1999). 'Soil Salinity – Electrical Conductivity and Chloride.' In: Peverill, K.I., Sparrow, L.A. and Reuter, D.J. (Eds.), Soil Analysis – An Interpretation Manual, CSIRO Publishing, Victoria.

Skaggs, R.W. (1978). *A Water Management Model for Shallow Water Table Soils*. Water Resources Research Institute, University of North Carolina, Report No. 134, Raleigh, USA.

Šimunek, J., Sejna, M., and van Genuchten, M.Th. (1999). HYDRUS-2D/MESHGEN-2D, Simulating Water Flow and Solute Transport in Two-Dimensional Variably Saturated Media, IGWMC – TPS 53c, Colorado School of Mines, USA.

Stevens, D. (2002). Groundwater on the Northern Adelaide Plains: Prioritising research and related communication requirements. Minutes of meeting 28th Nov. 2002. CSIRO Land and Water, Waite Campus, Adelaide, South Australia.

U.S Department of Agriculture – Agricultural Research Service, (1992). *Root Zone Water Quality Model (RZWQM).* Great Plains System Research Unit, Fort Collins, CO.

Utset, A. and Borroto, M. (2001). A modelling-GIS approach for assessing irrigation effects on soil salinisation under global warming conditions. Agricultural Water Management, 50: 53-63.

Van der Ploeg, R. R., Beese, F. (1977). *Model calculations for the extraction of soil water by ceramic cups and plates.* Soil Science Society of America Journal, 41: 466 – 470.

Van Genuchten, M. T., (1980). *A closed form equation for predicting the hydraulic conductivity of unsaturated soil*. Soil Science Society of America Journal, 44: 892-898.

Veihmeyer, F.J. and Hendrickson, A.H., (1927). *Soil moisture conditions in relation to plant growth*. Plant Physiology, 2: 71-82.

Veihmeyer, F.J. and Hendrickson, A.H., (1949). *Methods of measuring field capacity and permanent wilting percentage of soils.* Soil Science, 68: 75-94.

Wagenet, R.J. and Hutson, J.L. (1987) *LEACHM, Leaching Estimation and Chemistry Model: A process-based model of water and solute movement, transformations, plant uptake and chemical reactions in the unsaturated zone*. Continuum Water Resources Institute, Centre for Environmental Research, Cornell University, Ithaca, NY.

Wahba, M.A.S., El-Ganainy, M., Abdel-Dayem, M.S., Kandil, H. and Gobran, A., (2002). *Evaluation of DRAINMOD-S for simulating water table management under semi-arid conditions*. Irrigation and Drainage, 51: 213-226.

Wang, X., and Cui, P., (2004). *Linkage of ArcView GIS with the RZWQM*. Journal of Spatial Hydrology, Vol. 4, No. 2.

Western, A.W., Grayson, R.B. and Bloschl, G. (2002). *Scaling of soil moisture: a hydrological perspective.* Annual Review of Earth and Planetary Sciences, 30: 149-180.

Zhu, Y., Fox. R.H. and Toth, J.D. (2002). Leachate collection efficiency of zero-tension pan and passive capillary fibreglass wick lysimeters. Soil Sci. Soc. Am. Jnl. 66: 37-43.

Zhu, J.T., Mohanty, B.P. (2002). Upscaling of soil hydraulic properties for steady state evaporation and infiltration. Water Resources Research, 38 (9): 1178.